TUDelft

Delft
University of
Technology

Van Oord

Marine ingenuity

MASTER THESIS

Efficiency of a Sand Column Supported Embankment in Sabkha Soil

by

R. LAMORÉ

March 2016

Master Thesis

Efficiency of a Sand Column Supported Embankment in Sabkha Soil

Submitted in partial fulfilment of the requirements for the degree of

Master of Science (M.Sc.)

at Delft University of Technology.

To be publicly defended on March 24, 2016

Student:
R. Lamoré
St. Nr.   4052048
E-mail   rlamore@gmail.com

Graduation Committee:
Prof. Dr. M.A. Hicks (TU Delft)
Ir. W. Karreman (Van Oord)
Ing. H.J. Everts (TU Delft)
Dr. Ir. K.J. Bakker (TU Delft)

Acknowledgments

First I would like thank my graduation committee for their support during the project. Prof. dr. Hicks, I would like to thank you for your insight in the modeling part of this thesis and keeping guard of the academic level of this thesis. Ir. Karreman offered me the position as a graduate intern at Van Oord, which I am very grateful for. During the project you had many insights and helped me stay on track. The experience shared by ing. Everts was indispensable during my site visit preparation and the interpretation of my test results. You also reminded me of the subjects that are important during this project, so that I wouldn't wander of too far. Dr. ir. Bakker is thanked for helping me interpret my PLAXIS results, especially during the initial erroneous results. I appreciate that you reminded me to keep a structured investigation and to-the-point conclusions. Although not officially part of my graduation committee, I would like to thank Dr. Ir. Brinkgreve for his support and insight during the PLAXIS calculations.

The help of the laboratory staff of the soil mechanics lab at the University was indispensable for this project. I would like to thank ing. Verwaal for helping me prepare soil samples and taking the time to explain which tests to perform and how. Furthermore I would like to thank A. Mulder for helping me set-up a computer system to read out soil tests.

I would like to thank the staff of Van Oord, both at the Headquarters as well as at the site office in Kuwait. During the site visit I received a lot of aid in preparing and executing my tests. I was given the opportunity to discuss my findings with the people in the office which helped me in interpreting them.

Dr. ir. van Eekelen is thanked for her support during the literature study. You helped me understand the current state of art concerning column supported embankments and provided me with literature on the subject. I would also like to thank you for the invitation to your promotion and congratulate you with your achievements for the Concentric Arches model.

Last but certainly not least I would like to thank my family and friends for their support during this project. I wouldn't have been able to set up a soil sampling and testing campaign without the help of my father. Your experience and ability to see things in a different perspective were of great use in all phases of this project. The rest of my family and friends are thanked for their patience and insight during the project, especially at times it didn't run as smooth as I had wished it would.

Remco Lamoré
March 2016

Van Oord
Marine ingenuity

Preface

This thesis report concludes my master study of Geo-Engineering at the faculty of Civil Engineering and Geosciences at the Delft University of Technology. The project was supported by Van Oord Marine Contractors an has been conducted at Van Oord Headquarters in Rotterdam, the Van Oord site office in Al-Zour, Kuwait, and at the university in Delft.

For a current Van Oord project in Kuwait, an interesting soil improvement technique was employed, namely installing columnar sand inclusions in soft soil. While little attention to this specific method of soil improvement was given to the subject during the lectures at the university, it was very interesting to be involved in this project.

Soil improvement techniques such as sand and rock columns are suitable to be used in Dutch soil conditions. While settlement and bearing capacity are the main advantages of this technique highlighted in this report, the method can also be used to increase shear resistance of soil. In this respect the method may for instance be a suitable dike reinforcement technique.

For the future I hope that there will be more attention to soil improvement using columnar inclusions. The results show that there are many methods which can be implemented in the Dutch practice. The TU Delft has an excellent position to take a lead and make Dutch engineers aware of these methods and change the practice.

Abstract

This thesis report presents an investigation of a soil improvement technique that is being executed for a Van Oord project in Kuwait. The soil is improved by the use of a column supported embankment, consisting of sand columns installed in a soft soil layer and a sand platform. The efficiency of this method is defined in terms of stress transfer and settlement reduction. When the soil improvement is finished and the land will be used, there are conditions concerning bearing capacity and settlement behavior. To this extent two important parameters were defined. i.e. the incremental efficiency (the load increase in a sand column over the total surface load increase) and incremental settlement reduction ratio (the settlement of the improved soil over the settlement of the unimproved soil (i.e. soil that has not been improved by sand columns), under loading).

To determine the efficiency of the soil improvement, a number of tests were performed on site. Tests included plate load tests (in this thesis referred to as zone load tests). The load tests were simulated in PLAXIS, with the known load/settlement results the model could be benchmarked. Furthermore soil samples were taken and tested to determine the local soil characteristics. The parameters derived from the soil tests are also used in the PLAXIS calculations.

PLAXIS allows for a step-by-step consolidation of the soft soil in which the columns were installed. It can be seen that the stress distribution changes for different stages of consolidation. The columns are first constrained by the very stiff soft soil layer (due to high excess pore pressures under loading). When the pore pressures dissipate the constraining stress is lowered and the column head expands. Under vertical loading the stress in the column head has a funnel shape, due to the displacements in the outer ring of the column head.

Based on the PLAXIS calculations it can be concluded that when a load is activated on top of a surface of soil that has been improved by the use of sand columns (with a center-to-center distance of three meters), given that the platform is thick enough, 60% of that load is transferred to the column. With a greater center-to-center distance between the columns that percentage decreases, e.g. 28% for a column spacing of five meters.

Compared to existing theories by Hewlett and Randolph (1988) and Zaeske (2001) (it should be noted that most existing theories assume presence of geosynthetic reinforcement, which is not the case for this project) the calculated column force is relatively low.

A minimal thickness of the sand platform is needed to facilitate maximum efficiency. The thickness as determined by the PLAXIS calculations are lower compared to existing literature. With platform heights of up to seven meters no full arching was observed, however partial arching did occur as evidenced by the efficiency values.

Van Oord
Marine ingenuity

Samenvatting

Deze scriptie beschrijft een onderzoek naar een grondverbeteringstechniek die wordt toegepast voor een bestaand Van Oord project in Koeweit. De grond aldaar wordt verbeterd door het gebruik van een soort paalmatras, bestaande uit zandkolommen en een zandplatform. De efficiëntie van deze methode wordt gedefinieerd in termen van spanningsverdeling en zettingsvermindering. Nadat de grondverbetering klaar is en het terrein in gebruik wordt genomen moet de ondergrond voldoen aan bepaalde draagkrachts- en zettingseisen. Om deze eisen te kwantificeren en veralgemeniseren worden er twee parameters gedefinieerd, namelijk de incrementele efficiëntie (Engels: incremental efficiency) en het zetting verminderingsratio (Engels: Settlement Reduction Ratio). De incrementele efficiëntie wordt gedefinieerd als de hoeveelheid kracht die naar de kolom gaat over de totale kracht van een uniform verdeelde belasting. Het zettings verminderingsratio wordt gedefinieerd als de hoeveelheid zetting die optreedt in verbeterde grond over de hoeveelheid zetting die optreedt in onverbeterde grond.

Om de efficiëntie van het paalmatras dat in Koeweit wordt aangelegd te bepalen, is er een aantal testen verricht op locatie. Een van deze testen was een serie plaatbelastingtests. Deze plaatbelastingtests werden vervolgens gemodelleerd in PLAXIS, zodat het model geijkt kon worden aan de hand van het bekende belasting/zet gedrag. Verder werden er grondmonsters gestoken, deze zijn vervolgens getest in het lab van de TU Delft. De sterkte- en stijfheidsparameters die bepaald zijn met lab testen zijn gebruikt voor het PLAXIS model.

PLAXIS beschikt over een functie om consolidatie van de slappe grondlaag te modelleren in verschillende fasen. Uit de verschillende stappen kunnen de spanningsverdelingen per fase achterhaald worden. De kolommen zijn eerst opgesloten door de relatief stijve slappe grondlaag (de laag bevat namelijk bij 0% consolidatie een wateroverspanning ter hoogte van de belasting). Als de poriedrukken afnemen neemt de spanning op de zandkolommen af. De verticale spanning op de kolommen neemt hierna toe en krijgt een trechtervormige verdeling in de kolomkop door de horizontaal uitzettende kolom.

Gebasseerd op PLAXIS berekeningen kan men concluderen dat wanneer een uniform verdeelde belasting op het maaiveld wordt gezet, aangenomen dat het platform voldoende dik is, wel 60% van de belasting naar de kolommen kan worden geleid (bij een hart-op-hart afstand van drie meter). Als de h.o.h. afstand tussen de kolommen wordt vergroot neemt dit percentage af, bijvoorbeeld tot 28% voor een h.o.h. afstand van vijf meter.

Vergeleken met bestaande theorieën uit Hewlett and Randolph (1988) en Zaeske (2001) is de kracht in de kolom die uit de PLAXIS berekeningen volgt relatief laag. Men dient wel in achting te nemen dat de meeste theorieën gebasseerd zijn op het gebruik van geotextiel of geogrid, wat echter niet het geval is voor het project in Koeweit.

Een minimale dikte van het zandplatform is vereist om maximale efficiëntie te behalen. De diktes die af te leiden zijn uit de PLAXIS berekeningen zijn lager dan door de literatuur wordt voorgeschreven. Met platformhoogtes tot wel zeven meter is er geen volledige boogwerking ontdekt in de PLAXIS modellen. Echter is er wel gedeeltelijke boogwerking bewerkstelligd, wat wordt bewezen door de gevonden waarden voor de efficiëntie.

TUDelft

Delft
University of
Technology

Contents

Van Oord
Marine ingenuity

Van Oord
Marine ingenuity

Nomenclature and Abbreviations

Column Supported Embankment

a	m	Cap width of a pile or column
A	m^2	Area (of a unit cell), $=s^2$
A	kN/column	Load part transferred directly to the column
$A\%$	[-]	Arching as a percentage of the total load, $=E$
A_c	m^2	Area of the column
ΔA	%	Incremental arching
b	m	Pile cap / column width by Hewlett and Randolph (1988)
B	kN/unit cell	Load part that passes through the geosynthetic reinforcement
C	kN/unit cell	Load part that is carried by the soft soil between the columns
CSR		Column Stress Ratio
d	m	Pile or column diameter
E	%	Efficiency, A as a percentage of the total load, see eq. 2.6
ΔE	%	Incremental efficiency
h_m	m	Critical height by Jenck (2004)
H	m	Platform height
H_{crit}	m	Critical height
H_g	m	Height of the arch by Zaeske (2001)
m	[-]	Stiffness ratio, $= \frac{E_c}{E_s}$
n	[-]	Stress concentration ratio
s	m	Center to center distance between colums
s'	m	Half of the diagonal distance between columns minus the radius
s_d	m	Diagonal distance between two columns
s_x	m	Center to center distance between colums, x axis
s_y	m	Center to center distance between colums, y axis
S_r	%	Settlement reduction ratio, $= \frac{U_z}{U_z^*}$
ΔS_r	%	Incremental settlement reduction ratio
SSR	(%)	Stress Reduction Ratio, $= \frac{\sigma_s}{\gamma H + q}$
ΔSRR	%	Incremental SRR
q	kPa	Surcharge
U_z	mm	Settlement
U_z^*	mm	Settlement without soil improvement
α	[-]	Replacement ratio, $= \frac{A_c}{A}$
δ	[-]	Column width over spacing ratio, $= \frac{b}{s}$
Δ	[-]	Increment
ζ	[-]	Ratio of platform height over column spacing, $= \frac{H}{s-a}$
ρ	[-]	Arching ratio used by Han and Gabr (2002), $= \frac{p_b}{\gamma H + q_0}$

Van Oord
Marine ingenuity

Soil (Testing) Parameters

c	kPa	Cohesion
C_c	[-]	Compression index
C_s	[-]	Swelling index
e	[-]	Void ratio, $= \frac{V_v}{V_s}$
E	(%)	Efficacy or Efficiency, $= A\%$
E_{50}	MPa	Secant stiffness modulus
E_{50}^{ref}	MPa	Reference secant stiffness modulus
E_c	MPa	Stiffness modulus column
E_{oed}	MPa	Oedometer modulus, $= M$
E_{oed}^{ref}	MPa	Reference Oedometer modulus
E_s	MPa	Stiffness modulus soft soil (in between columns)
f_s	MPa	Skin friction
M	MPa	Constrained modulus
n	[-]	Porosity, $= \frac{V_v}{V_t}$
s_u	kPa	Undrained shear strength, $s_u = c + \tau \cos\varphi$
$s_{u,PMT}$	kPa	Undrained shear strength from a PMT test
$s_{u,vane}$	kPa	Undrained shear strength from a Vane test
K_0	[-]	At rest coefficient of lateral earth pressure
K_a	[-]	Active coefficient of lateral earth pressure
K_{krit}	[-]	Critical coefficient of lateral earth pressure
K_p	[-]	Passive coefficient of lateral earth pressure
m	[-]	Power for stress-level dependency of stiffness in HSM
p	kPa	Pore pressure
P	kPa	Pore water pressure
q_c	MPa	Cone resistance
q_t	MPa	Corrected cone resistance
R	[-]	Friction ratio ($= \frac{f_s}{q_c}$)
U	%	Degree of consolidation in PLAXIS, $= 100(1 - \frac{p_{min}}{p_{max}})$
V_s	m^3	Volume of solids
V_t	m^3	Total volume
V_v	m^3	Volume of void space (air + water)
α	°	Angle of linear failure surface from vertical
$\gamma_{d,w}$	kN/m^3	Unit weight, dry and wet respectively ($= \rho \cdot 9.81 \text{m/s}^2$)
$\rho_{d,w}$	kg/m^3	Unit mass, dry and wet respectively
ρ_{max}	kg/m^3	Maximum density
ρ_p	g/cm^3	Particle density
$\sigma_{1,2,3}$	kPa	Principal stresses
σ_c	kPa	(Pre)Consolidation stress
σ_h	kPa	Horizontal stress
σ_t	kPa	Tensile strength
σ_v	kPa	Vertical stress
σ_w	kPa	Water pressure ($= p$)
τ	kPa	Drained shear strength, $s_u = c + \sigma'_v \tan\varphi$
φ	°	(effective) Friction angle
φ_p	°	Peak (effective) friction angle
ψ	°	Dilatancy angle

T U Delft
Delft
University of
Technology

Subscripts

c	Column
influence	Influence area or volume on top of a column
r	Ratio
s	Soft soil
s=3	Spacing equals 3.0 m
s=5	Spacing equals 5.0 m
t=0	Before activating a load
t=1	After activating a load
U=0%	Consolidation equals 0%
U=99%	Consolidation equals 99%
U=100%	Consolidation equals 100%
x	x-direction
y	y-direction
z	z-direction

Abbreviations

BH	Borehole
CPT	Cone Penetration Test
CPV	Contrôleur Pressure et Volume, pressure and volume control unit in a PMT
CSE	Column Supported Embankment
DC	Dynamic Compaction
DMT	Dilatometer Test
DR	Dynamic Replacement
DSS	Direct Simple Shear test
FVT	Field Vane Test
GR	Geosynthetic reinforcement
GWL	Groundwater Level
$HEIC$	High Energy Impact Compaction
HSM	Hardening Soil Model
MP	Mackintosh Probe
PLT	Plate Load Test
PMT	Pressuremeter Test
SPT	Standard Penetration Test
SSM	Soft Soil Model
VO	Van Oord
ZLT	Zone Load Test
ZOR	Al-Zour Refinery Project

Van Oord
Marine ingenuity

1

Introduction

1.1 The Project

Currently a land fill and soil improvement project by Van Oord is running in Kuwait. The project is located in the Southeast of the country, approximately 90 km south of Kuwait City. The Al-Zour power plant is situated approximately 10 km to the East. A map of Kuwait and the project location is included in the appendix, see chapter A.

The client of the project is the Kuwait National Petroleum Company, interested in building a new refinery in the area. Before the refinery can be built, soil improvement is necessary to increase bearing capacity and reduce settlements over a relatively large area. The refinery will be built on an approximately 5 m high embankment, consisting of dredged sand. The dredged sand is transported ashore over several kilometers by pipelines.

Different methods exist to improve soft soils. One of these methods is to install columnar inclusions. These columnar inclusions have a higher stiffness compared to the surrounding soil, leading to an increase in bearing capacity and a reduction of settlement. These inclusions can consist of any granular material, i.e. everything between rock and sand. There are different techniques of installing the inclusions, such as dynamic replacement and vibrocolumns.

The sand columns in the Al-Zour Refinery Project (ZOR) are installed using the dynamic replacement (DR) technique, which is a technique that shows considerable similarities to dynamic compaction and is also developed by Ménard. The technique employs a crane with a steel block and a dozer.

An illustration of the technique is shown in figure 1.1.
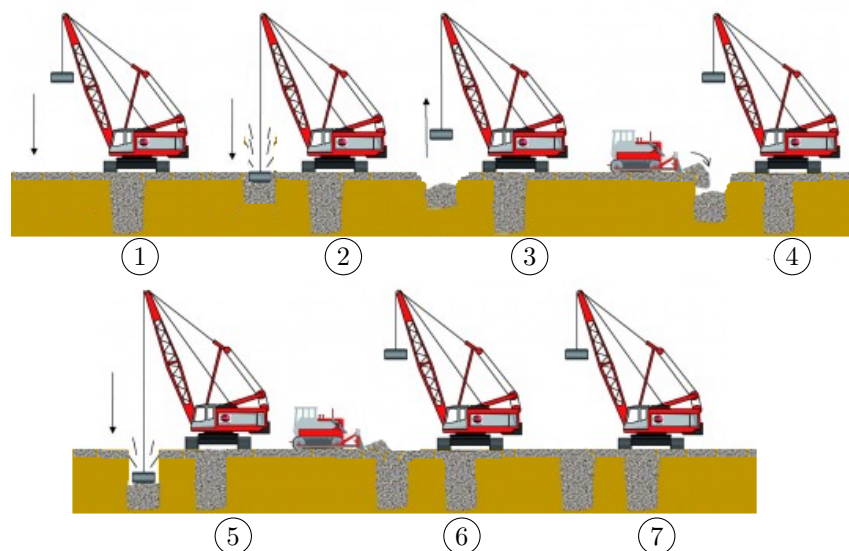

Figure 1.1: Dynamic Replacement, edited figure from Vibro Menard UK

The crane drops the block multiple times at the same location where a sand layer of 1 - 2 m is already present, forming a crater of approximately one meter depth (steps 1-3). The crater is backfilled and the operation is repeated (steps 4-5), after which the crater is again backfilled (step 6). The result is a sand column formed by displacing the existing soft soil (step 7). Because of the high energy impact of the DR blocks, the columns have a relatively high density and stiffness. After DR is finished the sand platform is compacted using dynamic compaction. The depth of the sand columns is dependent on the amount of cycles and the weight of the block. In the ZOR project depths of 4 - 5 m were reached in most cases and the column met a bearing layer. The diameter of the formed columns is dependent on the weight and dimensions of the block and to a lesser extent on amount of cycles. Generally a diameter of approximately 2.2 m was accomplished. In some locations the method was slightly changed, reducing the diameter to 1.0 m. The center-to-center distance of the columns in the ZOR project is 6 m for the 2.2 m diameter columns and a distance of 5 m was used for the 1 m diameter columns.

A photo taken on site is given in figure 1.2, in this photo the craters formed by dynamic replacement can be seen. A dozer is backfilling the craters (step 4 in figure 1.1), while in the background of the photo the cranes are in operation.

Figure 1.2: Area where DR is being executed

The DR technique is suitable for relatively soft soils, e.g. peat, clay and some silts. The prominent soft soil encountered in the ZOR project is locally referred to as sabkha. Sabkha is a collective noun for very soft, sometimes silty or sandy clay. Sabkha is deposited in supratidal flats along the coastline. Evaporate cycles of the seawater from the Arabian Gulf have caused deposition of salt minerals from the relatively extreme saline groundwater, which are a source of cementation for the sabkha. Freshwater or relatively low-saline water may destroy the salt cementation in sabkha.

The subsoil layering was determined based on soil borings and CPT. Starting from surface level, the soil layers are elaborated below.

1. **Sand** the first 1-2 m consist of reclaimed sand;

2. **Silty/sandy clay/silt** below the sand, at the former surface level, a mixture of clay and silt was observed. This layer is generally 1 m thick. Although this soil layer has the characteristics of sabkha, it is generally stiffer and has a higher cone resistance. Compared to sabkha, this layer has a higher course grain content;

3. **Sabkha** below the former surface level a layer of sabkha is found, varying in thickness from 1-4 m;

4. **Sand** In some cases stiff clay, however generally slightly silty dense sand is generally found under the sabkha layer. In some cases first a layer of loose sand is present under the sabkha.

The subsoil layering as described above was valid during the soil sampling campaign. After the columns are finished, the surface level is once more increased by 3-4 m to a final level of approximately 5 m above the original surface level.

The soil improvement is finished when all the columns have been installed and the sand platform is in place. The combination of (sand) platform and columns is often referred to as a Column Supported Embankment (CSE). A cross-sectional sketch of a CSE is given in figure 1.3. Note that on the right side of the figure the soils that are enumerated above are shown.
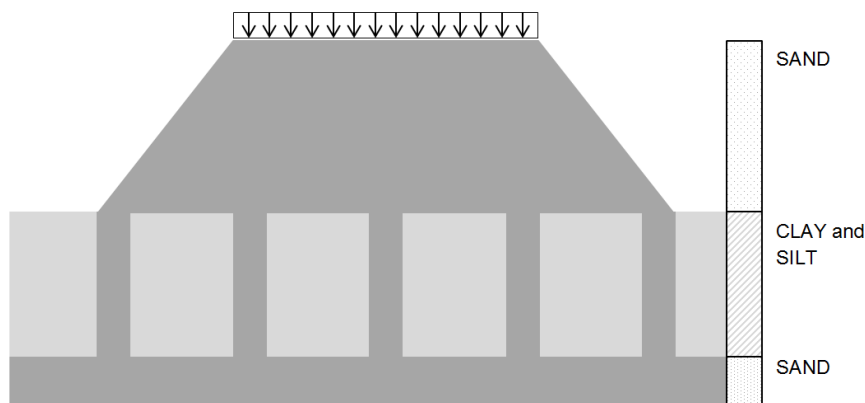
Figure 1.3: Cross-section of a CSE

The stress transfer in a CSE is based on stiffness difference between the columns and surrounding soft soil. The columns will draw more stress due to this difference. Using a granular platform with high friction angle further enhances stress transfer to the columns due to a higher spread in stress distribution. The platform is in the literature referred to as a transfer platform. The sand columns have a higher strength compared to the surrounding soft soil and will thus increase bearing capacity. The sand columns are also relatively stiff and will thus settle less than the soft soil would. The fact that a CSE is relatively economical, is one of the main advantages of the method. The versatility concerning the installation method (dynamic replacement, vibrocolumns etc.) makes the method adaptable for a variety of soils.

It is known that the friction angle of the soil under a shallow foundation determines for a great part the stress distribution imposed by the foundation. In the design phase account was taken hereof, resulting in a relatively highly compacted sand platform. The bearing capacity and settlement calculations, however, did not take into account the interaction between the platform and columns.

Van Oord
Marine ingenuity

1.2 Research

The design of the soil improvement was made based on the experience by the subcontractor, Ménard[1]. There was however no experience by Van Oord employing this technique.

The current method of calculating the stress distribution and settlements is based on the stiffness ratio between the columns and soft soil. It is however not known whether this relatively straightforward method is suitable. Additional investigation is needed to determine the efficiency of the improvement method, in terms of bearing capacity increase and settlement reduction. It is known that these parameters are dependent on column spacing, it is however not known how to quantify this dependency.

1.2.1 Research Questions

The main question is defined as: *What is the efficiency of a Column Supported Embankment in sabkha soil?* and can be answered by answering the following subquestions:

i *Are there existing methods to determine stress transfer and settlement?*

ii *How is the load, imposed by a surcharge, transferred in a CSE?*

iii *How does platform height and column spacing influence stress distribution?*

iv *How does platform height and column spacing influence settlement?*

v *Does the local soil composition influence the efficiency and settlement of a CSE?*

vi *How does consolidation influence the efficiency of a CSE?*

vii *What are the requirements for an efficient CSE?*

viii *Can existing theories be used to design unreinforced CSE?*

ix *Can a composite stiffness be applied to calculate settlements?*

x *When should a CSE be used as a soil improvement technique?*

1.2.2 Assumptions and Limitations

The boundaries and limitations of the investigation are defined as follows:

- The installation effects of the DR columns on the soft soil is not explicitly taken into account. The soil samples were however taken (months) after DR works, any improvement is thus implicitly taken into account.

- The sand platform and subsoil are assumed to be consolidated to the weight of the platform at the time of loading.

- The sand columns are assumed to be cylindrical volumes with a diameter of 1.0 m, that have not influenced the surrounding soil during installation.

- The sand columns are assumed to be founded on a sand layer:
    - > Settlement of the layer under the sand column is taken into account;
    - > The compaction of the soil under the column due to the DR is not taken into account;
    - > Any creep behavior of the soil under the column is not taken into account.

- In long-term calculations the consolidation is investigated, creep behavior is however ignored.

- The sand columns used in a CSE are also used to increase the shear strength of soil, for example in dike reinforcement projects. This favorable feature of sand columns is however not analyzed nor was it taken into account.

---

[1]See the companies section on page 121 for a list of companies

TUDelft
Delft
University of
Technology

1.2.3 Activities

To answer the questions stated above, a number of activities was summarized at the start of the project. The activities are enumerated below:

1. Familiarize with the subject through a literature study;

2. Present the findings of the literature study to the committee and discuss the activities for the site visit;

3. Go on a site visit to:

   - Inspect Dynamic Replacement execution;

   - Gather soil information (sabkha and sand);

   - Gather CPT data;

   - Execute load tests to determine load/settlement behavior.

4. Process all the data acquired during the site visit;

5. Present the information gathered on site to the committee;

6. Build a PLAXIS model using the parameters acquired during the site visit;

7. Perform multiple calculations with varying soil/geometry parameters;

8. Discuss the findings with the committee;

9. Present the findings of the investigation in the form of a written report and oral presentation.

Van Oord
Marine ingenuity

1.3 Reader's Guide

The literature study is summarized in the first part of this report. This part consists of three chapters. The first chapter describes the column supported embankment. The main elements, i.e. the columns and platform are described and a number of parameters are defined. The second chapter is concerned with the predominant soft soil that is found at the project site, which is sabkha. Characteristics and their relative importance to the soil improvement method are described in this chapter. The first part concludes with a chapter elaborating the dynamic replacement technique. This technique is used to install the sand columns.

The second part of this thesis describes the field work that has been performed on site and in the lab at the University. The first chapter discusses the soil tests that were necessary for the PLAXIS calculations which were performed in a later stage. The second chapter reviews the tests and their respective results, for the tests that have been executed in Kuwait as well as the tests that were performed in the TU Delft soil mechanics laboratory. The last chapter of this part specifies the parameters that have been acquired and will be used for the PLAXIS calculations.

The third part is concerned with the PLAXIS calculations that were carried out based on the parameters found in the previous part. This part is made up of two chapters. In the first chapter an analysis of the calculations is given for the short-term behavior of the column supported embankment. The second chapter analyzes the long-term behavior of the model.

The final part of this thesis is divided into three chapters. The first chapter discusses the results that were acquired from field and PLAXIS tests and calculations. The subsequent chapter gives the conclusions that can be drawn from the findings in this thesis. The last chapter is concerned with recommendations for further research.

The appendices are divided into relevant categories. These categories are displayed in the table of contents. Throughout the main report references are made. These reference are hyperlinked to the appendix.

Part I

Literature study

2

Column Supported Embankment

It was described in the introduction that the foundation in the ZOR project essentially consists of two elements, namely columns and a sand fill on top. This is commonly called a Column Supported Embankment (CSE).

The literature study part of the thesis, of which this is the first chapter, elaborates the CSE. The current chapter is mainly concerned with definitions and stress distributions. The next chapter discusses the soil that is being improved, namely soft clay locally known as sabkha. The last chapter in the literature study, chapter 4, elaborates the method of column installation, which is dynamic replacement. Two reference projects are described in that same chapter.

In order to keep this chapter brief and to the point some subjects and derivations were moved to the appendix, these can be found in chapter B.

2.1   Arching

The stress transfer in a CSE is based on an arching effect, described by Terzaghi (1943). Terzaghi's trapdoor experiment is shown in figure 2.1.
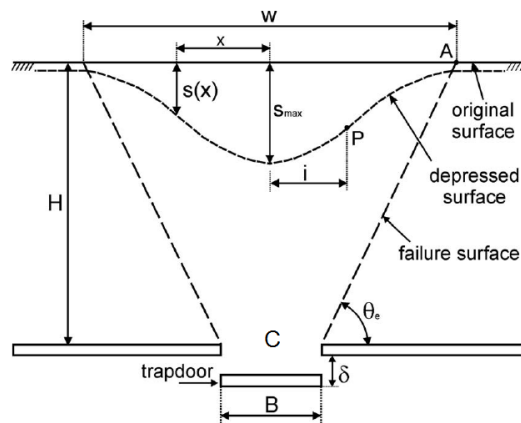

Figure 2.1: Trapdoor experiment (Costa et al., 2009)

Classic soil mechanics dictates that the stress in point C, before opening the trapdoor, (see figure 2.1) is calculated as follows:

$$\sigma_v = H\gamma + q \tag{2.1}$$

Where:

σ_v	=	Vertical stress;
H	=	Depth (height of the sand profile);
γ	=	Unit weight of the soil;
q	=	Surcharge (if applicable).

The soil on top of the trapdoor will not remain stationary upon lowering of the trapdoor, it will start to yield and move in a downwards direction. The yield surface is shown by the dashed line in figure 2.1. The downward movement is resisted by the stationary soil above the columns. Terzaghi (1943) notes that, since the shearing resistance tends to keep the yielding mass in its original position, the pressure on the yielding part of the support is reduced, and the pressure on the adjoining stationary part is increased. This is commonly called the arching effect (Terzaghi, 1943). The arching effect essentially transfers a relatively wide spread load to a more concentrated load on the structure next to the trapdoor.

The trapdoor experiment is comparable to the soft soil and sand columns in the ZOR project. In this case the soft soil in between the columns represents the trapdoor (the soft soil will settle upon loading). Because of the arching effect described above, the stress will be transferred to the columns. There will still be a load on top of the soft soil in between the columns, however significantly lower than the σ_v in equation 2.1. The stress on top of the columns will be higher than the σ_v calculated above.

Vertical equilibrium is always applicable:

$$\underbrace{H\gamma + q}_{\text{Total load}} = \underbrace{\alpha\sigma_c}_{\text{Column term}} + \underbrace{(1-\alpha)\sigma_s}_{\text{Soft soil term}} \qquad (2.2)$$

Where α, the replacement ratio, is defined as the area of the column divided by the total area of the square cell. The replacement ratio will be further elaborated in section 2.3.

A parameter quantifying the arching effect will be defined later. It can be seen however that when the column term in equation 2.2 increases, the second term decreases and arching develops.

The arching will continue until an equilibrium is reached. When an equilibrium is reached, the column term in equation 2.2 will have a threshold value. The (absolute) value is dependent on the form of the arch that has developed. Figure 2.2 shows different arch forms.
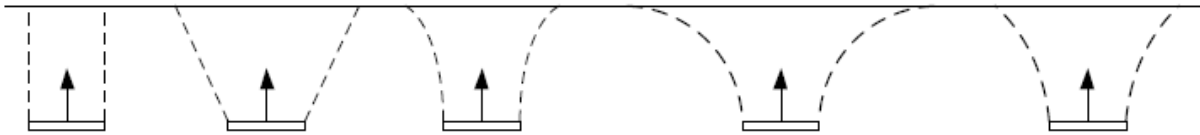
Figure 2.2: Arch forms (Mcguire, 2011), f.l.t.r.: cylinder, cone, trumpet, circular arch and log spiral

It can be seen in figure 2.2 that the part of the total stress that is transferred to the column is dependent on the form of the arch. Many authors (see table 2.1) agree that curved failure surfaces can be approximated by a linear failure surface as shown in figure 2.3, defined by a line between the origination point of shearing and the location where the shearing intersects the ground surface (Mcguire, 2011).
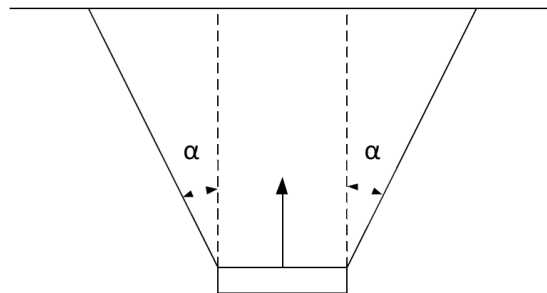
Figure 2.3: Linear failure surface (Mcguire, 2011)

Different authors have come up with recommendations for the angle α, usually dependent on the friction angle φ. A selection of recommendations is given in table 2.1.

TUDelft
Delft
University of
Technology

Table 2.1: Linear failure surface angle

Publication	Angle of linear failure surface from vertical α
Fadl (1981)	$\varphi/4[D_r(\frac{1+\cos^2\varphi}{2}) + (\frac{1+\sin^2\varphi}{2})]$
Murray and Geddes (1989)	$\varphi/2$
Ilamparuthi and Muthukrishnaiah (1999)	$\varphi/2 \pm 2°$
Meyerhof and Adams (1968)	$\varphi/3$
Kumar and Kouzer (2008)	φ

2.2   Design method

The design steps from CUR226 (2010) are given in section B.1.1. The first step in the design of a CSE is determining the critical height. This will be elaborated on in section 2.5. The second step, calculating bearing capacity of the columns, is not elaborated in this thesis.

Although Filz et al. (2012) do not give any concrete design steps, recommendations are given for the (preliminary) design of a CSE. These recommendations can be found in section B.1.2.

2.3   Load Distribution

2.3.1   Unit cell definition

To study the load distribution over the CSE, it is convenient to define a grid with an unit cell. Since a square grid is chosen in this project, a square unit cell is defined. The geometry of the unit cell is given in figure 2.4.
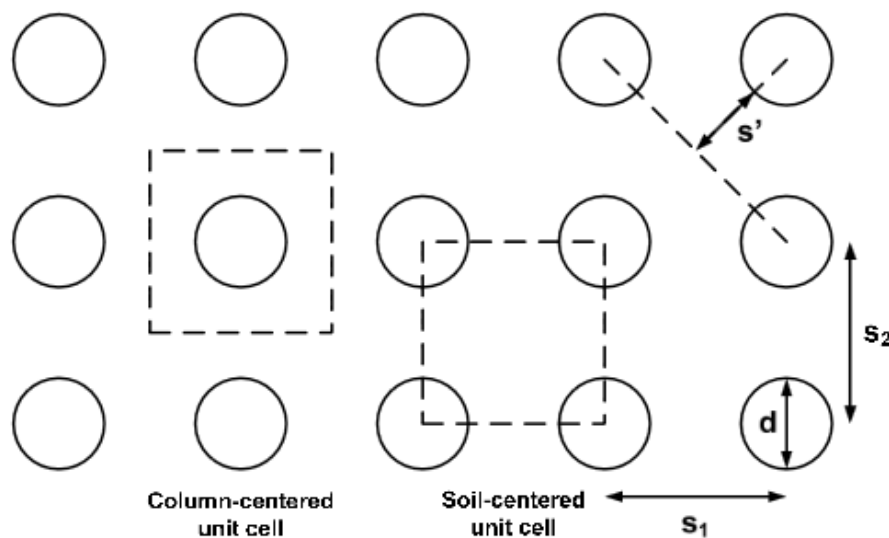
Figure 2.4: Square unit cell (Mcguire, 2011)

The parameters in this figure are defined in table 2.2.

Table 2.2: Unit cell parameters

Parameter	Definition
d	Diameter of the column
s_1 or s_x	Distance between columns in x-axis
s_2 or s_y	Distance between columns in y-axis
s'	Half of the diagonal distance between columns minus the radius.

In case $s_1 = s_2 = s$, then $s' = \frac{\sqrt{2}s - d}{2}$. Note that in the literature the term s_d is also used, which is the diagonal distance between columns, defined as $s_d = \sqrt{s_1^2 + s_2^2}$

Filz et al. (2012) present a terminology to describe parameters for stress transfer in a CSE. This terminology is used and elaborated below.

To provide an indication of the amount of support provided to the surcharge, a dimensionless quantity is used -the spanning ratio- defined as:

$$SR = \frac{s'}{d} = \frac{s}{\sqrt{2}d} - \frac{1}{2} \tag{2.3}$$

With a decreasing SR, the support provided by the columns increases.

The time that is necessary to improve an area is dependent on the amount of columns within that area. It is thus useful to define a parameter which defines the area of the columns per area of land. This parameter is calculated as follows:

$$\alpha = \frac{A_c}{s^2} = \frac{\pi}{4}\left(\frac{d}{s}\right)^2 \tag{2.4}$$

2.3.2 Stress transfer

In the case that there is no differential settlement between the part of the platform on top of the column and next to the column, the stress acting on the soil would be uniform. The stress is then calculated by adding the overburden pressure and surcharge, i.e. $\sigma_0 + q$ where $\sigma_0 = \gamma H$. The overburden stress is transferred to both soil and column, the ratio of stress transferred to the soil over the total stress is defined in equation 2.5.

$$SRR = \frac{\sigma_s}{H\gamma + q} \tag{2.5}$$

Where σ_s is the stress in the soil between the columns. The SRR is a ratio of stress borne by the soft soil over a total stress, and has a value between 0-1. A value that approaches 0 corresponds to a perfect arching effect. The SRR can however never have a value of exactly 0, because there is always soil below the arch that is borne by the soft soil. A value of 1 means that there is no arching.

2.3.3 Arching

The 'amount of arching' is defined by the ratio of stress transferred to the pile and the total stress (from the overburden). Eekelen et al. (2013) called this parameter the *arching A%*, Hewlett and Randolph (1988), Jenck et al. (2007) and Sloan (2011) called it the *efficacy*. The definition of the names is however the same, and will be referred to as the efficiency E. Note that Eekelen et al. (2013) uses two almost similar parameters, namely arching $A\%$ and arching A. The former is a ratio of the load transfer (see equation 2.6) as a percentage, the latter is the part of the load that is transferred to the pile in kN/pile.

Efficiency

The efficiency as it is defined in this thesis is given in equation 2.6, edited from Eekelen et al. (2013).

$$E = \frac{A}{A + B + C} = \frac{A}{(H\gamma + q)s_x s_y} = 1 - \frac{B + C}{(H\gamma + q)s_x s_y} \tag{2.6}$$

Where:

E	=	Efficiency;
A	=	Load part transferred to the pile;
B	=	Load part that passes through the geosynthetic reinforcement;
		(=0 in case no GR is used)
C	=	Load part that is carried by the soil in between the columns;
q	=	Surcharge;
s_x, s_y	=	Pile spacing in x or y direction.

In case no GR is used $B = 0$, so that:

$$\sigma_s = \frac{C}{s^2 - A_c} = \frac{C}{s^2 - \frac{1}{4}\pi d^2} \ \rightarrow \ E = 1 - SRR\frac{s^2 - \frac{1}{4}\pi d^2}{s^2} = 1 - SRR(1 - \alpha) \tag{2.7}$$

Incremental Efficiency

If a distributed load is modeled, which is usually the case, the efficiency can also be defined in terms of stress increments over surcharge increase. Using an incremental efficiency, one can determine the stress increment in the subsoil and columns, without having to take the weight of the soil into account. Note that the incremental stress is defined at the end of the consolidation period (when $p_{excess} \approx 0$ kPa).

$$\Delta E = \frac{\Delta A}{\Delta q s^2} = \frac{A_{t=1} - A_{t=0}}{[(\gamma H + q_{t=1}) - (\gamma H + q_{t=0})]s^2} = \frac{A_{t=1} - A_{t=0}}{(q_{t=1} - q_{t=0})s^2}$$

$$= 1 - \frac{(\sigma_{s,t=1} - \sigma_{s,t=0})(s^2 - \frac{1}{4}\pi d^2)}{(q_{t=1} - q_{t=0})s^2} \tag{2.8}$$

In a similar matter the SRR can be rewritten to represent an incremental ratio, using equation 2.9.

$$SRR = \frac{\sigma_s}{H\gamma + q} \rightarrow \Delta SRR = \frac{\sigma_{s,t=1} - \sigma_{s,t=0}}{q_{t=1} - q_{t=0}} \tag{2.9}$$

With equations 2.8 and 2.9 the efficiency is defined in terms of SRR and α in equation 2.10.

$$\Delta E = 1 - \Delta SRR\frac{s^2 - \frac{1}{4}\pi d^2}{s^2} = 1 - \Delta SRR(1 - \alpha) \tag{2.10}$$

2.3.4 Calculation Models

There are many models to calculate the amount of arching in a CSE. The majority of the models are limited to the case where geosynthetic reinforcement (GR) is used, since this is daily practice. These models are not or very limited elaborated in this thesis.

There are four approaches to describe arching. These models are summarized in the following sections.

Frictional models

Terzaghi (1943) performed experiments with a sand platform on top of a trapdoor, described in 2.1. Russell and Pierpoint (1997) extended the model in the third dimension, however the use of frictional models is less widespread compared to other models. Their main advantage, being theoretically based and therefore universally applicable, is often overshadowed by the disadvantage of the required parameters (Peet, 2014).

Empirical models

The empirical models, as the name suggests, are based on experimental data. The advantage of these models is simplicity. The disadvantage however is, as it is with nearly all empirical models, the dependence on the specific situation. That situation may not be suitable for extrapolation and thus limits the recommendations based on that model.

Rigid arch models

In these models, the arch that is formed is assumed to have a fixed shape (see figure 2.3). The weight of the soil outside of the arch (including any surcharge) is transferred directly to the pile or column. The soil inside the arch is carried by the subsoil.

Equilibrium models

The equilibrium models are the most used models in Western Europe (Peet, 2014). In these models the soil is assumed to be in limit state (i.e. the ratio of horizontal over vertical stress equals K_p). The stress on the columns and subsoil is calculated from the equilibrium of the critical part of the arch.

Hewlett and Randolph (1988) developed an equilibrium model, with a distinct first and second step of calculations. In the first step the GR is excluded from the calculations. This model will be described in section 2.3.5.

2.3.5   Hewlett and Randolph (1988)

The model of Hewlett and Randolph (1988) does not use GR in the first calculation step (presented in his paper). It is included in the second step of the design calculations, so that the effect of GR is not integrated in the arching calculation. Because of these separate steps the model may be applicable for the project. The model is adopted in the French ASIRI (2012) guideline and the British Standard BS8006.

The efficiency formulas derived can be found in B.3. Two formulas are presented, one considers the equilibrium in the crown of an arch while the other formula considers the base of the arches (at the pile caps). The lower result of the two formulas should be used for design. Figure 2.5 shows a plot of the formulas presented in section B.3.
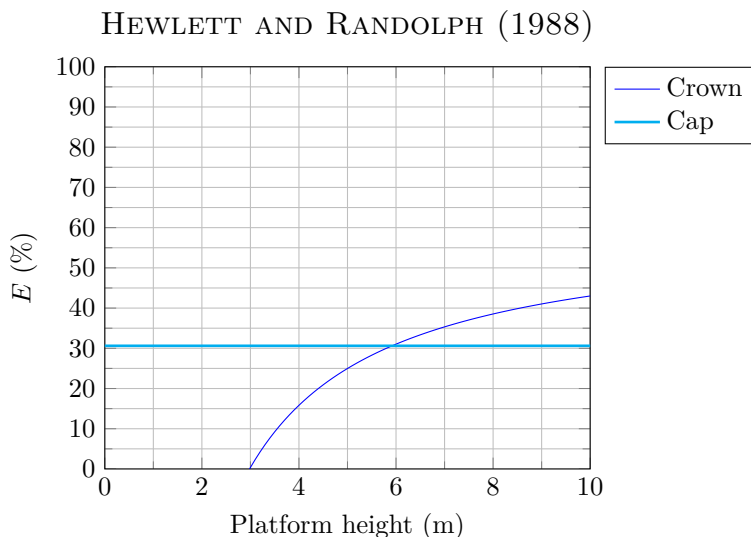
Figure 2.5: Design plots based on Hewlett and Randolph (1988) for $\varphi = 30°$ and $\frac{b}{s} = \frac{1}{3}$.

2.3.6 Zaeske (2001)

The model by Zaeske (2001) assumes arches to develop between columns. The arch thickness increases with arch radius, see figure B.3. The vertical stress acting on the soft soil between the columns is calculated and assumed to be constant over the area between the columns. The theory presented by Zaeske (2001) is used in the German EBGEO (2010) and the Dutch CUR226 (2010).

A more elaborate description including the equations by Zaeske (2001) can be found in B.4. The efficiency calculations do not require modification to calculate ΔE rather than E, which is shown in section B.4.1.

A design graph by Zaeske (2001) is given in figure 2.6.
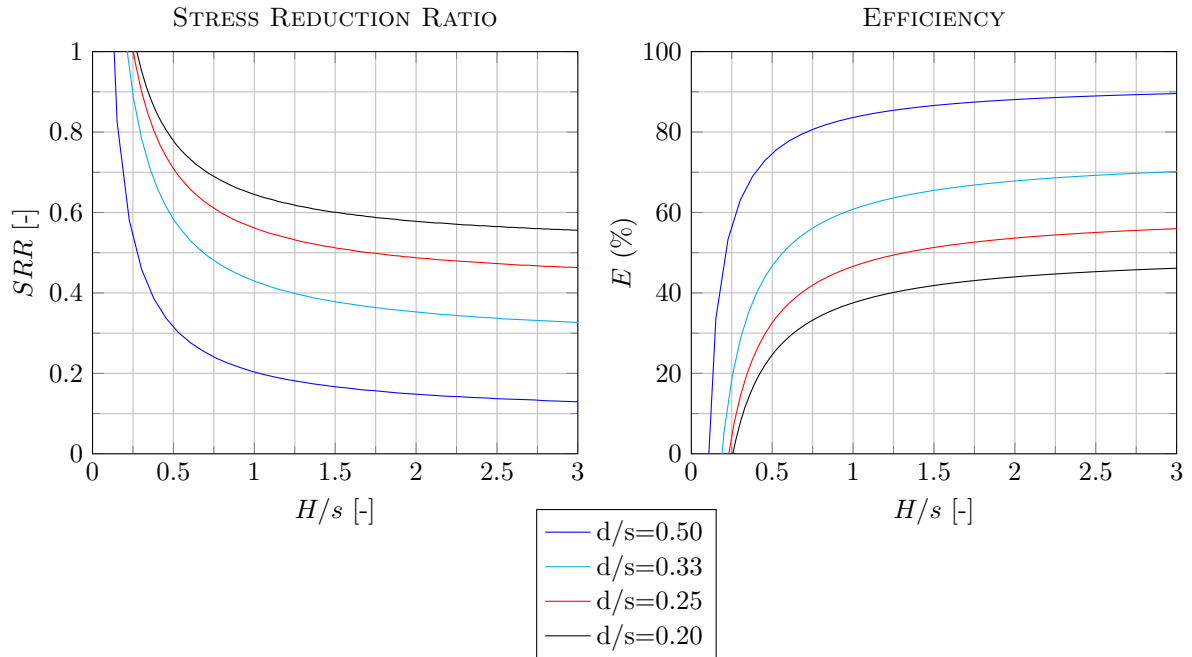
Figure 2.6: Design plots based on Zaeske (2001) for $\varphi = 30°$

The plots shown on the left in figure 2.6 are based on the formulas by Zaeske (2001), see equation B.6. This formula can be rewritten to calculate the efficiency, E, as defined before. Rewriting leads to plots given on the right in figure 2.6.

It is noted that Zaeske (2001) assumes that GR is used. The strength of the GR is however no input parameter for the calculations.

2.4 Settlement

The efficiency of a CSE is usually defined in terms of stress (E, SRR etc.). To quantify the improvement in terms of settlement rather than stress another ratio is used, i.e. the Settlement Reduction Ratio, S_r. S_r is the reciprocal ratio of the displacement that occurs if no improvement is used over the displacement that occurs in an improved soil. The settlement of both an improved as well as an unimproved CSE is shown in figure 2.7. S_R is defined in equation 2.11.

Van Oord
Marine ingenuity

(a) Settlement in unimproved soil   (b) Settlement in improved soil
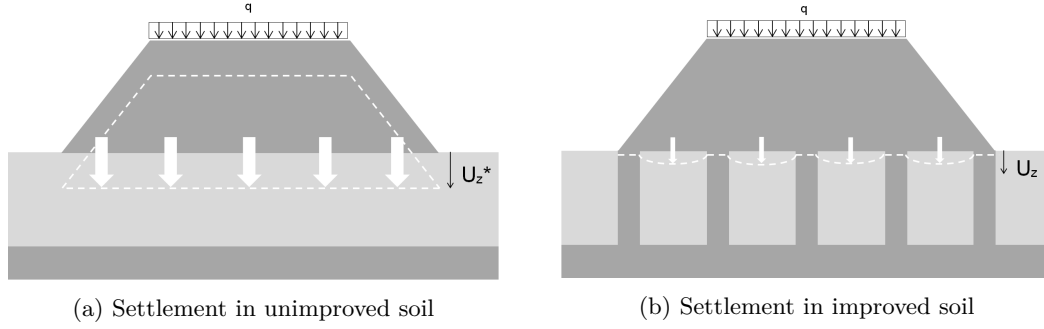
Figure 2.7: Settlement of a CSE

$$S_r = 1 - \frac{U_z}{U_z^*} \tag{2.11}$$

Where:
S_r	= Stress reduction ratio;
U_z	= Settlement after improvement;
U_z^*	= Settlement without improvement.

2.4.1 Incremental Settlement Reduction

The lower the Settlement Reduction Ratio, the more improved the soil is in terms of settlement. To determine the settlement reduction based only on a surcharge, q, an incremental S_r can be defined, using equation 2.12.

$$\Delta S_r = 1 - \frac{\Delta U_z}{\Delta U_z^*} = 1 - \frac{U_{z,t=1} - U_{z,t=0}}{U_{z,t=1}^* - U_{z,t=0}^*} \tag{2.12}$$

While S_r is a very useful parameter, it may prove difficult to be determined in practice. Stress distribution calculations are relatively straightforward, settlement calculations are more complicated. The S_r can be empirically based on comparable projects where different soil improvement techniques have been employed.

2.5 Platform height and column spacing

Whether arching develops is greatly dependent on the thickness of the platform on top of the columns. McNulty (1965) found in his trapdoor experiments that a low embankment height does not develop maximum arching. With the increase of embankment height the pressure on the soft soil decreased, because of the increase in shear resistance enhancing soil arching.

The minimum height is referred to as critical height, and defined as the embankment height above which settlements at the base of the CSE do not produce measurable differential settlement at the embankment surface (Filz et al., 2012). At the critical height lies the plane of equal settlement (Naughton, 2007), at which no differential settlements occur. The critical height is illustrated in figure 2.8.
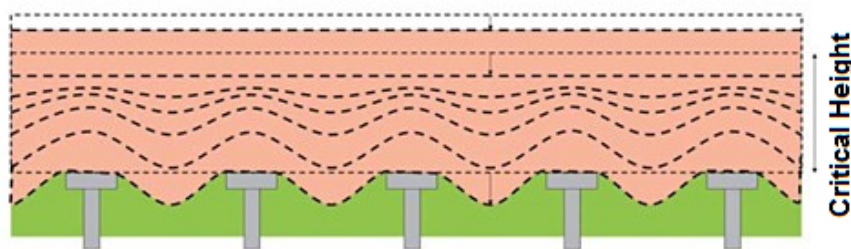
Figure 2.8: Critical height (CUR226, 2010)

It is important for nearly all construction projects that no differential settlements occur. Factors that influence differential surface settlements include column spacing, column diameter, embankment height, quality of subgrade support relative to column stiffness and loading acting on the embankment surface Filz et al. (2012). Low differential settlements can be achieved with a high embankment and a narrow column spacing.

Numerous investigations to determine the critical height have been performed. Most of these investigations were aimed at a CSE with GR. A summary is given in chapter B.2.

The remainder of this section is concerned with a summary of the critical height as determined by Han and Gabr (2002), Jenck et al. (2007) and Filz et al. (2012).

2.5.1   Han and Gabr (2002)

Han and Gabr (2002) used numerical analysis to investigate maximum- and differential settlements for different heights. The program used in his calculations was FLAC (Fast Lagrangian Analysis of Continua), with a square pattern of columns. A clear spacing of the piles is not described, however a 'zone of influence' is defined and equal to three meters and and approximately equal to the c.t.c. distance. The diameter of the pile is equal to 0.7 m. The sand that was used for the platform had a rather low friction angle of 30°.

The results in figure 6 in Han and Gabr (2002) show an increase in maximum settlement with increasing embankment height. As expected, the settlements were lower for the case where reinforcement was used. The difference increased to about 15% at a height of one meter and 25% at a height of four meters.

In figure 9 in Han and Gabr (2002) it is shown that the differential settlement at the pile caps continues to increase with an increase in the height of the embankment. Essentially this illustrates that when the embankment height is increased the settlement continues to increase, showing that arching cannot develop to a 0% SRR. For the reinforced case, the differential settlement is approximately 25% higher at an embankment height of four meters. The differential settlement at the surface reduces for an increase in embankment height. The differential settlement for both the unreinforced and reinforced case converge to zero at an embankment height of three meters. The latter finding is explained by the fact that soil arching develops (Han and Gabr, 2002). The ratio of embankment height over spacing ($\frac{H_e}{s-a} = 1.3$), which is different from the results by Jenck et al. (2009).

Han and Gabr (2002) also performed calculations determining stress distributions. It was found in figure 16 in Han and Gabr (2002) that an increase in embankment height leads to a higher value for the stress concentration ratio $n = \frac{\sigma_c}{\sigma_s}$. It was also found that the use of GR causes an increase in n. In figure 18 in Han and Gabr (2002) it is shown that an increase in the elastic modulus of the piles leads to an increase in n, up to a value of approximately 1000 MPa. The stress concentration ratio is higher for the case where GR is used.

2.5.2 Jenck et al. (2007)

The tests were performed with a steel rod assembly, known as a Schneebeli[1] soil. Two tests configurations have been used, one with a ratio $\frac{H}{s-a} = 1.3$ and the other $\frac{H}{s-a} = 2.0$. Both configurations use an α of 22%.
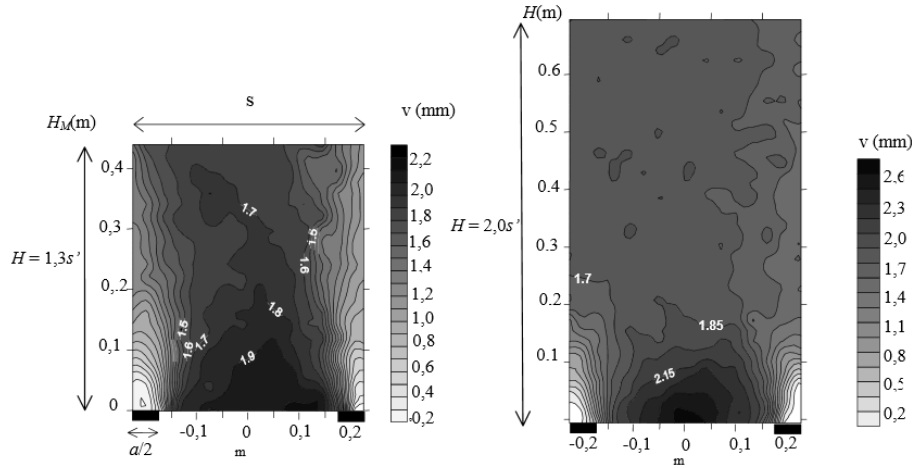
Figure 2.9: Settlements found by Jenck (2004)
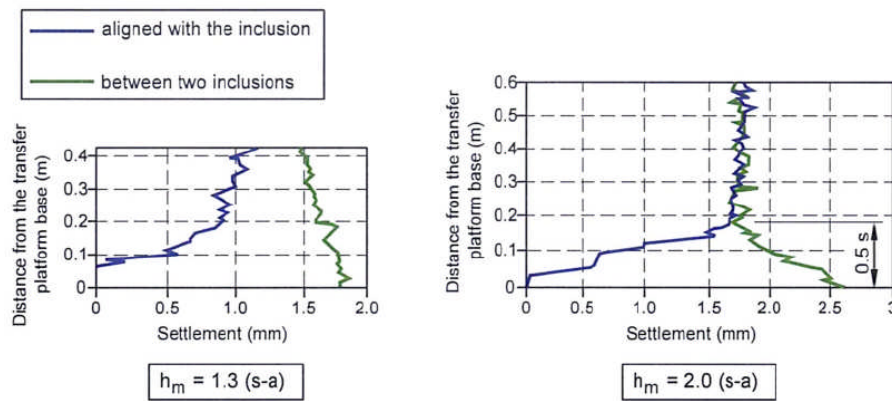
Figure 2.10: Differential settlement (Jenck, 2004)

It can be seen in figure 2.9 left that differential displacement will occur at the surface for a ratio of 1.3. Figure 2.9 right shows uniform settlement. Figure 2.10 shows limited differential settlement in the right figure. The latter figure also shows that almost no differential settlements occur above a length of half the column span, measured from the bottom. An important conclusion can be drawn from this, namely that more embankment height may be needed to develop a plane of equal settlement, than the actual height at which that plane lies.

2.5.3 Filz et al. (2012)

Filz et al. (2012) reported on tests by Mcguire (2011) and Sloan (2011). Mcguire (2011) used five bench-scale tests with different cap widths and spacings to determine the critical height (as defined before). Sloan (2011) performed field scale tests. The diagram showing their results is given in figure 2.11.

---

[1]Schneebeli soil is an analogical soil, which is an assembly of 3, 4 and 5 mm diameter steel rods which have a length of 60 mm.
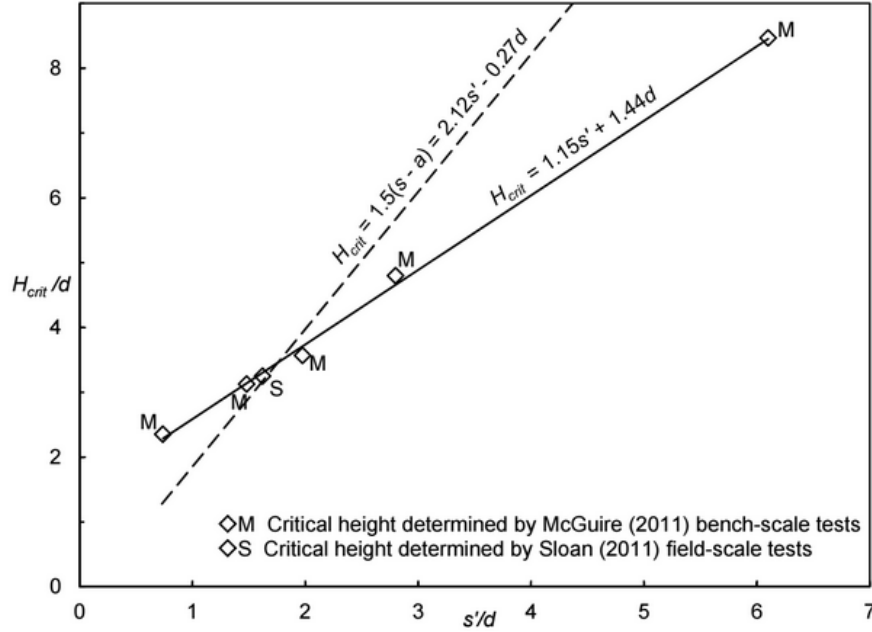
Figure 2.11: Tests results from Mcguire (2011) and Sloan (2011)

A trend line is drawn through the data points. The other line is referred to as the conventional approach (Filz et al., 2012). As in other literature ((CUR226, 2010), (Jenck, 2004), (Eekelen et al., 2013) the parameters s and a are used instead of s' and d. This requires re-arranging and results in:

$$H_{crit} = 1.15s' + 1.44d = 0.81s + 0.51a \qquad (2.13)$$

Filz et al. (2012) compared results published in literature with equation 2.13. The results are given in chapter B.2.

A summary of the recommendations is given in table 2.3.

Table 2.3: Summary of critical height design recommendations

Standard/recommendation	Critical height	Applicability
British Standard 8006	$H \geq 0.7(s_x - a)$	+/-
EBGEO	$H \geq 0.8(s_d - d)$	+/-
CUR226	$H \geq 0.66(s_d - d)$	-
Concentric Arches	$H \geq 0.5s_x$	-
Filz et al. (2012)	$H \geq 1.15s' + 1.44d$	+/-
Jenck et al. (2007)	$\frac{H}{s-a} = 1.3 \leq \frac{H}{s-a} = 2.0$	-

The last column of table 2.3 shows the applicability of the standards and theories in case no geosynthetic reinforcement is used. For instance, CUR226 and Concentric Arches are not applicable because geosynthetic reinforcement is an important parameter in that standard or model.

Note that none of the standards in table 2.3 take soil parameters into account. Soil parameters do have great influence on the CSE however, which will be elaborated in section B.6.

2.6 Synthesis of parametric study

The influence on the parameters described above are summarized in table 2.4. A more extensive elaboration can be found in section B.6.

Table 2.4: Influence of different parameters, partly derived from Jenck et al. (2007)

Soil	Parameter	Description	Load transfer	Surface settlement
Platform	φ	Friction angle	++	++
	c	Cohesion	++	++
	ψ	Dilatancy angle	-	+
	E	Young's Modulus	+	+
Soft soil	ND	Compressibility	++	++

Note that Jenck et al. (2007) does not define the compressibility in terms of engineering parameters. It is assumed by the author that stiffness is meant here.

From table 2.4 can be derived that the strength parameters (φ and c) have a great influence on both the load transfer and surface settlement. The compressibility of the soft soil has a great influence on both the load transfer and settlement. The author's opinion is that Jenck et al. (2007) does not fully fathom the influence due to the limits of the investigation (only two compressibility values were used next to the reference case).

3

Sabkha

In the previous chapter it was elaborated that the soft soil characteristics surrounding the sand columns have an influence on the efficiency and settlement reduction of a CSE. Also, consolidation has an influence on the final efficiency. It is therefor relevant to discuss the soft soil present at the ZOR project. This soil is known in the Middle-East as sabkha, and described in this chapter.

3.1 General

A remarkable soil that is predominantly found in the Middle-East is sabkha. Sabkha is not found in the Netherlands, Dutch companies consequently have limited experience with this soil. This chapter elaborates the geology of sabkha. It is concluded from literature that sabkha has some specific characteristics, mainly fueled by the presence of fresh or relatively weakly salted water. Some characteristics are described in section 3.3. The chapter concludes with a summary of soil investigations found in literature, described in section 3.4. A more elaborate description of the soil investigations that have been performed in the area can be found in the appendix in chapter C.

3.2 Geology

Supratidal flats along desert coastlines, notably along the western and southern coasts of the Arabian gulf but also elsewhere, have led to the formation of soils with substantial deposits of evaporite materials. Considered as a simple model, the high rate of evaporation from the sabkha surface causes concentration of the saline groundwater and deposition of evaporite minerals above and below the shallow groundwater, forming cemented layers and zones, particularly near the surface. (Walker, 2012)

Along the Western and South-Western coast of the Arabian Gulf, sabkha soils are generally viewed as unconsolidated, heterogeneous, layered or unlayered sediments, that are bathed in highly concentrated brines (Al-Amoudi and Abduljauwad, 1991). The distinct feature of sabkha deposits is their poor mechanical properties. Being a highly compressible material with low bearing resistance, often serious geotechnical problems are met where sabkha deposits are encountered (Akili and Torrance, 1981),(Khan and Hasnain, 1981), (Juillie and Sherwood, 1983), (Khan and Layas, 1984).

Sabkha is deposited by fluctuating sea levels, making the deposit highly variable in vertical extent. Also, as the lateral variation appears to be dependent on the proximity to the shoreline, the lateral extent is very variable. (Akili and Ahmed, 1983).

The salt minerals are a major source of cementation that appears to hold sand and silt particles together to form cemented layers and cemented zones, particularly in the portion of the sabkha near the surface (Akili and Ahmed, 1983). A drawing of the grains with cementation is given in figure 3.1.

3.3 Interaction with surface- and groundwater

Water is extracted from sabkha by evaporation. The high rate of evaporation from the sabkha surface causes concentration of the interstitial pore fluid and eventual formation of new evaporate minerals
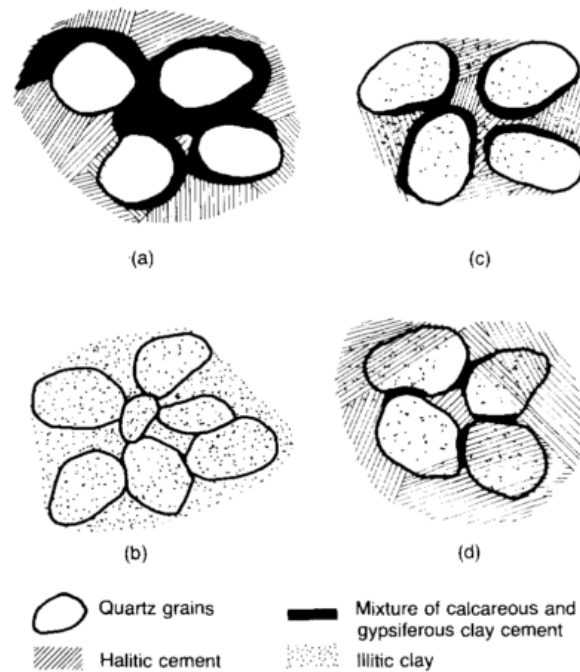
Figure 3.1: Grains with cementation (figure 14 in Abduljauwad and Al-Amoudi (1995))

above and below groundwater. Different evaporative salts will be precipitated at different humidities (Kinsman, 1969). At a relative humidity of 93-76% sulphate minerals will precipitate, at 76-67% halite will precipitate. For the arid coastal evaporite areas of the Arabian Gulf with mean relative humidities ranging from 50-80%, mainly sulphate minerals and, to a lesser degree, halite are suitable for precipitation.

On the top layers of the soil the temperature fluctuation is the highest. Gypsum is present at temperatures less than 42°. At higher temperatures the relatively unstable gypsum dehydrates to form anhydrite. This reaction is accompanied by a volume decrease of 39% if the water evaporates. The hydration of anhydrite results in a 63% volume increase. (Ismael, 1993)

Water can be supplied to the sabkha in two forms: by stormwater (rain event) and by the upward flow of groundwater to replace water lost by capillary evaporation (Hso and Schneider, 1973), these are described below.

3.3.1 Precipitation

The supply of water could cause the destruction of the natural cementation that has been formed due to the deposition and evaporation cycles by dissolution or leaching of salts (Abduljauwad and Al-Amoudi, 1995). The outer surfaces are generally composed of hygroscopic salts which, when dampened, can render the normally stable surface crust impassable (Ellis, 1973),(Johnson and Kamal, 1978). This phenomenon is called *collapse upon wetting.*

3.3.2 Groundwater

The groundwater found in sabkha soils, often referred to as brine, is typically high in chloride and sodium concentrations (Abduljauwad and Al-Amoudi, 1995). The chloride and sodium concentrations are approximately six times higher than in typical sea water; Taylor and Illing (1969) have reported that an eight-fold concentration of the interstitial sabkha brine is not unusual. Additionally, it was found that the ratios of the various ions, except for Ca^{++} and SO_4^{--}, are almost the same as to those normally found in sea water. The reduction in the calcium and sulphate ions is attributed mainly to the precipitation of gypsum from the concentrated brine (Abduljauwad and Al-Amoudi, 1995).

The groundwater flow is directed towards the Arabian Gulf (discharge area). Also, there is a topographic depression east of the ZOR project, which is also a hydraulic depression. The groundwater levels are observed to be under mean sea water level. The cause of the low groundwater level is the evaporation at the surface (Fugro, 2013). The average groundwater conditions are drawn in figure 3.2. It can be seen that there is shallow groundwater near areas seven and eight. The depth to groundwater is approximately one to two meters in the east. The depth increases to five meters in the West.
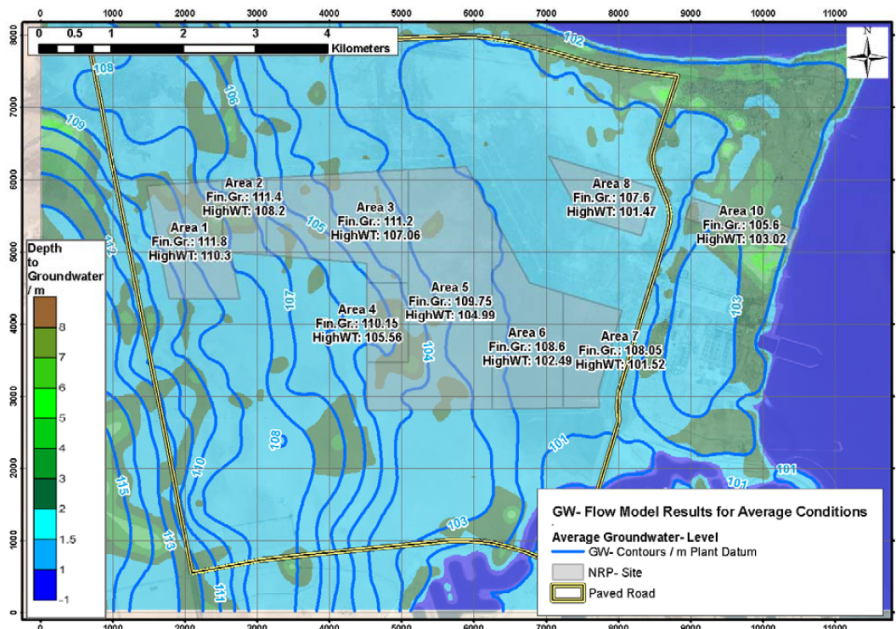
Figure 3.2: Average groundwater flow conditions and depth to groundwater (Fugro, 2013)

3.4 Soil investigations

This section describes the conclusions from the relevant soil investigations that have been performed in the Middle-East. A more elaborate description can be found in section C.

The engineering behaviour of sabkha soils is strongly influenced by the groundwater conditions, the soil and groundwater chemistry, and the effects of dissolution or leaching of salts (Walker, 2012). The effects of water on permeability, California Bearing Ratio, bearing capacity and settlements have been quantified in the described soil (lab) investigation. Water leaches the bonds between particles in sabkha, resulting in reduced strength.

The findings from Abduljauwad and Al-Amoudi (1995) are very relevant for the NRP. When the hydraulic fill is placed, seawater will be used as a transporting agent. As can be seen in Taylor and Illing (1969), the groundwater (brine) in sabkha soils is up to eight times higher in salt concentrations compared to seawater. The seawater having lower concentrations of dissolved salts, will result in osmosis between the sabkha and the hydraulic fill. Osmosis will lead to a lowering of salt concentrations of the brine in the sabkha soil. Lowering of the concentration leads to dissolution, or leaching, of the cementation between the particles in sabkha soil, as described by Abduljauwad and Al-Amoudi (1995).

The sand columns that are formed in the sabkha soil can be considered drains. The columns may function as a water supply to the sabkha soil, driven by osmosis. This system is also seen in the interaction between precipitation and groundwater, as described in section 3.3. The intrusion of relatively fresh water will be coupled with a reduction in strength. Reduction in strength will lead to reduced support for the sand columns.

As was concluded from the results of Abduljauwad and Al-Amoudi (1995) in paragraph C.1, permeability decreases with an increase of pressure. The pressure on the sabkha drastically increases during the formation of the piles (because of the DR), there will however be an excess pore pressure at this time. The pressure from the five meter sand platform should result in a lower rate of osmosis and in turn a lower rate of strength reduction after consolidation of the sabkha.

Ismael (1993) reported that the void ratio (and in this case the permeability) are actually lower for leached samples at high confining pressures compared to natural samples. Furthermore, the influence of soaking the topsoil in a field test turned out to be only 1 - 1.5 m depth. As there will be a sand platform of approximately 3 - 6 m on top of the soft soil, plus a distributed load, it is assumed that the sabkha is under relatively high confining pressure.

In the long term it is not known whether the low-concentration water from the columns will penetrate the sabkha (either under or next to the column). With a change in phreatic water level the pore pressures may increase and penetration occurs. Contrary, because of the higher weight of the brine, there may be an equilibrium somewhere along the height of the column. Before any calculations concerning bearing capacity (loss) or settlements can be done, more investigations should take place. Especially investigations after the long-term characteristics of sabkha soil. However, based on the results presented by Ismael (1993), a likely scenario is the following:

1. Hydraulic fill is placed, top soft soil reduces in strength and increases in permeability;

2. The sand columns are made and along the edges of the column the soft soil reduces in strength and increases in permeability;

3. As the pressure increases the voids start to collapse and the void ratio decreases;

4. Because of the void collapse the soil consolidates and effective stress increases;

5. The soft soil has increased in strength and the permeability is low(er).

4

Dynamic Replacement

It was described in chapter 2 of the literature study part that the stiffness of the sand columns have a great influence on the efficiency and settlement reduction in a CSE. Furthermore, this technique is not often employed thus a brief elaboration may be in order.

4.1 General

Dynamic replacement (DR) is a method developed by Ménard. DR is based on the frequently employed dynamic compaction (DC) method. DC improves soil by dropping a weight of up to tens of tons on the surface. The weight is often referred to as a tamper or pounder.

The impact from the tamper compacts the soil, given that the soil is suitable for compaction. Clay for instance, is not suitable to be compacted with DC. Granular soils, e.g. sand, can very well be compacted by DC to certain depths. The depth to which the sand is compacted is the depth of influence. This depth can be up to several meters. The depth of influence is dependent on soil properties, falling height, tamper weight and height of the water table in the area.

DR is a modified method based on DC. Compared to DC, DR uses heavier tampers, higher drop heights and thus a higher impact energy. DR requires a sand platform (also known as 'blanket') to be in place before the operation can start.

A selection of terms referring to DR works, that will often be used in this thesis, are clarified below.
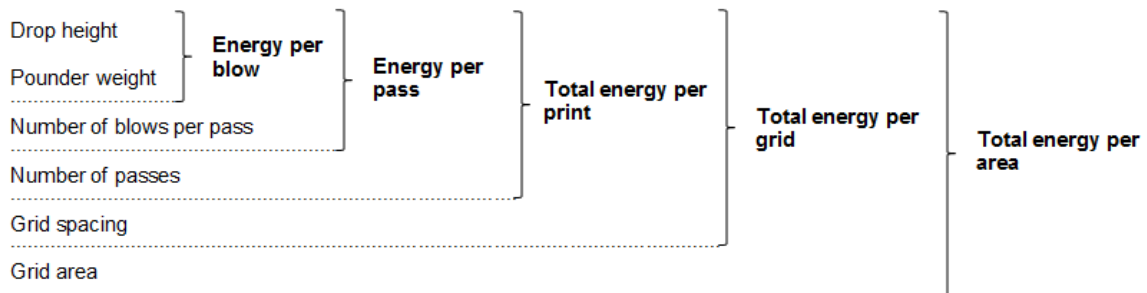
DCDR works are executed in a number of phases and passes. Both terms are elaborated using figure 4.1 and 4.2.
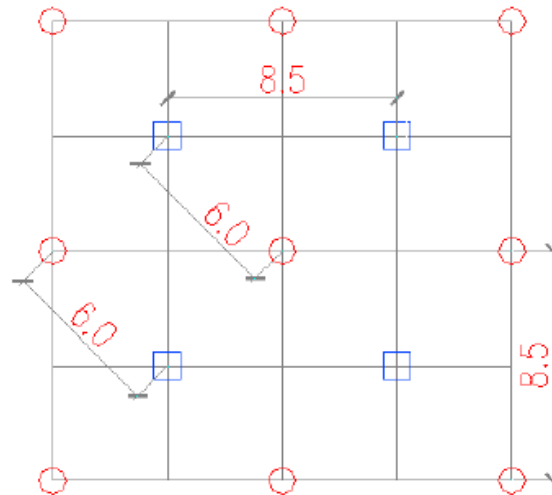
Figure 4.1: DR passes
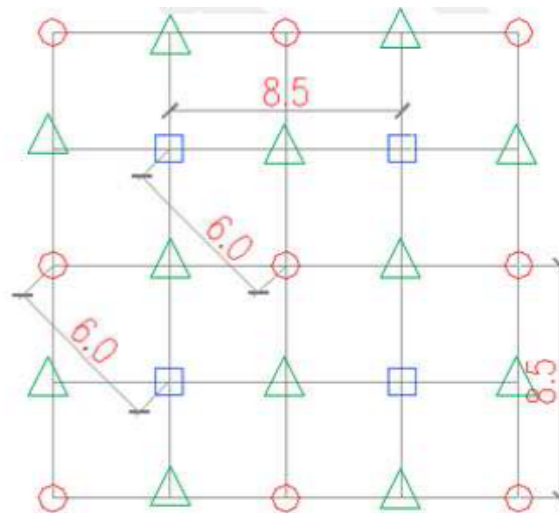
Figure 4.2: DR phases

The circles in figure 4.1 represent the first phase. In the first phase DR is executed in every other row. In the second phase DR is executed every row in between two rows which have been finished during phase one.

When the entire grid is finished pass one is complete. The complete grid is subject to another DR pass after this. It may well take three passes to finish an area.

After the DR passes the DCDR pass starts. The DCDR points are located on top of the DR columns, as well as in between the existing DR columns (illustrated by the green triangles in figure 4.2).

4.2   Working sequence

The working sequence for a DR operation is summarized below:

1. A sand platform is placed on top of the existing surface;

2. The crane with the tamper is brought in;

3. The crane drops the tamper at one certain location multiple times (e.g. 20 times);

4. Tampering stops when the penetration of the tamper is less than a pre-defined penetration;

TUDelft

5. The crane moves on to a second location to allow the formed crater to be backfilled with platform material;

6. The crane moves back to the previous location for a second pass;

7. When sufficient soft soil has been replaced, the operation is finished.

After the last pass CPTs are performed to check the DR operation. Based on the results of the CPT it may be deemed necessary to perform additional compaction. This is executed in an ironing-pass. An ironing-pass consists of further compacting the existing columns. The result of an ironing-pass is an increased compaction; it usually does not influence column depth.

It can be seen in figure that the high energy results in penetration of the sand layer into the soft soil. Contrary to DC, where craters form due to compaction of the sand, DR forms craters predominantly because of plastic deformations in the soft soil. The soft soil is replaced by a dense sand column, hence the name of this method.

After the last step in the enumeration above an extra step can be added, namely using a heavier tamper to mix the soft soil and the sand columns. If that step is included, the method is known as Dynamic Replacement and Mixing (DRM). DRM method is not used in the ZOR project, nor elaborated in this thesis.

4.3   Equipment

The DR method essentially requires the following equipment:

Crawler crane	The cranes that are used often have a relatively large counterweight to increase production (faster lift of the tamper). The cranes generally have a single lifting cable and allow free-fall of the tamper.
Pounder	A tamper is usually made from high quality steel plates mounted together.
Dumper & dozer	A dumper and dozer are necessary to respectively supply and distribute sand.

4.4   Column Compaction Depth

Granular soils are compacted by the impact energy from the tamper. The particles in the soil will re-arrange resulting in a lower void ratio. In soils with a sufficiently high void ratio and a high water table, the pore pressure will increase due to re-arrangement of the grain skeleton. After some passes with the tamper liquefaction can be induced (Moseley and Kirsch, 2004). Dissipation of the excess pore pressures will result in a further increase in compaction.

It is known from DC that during tamping the deeper layers compact first (Moseley and Kirsch, 2004). The compaction then progresses upwards to shallower layers. Generally, a homogeneous sand profile will thus show an overall increasing compaction with depth, down to the influence depth. The top sand layers can be compacted by using lower impact energy or other means e.g. Rapid Impact Compaction (RIC) or High Energy Impact Compaction (HEIC).

4.5   Soft Soil Response

Soft soil in which the DR is used generally has a lower permeability compared to the granular soil that is used to replace the soft soil. This means that consolidation will take a longer period compared to the consolidation of the dynamically replaced columns.

The impact of the tamper increases the pore pressure in the clay rapidly. The time intervals between the drops, which are in the order of a few minutes, are not sufficient for consolidation. The high impact energy does induce shear and hydraulic failure (Moseley and Kirsch, 2004), which enhances dissipation of excess pore pressure. It is thus believed that consolidation does occur more rapidly compared to normal static loading. Another factor enhancing consolidation is the reduce in drainage path, namely by the creation of a sand drain (i.e. the column).

Between the passes the soft soil can consolidate, increasing its strength. Faster DR operation results in a lower degree of consolidation between passes. The contractor should always consider the following two options:

1. **Fast operation:** no or very little consolidation occurs between passes. The soft soil behaves stiff due to the excess pore pressures. The sand columns penetrate relatively easily Excessive heave may result from displacing the stiff soil volume.

2. **Slow operation**: consolidation does occur between passes and the soft soil increases in strength. Penetration of sand columns will be more difficult due to the strength increase.

4.6 DR Projects

In this section a selection of projects where the DR method was employed will be discussed.

4.6.1 NCIG Coal Export Terminal 3

A paper written by Chua et al. (2008) reports on the DR works and the CPT results for the foundation of a Newcastle Coal Infrastructure Group (NCIG) coal stockyard on Kooragang Island, New South Wales, Australia.

The stockyard covers an area of approximately 1200 by 300 m. The subsoil consists of 2 m of very loose to medium dense sand, overlying 2-3 m of soft clay. Underneath the soft clay medium dense to dense sand is present, underlain by bedrock. A typical CPT is shown in figure 4.3.
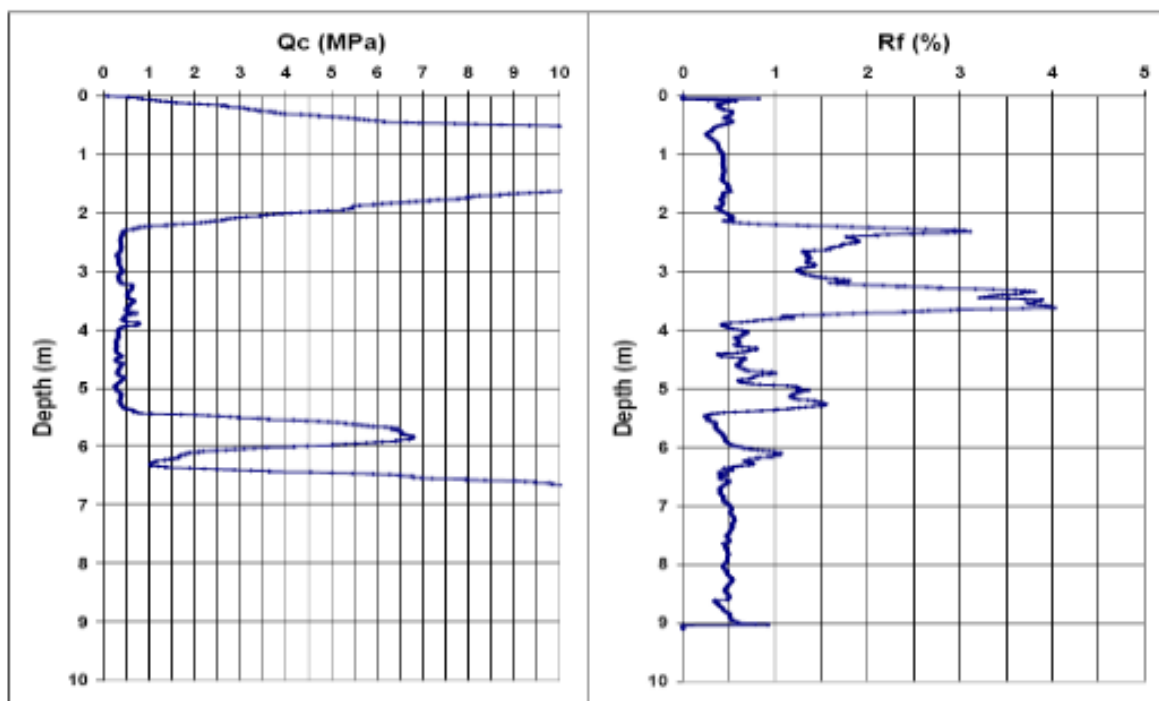
Figure 4.3: Typical CPT (Chua et al., 2008)

Chua et al. (2008) shows a selection of pre- and post-CPTs in and around the DR columns. The CPT diagrams can be found in figure 4.4
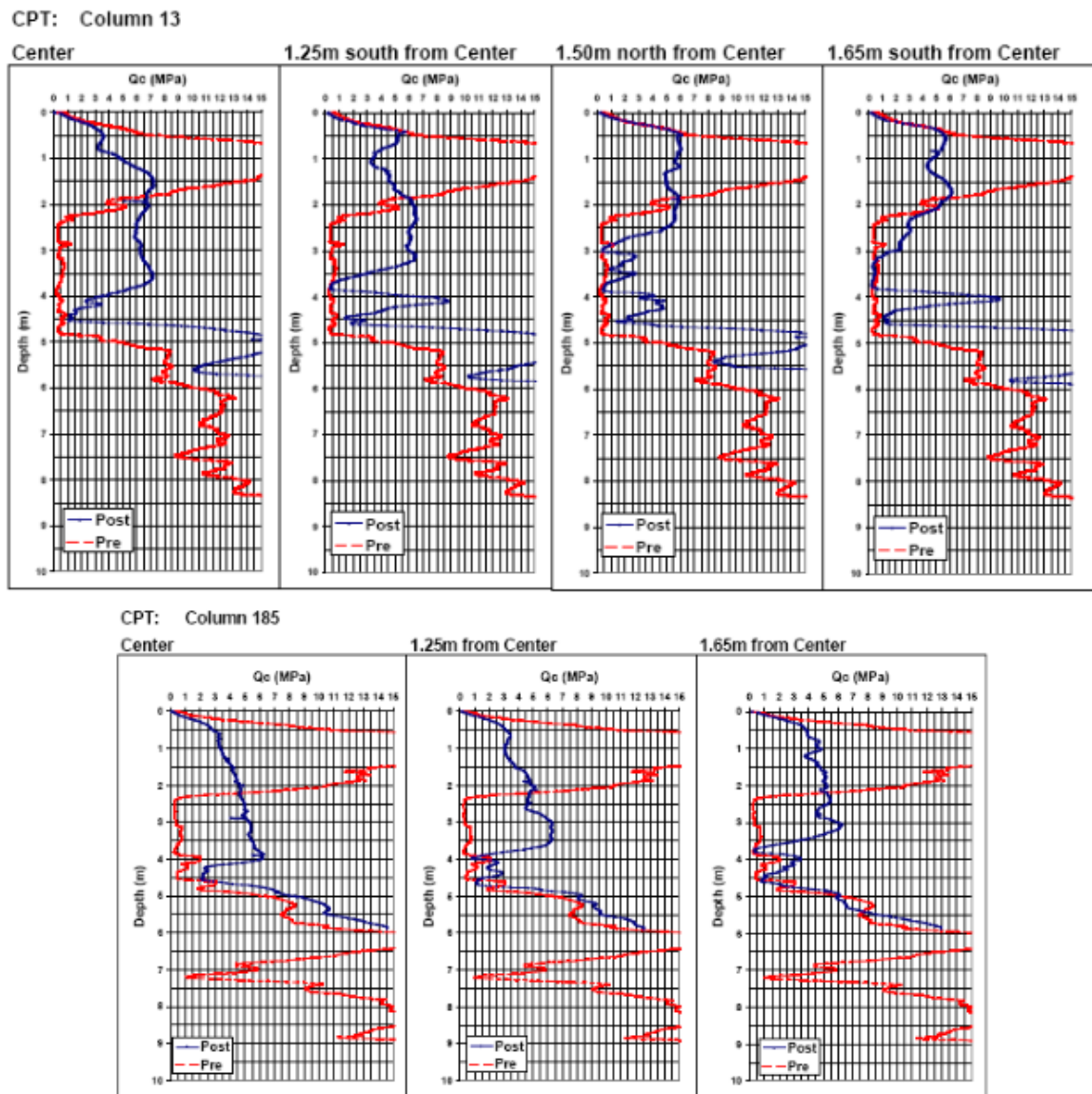
Figure 4.4: CPT diagrams in and around two DR columns (Chua et al., 2008)

While the (very) low cone resistances between 2.3-4.5 m are definitely improved, it can be seen that the peak cone resistance two meters from surface level have disappeared.

After DR operations were finished PLTs have been performed. The diameter of the plate that was used is 1.2 m. The author of the paper recognizes the limited influence depth of a PLT with a diameter of only 1.2 m. It cannot be concluded with certainty from the text, however it is assumed that the PLT took place on top of a column. The results from the PLT are given in figure 4.5.
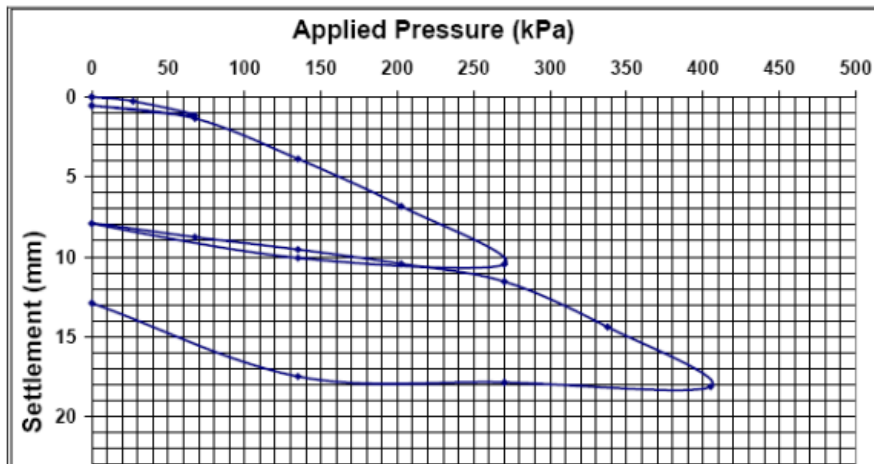
Figure 4.5: Load-settlement diagram (Chua et al., 2008)

4.6.2 Al Jazira Steel Pipe Factory

A paper written by Hamidi et al. (2011) reports on the DR works and results for the foundation of a steel pipe factory in Abu Dhabi, United Arab Emirates. This section summarizes the findings and conclusions.

The foundation loads for the steel factory ranged from 40 kPa to 200 kPa. Borings showed 11-12 m of soil on top of bedrock. CPT showed a soft layer of clayey material with minimum cone resistance of 0 MPa at a depth of 1.5-2.0 m. PMT Limit Pressure was in the range of 2 MPa in the soft soil, the Menard modulus was as low as 15 kPa.

For this project the column holes were excavated and backfilled with sand. After backfilling the column would be compacted by DC. Hamidi et al. (2011) do not elaborate the method of excavation nor do they discuss whether the excavated hole remained open without stabilizing.

After the columns were finished another set of PMTs were performed. The results of these PMT can be found in figure 4.6. It is noted that in Hamidi et al. (2011) the author mentions that the improvement in the soft soil is less than the improvement of the prints. It is thus assumed by the author of this thesis that Hamidi swapped two lines (the dotted and the dashed) in the graph's legend.
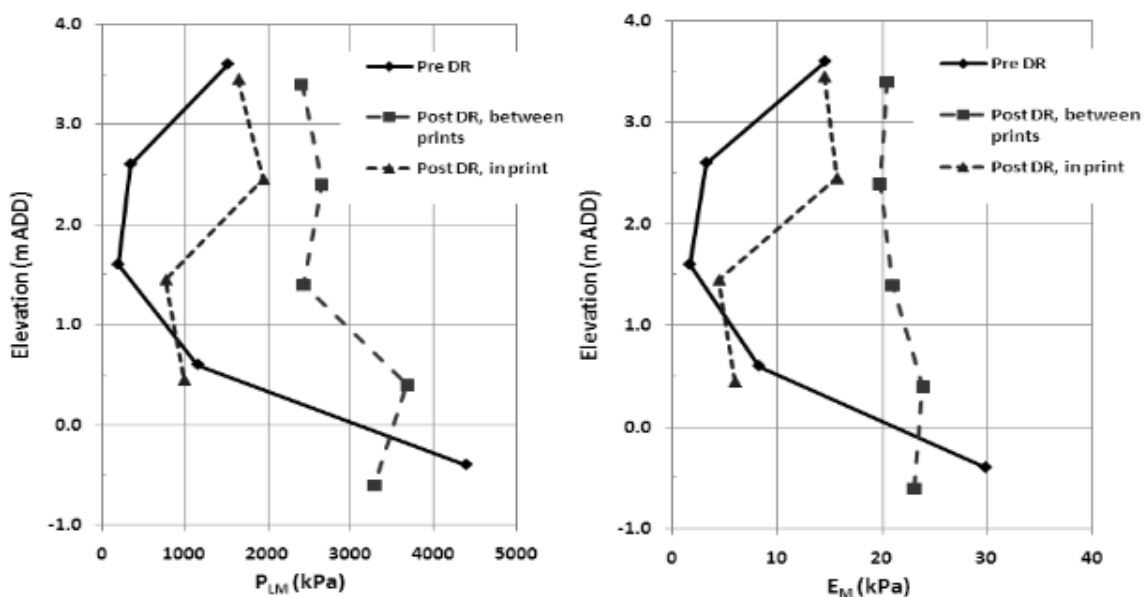
Figure 4.6: PMTs before and after, inside and between DR columns (Hamidi et al., 2011)

In figure 4.6 it can be seen that a soft soil layer is present at approximately 2.0 m below surface. It is evident that the both PMT limit pressure and Menard modulus have increased considerably. It is however also very interesting to see that the soft soil has increased in strength by 700% at some depths. This means that the soft soil in between the columns, which was not expected to improve, actually did improve.

4.7 Trial Area

Before the start of the DCDR works by Menard, a trial area was set up. During the trial three different column spacings were used, see table 4.1.

Table 4.1: Column spacing for the trial area

Area	Grid spacing (m)	Angular distance between columns (m)
TA1	6.0 x 6.0	$6.0\sqrt{2} \approx 8.5$
TA2	6.5 x 6.5	$6.5\sqrt{2} \approx 9.2$
TA3	7.0 x 7.0	$7.0\sqrt{2} \approx 9.9$

The trial was assumed to be successful if the result met the acceptance criteria, which is $q_{c,average} > 8$ MPa.

During the trial the penetration and heave were recorded. Figure 4.7 shows the heave and penetration during the DR operation. It can be seen that the penetration reaches a peak value at the first blow. The penetration then decreases from 23 cm to 10 cm in the following three blows. After the fifth blow the penetration stays approximately constant at 3 cm. The bottom graph in figure 4.7 shows the volume change in the DR crater. The volume steadily increases with the number of blows. The green line shows that the heave increases with approximately the same increment. It can thus be concluded that most of the volume change of the crater is probably caused by the formation of a heave ring.

Van Oord
Marine ingenuity

PENETRATION TEST

PROJECT:	KNPC-NRP		Project Ref.	FK14014
CLIENT:	VAN OORD		Date	28-Aug-14
LOCATION	TRIAL AREA 1 (6X6)		Site Manager	

Soil Improvement Method		DC/DR			
Test No.	HPT-TA1-B11.B				
Grid:	6m X 6m		Phase	2	Pass	2	Print Ref	TA1-PH2-012
Pounder Dimensions		1.60 m	Pounder Weight		16 Ton	Drop Height	20 m

Blows number	Upper Diameter of print (m)	Pounder References Levels (m)					Penetration (m)	Cumulated Penetration (m)	Vol Crater (m3)
		1	2	3	4	Average			
0	0	0.332	0.298	0.288	0.312	0.308	0.00	0.00	0.00
1	1.8	0.915	0.877	0.868	0.893	0.888	0.58	0.58	1.32
2	2	1.090	1.142	1.160	1.098	1.123	0.23	0.82	2.08
3	2.2	1.269	1.248	1.285	1.301	1.276	0.15	0.97	2.77
4	2.5	1.401	1.330	1.382	1.443	1.389	0.11	1.08	3.63
5	2.7	1.479	1.422	1.509	1.558	1.492	0.10	1.18	4.39
6	2.9	1.628	1.448	1.435	1.603	1.529	0.04	1.22	4.99
7	3.1	1.618	1.524	1.552	1.637	1.583	0.05	1.28	5.72
8	3.3	1.649	1.501	1.580	1.717	1.612	0.03	1.30	6.40
9	3.4	1.572	1.557	1.743	1.751	1.656	0.04	1.35	6.90
10	3.4	1.632	1.489	1.742	1.873	1.684	0.03	1.38	7.05
12	3.7	1.691	1.732	1.695	1.748	1.717	0.02	1.41	8.18
14	3.9	1.701	1.812	1.753	1.885	1.788	0.04	1.48	9.30
16	4	1.831	1.775	1.874	1.824	1.826	0.02	1.52	9.92
18	4	1.883	1.842	1.871	1.840	1.859	0.02	1.55	10.14
20	4.1	1.943	1.928	1.931	1.923	1.931	0.04	1.62	11.02

Figure 4.7: Heave and penetration records

During the trial three CPTs were performed per location. The locations of the CPTs are sketched in a top view in figure 4.8.
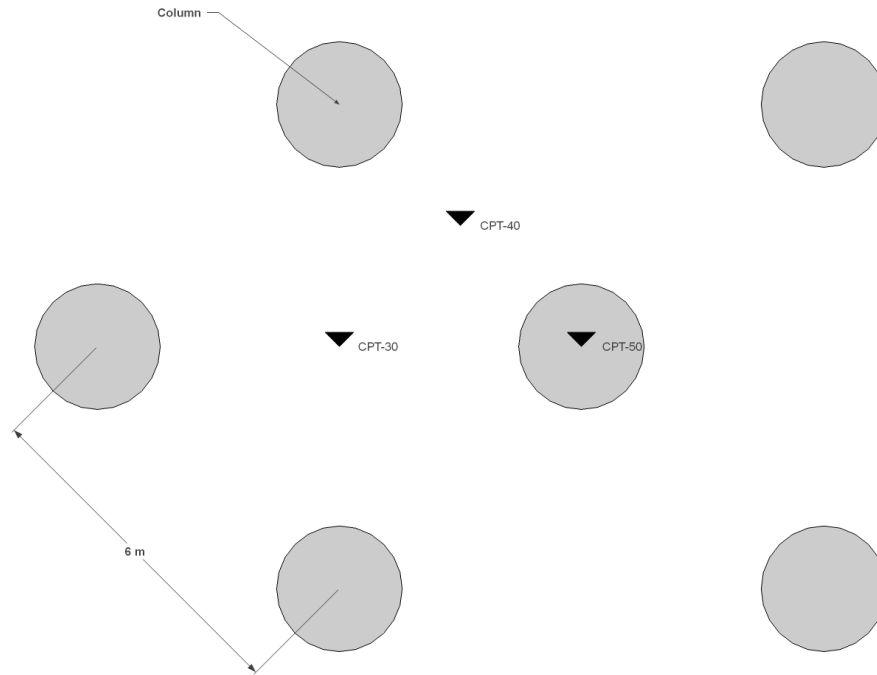
Figure 4.8: CPT locations with respect to the DR columns

The results of the CPTs in the three trial areas can be found in figure 4.9.
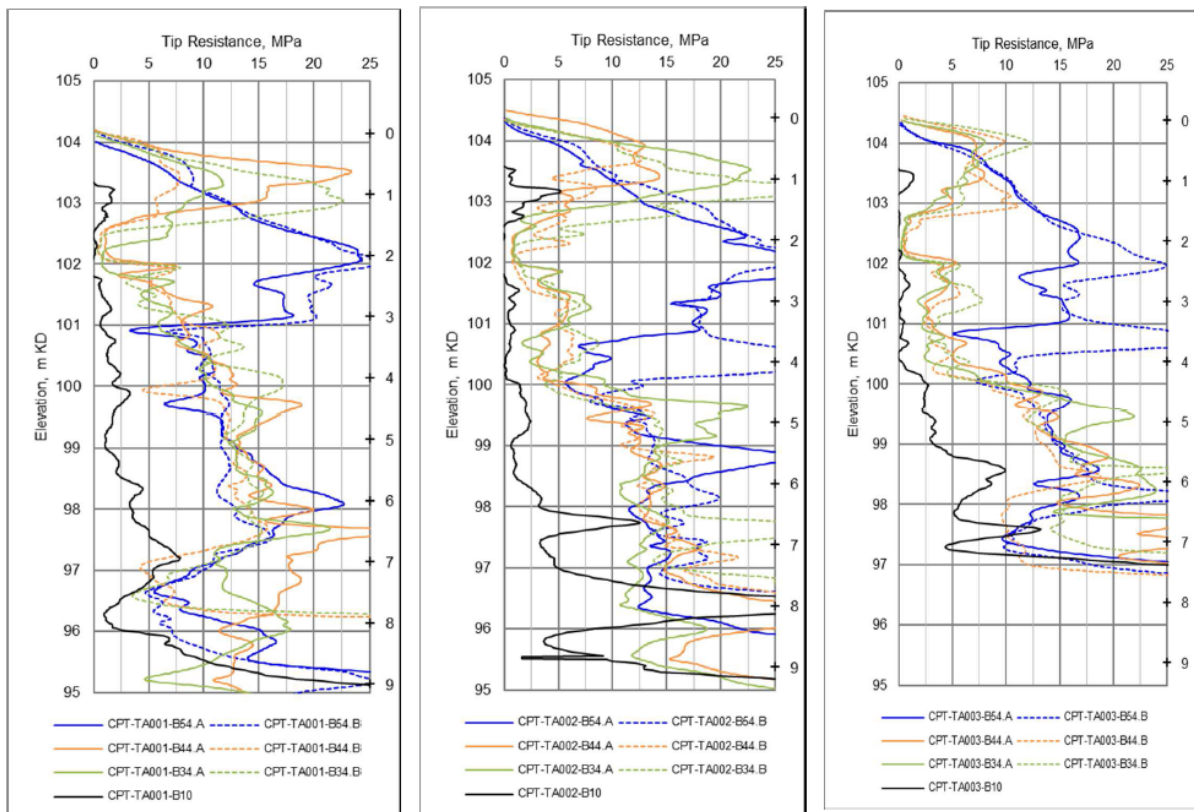
Figure 4.9: Pre and post DR improvement CPTs

Part II

Field Work and Soil Testing

5

Field Tests

It was elaborated in previous chapters, e.g. chapter 2, that there is a selection of parameters that are important for the efficiency of a CSE, these are described below.

- Subsoil parameters

  1. Soil Stiffness
     The stiffness of the soil, or rather the difference between the soft soil and the columns, determine for a great part the efficiency of the system.

  2. Soil Strength
     The soil strength of the platform, in terms of the friction angle φ, determines the load distribution and transfer to the columns.

- Subsoil composition

  1. Soil Layers
     The composition of the soil in terms of layering is important. For instance, the thickness of the sand platform has a great influence on the efficiency.

Below four tests that will be performed on-site are summarized, including the parameters that can be derived from those tests.

5.1 Soil Sampling

Although literature offers extensive information about sabkha (see chapter C), the heterogeneous nature of the soil requires additional soil investigation. To this extent, soil borings were be performed. Soil samples were taken and tested.

Based on previous investigations and CPT results, the following soil layers were to be expected (from surface to depth):

1. **Sand** the first 1-2 m will consist of reclaimed sand;

2. **Silty/sandy clay/silt** below the sand, at the former surface level, a mixture of clay and silt can be expected. This layer is generally 1 m thick. Although this soil layer has the characteristics of sabkha, it is generally stiffer and has a higher cone resistance. Compared to sabkha, this layer has a higher course grain content;

3. **Sabkha** below the former surface level a layer of sabkha is found, varying in thickness from 1-4 m;

4. **Clay/sand** Stiff clay or dense sand is generally found under the sabkha layer. In some cases loose sand is present under the sabkha.

The layers of special interest are the sabkha and silt layer.

5.1.1 Test Description

The soil borings were be performed using a drill rig. This rig was capable of executing 4-inch soil borings.

The borings commenced by drilling through the sand layer. Water is present in this layer at relatively shallow depths, so borehole stabilizing is necessary. The preferred drilling system is the auger (this was the only system available). When sabkha was encountered the borehole was cleaned from cuttings. After cleaning the borehole the the tube samples were taken.

The samples were extruded in the GIICO[1] lab in Kuwait City. After extrusion the samples were made ready for transport and sent to Rotterdam.

The soil samples were tested in the TU Delft soil mechanics lab. The main tests that have been performed are:

1. **Consolidation Tests**, an Oedometer setup was used to determine consolidation and stiffness parameters.

2. **Shear box**, a DSS was used to determine the shear strength, in the drained situation.

3. **Soil classification tests**, the samples were sieved to determine the sieve curve. A hydrometer was used to determine the fines content. Also Atterberg's limits were determined.

5.1.2 Parameter Derivation

From the abovementioned tests the following parameters can be derived:

E_{oed}, E_m	=	Oedometer modulus
φ	=	(Effective) Friction angle
c	=	(Effective) Cohesion
s_u	=	Undrained shear strength
ρ	=	Density

Based on these parameters other parameters can be derived, i.e. the compression and swelling index (C_c and C_s, respectively), which can be used in a Plaxis model.

5.1.3 Reliability

The reliability of soil samples is for a great part determined by the boring method and the retrieval of the samples. A method statement with executional aspects is included in section E.3.

After the samples have been taken the tubes were sent to the Netherlands. While the samples will be sealed and packaged according to ASTMD4220, it is inevitable that the tubes were subject to disturbance during transport. Among these disturbances the major influences come from vibrations and heat/cold cycles. The respective consequences are summarized below:

- Vibrations
  - Denser sample
  - Relaxation of the sample
  - Lower water content
- Temperature
  - Lower water content

5.2 Cone Penetration Test

In the ZOR project many parameters are derived from CPT results, which is extensively described in section H.2.

---

[1]see companies, on page 121

5.2.1 Test Description

For a detailed test description of a CPT, reference is made to Robertson and Cabal (2015).

5.2.2 Parameter Derivation

CPT results can be used to distinguish soil layers. Furthermore, using correlations, the following parameters were estimated:

E_m	=	Constrained Young's modulus
φ	=	Friction angle
s_u	=	Undrained shear strength
MDD	=	Maximum Dry Density

The correlations are not limited to the parameters mentioned above, however these are the only correlations used in this thesis.

5.2.3 Reliability

The CPT equipment (Geomil) that is used on site is produced by Geomil and certified, and will not be discussed here.

The CPT is essentially a strength test. This would imply that strength parameters generally have a strong correlation with CPT results. Stiffness parameters have a weaker correlation.

5.3 Zone Load Test

In section 2.5 a selection of theories was presented, calculating the height of a platform in a CSE. That height is usually calculated from a known ratio between the height of the platform and the column spacing.

The center to center distance in the ZOR project is 6 meters with a column diameter of 2.2 m in the coarse grid. The denser grid has a center to center distance of 5 m with a column diameter of 1 m. The height of the platform is approximately 5 m (at final level). The ratio between the height and spacing is then given by equation 5.1.

$$\frac{H}{s-a} = \frac{5}{6-2.2} = 1.3 \tag{5.1}$$

Where H is the platform height, s is the center-to-center distance between the piles and a is the pile diameter. The parameters are elaborated in section 2.5. The ratio is higher compared to the theories. Taking into account stress distribution, the stress imposed by the ZLT will be low at the depth of the former surface level. It is thus decided to perform additional ZLTs on lower platform heights. It is furthermore noted that there is a significant spread of the stress induced by the ZLT. At the former surface level the stress will be relatively low, because of the increase in area due to this spread.

5.3.1 Test Description

For an elaborate description of the working sequence of a ZLT, reference is made to chapter D.2.

A total of three tests have been performed. These tests were be executed on a platform which has a lower surface level than the design level (i.e. less than the 5 meters mentioned in equation 5.1). It was decided to execute the test on a lower platform to be sure to measure the CSE system. If a ZLT performed on a 5 meter sand platform would be used, the derived settlement would be mainly settlement of the sand. The first ZLT will be located on top of a column in an area where the column spacing is 6 meter c.t.c., a drawing of the location is given in figure 5.1. Due to unavailability of the ZLT set-up, it was only possible to perform a single ZLT in this location. Two of the ZLTs, number 2 and 3, will be located in an area where the column spacing is 5 m c.t.c., a drawing of the location is given in figure 5.2. Based on the previous ZLT (number 1) plastic strains could be expected. It was thus decided not to execute the ZLT in near proximity, to minimize any influence the first test may have on the second test. Taking account

of a smooth set-up and breakdown of the test (cranes and trucks are needed, which require space to move around), the two locations were set out 13 m from each other. It is concluded in chapter 8 that this was in fact out of the immediate influence zone of the ZLT.
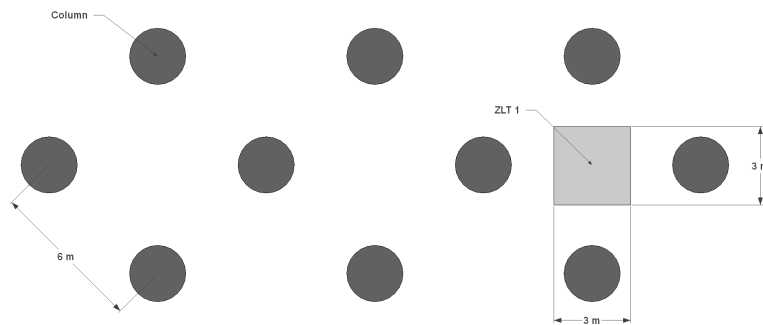
Figure 5.1: ZLT location 1 with respect to the DR columns
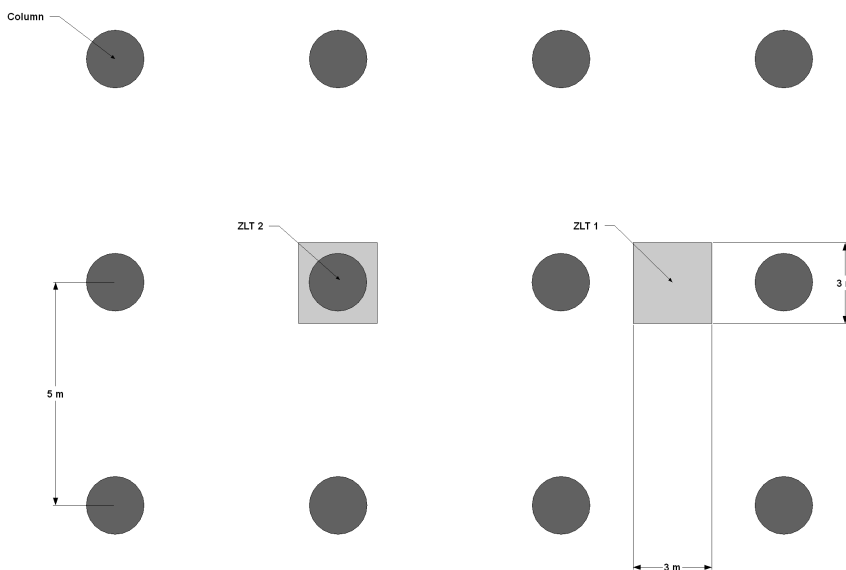
Figure 5.2: ZLT locations 2 and 3 with respect to the DR columns

5.3.2   Parameter Derivation

In the ZLT the settlement of a concrete block is measured at certain load intervals. The settlement is measured during load increase and load decrease. From these two sets of measurements both the elastic and plastic response can be derived.

The results of the three tests can be compared. From the comparison conclusions can be drawn with respect to the homogeneity of the composite soil.

Another valuable use of the results is the calibration (or 'benchmarking') of the Plaxis model. After the model is finished and a ZLT is simulated, the results can be compared to actual ZLT results.

TUDelft
Delft
University of
Technology

5.3.3 Reliability

Similar to every soil test that is performed in the field, the ZLT results are dependent on the exact subsoil composition in that particular area. In other words, a ZLT performed only a few meters from a previous test may deliver different results.

5.4 Considerations

The writer would like to remind the reader about the order of sand placement in the ZOR project. The order is elaborated below, up to the placement of the second sand layer.

1. At this time the surface level is at its original level and the soil is in its virgin state.

2. The sand that has been dredged it pumped ashore and distributed over certain areas. At this time the soil starts to adapt to the new load imposed by the sand.

3. DR works start, the sabkha and silt are replaced by sand and subsequently the pore pressures in the soft soil increase.

4. The DR results are checked using CPT and some time passes before the next layer of sand is brought in. If necessary DC works continue to increase the compaction of sand.

5. Another load of sand is brought in and distributed over the area.

The samples are taken between item number 4 and 5. The soil has already adapted to the new stress imposed by the first sand platform. This should be taken into account when the PLAXIS calculations will be run later.

6

Field and Laboratory Results

This chapter describes the results from the test described in the previous chapter. This chapter is divided into three sections. The first section describes the three ZLT that have been performed. The second section elaborates the CPT that have been executed. The CPT diagrams can be found in chapter L. The third section is concerned with the soil samples and test results.

6.1 Zone Load Test

The exact ZLT location was based on the availability of a particular area in the ZOR project.

The ZLT are performed on at least 2 m of soil to reduce the risk of the foundation slab punching through the sand platform. Also, if the ZLT would be executed on the final platform level, which is (dependent on the location) approximately 5 m, the settlement would be governed by the sand (due to the spread of the ZLT-imposed stress in the platform).

The results of the ZLT are given in figures 6.1 through 6.3.
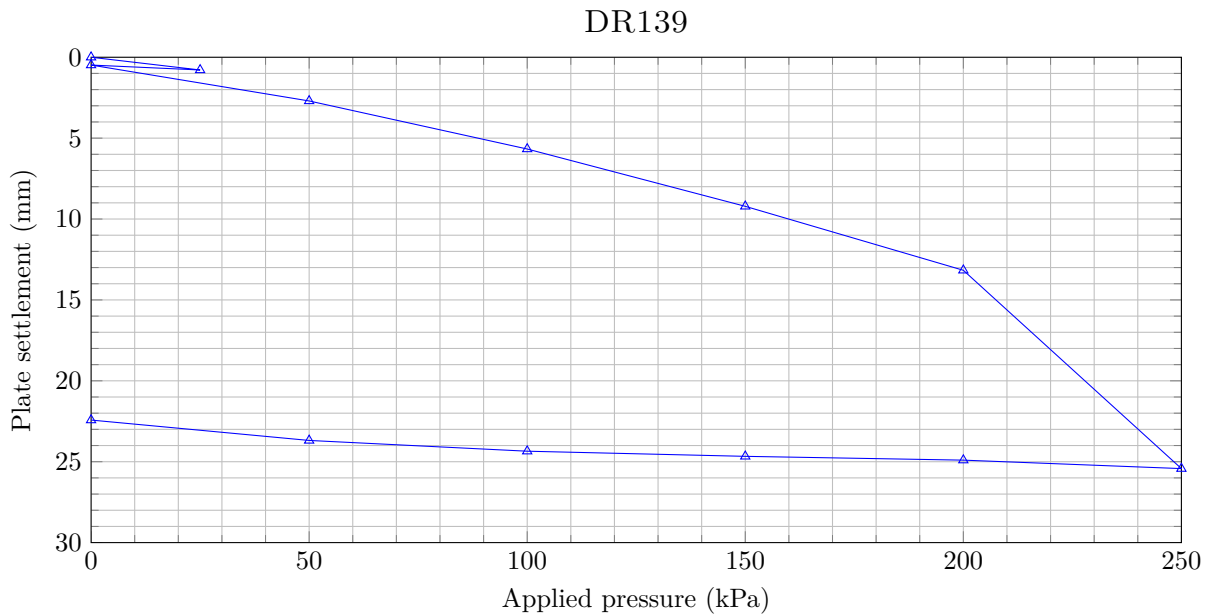
Figure 6.1: ZLT settlement at box DR139
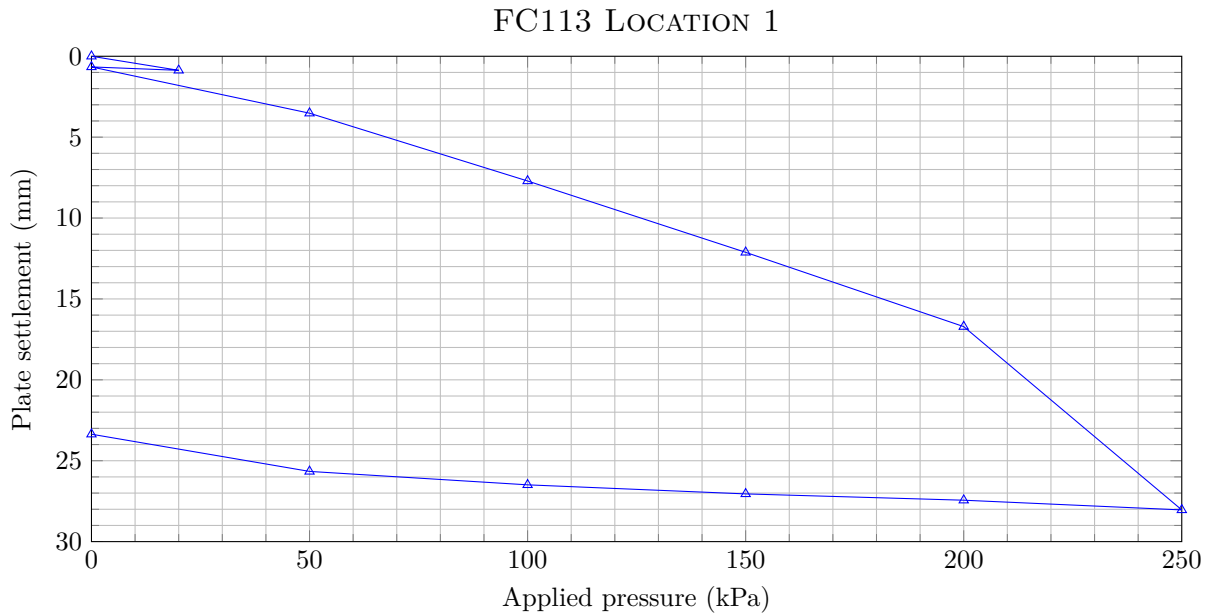
FC113 Location 1

Figure 6.2: ZLT settlement at box FC113, location 1
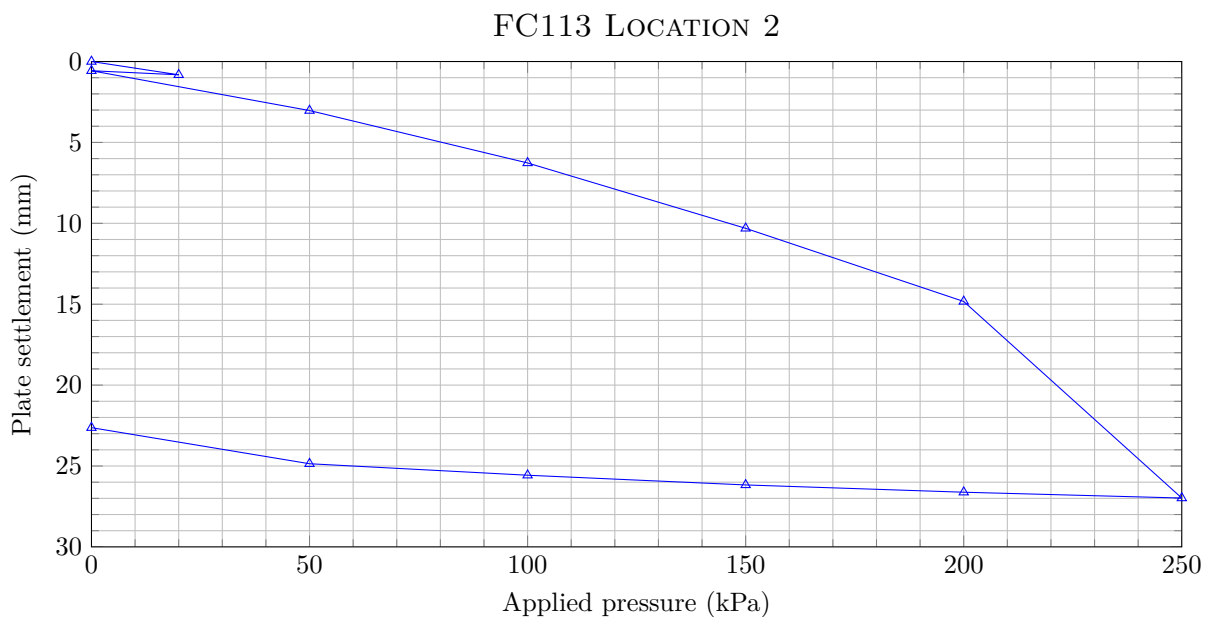
FC113 Location 2

Figure 6.3: ZLT settlement at box FC113, location 2

The ZLT performed in location 1, which is on top of a sand column, is shown in figure 6.2. The maximum settlement equals 28 mm at 250 kPa. It can be seen that especially the last part, i.e. between 200 and 250 kPa, the settlement is relatively high. This load interval is kept at 250 kPa for 48 hours. Upon offloading, the settlement reduces approximately 5 mm to 23 mm. This means that most of the settlements that have occurred are plastic deformations. Approximately 40% of the deformation during offloading occurs in the last (i.e. 50 to 0 kPa) interval.

The ZLT performed in location 2, which is between sand columns, is shown in figure 6.3. The settlement at 250 kPa is in this case 27 mm, which is one millimeter less compared to the previous test. Similar to the previous test, the settlement during the last part of loading is relatively high. Again the load is kept at 250 kPa for 48 hours. Upon offloading the settlement reduces to approximately 23 mm. Approximately 50% of the deformation during offloading occurs in the last (i.e. 50 to 0 kPa) interval.

6.2   Cone Penetration Tests

The CPT can be used to determine the subsoil layering. One CPT campaign was executed to determine the shape of the sand columns, these CPTs were not particularly successful and shall not be elaborated here. A short discussion of these CPTs can be found in section F.2.

Another CPT campaign was executed to determine the subsoil composition under the ZLT. To this extent one CPT is executed in all the four corners of the ZLT base block, totaling to four CPTs per ZLT. The results of these CPTs are used for the Plaxis calculations in chapter 8.

6.3   Soil Sampling and Testing

Section F.1 elaborates the soil sampling works.

Five 4-inch tube samples of approximately 0.5 m were taken and brought to the laboratory. The samples were sealed and packaged and transported back to Van Oord site office. A photo report concerning the sealing and packaging of the samples in Kuwait can be found in F.1.1.

The samples were sent to the TU Delft afterwards. The samples are tested at the TU Delft, this is described in chapter G.

6.3.1   Sand

The parameters for the sand platform and columns are derived from FDT and CPT (see section F.4 and chapter H.2, respectively.

Field Density Test

Table 6.1 summarizes the density of the sand, derived from FDT results.

Table 6.1: Sand density

Parameter	Description	Unit	Value
ρ_w	Wet density	kg/m^3	1813
ρ_d	Dry density	kg/m^3	1720
$\rho_{d,max}$	Max. dry density	kg/m^3	1802
	Relative compaction	%	95.5

Cone Penetration Test

As described in chapter 5 many parameters can be derived from the CPT. Robertson and Cabal (2015) and Mayne (2014) describe many correlations. The correlations that are used to determine the parameters defined in this paragraph are given in chapter H.2. The CPT on which the correlations are based are given in chapter L.

Table 6.2: Sand parameters

Parameter	Description	Unit	Value
E_{oed} or M	Constrained or Oedometer modulus	kPa	54310[1]
φ'_p	Friction angle	°	45

[1] $P_{ref,z} = \sigma_{v,0}$

6.3.2 Sabkha and Silt

At the laboratory classification tests, consolidation tests and shearbox tests were performed. The results of these tests are given in table 6.3.

Table 6.3: Laboratory Test Results

Parameter	Unit	Borehole 16	Borehole 17	Borehole 17 Silt	Borehole 18
W	%	83.3	84.6	40.5	73.6
ρ_w	kg/m^3	1536.9	1535.5	1607.25	1527.9
ρ_p	g/cm^3	2.6099	2.5909	2.7238	2.6211
% Fines	%	99	99	69	100
LL	%	93	86	-	89
PL	%	55	37	-	38
PI	%	38	49	-	51
τ (σ_c)	kPa (kPa)	32.76 (47.1)	8.2 (15.6)	-	-
		54.25 (94.3)	23.5 (33.0)	-	-
		71.14 (138.7)	40.7 (71.0)	-	-
c	kPa	14	1.5[1]	-	-
φ	°	22.6	29.9[1]	-	-

[1] These values are not considered realistic, see figure 6.6.

Consolidation

The consolidation and swelling characteristics in terms of consolidation stress, σ_c, and compression index, C_c, can be found in figure 6.4 and 6.5, respectively. The equation for the compression index is given in equation 6.1.
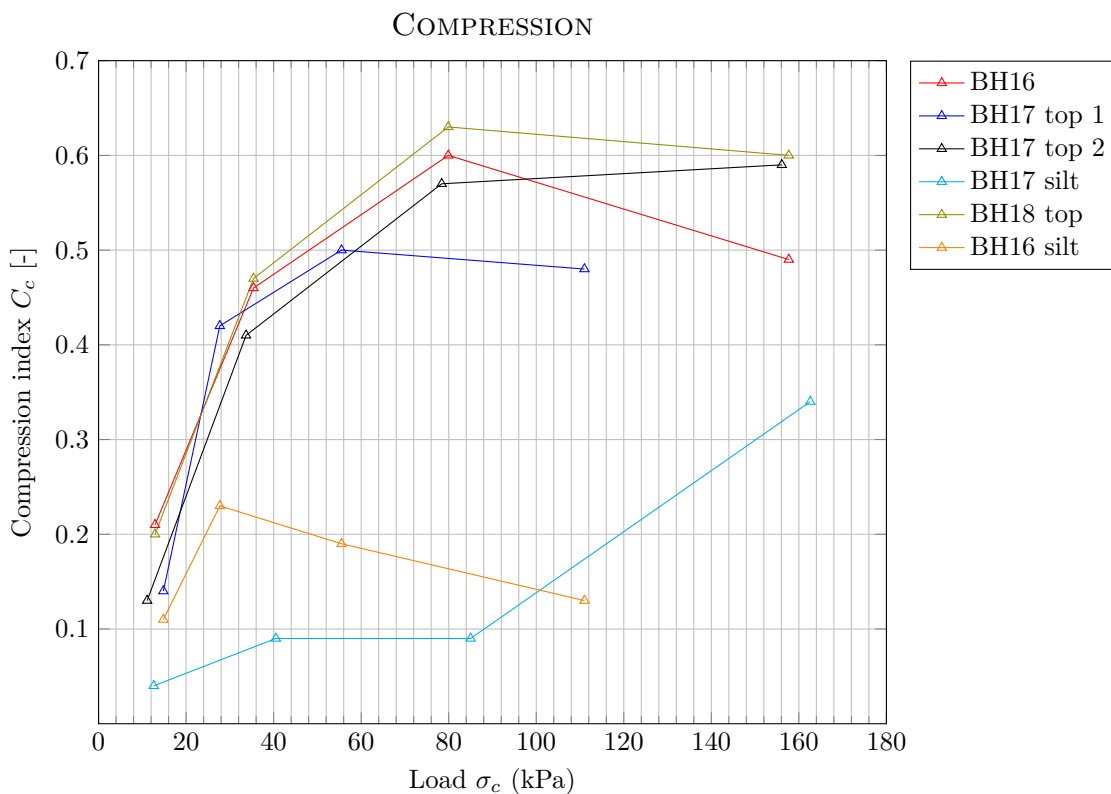
Figure 6.4: Compression plots
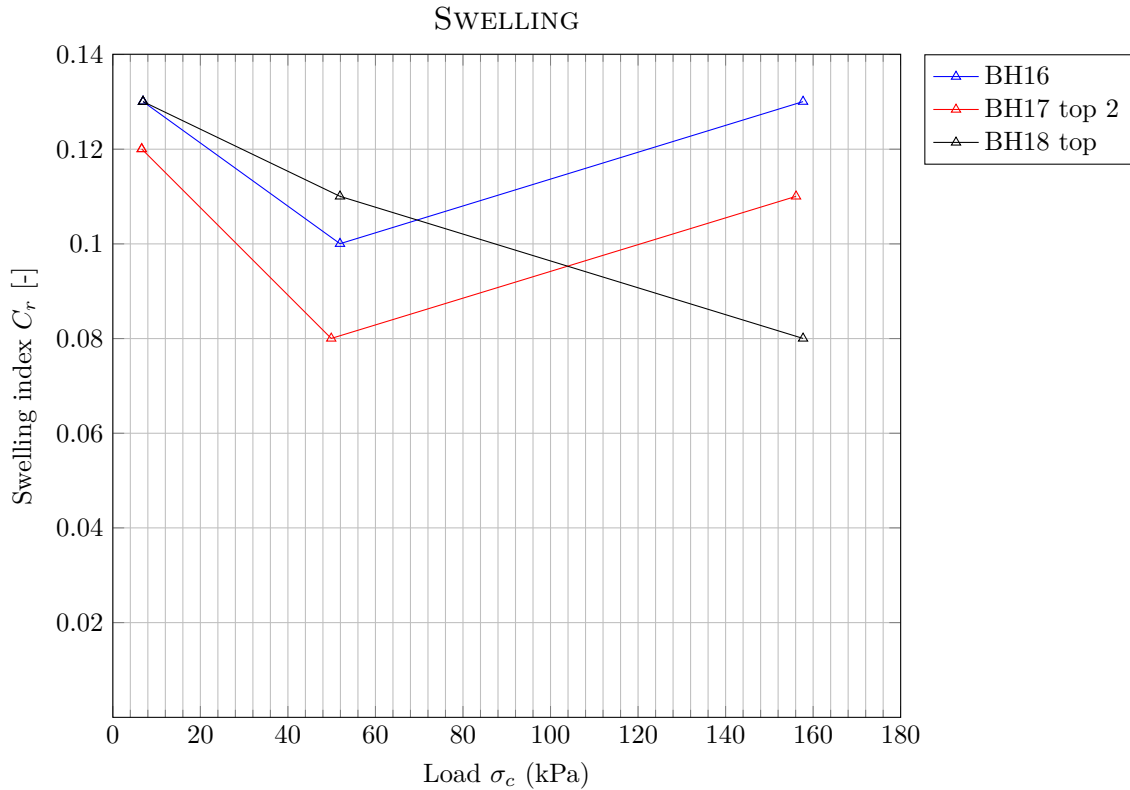
Figure 6.5: Swelling plots

$$C_c = \frac{e_1 - e_0}{\log(\sigma_{c,1}/\sigma_{c,0})} \tag{6.1}$$

Where:

C_c	=	Compression index;
e	=	Void ratio;
σ	=	Consolidation stress.

It can be seen in equation 6.1 that a lower value of C_c will imply a stiffer soil (the enumerator, the void ratio, wil increase with displacement, the denominator, $\log \sigma$ will be smaller when there is little stress needed for a displacement) see NEN (2012) table 2b for more information. It can seen in figure 6.4 that the compression index increases to a peak value. After the peak the C_c decreases.

Based on figure 6.4, it can be concluded that the sabkha has some apparent preconsolidation stress which is lost upon loading. After a certain load, the sample will start gaining strength again and behave stiffer (and will thus show a lower C_c upon strength increase).

It was already mentioned in the literature study in section 3.4 that salt minerals are a major source of cementation in sabkha, as mentioned in Akili and Ahmed (1983). A drawing of the cementation is given in figure 3.1.

The results from the investigations by Abduljauwad and Al-Amoudi (1995) and Ismael (1993), described in detail in section 3.4, show lower sabkha strength in case the sample is first leached by fresh water. The results from the consolidation test in figure 6.4 clearly show strength loss (in fact the mentioned diagram shows a decrease in stiffness which can be attributed to a loss of strength) after a threshold consolidation stress.

The preconsolidation stress of the tested sabkha is most likely due to the sand platform on top of the sabkha, which has been there for a period in the order of months. The salt cementation found by e.g. Abduljauwad and Al-Amoudi (1995) was not observed as the preconsolidation stress of the sand platform is higher than the cementation strength. It is therefor assumed that the cementation has already been destroyed by the stress imposed by the sand platform.

Strength

It was concluded in the previous paragraph that the tested soil has a preconsolidation stress, which is most likely due to the sand platform. The results from two tests are given in figure 6.6.

DIRECT SIMPLE SHEAR TESTS
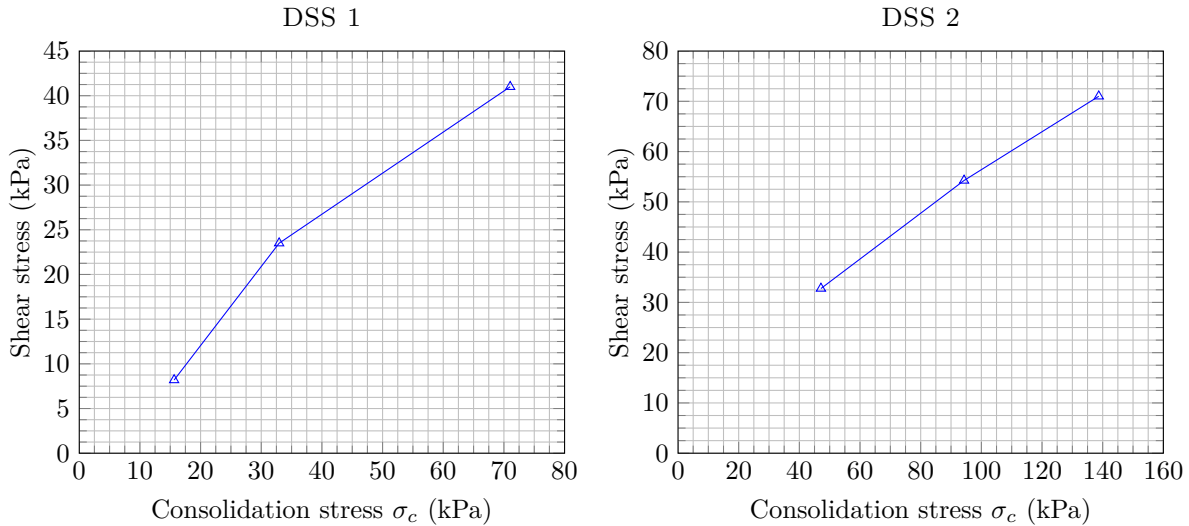
Figure 6.6: DSS tests for different σ_c

It can be seen in figure 6.6 left that the σ_c=15.65 kPa test has a relatively low strength. The cohesion is less than 0 kPa, if a line is plotted for runs 1 and 2 while the cohesion equals 10 kPa when a line is plotted between run 2 and 3.

Figure 6.6 right shows test results where a clear trend line is visible. All test results are approximately on a linear line.

It was concluded in the previous paragraph that the samples show a decreasing stiffness after a threshold value, before reaching another threshold value after which the sabkha starts to increase in strength again. It can be concluded that the σ_c in DSS test 1 was lower than the σ_c in the field.

6.3.3   Silty Sand

Below the sabkha and silt layer, a silty sand layer is present. The engineering parameters of this layer are determined based on CPT results and NEN (2012). The parameter values can be found in chapter 7.

7

PLAXIS Soil Models Input

PLAXIS uses different soil models, dependent on soil characteristics, composition, load, stress et cetera. The models used in the calcuations for this report are the Hardening Soil model and the Soft Soil model, described in section 7.1 and 7.2, respectively.

7.1 Hardening Soil model

The Hardening Soil model (HSM) is used to model the sand platform and the sand columns. HSM accounts for soil hardening during (shear) loading.

7.1.1 Model Parameters

The input for the sand platform is summarized in table 7.1. For the determination of these parameters, reference is made to chapters 6, H and H.2.

Table 7.1: HSM input for the sand platform

Parameter	Description	Value	Unit
E_{50}^{ref}	Secant stiffness in standard drained triaxial test	110,000	kPa
E_{oed}^{ref}	Tangent stiffness for primary Oedometer loading	110,000	kPa
E_{ur}^{ref}	Unloading/reloading stiffness $(=3E_{50}^{ref})$	330,000	kPa
m	Power for stress-level dependency of stiffness	0.5	[-]
c	Cohesion	0	kPa
φ	Friction angle	38	°
ψ	Dilatancy angle	8	°
γ_d	Dry unit weight	17.13	kN/m^3
γ_w	Wet unit weight	18.20	kN/m^3

[1] $P_{ref,v} = 100$ kPa
[2] The tensile strength is set to zero in the Plaxis model (which is a very reasonable assumption, particularly in sand). Should there be any numerical problems during the calculation, it may be necessary to adjust this value.

It is noted that for the advanced parameters in the HSM the default settings are used.

The HSM considers a specific parameter for unloading/reloading cases, the E_{ur} which is generally equal to three times the primary stiffness E_{oed}. The resulting reloading stiffness would be 330 MPa, which is unrealistically high.

The model uses stiffness moduli for primary loading, E_{50} and E_{oed} which may not be realistic. The amount of stress which the soil has been subject to during DR works has been higher than the stress

imposed by a ZLT. With that insight, it may be applicable to use E_{ur} instead. If one considers the already relatively high primary stiffness moduli however, which are in the order of 100 MPa, it may very well be justified to use primary loading parameters. It is likely that this would result in a significant amount of plastic points in the model.

It is concluded from the CPT results, as presented in chapter L, that the sand columns have a higher degree of compaction. This increases both strength and stiffness, compared to the sand platform. The input parameters for the sand column are given in table 7.2.

Table 7.2: HSM input for the sand platform

Parameter	Description	Value	Unit
E_{50}^{ref}	Secant stiffness in standard drained triaxial test	125,000	kPa
E_{oed}^{ref}	Tangent stiffness for primary Oedometer loading	125,000	kPa
E_{ur}^{ref}	Unloading/reloading stiffness ($=3E_{50}^{ref}$)	375,000	kPa
m	Power for stress-level dependency of stiffness	0.5	[-]
c	Cohesion	0	kPa
φ	Friction angle	40	°
ψ	Dilatancy angle	10	°
γ_d	Dry unit weight	17.13	kN/m³
γ_w	Wet unit weight	18.20	kN/m³

The input for the deep silty sand layer is summarized in table 7.3.

Table 7.3: HSM input for the sand platform

Parameter	Description	Value	Unit
E_{50}^{ref}	Secant stiffness in standard drained triaxial test	70,000	kPa
E_{oed}^{ref}	Tangent stiffness for primary Oedometer loading	70,000	kPa
E_{ur}^{ref}	Unloading/reloading stiffness ($=3E_{50}^{ref}$)	210,000	kPa
m	Power for stress-level dependency of stiffness	0.5	[-]
c	Cohesion	2	kPa
φ	Friction angle	36.5	°
ψ	Dilatancy angle	6.5φ	°
σ_t	Tensile strength	0^2	kPa
γ_w	Wet unit weight	18.00	kN/m³

7.2 Soft Soil model

The Soft Soil model (SSM) is used to model the sabkha and intermediate silt layers.

7.2.1 Model Parameters

For the derivation of the following parameters, reference is made to chapters 6 and F.

The SSM uses modified compression index and the modified swelling index (the slope of the primary loading line and the slope of the unloading line in a log mean stress vs. volumetric strain, respectively) from the Cam-Clay model (CCM) as the primary stifness input. The indices are defined as λ^* and κ^*, while the original CCM indices lack the asterisk. (Brinkgreve and Swolfs, 2015)

The relationship between the modified CCM indeces and internationally recognized parameters for one-dimensional compression, C_c and swelling C_s, are defined in equation 7.1 and 7.2 (Brinkgreve and Swolfs, 2015).

$$\lambda^* = \frac{C_c}{2.3(1+e)} \tag{7.1}$$

$$\kappa^* \;=\; \frac{2C_s}{2.3(1\;+\;e)} \tag{7.2}$$

As can be read in chapter F, both the compression and swelling parameters are dependent on the normal stress applied in the Oedometer test. For the model a value determined in the applicable stress level is chosen. The input for the soft clay layer is summarized in table 7.4.

Table 7.4: SSM input for the sabkha layer

Parameter	Description	Value	Unit
C_c	Compression parameter	0.4	[-]
C_s	Unloading parameter	0.13	[-]
c	Effective cohesion	14	kPa
φ	Friction angle	22.6	°
ψ	Dilatancy angle	0	°
σ_t	Tensile strength	0^3	kPa
B	Skempton's B parameter	0.95	[-]
γ_w	Wet unit weight	15.13	kN/m^3

It is noted that for the advanced parameters in the SSM the default settings are used.

The input for the silt layer is summarized in table 7.5.

Table 7.5: SSM input for the silt layers

Parameter	Description	Value	Unit
C_c	Compression parameter	0.2	[-]
C_s	Unloading parameter	0.02	[-]
c	Effective cohesion	5	kPa
φ	Friction angle	28	°
ψ	Dilatancy angle	0	°
σ_t	Tensile strength	0^3	kPa
B	Skempton's B parameter	0.95	[-]
γ_w	Wet unit weight	16.07	kN/m^3

[3] Cohesion in clay or silt can be considered tensile strength. The tensile strength is however set to zero in the Plaxis model. Should there be any numerical complications during the calculation, it may be necessary to adjust this value.

Part III

Plaxis and Analytical Calculations

Van Oord
Marine ingenuity

8

PLAXIS Short-Term Calculations

8.1 PLAXIS Considerations

The writer would like to remind the reader about the chronological order of sand placement in the ZOR project. The order is briefly described in section 5.4. The conclusion was drawn that the samples that have been tested are already consolidated to the 2 - 3 m of sand that has been placed on top of the original surface level. After placement of the sand DR and DC works have been performed, as well as leveling operations. It is therefor decided to model the CSE in the phase during which the soil samples were taken. During this phase the CPTs that have been used to determine the sand characteristics were carried out. It should be stressed that the calculations have a significant deficiency. After placing the sand the soil will have settled under the weight of the platform. This is however not taken into account in the calculations.

In the remainder of this section the considerations for choosing particular PLAXIS inputs will be elaborated.

8.1.1 Model Geometry

Considering calculation speed, the PLAXIS calculations will be performed on a section of the CSE. To this extent a cell within the model was chosen (see section 2.3), shown in figures 8.1 and 8.2. A soil-centered unit cell could not be used because of the boundary conditions that are imposed by PLAXIS. The boundaries of the model always assume a horizontal boundary, i.e. $\frac{dx}{dz} = 0$ on the y-axis and $\frac{dy}{dz} = 0$ on the x-axis.

There are four symmetry lines in the model. Two of the lines intersect the ZLT because it is reasonable to assume that the settlements and stresses will be equal at these lines. Two other lines are assumed to be outside of the influence zone of the ZLT, and the displacement is thus equal to zero. The PLAXIS model for the configuration with the ZLT between the DR columns is given in figure 8.1. The other configuration, with the ZLT on top of a column, is given in figure 8.2.
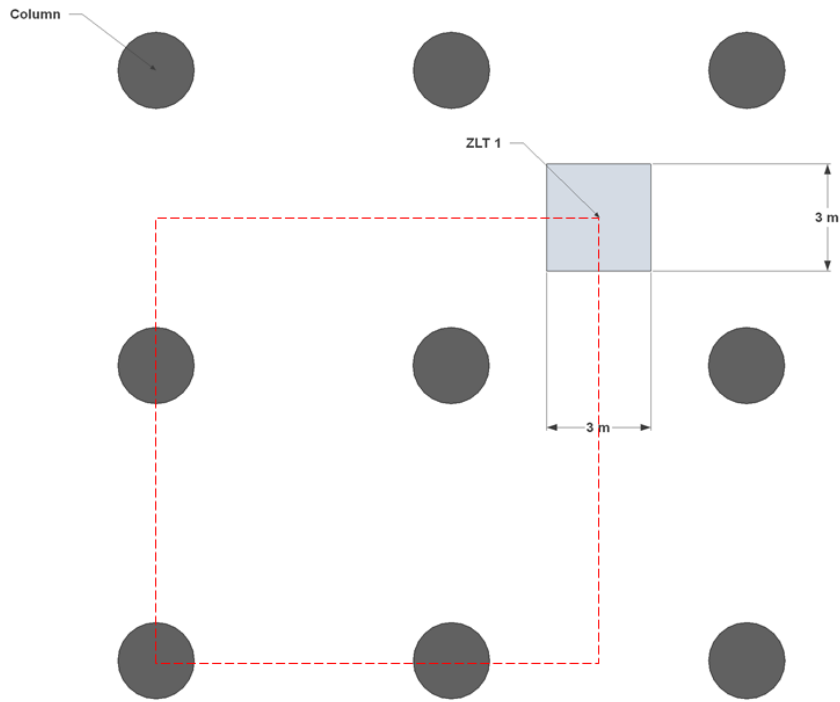
Figure 8.1: Plaxis model shown by the dashed line, ZLT between columns
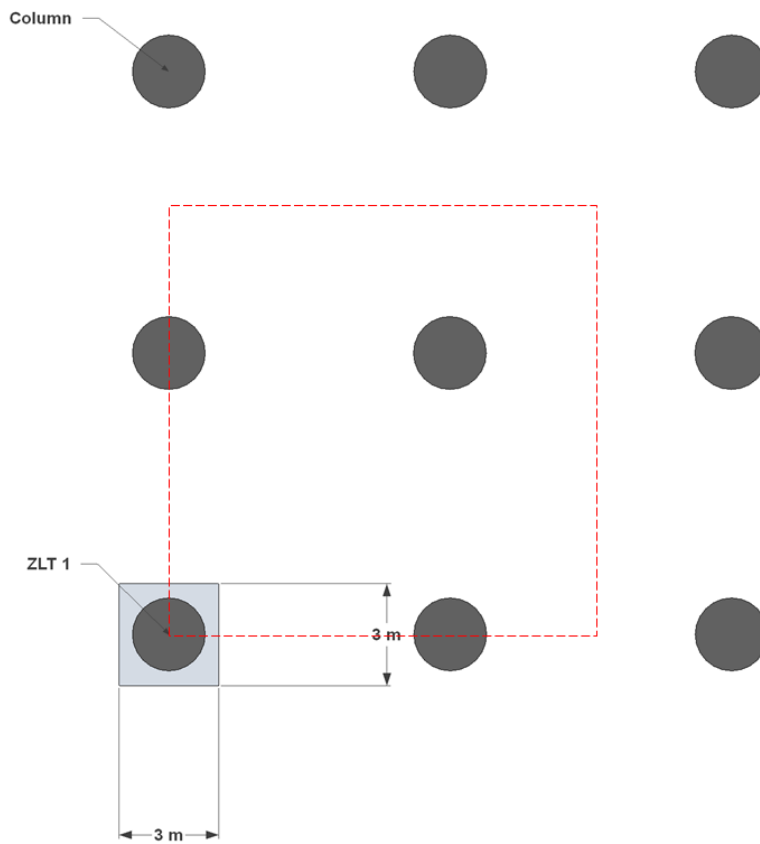
Figure 8.2: Plaxis model shown by the dashed line, ZLT on top of columns

Boundary Conditions

The boundary conditions that are used in the model are summarized in table 8.1.

Table 8.1: Boundary Conditions

Boundary	Deformation	Groundwater
Xmin	Hor. fixed	Closed
Xmax	Hor. fixed	Open
Ymin	Hor. fixed	Closed
Ymax	Hor. fixed	Open
Zmin	Fully fixed	Open
Zmax	Free	Open

8.1.2 Soil Models

For the benchmark calculations, the parameters mentioned in chapter 7 are used.

8.1.3 Phases

There are multiple phases used for the ZLT simulation. The *Staged construction* option is used, so that the ZLT foundation pressure can be increased over several phases. The phases are described in table 8.2.

Table 8.2: Calculation Phases for short term analysis

Phase 1	**Phase 2**
In the first phase the PLAXIS K_0 procedure is employed. During this phase PLAXIS determines the initial stresses in the model based on K_0.	The second phase comprises of a zero-step. In this step undrained behavior is ignored. Ignoring undrained behavior implies that the consolidation is finished and that there are no pore pressures in the soft soil. The result of this phase is used as a zero reading for the effective stress (before loading).
Phase 3-7	**Phase 7-11**
In this phase the load is activated and increased in intervals from 10% to 125%. For the load increase the *Staged Construction* option is used in PLAXIS. The exact interval loads and time periods can be found in section D.2.	The last set of phases consist of unloading the ZLT. The exact interval loads and time periods can be found in section D.2. Note that in the figure below the surface load is not shown to emphasize the displacement.
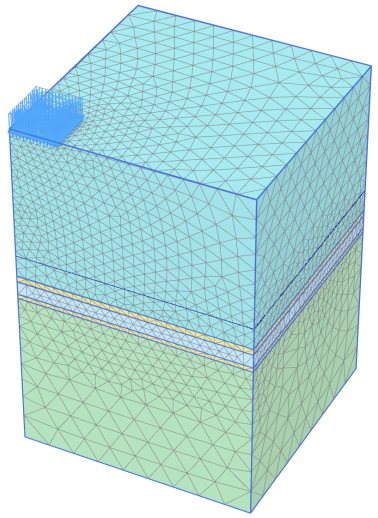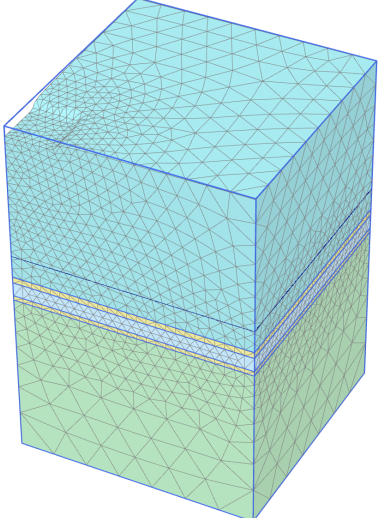
8.2 Calculations

This section describes the calculations that have been performed.

8.2.1 Parametric Analysis of the Platform

It became clear from section 2.6 that there is a number of soil parameters that have an influence on the amount of arching and (differential) settlement in a CSE. The PLAXIS calculations were run for a selection of these parameters. The model mesh was refined at the column heads, the colum shaft and the sand platform. The silt, sabkha and deep silt layers were calculated with a coarse mesh. The mesh configuration is further elaborated in I.1.

The most influential soil parameters that were investigated are $\varphi_{platform}$ and $E_{platform}$, the results of the calculations for these parameters are given in the following sections. The parametric analysis of the column revealed that φ_{column} and E_{column} only had a marginal influence on the settlement of the ZLT. The results of these calculations can be found in the appendix, section K.1.

Platform Friction Angle

The results from the platform friction angle calculations are given in figures 8.3 and 8.4.
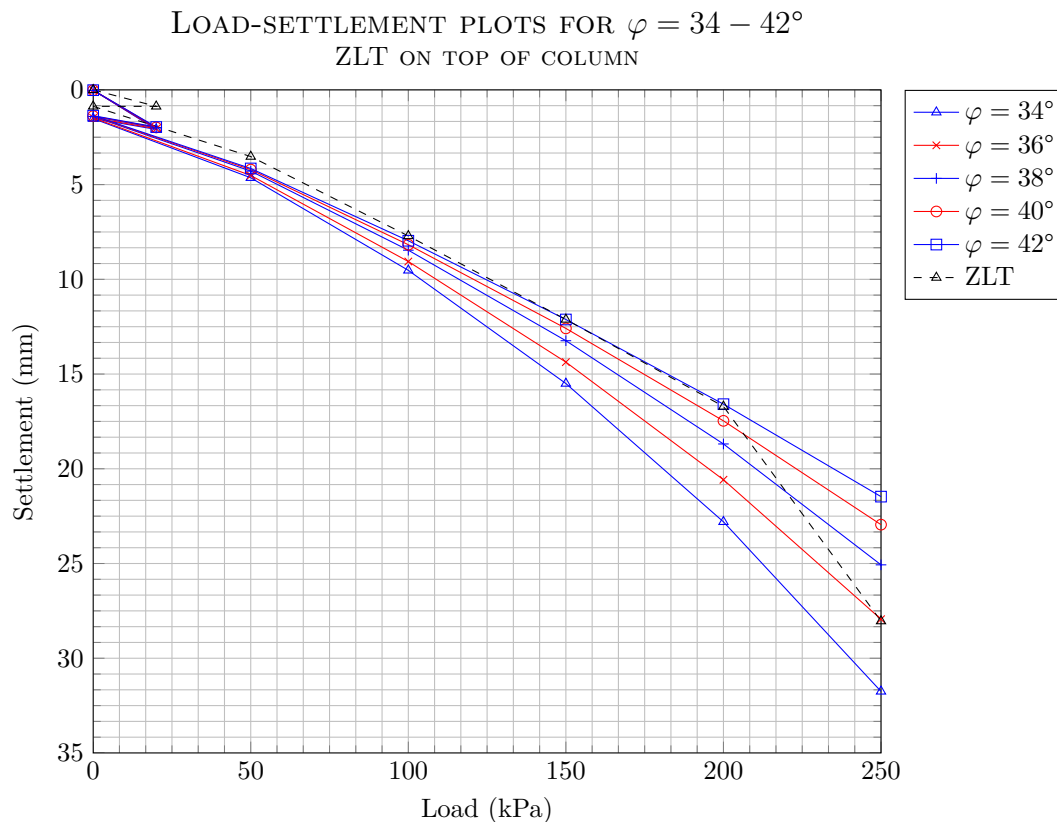
Figure 8.3: Load-settlement plots varying friction angle, ZLT on top of column

LOAD-SETTLEMENT PLOTS FOR $\varphi = 34 - 42°$
ZLT BETWEEN COLUMNS
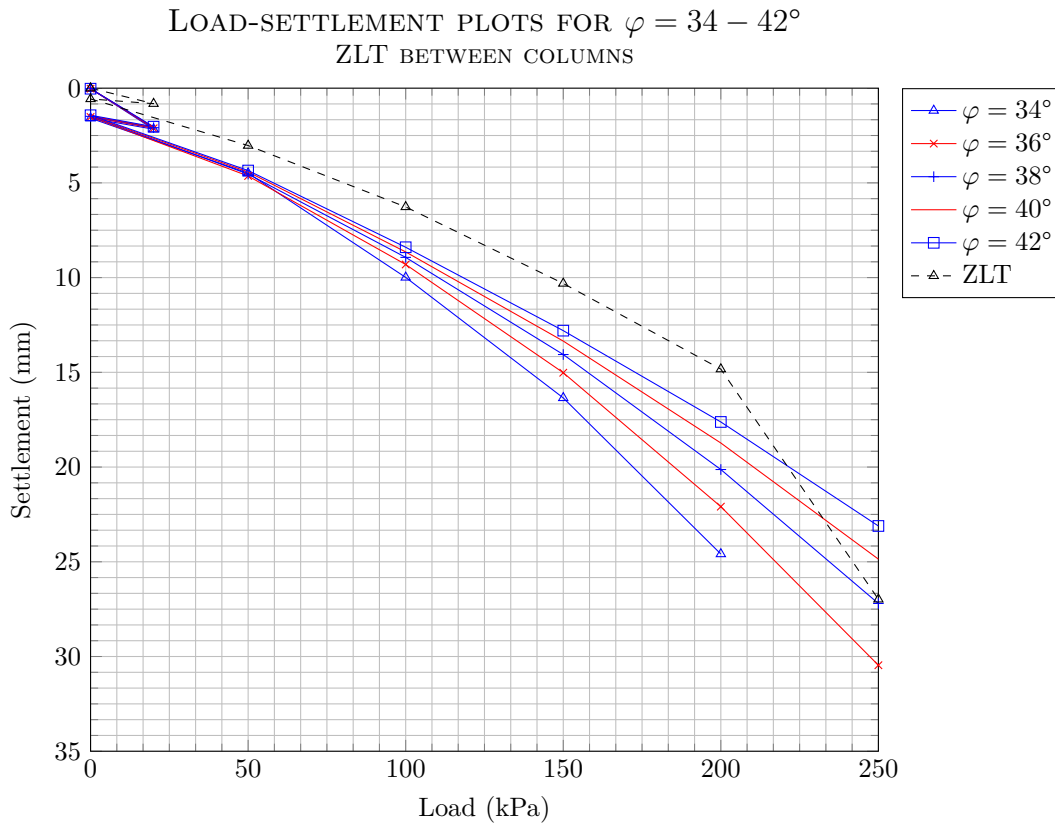
Figure 8.4: Load-settlement plots varying friction angle, ZLT in between columns

It can be seen that there is a significant influence from the friction angle of the sand platform on the settlement. The difference in settlement between the minimum ($\varphi = 34°$) and maximum ($\varphi = 42°$) is more than 10 mm for the model with the ZLT on top of the column. For the model where the ZLT is located between the columns, $\varphi = 34°$ leads to large deformations in the PLAXIS calculation. The difference in settlement for $\varphi = 36°$ and $\varphi = 42°$ is approximately 7 mm for a load of 250 kPa.

The difference in settlement between the ZLT on top and in between, for 250 kPa, is only 1.5 mm for $\varphi = 42°$. This suggests that the stress distribution for such a friction angle is approximately the same and thus results in nearly equal settlement.

Platform Stiffness

The results from the platform stiffness calculations are given in figures 8.5 and 8.6. Note that all PLAXIS stiffness input have been adjusted to a reference pressure of 100 kPa, as per chapter H.
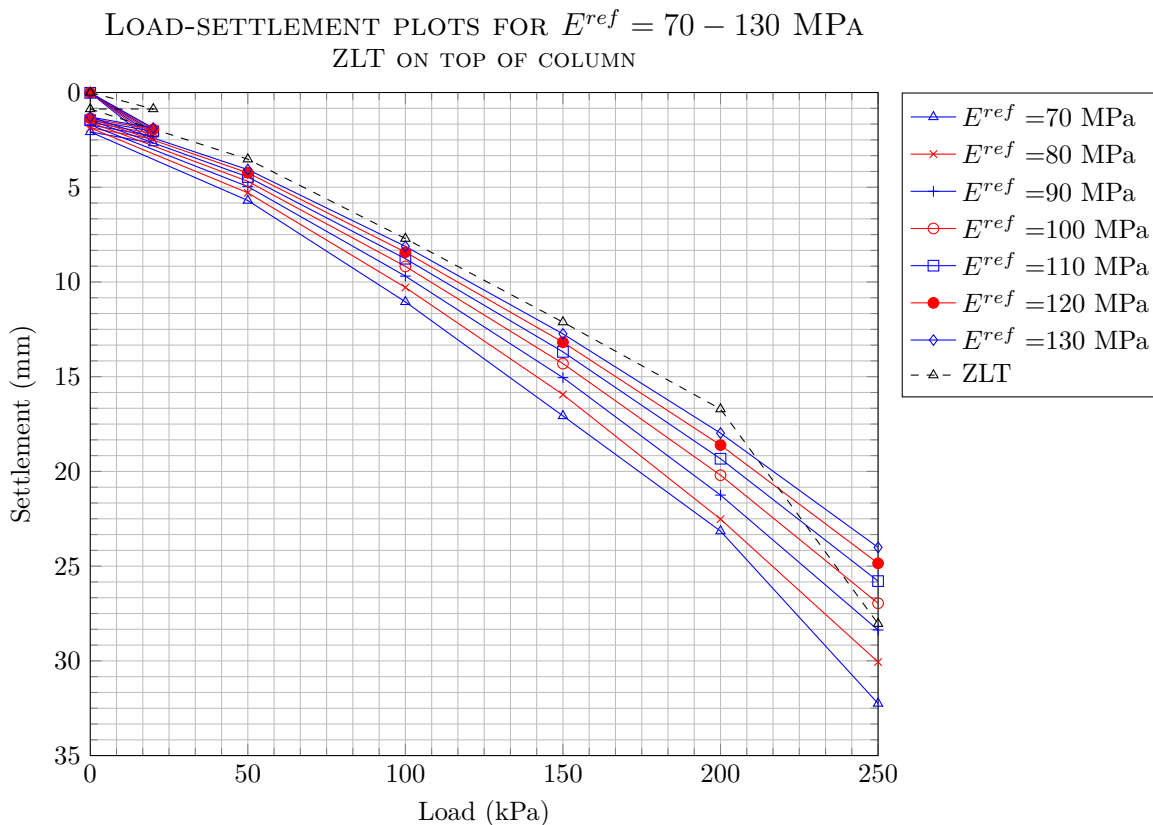
Figure 8.5: Load-settlement plots varying stiffness, ZLT on top of column
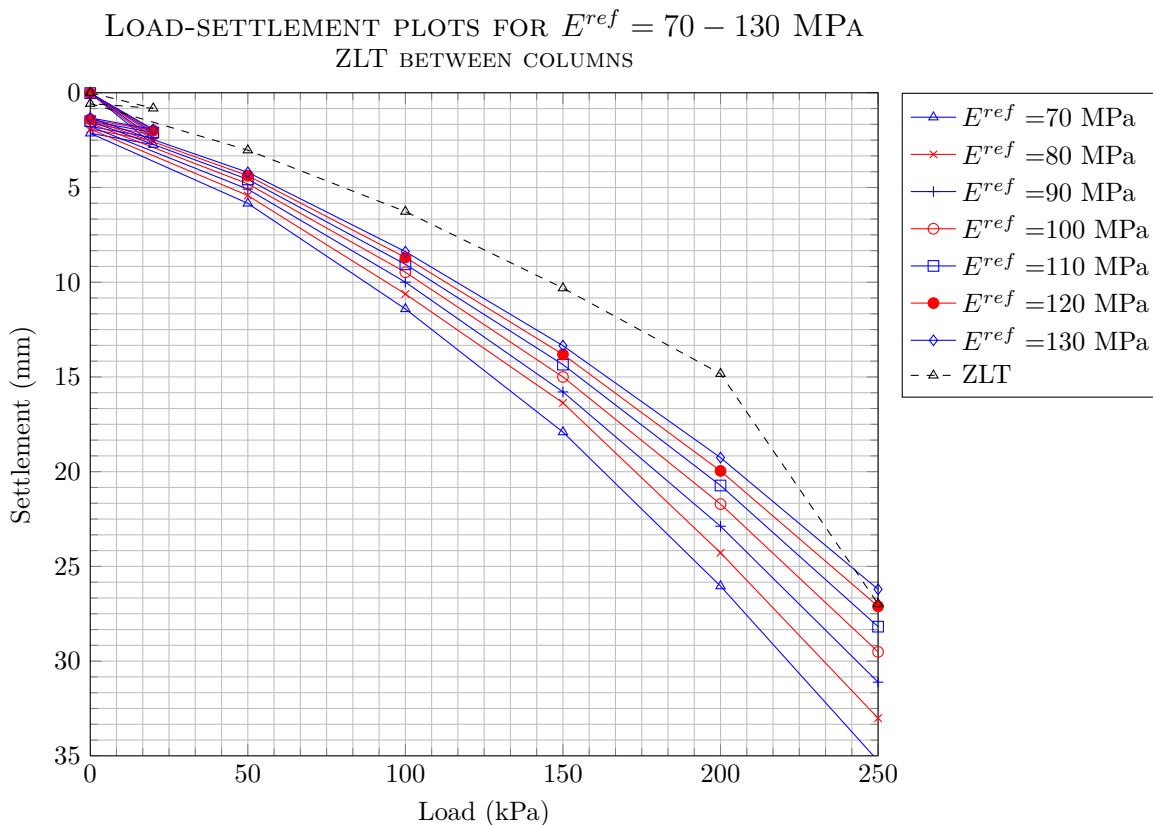
Figure 8.6: Load-settlement plots varying stiffness, ZLT in between columns

8.2.2 Platform Height

It was established in chapter 2 in the literature study that the arching in a CSE is dependent on the platform height. The arching increased with an increase in platform height.

The platform height that was used for the reference ZLTs was 2.2 m. Table 8.3 summarizes the platform heights on which the calculations were based. In the last column the ratio of platform height over column spacing, defined by ζ is given (see equation 8.1).

$$\zeta = \frac{H}{s - a} \qquad (8.1)$$

For the definitions of H, s and a reference is made to the nomenclature.

Table 8.3: Platform calculations

Calculation	Platform height (m)	$\zeta\,[-[$
1	2.2	0.55
2	2.5	0.63
3	2.8	0.70
4	3.1	0.78
5	3.4	0.85
6	3.7	0.93
7	4.0	1.00
8	5.0	1.25
9	6.0	1.50
10	7.0	1.75
11	8.0	2.00

The results of the calculations where the ZLT was modeled on top of a column are given in figure 8.7.
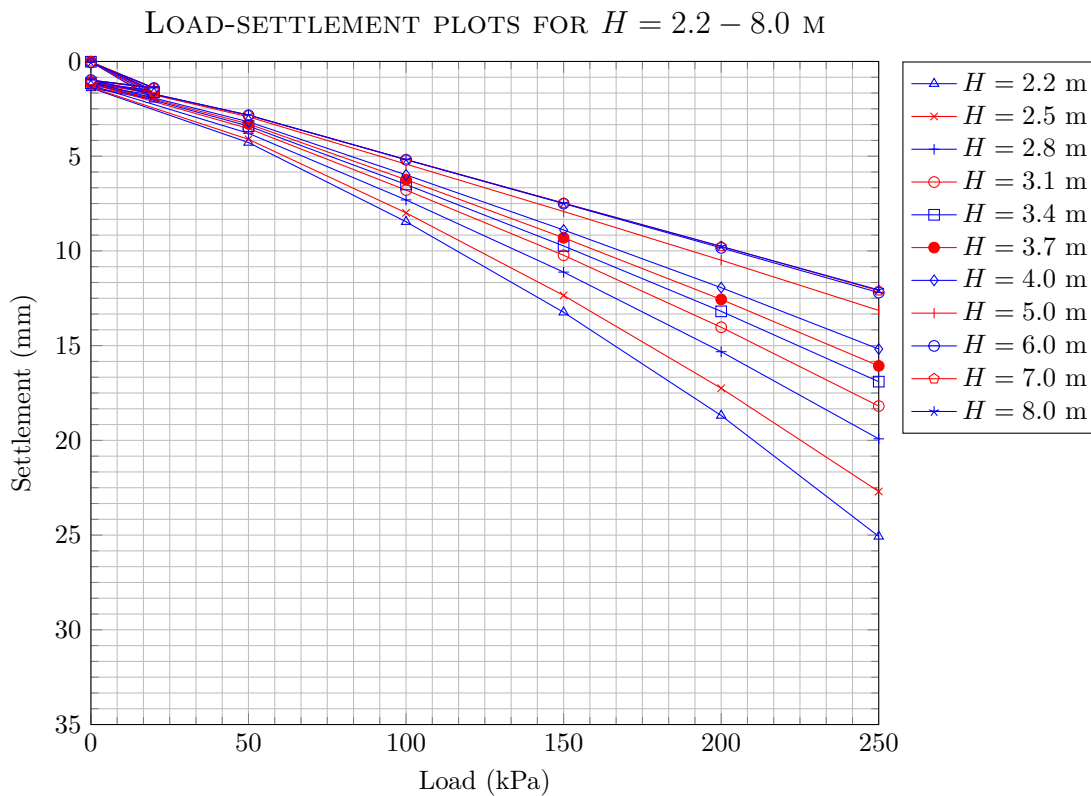
Figure 8.7: Platform height calculations, ZLT on top of column

It can be seen in the graph that there is a threshold value for the platform height above which the settlement does not increase anymore. It is assumed that at such platform heights the settlement is governed by the sand platform rather than the soft soil layer.

8.3 Analysis

It can be seen in figures 8.3 and 8.4 that the settlement is higher for a lower friction angle in both calculations. To aid in analyzing this behavior, the principal effective stress plots for the calculations where the ZLT is located in between the columns are given in figures 8.8 and 8.9.

Effective principal stresses (scaled up 2,00*10⁻³ times)

Maximum value = 0,000 kN/m² (Element 23886 at Stress point 95541)

Minimum value = -586,3 kN/m² (Element 24816 at Stress point 99261)
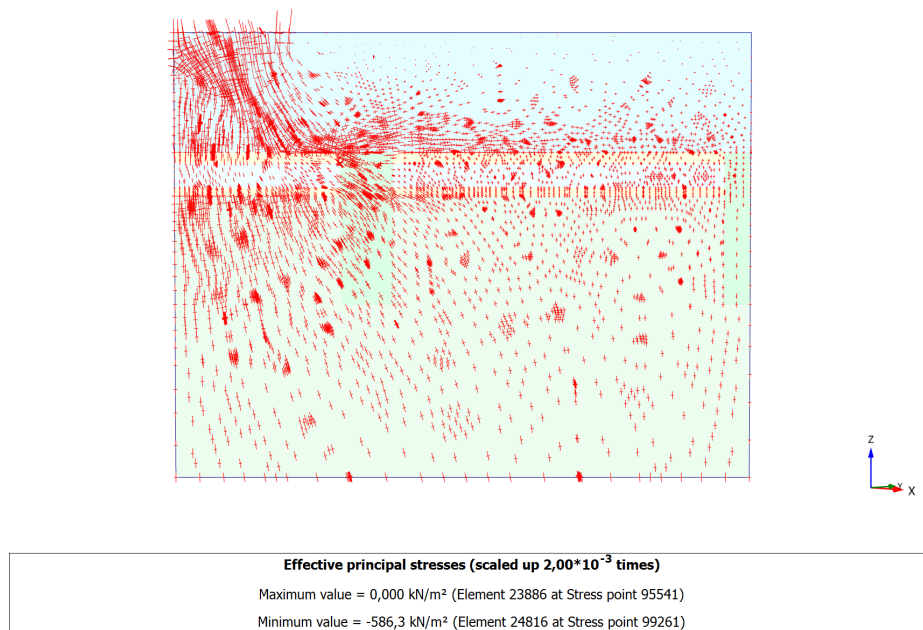
Figure 8.8: Effective stress for $\varphi = 36°$, ZLT in between columns

Effective principal stresses (scaled up 2,00*10⁻³ times)

Maximum value = 0,000 kN/m² (Element 23886 at Stress point 95541)

Minimum value = -505,9 kN/m² (Element 24159 at Stress point 96633)
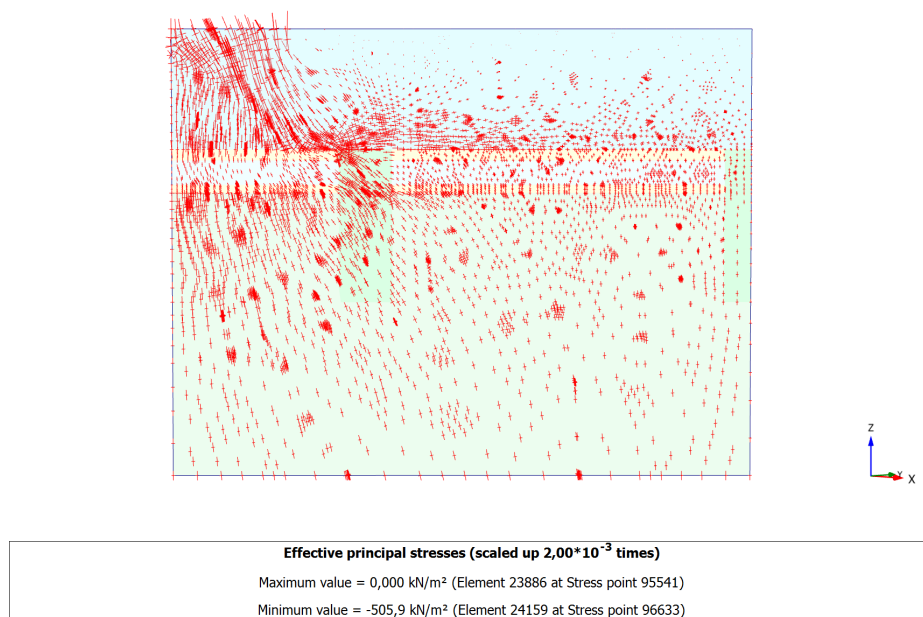
Figure 8.9: Effective stress for $\varphi = 42°$, ZLT in between columns

It can be seen in figure 8.8 that the load imposed by the ZLT (located in the far left of the figure) is transferred in a more concentrated stress compared to the stress in figure 8.9. The highest stress in figure ≈586 kPa while the maximum stress in figure ≈506 kPa. The concentrated stress that develops in a platform with a relatively low friction angle results in a higher horizontal displacement of the soft soil layer.

Total displacements |u| (scaled up 20,0 times)
Maximum value = 0,03046 m
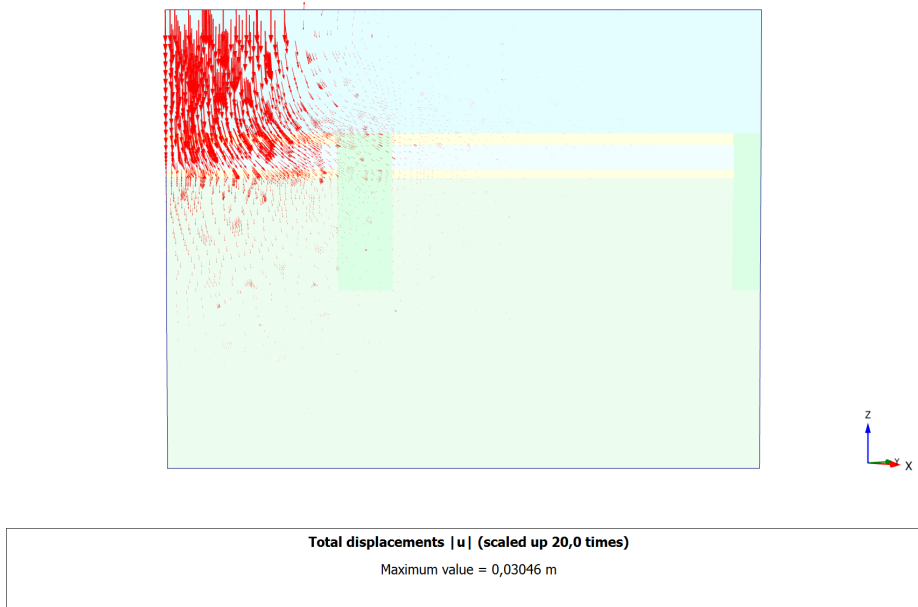
Figure 8.10: Displacement for $\varphi = 36°$, ZLT in between columns

Total displacements |u| (scaled up 20,0 times)
Maximum value = 0,02311 m
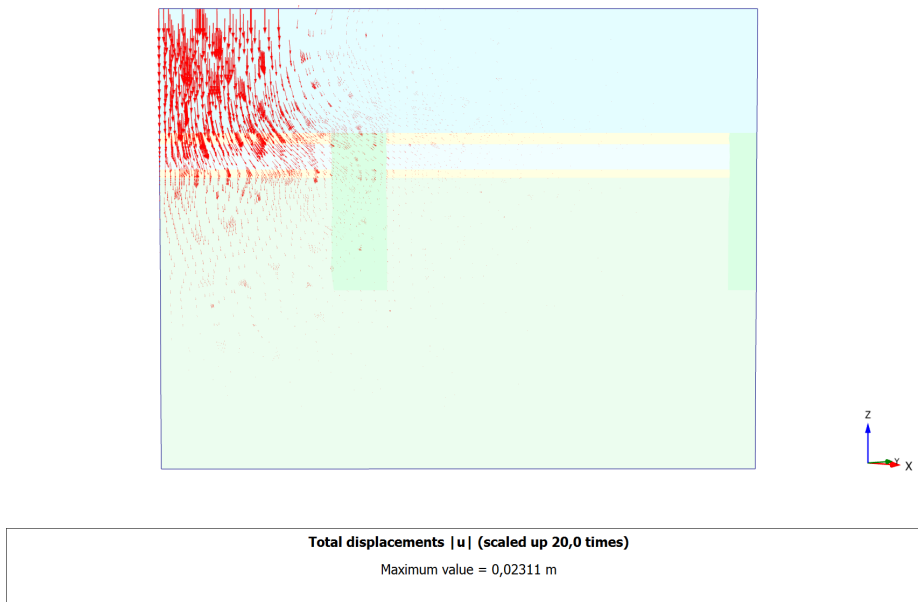
Figure 8.11: Displacement for $\varphi = 42°$, ZLT in between columns

It may be concluded from the figures above that the horizontal displacement is higher for a lower friction angle. Although not printed here, the excess pore pressure plots showed a higher local p_{excess} for a lower friction angle. This may most likely be attributed to the fact that there is less stress-spread under

the foundation in a platform with a low φ. While the force is the same for both calculations, due to a relatively high stress spread under the ZLT in the case of $\varphi = 42°$ the stress at the soft soil layer will be lower. Consequently, the stress and thus displacement will be higher for the calculations where $\varphi = 36°$. It may be concluded that the platform with a low friction angle will squeeze the soft soil farther away, resulting in higher settlements compared to a platform with a high friction angle.

It should be noted that, based on the theory presented for the calculations with the ZLT between the column, the area on which the ZLT load is distributed will be relatively small for the low φ and would thus imply a lower settlement (due to the higher stiffness of the sand column). Apparently the displacement of the soft soil layer is still governing, as the settlement is higher for the low φ. One should keep in mind however that the cross-sectional area of the column is only $\frac{\pi}{4}$ m^2 while the area of the ZLT equals 9 m^2. In short-term analysis the stress being drawn to the column due to the high relative stiffness is limited to non-existent as the stiffness of the soft soil layer approaches the stiffness of water.

The influence of the soil parameters on the short-term settlement response of a ZLT that have been investigated are summarized in table 8.4. Note that ++ represents great influence and – means no influence.

Table 8.4: Parameter influence

Parameter	Influence
Friction angle platform	++
Friction angle column	–
Stiffness platform	+
Height platform	++

Van Oord
Marine ingenuity

9

PLAXIS Long-Term Calculations

In the previous calculations, described in chapter 8, no account was taken of long-term behavior. In this report, long term behavior will include consolidation, no soil creep is considered however. For the long-term calculations a uniformly distributed load of 100 kPa is modeled, instead of the 250 kPa in a ZLT. This is assumed to be a more realistic long-term load.

For the long-term analysis three different types of models have been calculated. These models are briefly described in the enumeration below.

> **Calculation series 1:** The standard column spacing with s=5 and d=1, as executed in the ZOR project. Consolidation calculations were performed, of which the details are elaborated in section 9.1.3.

> **Calculation series 2:** The column spacing was changed to s=3 and d=1 to determine the effects of a denser column grid. On these analyses consolidation calculations were performed as well.

> **Calculation series 3:** For the last set of calculations the sand columns were removed. These calculations serve as a zero-type calculation to determine stress distribution and settlement in the non-improved situation.

The geometry and other PLAXIS configurations are described in the following sections. Section 9.2 describes the calculation results. These results are analyzed in the concluding section of this chapter, which is section 9.4.

9.1 PLAXIS Considerations

With reference to 8.1, the writer would like to remind the reader that the settlement and stress distribution that occured during the placement of the sand platform is not taken into account.

Based on the above mentioned approach to modeling it is not appropriate to calculate efficiency E, Stress Reduction ratio SRR and Settlement Reduction Ratio S_r. These calculations take account of the effect of an increasing platform height *and* the effect of surcharge. It is therefor decided to calculate and compare the incremental value of these parameters. The relations between the E and ΔE, SRR and ΔSRR are described in section 2.3.3, S_r and ΔS_r are described in section 2.4.1.

9.1.1 Model Geometry

Because of the high calculation load of consolidation analyses in PLAXIS, it was decided to decrease the size of the model. To this extent the previous model, as described in 8.1.1, was changed to a column-centered unit cell (see section 2.3.1). In the new model one sand column is modeled. This reduces the model to 5 x 5 m. The mesh of the model can be found in figure I.13. The coarseness of the elements is summarized in table I.7.

Based on symmetry considerations, the boundary conditions summarized in table 9.1 were applied.

Van Oord
Marine ingenuity

Table 9.1: Boundary Conditions

Boundary	Deformation	Groundwater
Xmin	Hor. fixed	Closed
Xmax	Hor. fixed	Closed
Ymin	Hor. fixed	Closed
Ymax	Hor. fixed	Closed
Zmin	Fully fixed	Open
Zmax	Free	Open

9.1.2 Soil Models

The soil model input as described in section 8.1.2 is used.

9.1.3 Consolidation

To prevent time-dependency between model geometry results, levels of consolidation (defined in %) were calculated rather than consolidation periods (defined in the time domain).

To determine the levels of consolidation PLAXIS consolidation calculation tool was used. The degree of consolidation, U, is calculated from 0% to 99%. Although generally the U is calculated based on the settlement (see chapter 16 in Verruijt and Baars (2007)), PLAXIS defines U based on pore pressure dissipation, see equation 9.1.

$$p_{min} \; = \; (100 \; - \; U) \, p_{max} \tag{9.1}$$

The intermediate consolidation steps are summarized in table 9.2.

Table 9.2: Degrees of Consolidation

Calculation	Consolidation [%]
1	0
2	25
3	50
4	75
5	99

9.1.4 Force in the Column

In order to compare existing arching theories by i.a. Hewlett and Randolph (1988) the force in the sand columns should be determined. PLAXIS does not include a tool or function to determine the force in a columnar soil reinforcement. Only when an embedded beam is used the structural force may be determined, it is however not assumed to be a valid modeling technique. The method of force calculation is elaborated in chapter J.

9.1.5 Phases

There are multiple phases used for the consolidation analyses. The phases are described in table 9.3.

Table 9.3: Calculation Phases for the long-term analysis

Phase 1	Phase 2
In the first phase the PLAXIS K_0 procedure is employed. During this phase PLAXIS determines the initial stresses in the model based on K_0.	The second phase comprises of a zero-step. In this step undrained behavior is ignored. Ignoring undrained behavior implies that the consolidation is finished and that there are no excess pore pressures in the soft soil. The result of this phase is used as a zero reading for the effective stress (before loading).
Phase 3	**Phase 4-7**
In this phase the load uniformly distributed load of 100 kPa is activated. For this phase an undrained analysis is performed. Since the previous phase was drained there are no excess pore pressures in the model. The excess pore pressures increase to 100 kPa in this phase however.	After the undrained analysis of the previous phase, the soft soil starts to consolidate in this phase. There are four consolidation intervals, described in table 9.2. These are subsequently calculated in phases 4 through 7.
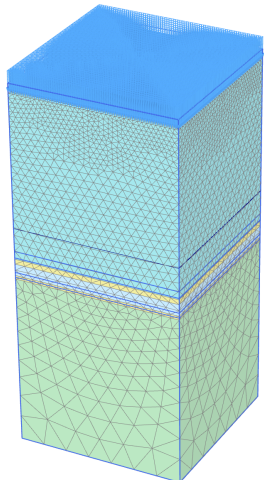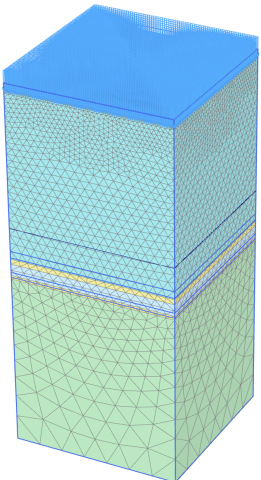
9.2 Calculations

For the long-term analysis no parametric analyses were performed. Calculations varying platform height and column spacing were carried out. Also a set of calculations where no sand columns were present was analyzed.

The reader is reminded that efficiency is defined as the portion of the total vertical stress over an area (which is a force) in a grid cell that is transferred to the column relative to the (vertical) soil stress integrated over the grid cell area. Efficiency was defined in equation 2.6. An incremental arching effect due to the introduction of a distributed load can be defined using equation 9.2.

$$\Delta E \;=\; 1 \;-\; \Delta SRR \, \frac{s^2 \;-\; \pi \, d^2}{4s^2} \;=\; 1 \;-\; \Delta SRR \, (1 \;-\; \alpha) \tag{9.2}$$

Where:
ΔE	= Incremental efficiency;
ΔSRR	= Incremental Soil Stress Reduction;
s	= Column spacing;
d	= Column diameter;
α	= Replacement ratio, $\frac{A_c}{s^2}$.

For a more elaborate description of the terms in equation 9.2 reference is made to equation 2.6.

A more elaborate description of equation 9.2 can be found in section 2.3.3. The efficiency based on SRR is elaborated in equation 2.10, which can also be found in the aforementioned section.

9.2.1 Consolidation with Columns

PLAXIS allows for different cross-sections to determine stress/strain behavior in multiple sections. Using these cross-sections at varying consolidation times, one can determine the behavior of the CSE during loading. This behavior is elaborated below. Please note that when cross-section A-A* is mentioned a vertical section through the center of the column is meant. Cross-section B-B* is a horizontal section through the interface between the sand platform and soft soil. The cross-sections are shown in figure 9.1.
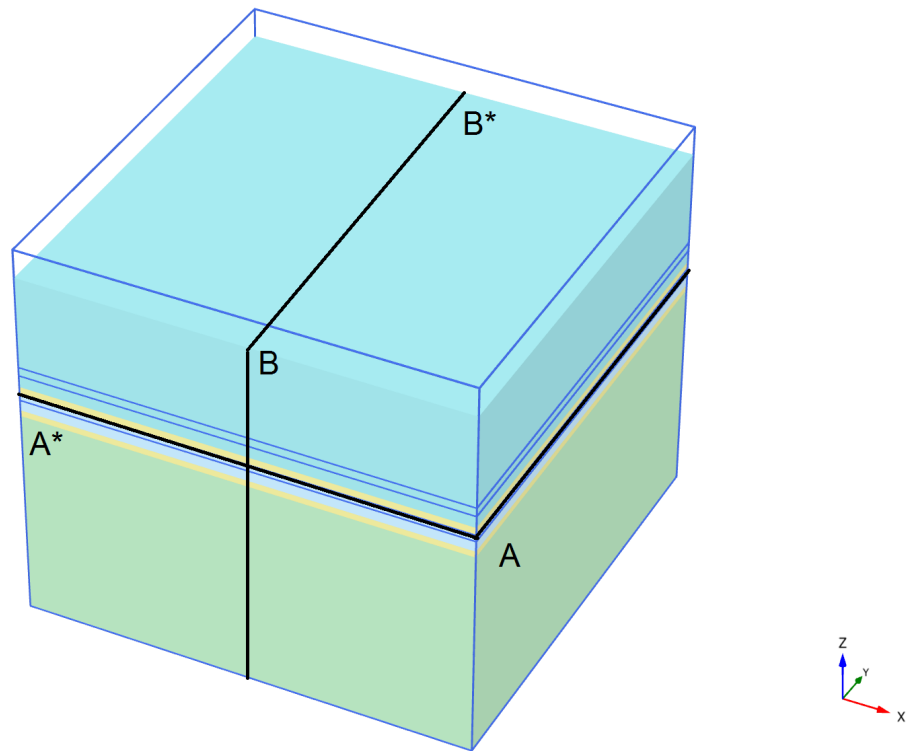
Figure 9.1: Cross-section locations A-A* and B-B*

0% Consolidation

The stress imposed by the distributed load is carried by the water. It can be seen in figure 9.2 that the excess pore pressure in the clay layer is approximately 100 kPa, which is equal to the distributed load. Note that near the columns the consolidation starts.
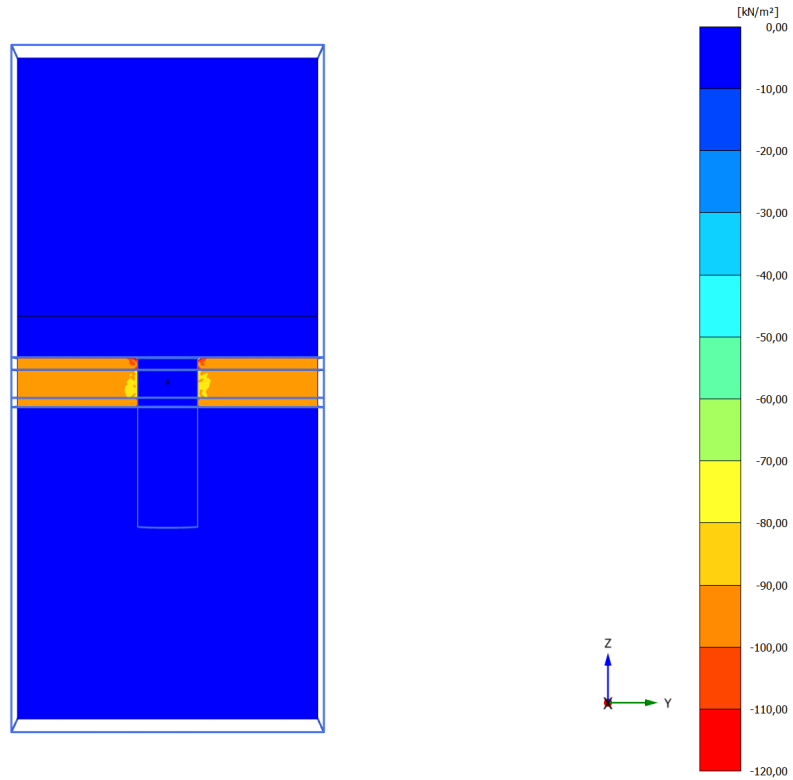
Figure 9.2: Pore pressures in cross-section B-B*

It can be seen in figure 9.3 that the excess pore pressure in the sabkha and silt leads to a (inwards) lateral displacement of the sand column. A cross-sectional stress distribution of the top of the column is plotted in figure J.2. In this figure it can be clearly observed that the stress is relatively high at the outer ring of the column cap. A horizontal B-B* cross-section is given in figure 9.4.

Total displacements u$_y$ (scaled up 400 times)
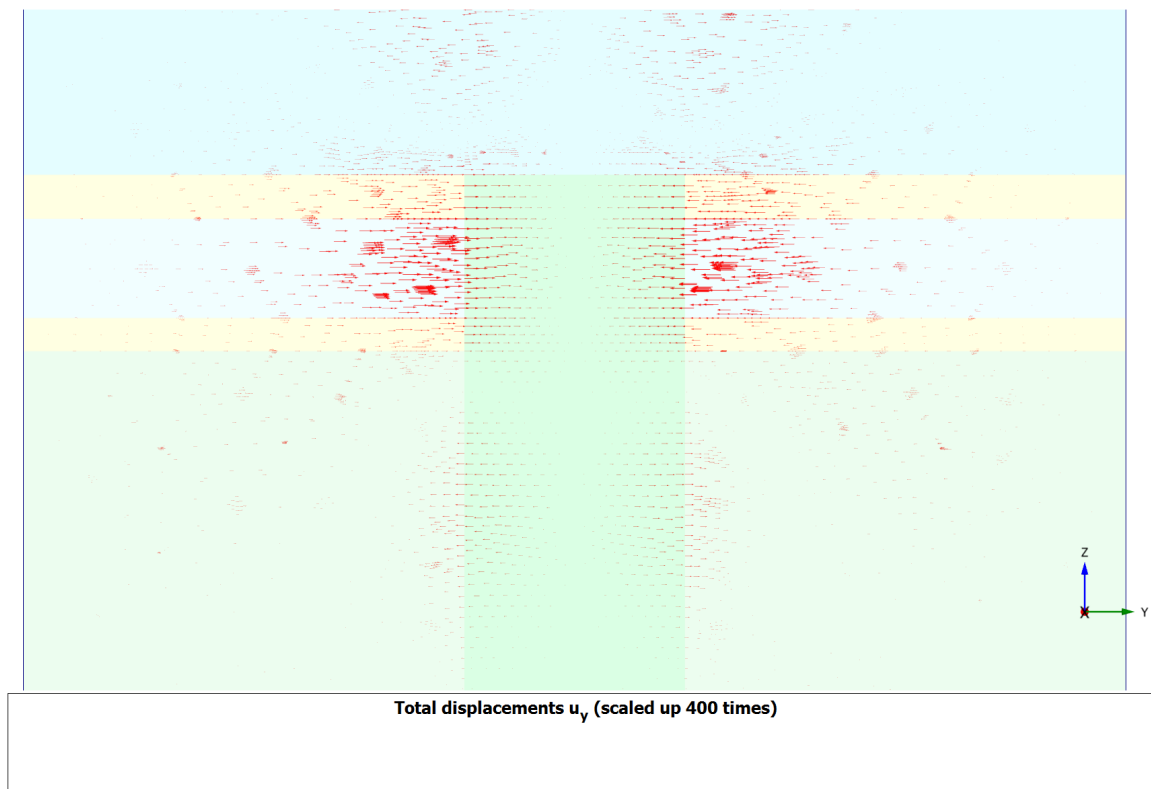
Figure 9.3: Deformation in cross-section B-B* for 0% consolidation

Principal effective stress σ'$_1$
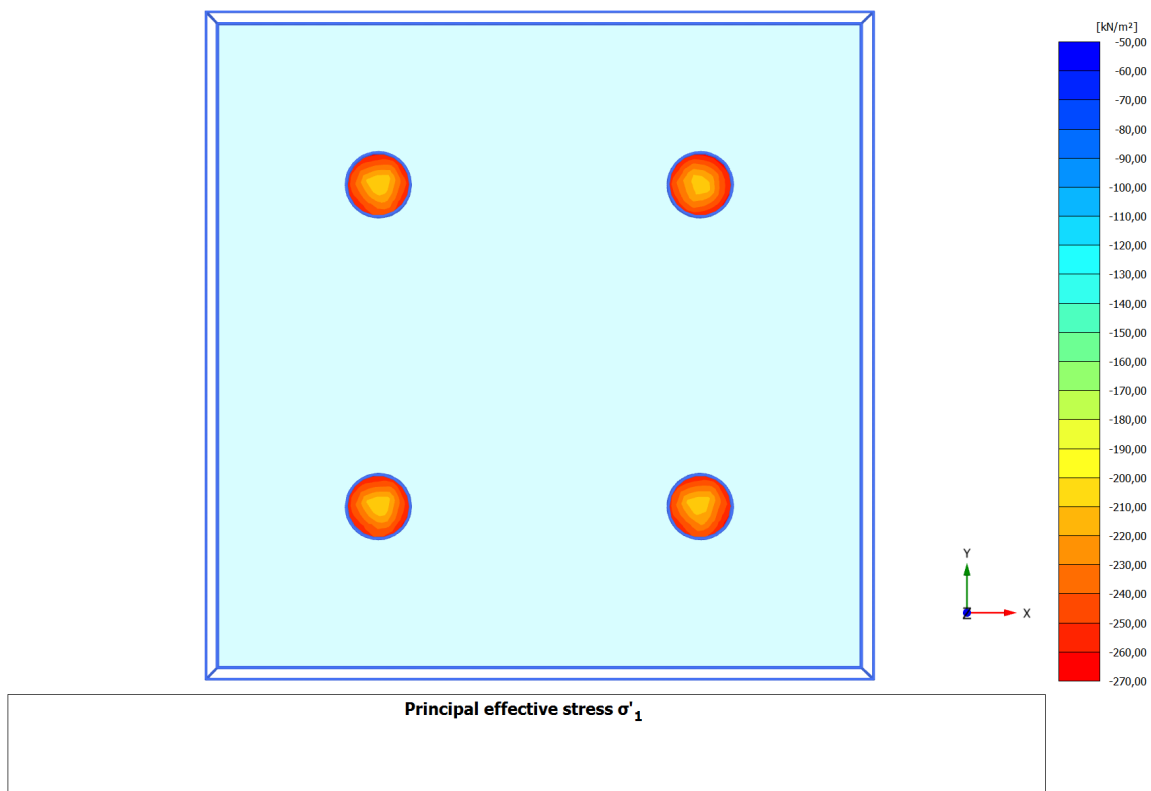
Figure 9.4: Effective stress σ'_1 in cross-section A-A* for 0% consolidation

The effective vertical stress is uniformly transferred through the column to the lower silty sand layer as can be seen in figure 9.5.

Effective principal stresses (scaled up 0,100*10^{-3} times)
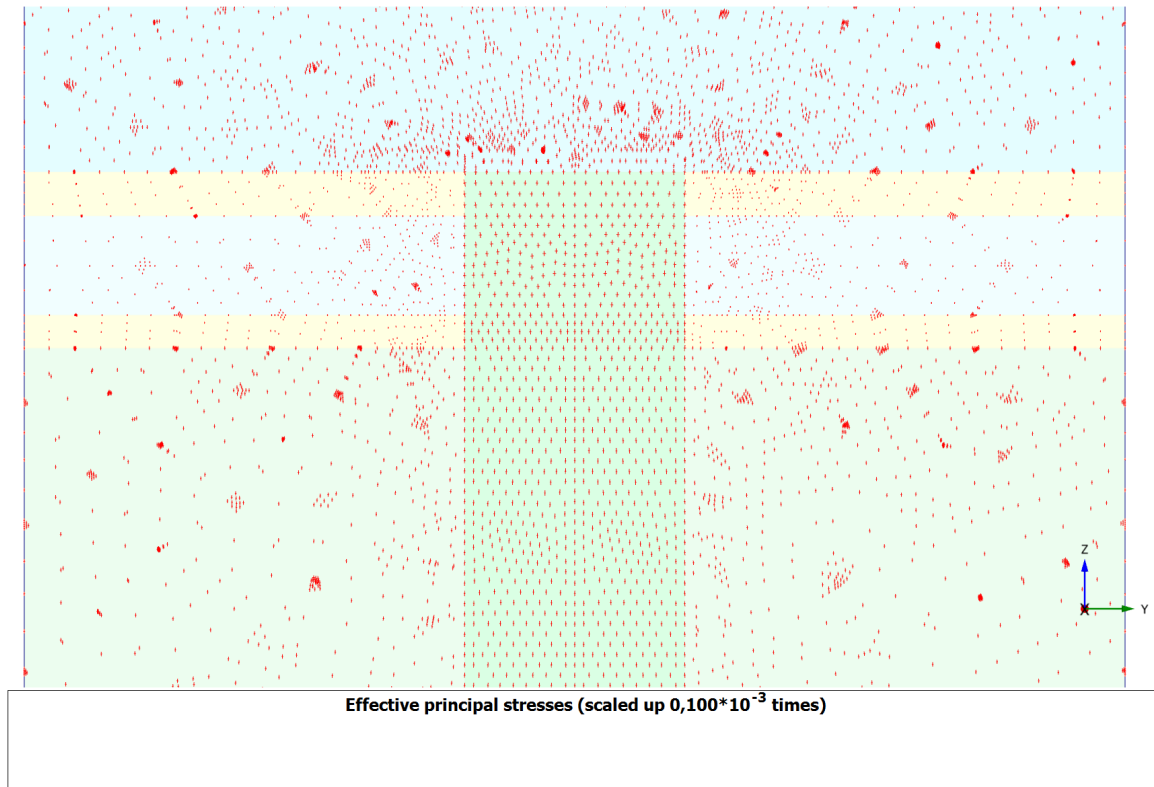
Figure 9.5: Effective stresses in cross-section B-B* for 0% consolidation

50% Consolidation

Figure 9.6 shows that the excess pore pressure decreases at the interfaces with the sand layers, as the permeability of these layers is orders of magnitude higher compared to the soft soil.
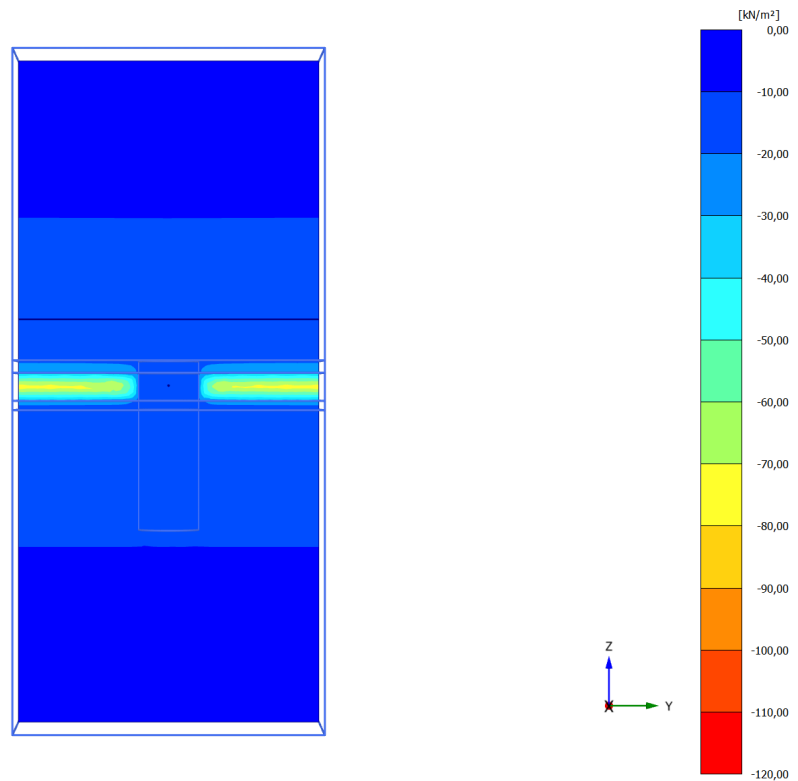
Figure 9.6: Pore pressures in cross-section B-B* for 50% consolidation

Because of the decrease in pore pressure in the soft soil layers, the confining pressure around the sand columns decreases. While the confining stress is lower, the load on the column increases. This results in an outward displacement of the sand column. The vectors of this displacement are shown in figure 9.7. Figure J.3 also illustrates the higher stresses inside the column by means of a cross-sectional stress distribution plot. A horizontal B-B* cross-section is given in figure 9.8.
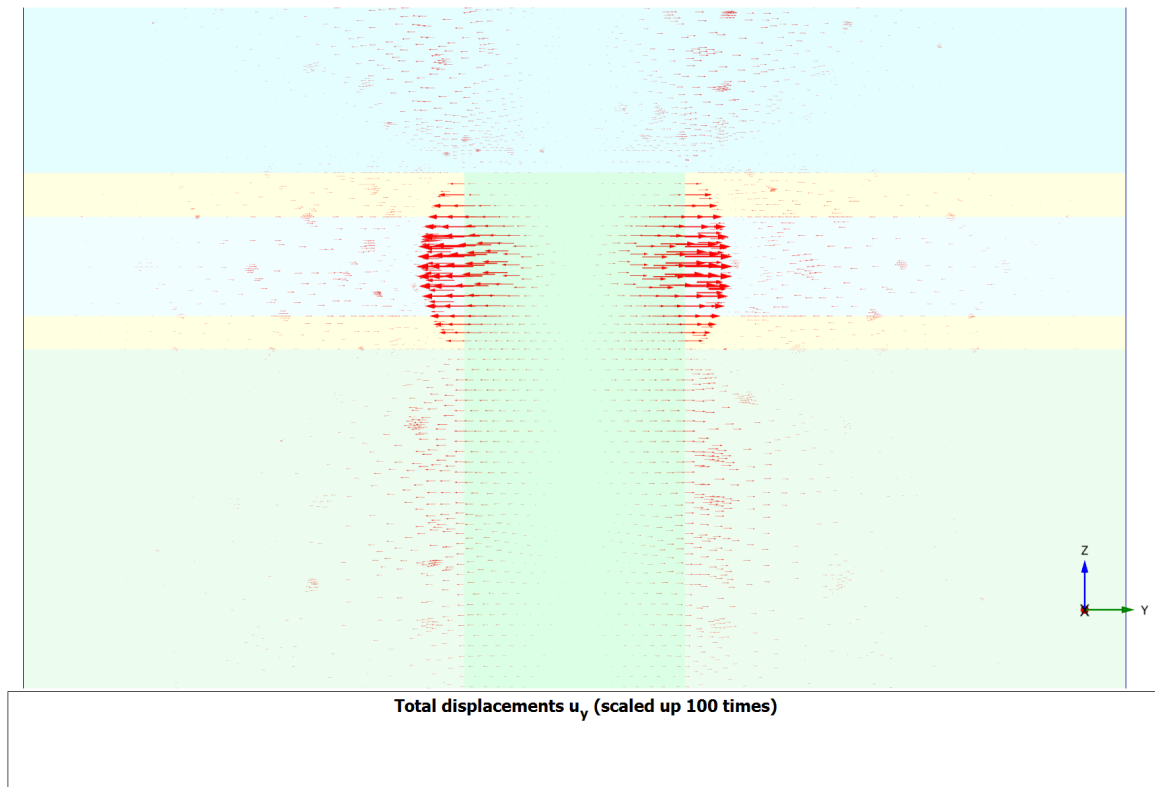
Figure 9.7: Deformation in cross-section B-B* for 50% consolidation
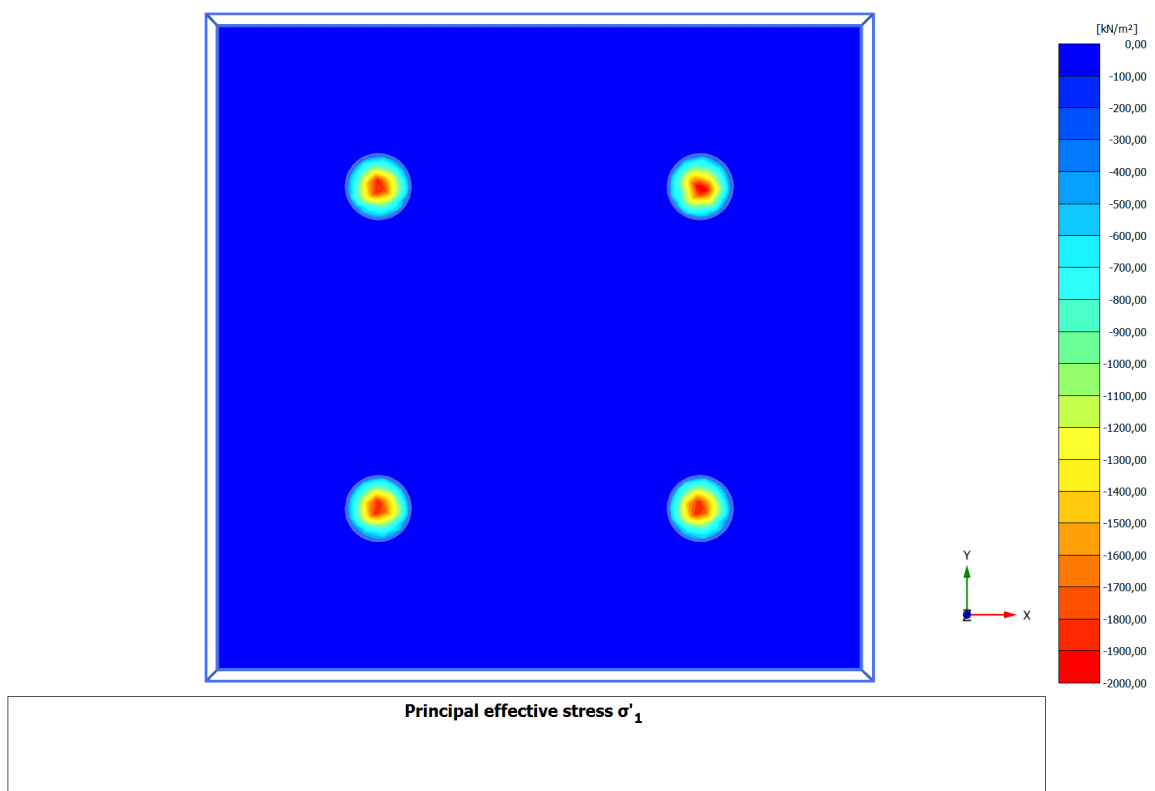
Figure 9.8: Effective stress σ'_1 in cross-section A-A* for 50% consolidation

Because of the outward displacement of the sand column, the stress decreases at the outer ring of the column cap. The core cylinder of the column does not deform as much as the outer ring however. The effective stress in the core cylinder is relatively high compared to the outer ring. The stress concentration in the column cap results in a funnel shape, which can be seen in figure 9.9.

Effective principal stresses (scaled up 0,100*10⁻³ times)
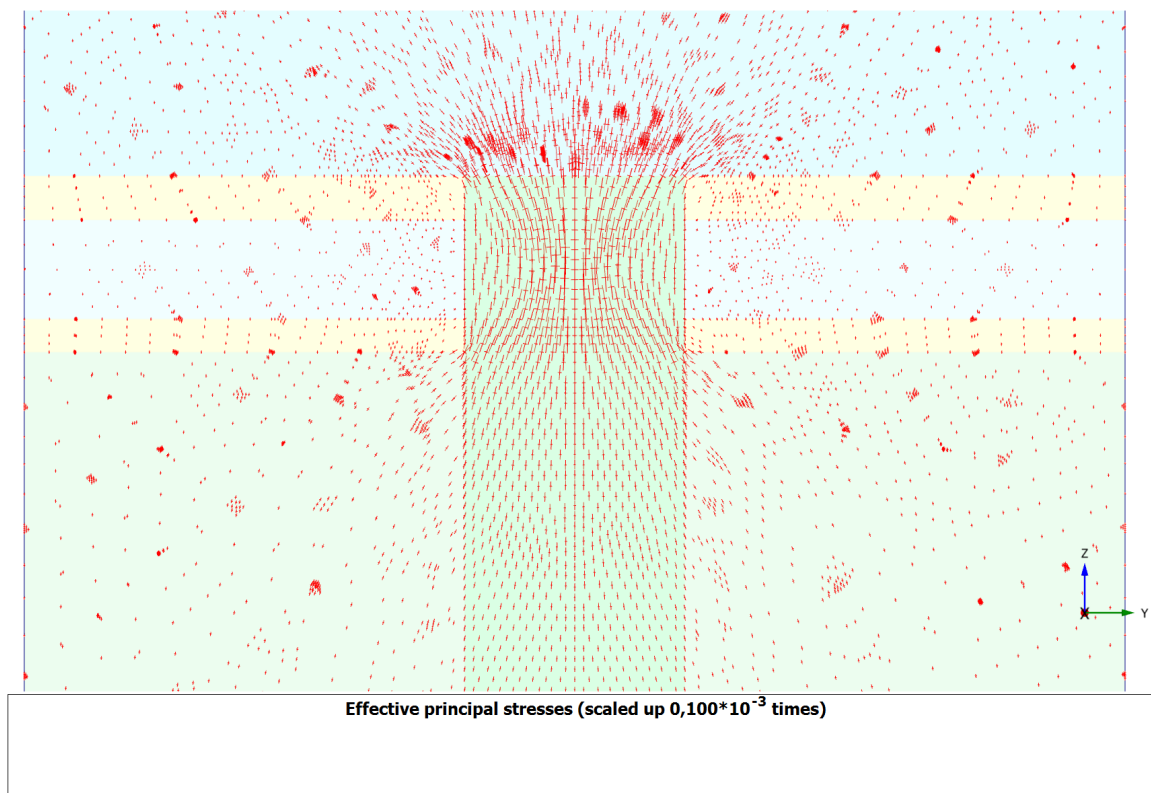
Figure 9.9: Effective stresses in cross-section B-B* for 50% consolidation

99% Consolidation
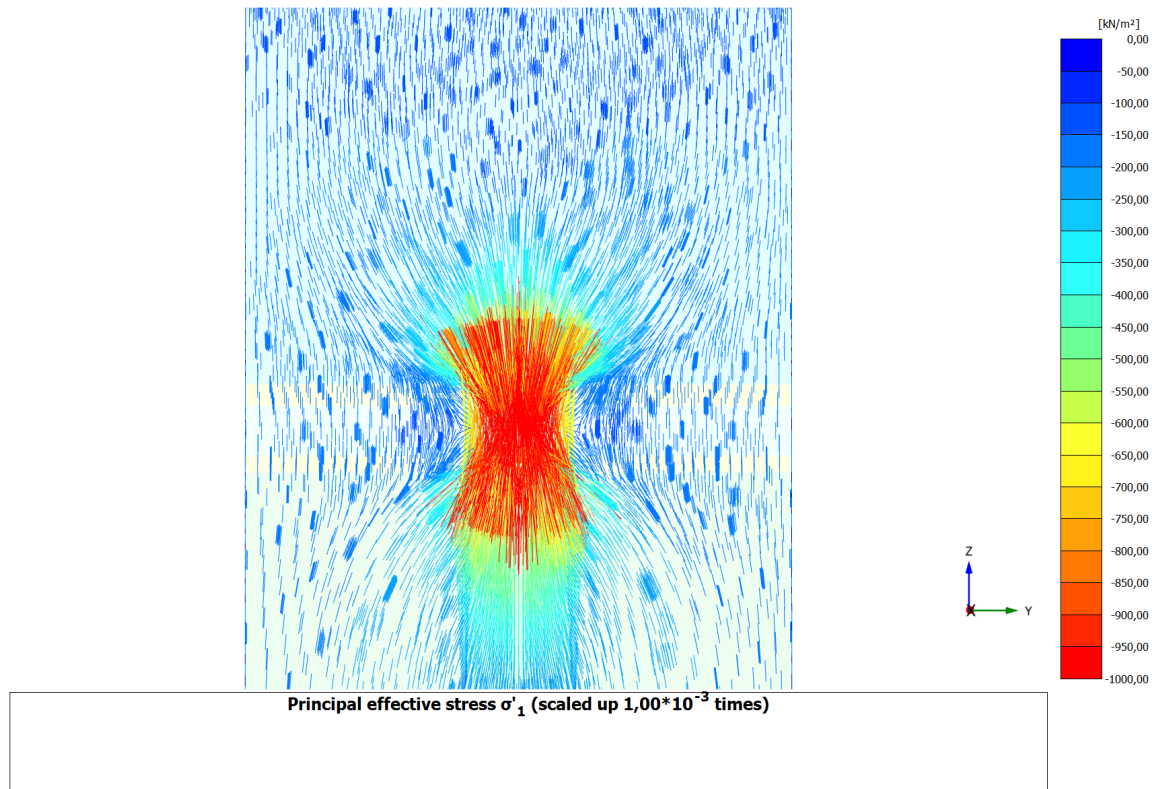
Figure 9.10: Effective stresses in cross-section B-B* for 99% consolidation

Soil Volume

Figure 9.11 shows the volume of soil, marked in red, that is influenced by the presence of a sand column for a spacing of $d = 5$ m. The diameter of the sand volume is approximately 3 times the diameter of the column.
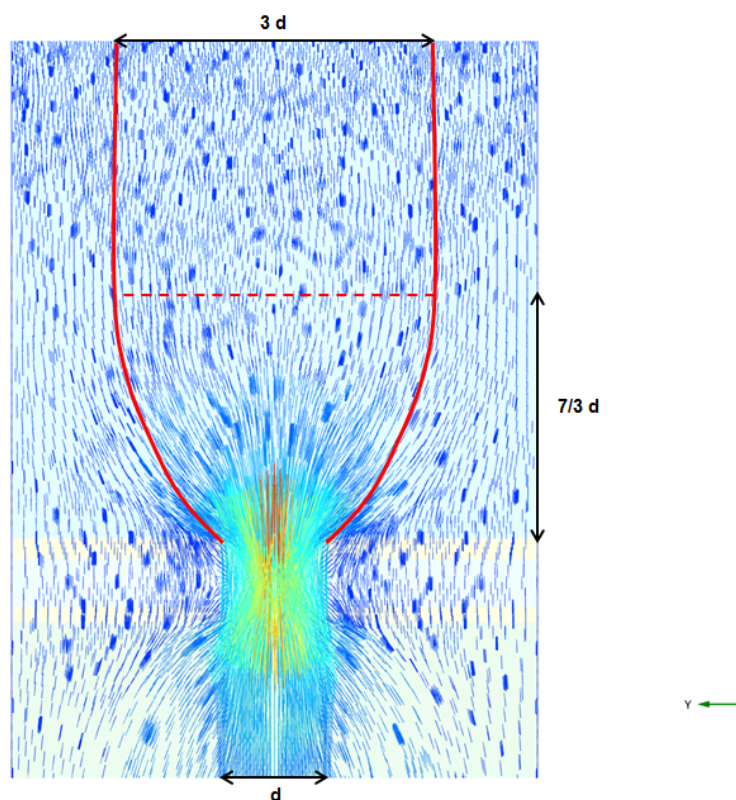
Figure 9.11: Soil volume influenced by the presence of a sand column ($s = 5$ m) at 99% consolidation, cross-section B-B*

The sand volume described above would occupy a cross-sectional area (in the XY plane, see axes in the bottom-right part of figure 9.11) of $3d \rightarrow \frac{9}{4}\pi d^2$. The area relative to the unit cell is then (for $d = 1$ and $s = 5 = 5d$):

$$\frac{A_{c,influence}}{A} = \frac{9}{4}\frac{\pi\, d^2}{25d^2} = \frac{9\pi}{100} = 28.3\% \tag{9.3}$$

9.2.2 Denser Column Spacing

To investigate the influence of a denser column grid, i.e. $s < 5$, three calculations have been performed with $s = 3$ m. The result of these calculations are compared with the results for the spacing of $s = 5$ m in the following sections.

The soil model and consolidation phases are left unchanged. The model geometry is reduced to 3 x 3 m with a column diameter of $d = 1$ m. The behavior of the CSE during consolidation is essentially the same for both column spacings analyzed, for a description of the behavior the elaboration in section 9.2.1 holds.

Soil Volume

In a matter similar to section 9.2.1 the influence area of a column with a spacing of $d = 3$ m can be determined. The plot can be found in figure 9.12.
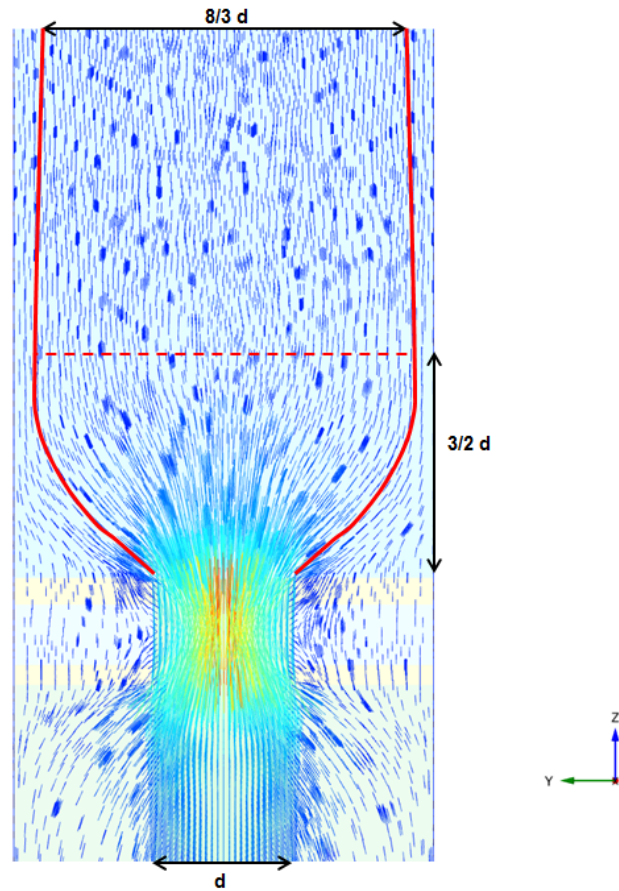
Figure 9.12: Soil volume influenced by the presence of a sand column ($s = 3$ m) at 99% consolidation, cross-section B-B*

The figure shows that the diameter of the area above the column is $\frac{8}{3}d$. The efficiency based on the area, as illustrated in figure 9.12 is calculated using equation 9.3 with $A_{c,influence} = \frac{16\pi}{81} = 62\%$.

9.2.3 Consolidation without Columns

For a selection of geometries Plaxis calculations were run without the sand columns, to compare the improvement relative to the unimproved situation.

The following calculations were run:

Table 9.4: Platform height calculations without sand columns

Calculation	Platform height (m)
1	2.0
2	4.0
3	7.0

It can be seen in figure 9.13 that no more than the at-rest horizontal stress (determined by K_0 rather than K_{krit} or K_p) develops in the cross-section. Contrary to the calculations with a sand column, where significant horizontal stress was developed due to arching effects, the horizontal stress is equal to $\sigma'_h = K_0 \, \sigma'_v$.

TUDelft

The results of the calculation with a platform height of 2.0 m will be given in the following section. The results of the calculations for different platform heights will be given along with the results of the other calculations.

Platform height 2.0 m

Figure 9.13 shows an B-B* cross-section of the principal effective stress.
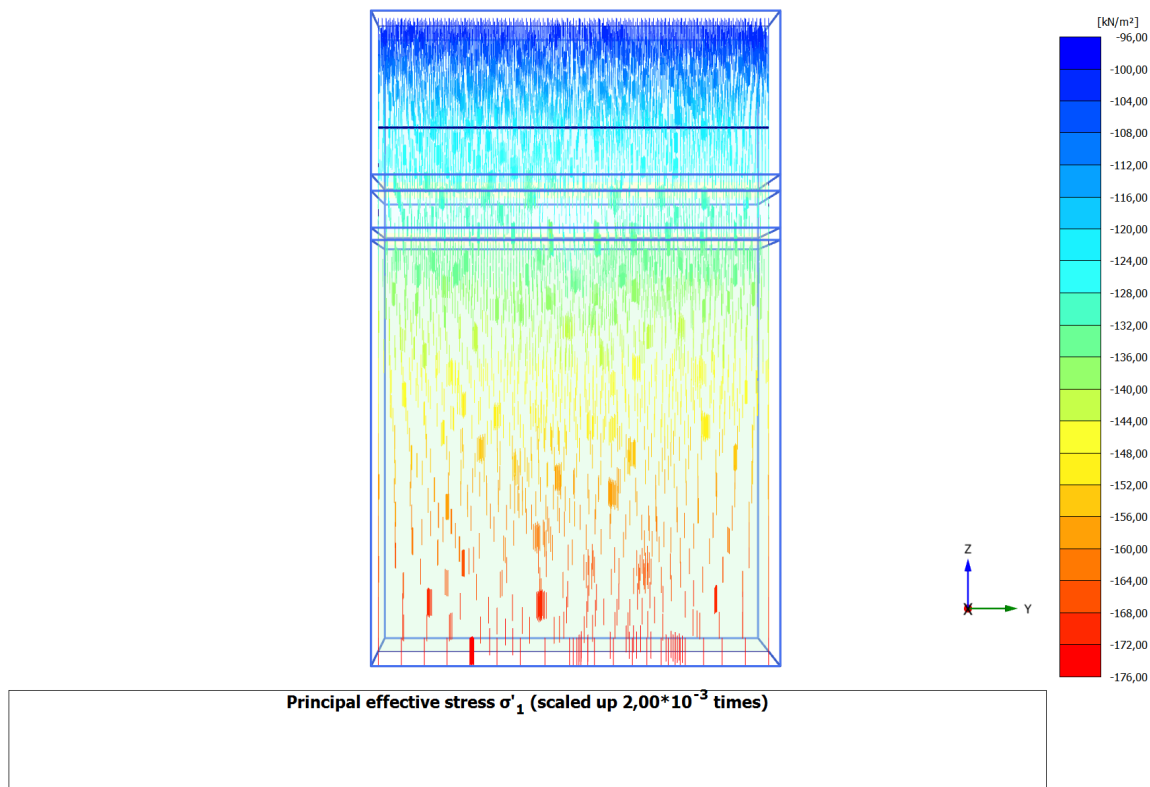
Figure 9.13: Effective stresses in cross-section B-B* for 99% consolidation

It can be seen in figure 9.14 that the vertical stress is nearly uniform over cross-section B-B*. The average effective vertical stress at 99% consolidation in this cross-section is 127.5 kPa.
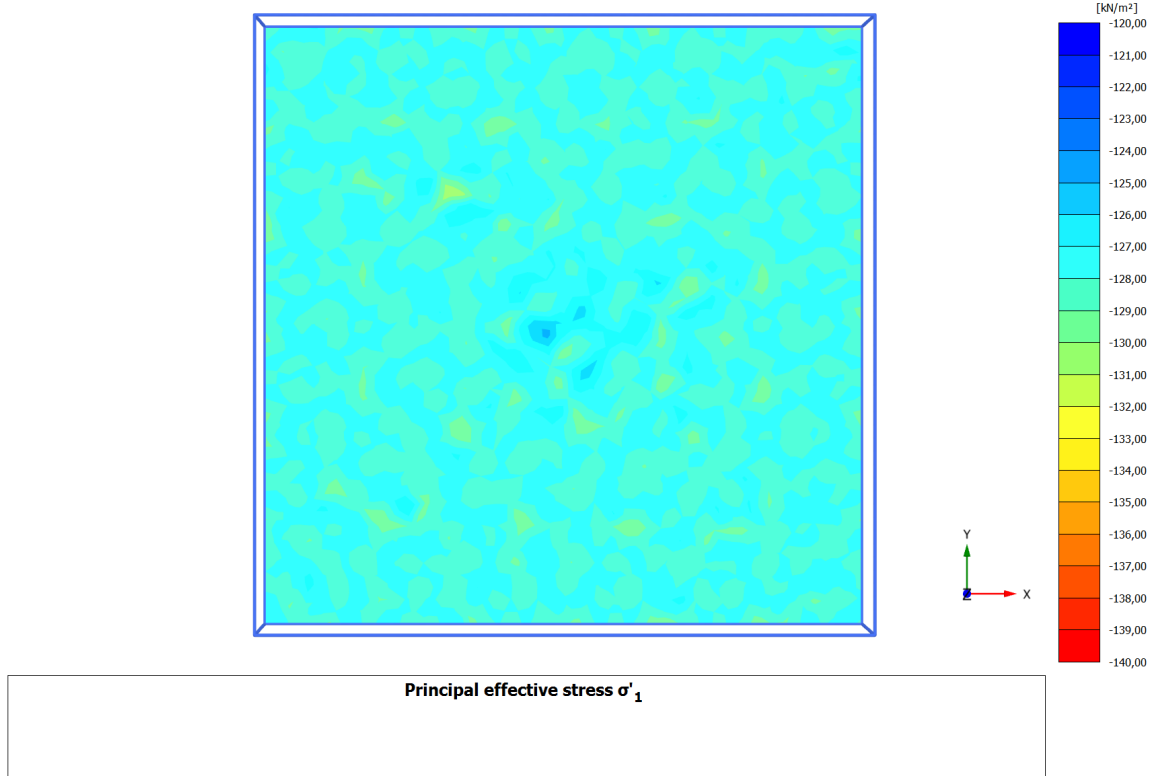
Figure 9.14: Effective stresses in cross-section A-A* for 99% consolidation

9.2.4 Combined Results

The calculations varying the platform height and column spacing are summarized in table 9.5.

Table 9.5: Platform height calculations

Calculation	Platform height (m)	Spacing (m)	ζ [-]
2.0	2.0	5.0	0.50
3.0	3.0	-	-
3.1	3.0	3.0	1.50
3.2	3.0	5.0	0.75
4.0	4.0	5.0	1.00
5.0	5.0	-	-
5.1	5.0	3.0	2.50
5.2	5.0	5.0	1.25
6.0	6.0	5.0	1.50
7.0	7.0	-	-
7.1	7.0	3.0	3.50
7.2	7.0	5.0	1.75

Stress Reduction Ratio

The results of the calculations with columns are compared with the set of calculations without sand columns to determine the incremental SRR. The results are summarized in table 9.6.

Table 9.6: Stress Reduction Ratio

Platf. height (m)	No columns $\sigma'_{s,U=0\%}$ (kPa)	$\sigma'_{s,U=99\%}$ (kPa)	$s=3$ $\sigma'_{s,U=0\%}$ (kPa)	$\sigma'_{s,U=99\%}$ (kPa)	ΔSRR (%)	$s=5$ $\sigma'_{s,U=0\%}$ (kPa)	$\sigma'_{s,U=99\%}$ (kPa)	ΔSRR (%)
0.0	0.00	99	0.00	100	99.0	0.00	100	99.0
1.0	10.45	110.9	10.45	80.1	69.6	10.45	105.1	94.6
2.0	27.66	127.9	27.66	77.2	49.3	27.66	108.4	80.3
3.0	44.80	144.8	44.80	91.2	46.4	44.80	118.59	73.8
4.0	-	-	-	-	-	61.89	135.64	73.7
5.0	78.99	178.6	78.99	124.1	45.1	78.99	152.64	73.6
6.0	-	-	-	-	-	96.08	169.55	73.5
7.0	113.2	212.8	113.2	157.2	43.7	113.2	186.59	73.4

Note that the σ_s and ΔSRR for $H=0$ are (conservative) estimates rather than PLAXIS results.

Efficiency

The efficiency is determined for both the $s=3$ and 5 m calculations and given in table 9.7.

Table 9.7: Efficiency calculation results

Platform height (m)	$s=3$ ΔE (%)	$s=5$ ΔE (%)
0.0	8.7	3.1
1.0	36.5	8.4
2.0	55.0	22.2
3.0	57.6	28.5
4.0	-	28.6
5.0	58.8	28.7
6.0	-	28.8
7.0	59.4	28.9

Note that the efficiencies for $H=0$ are based on the area ratio α rather than PLAXIS results, the exact results for ΔE are 100α, with $\alpha = \frac{\pi}{36}$ for $s=3$ m and $\alpha = \frac{\pi}{100}$ for $s=5$ m.

Figures 9.15 and 9.16 show the stress distribution for $H=3$ and 5 m and $s=5$.
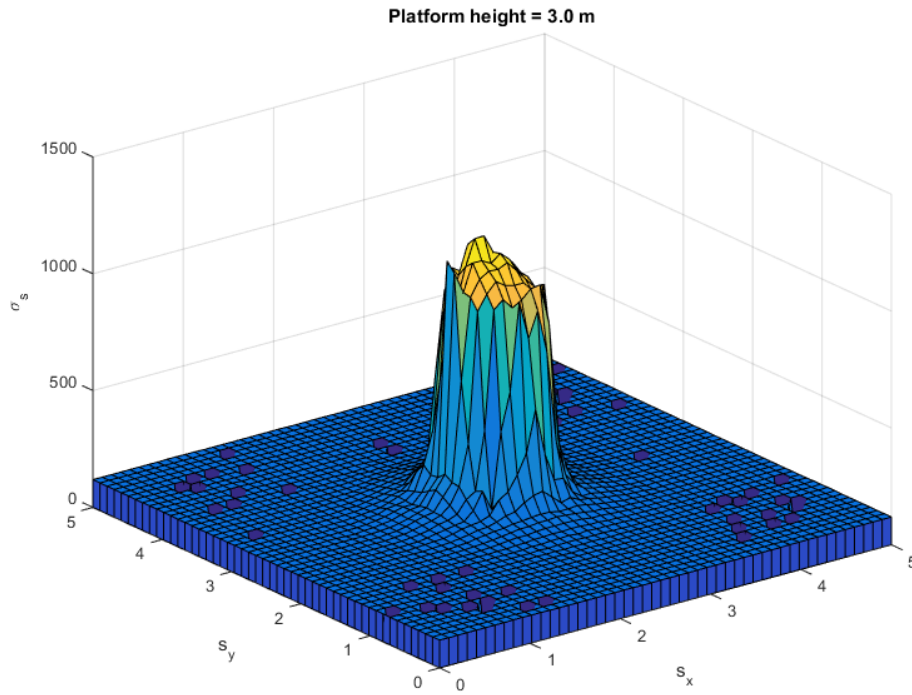
Figure 9.15: Stress distribution for $H = 3$ m
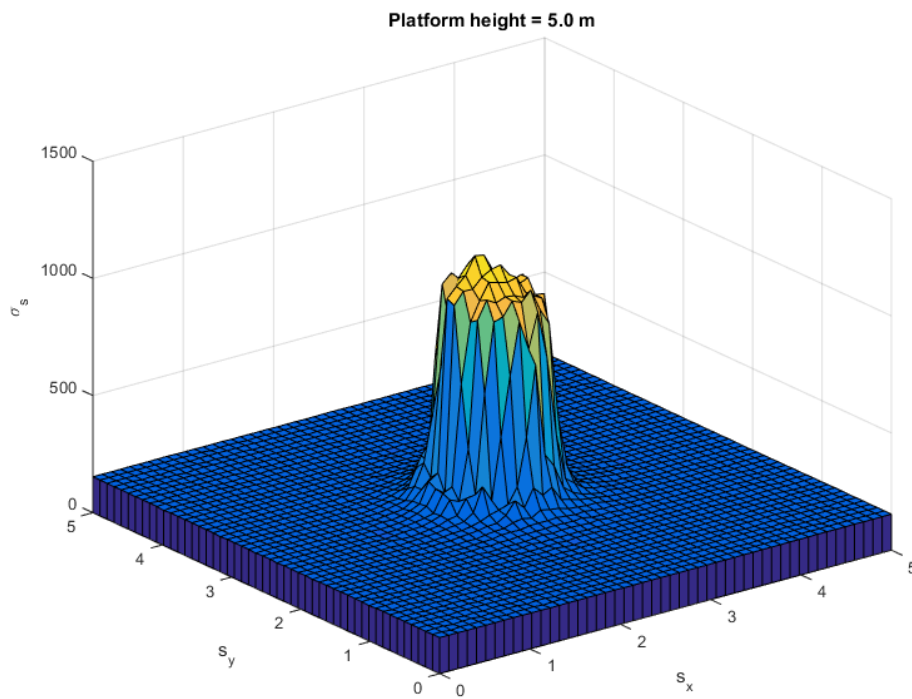
Figure 9.16: Stress distribution for $H = 5$ m

Settlement Reduction Ratio

The results of the calculations with columns are compared with the set of calculations without sand columns to determine ΔS_r. The results are summarized in table 9.8.

Table 9.8: Settlement Reduction Ratio

Platform height (m)	ΔU_z^* (mm)	$s = 3$ ΔU_z (mm)	ΔS_r (%)	$s = 5$ ΔU_z (mm)	ΔS_r (%)
1.0	75.4	61.0	17.1	71.1	5.8
2.0	57.6	38.1	34.0	51.0	11.5
3.0	48.6	31.1	36.2	41.5	14.6
5.0	39.0	25.5	34.5	33.5	14.0
7.0	34.4	23.0	33.1	29.5	12.2

9.3 Plotted Results

The increase in effective stress, is given for multiple platform heights at multiple consolidation intervals, in figure 9.17. Note that the σ_s increase in figure 9.17 is due to the distributed load on top of the surface, so the σ_s value at x-axis $= 0$ represents the stress before activating the 100 kPa.
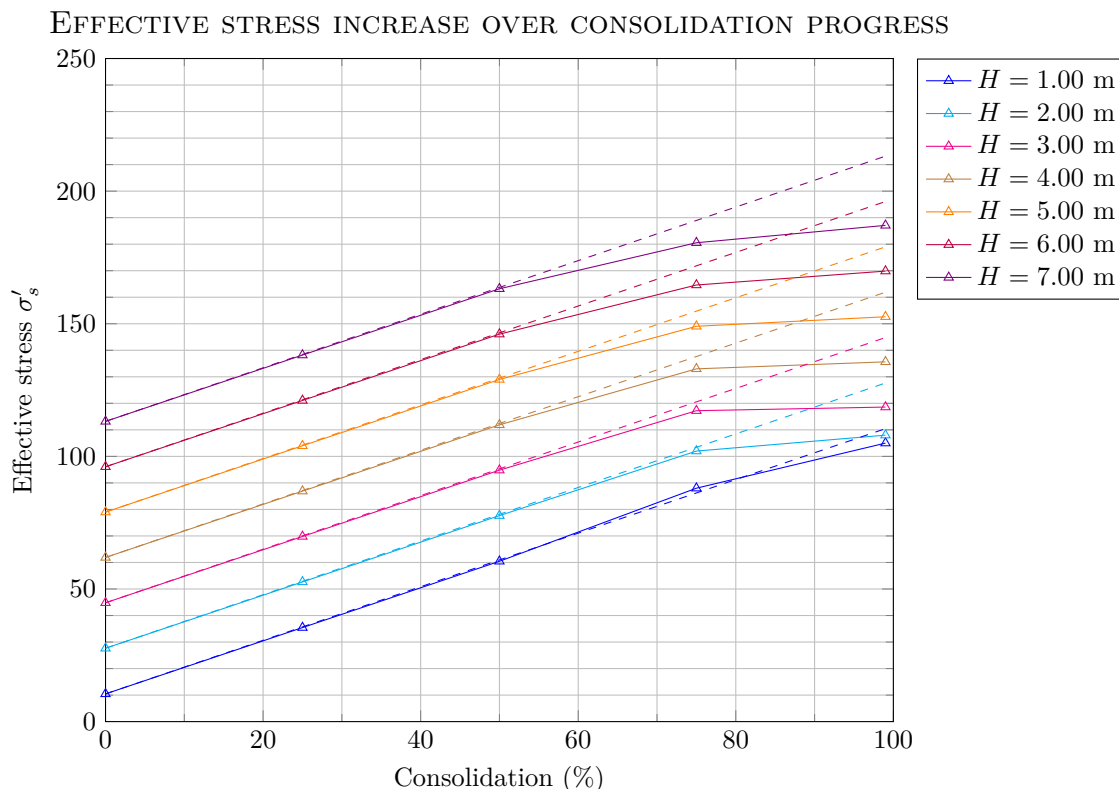
Figure 9.17: Effective stress increase with consolidation progress, dashed lines represent the normal consolidation line

It can be seen in figure 9.17 that the plots for the varying platform height are almost linear for low embankment heights. When H increases the stress increase under consolidation follows a different path however. For $H = 3$ there is a sharp increase of effective stress at 50% consolidation. That sharp increase is less prominent for higher values of H. The plots seem to flatten out after 50% consolidation, meaning that most of the stress is drawn to the column rather than the soft soil.

For $H = 1$ m the stress increase follows approximately the normal consolidation line. It can be seen there there is a slight improvement at the end, leading to an efficiency just over α.

Figure 9.18 shows the effective stress increase with platform height for $s = 5$, $s = 3$ is shown in figure 9.19. On the second vertical axis the efficiency is plotted.
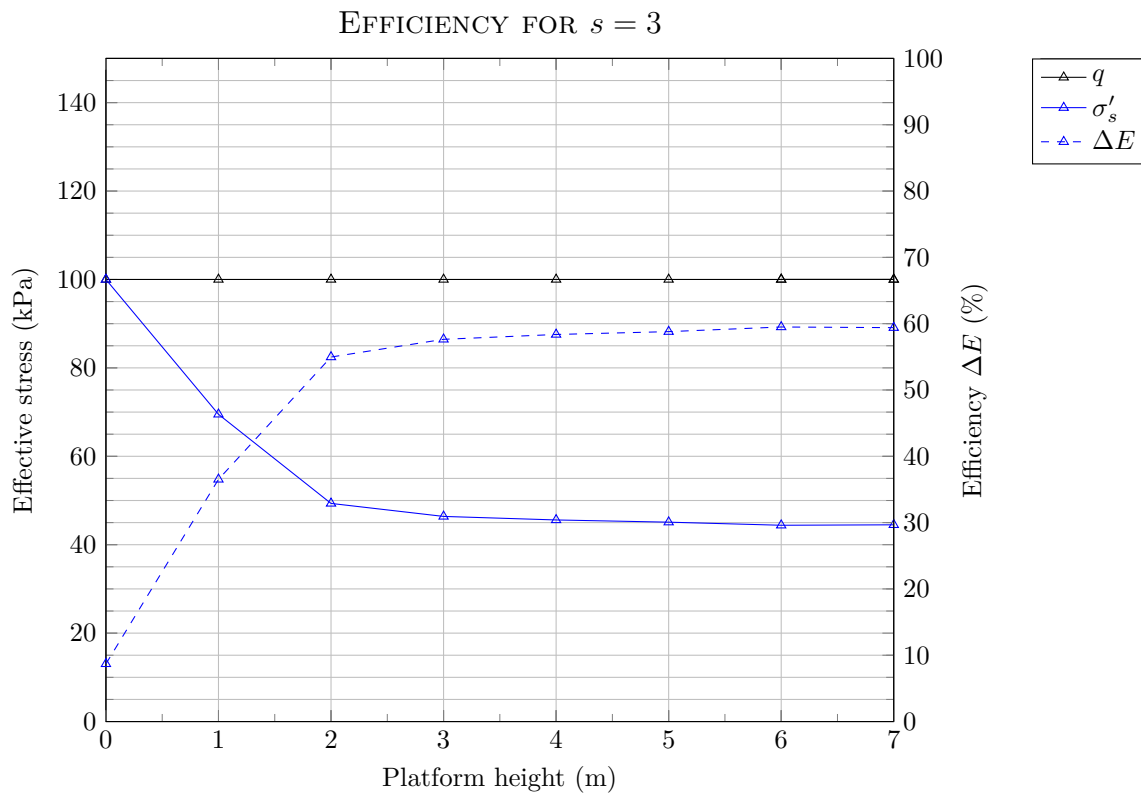
Figure 9.18: Effective stress and efficiency increase with platform height for $s = 3$
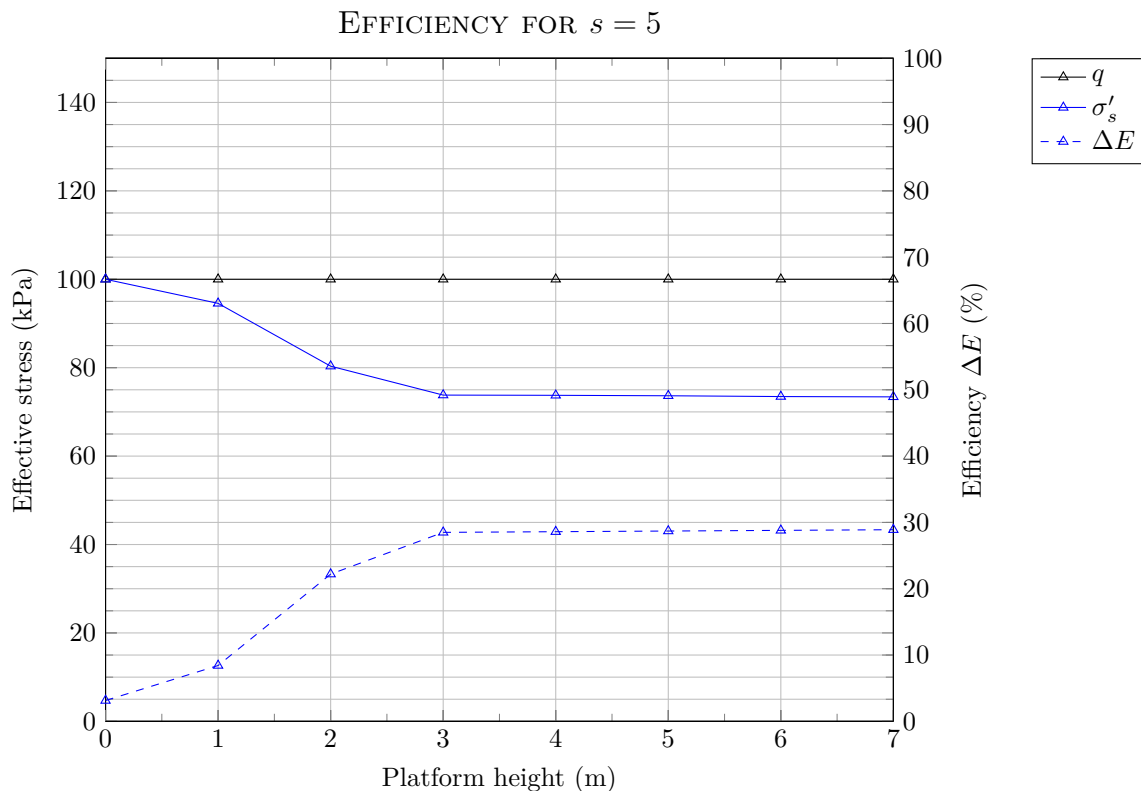
Figure 9.19: Effective stress and efficiency increase with platform height for $s = 5$

One should keep in mind that the plot shown in the figure above is a straight line drawn between points. The effective stress decreases starting at $H > 0$ which may be too abrupt.

Figure 9.20 shows the Settlement Reduction Ratio for both $s = 5$ and $s = 3$.
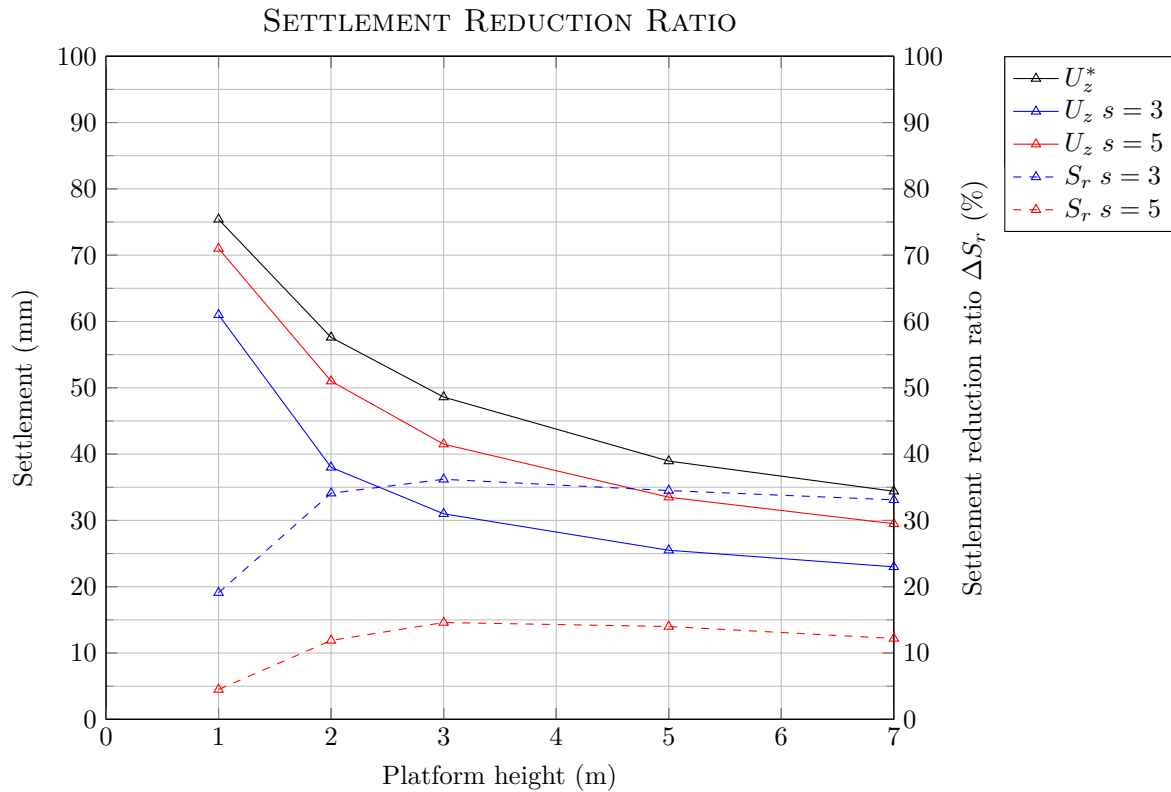
Figure 9.20: Settlement reduction ratio with platform height for $s = 3$ and $s = 5$ m

9.4 Analysis

While there is a significant stress transfer to the sand columns, as evidenced by the efficiency values in table 9.7, no full arches between columns are observed.

9.4.1 Column Spacing

It can be seen in tables 9.6 and 9.7 that the SRR is lower for a denser column grid, while the efficiency is higher. This means that a CSE with a spacing of $s = 5$ is less efficient than a CSE with a spacing of $s = 3$ in terms of stress transfer. The absolute values of the force in the column will be lower in a denser grid, however the amount of force relative to the coarser embankment is higher. This is an important observation since the settlement is greatly dependent on stress transfer. If the amount of stress that is transferred to the column is relatively high, the total settlement will be governed by the stiffness of the sand columns. The stiffness of sand is generally significantly higher than the stiffness of clay (see e.g. chapter 7) and would thus lead to less settlement.

9.4.2 Settlement

It was already stated in section 9.1 that the settlement due to the placement of the sand platform is not taken into account. Instead, all the settlement that is considered is the settlement due to the introduction of an uniformly distributed load of 100 kPa. This led to a incremental settlement S_r. It should be noted that when the sand platform is placed, high settlements are expected. The settlement will be higher for increasing platform heights. Because of the stiffness improvement in a CSE, this settlement (due to the weight of the platform) will be lower than in an unimproved situation. Based on these assumptions, S_r would increase with an increasing platform height.

If the settlement imposed by the weight of the sand platform is ignored, the settlement due to the distributed load will be governed by the settlement in the sand platform. When the platform height is

increased, the settlement will be lower because the soft soil was already consolidated by the relatively thick sand platform. The calculations where no sand columns were present - the zero calculations - thus provide an underestimate of the settlement. As U_z^* is in the denominator in the ΔS_r calculation, the ratio will increase while this may not be very realistic.

When the sand platform continues to increase in height, the effective stress in the soft soil under the platform decreases rapidly. ΔS_r approaches 1.0 for $\lim_{H \to \infty}$, because only the settlement in sand is then considered.

9.4.3 Efficiency

When the efficiency based on the soil volume, as shown in figure 9.11, is compared with the efficiency based on the calculation in equation 9.3, the values are close. This implies that the volume drawn in figure 9.11 may be a fairly accurate illustration of the sand volume that is borne by the column.

For $s = 3$ m the efficiency based on the soil volume shown in figure 9.12 equals 62%, that is approximately 3% higher compared to ΔE based on σ_s.

10

Analytical Calculations

Section 2.5.3 elaborated the critical height recommendations for several standards and theories. The recommendations are compared with the PLAXIS calculations in the first section of this chapter.

In sections 2.3.5 and 2.3.6 a description of the methods by Hewlett and Randolph (1988) and Zaeske (2001) was given. Also, a method based on the stiffness ratio m was described. This chapter elaborates calculations based on these three methods, slightly adapted to represent the incremental efficiency ΔE.

10.1 Critical Height

The recommendations concerning critical height are given in table 10.1, including the results from PLAXIS calculations.

Table 10.1: Summary of critical height design recommendations

Standard/recommendation	Critical height (m)	$s = 3$ (m)	$s = 5$ (m)
PLAXIS	$\frac{3}{2}d$, $\frac{7}{3}d$	1.5	2.33
British Standard 8006	$H \geq 0.7(s_x - a)$	1.4	2.8
EBGEO	$H \geq 0.8(s_d - d)$	2.6	4.9
CUR226	$H \geq 0.66(s_d - d)$	2.1	4.0
Concentric Arches	$H \geq 0.5s_x$	2.5	1.5
Filz et al. (2012)	$H \geq 1.15s' + 1.44d$	2.9	4.6
Jenck et al. (2007)	$\frac{H}{s-a} = 1.3 \leq \frac{H}{s-a} = 2.0$	2.6-4	5.2-8

The PLAXIS results shown in 10.1 suggest that the critical height decreases with a decrease of column spacing s, which is in line with the recommendations.

Except for the Concentric Arches model, all recommendations overestimate the critical height. The reader is reminded that the critical height as determined by the recommendations is based on a plane of equal settlement, described in 2.5. The critical height from the PLAXIS calculations is based on maximum efficiency. While these two parameters are interrelated, it may not be suitable to compare the results one on one.

10.2 Design Plots Hewlett (1988)

The efficiency calculation by Hewlett and Randolph (1988) is described in the main report. The variables in Hewlett's equations (given in equationB.2 and B.3) are b, s, H, φ, γ. For the plots given in this chapter the following values given in table 10.2 have been used.

Van Oord
Marine ingenuity

Table 10.2: Variable values for the Hewlett calculations

Variable	Unit	Value
b	m	1
s	m	3.0, 5.0
H	m	0 - 15
φ	°	38
γ	kN/m^3	17.13

The method was modified to represent ΔE rather than E in section B.3.1.

The design plots for $s = 3$ and $s = 5$ are given in figure 10.1.
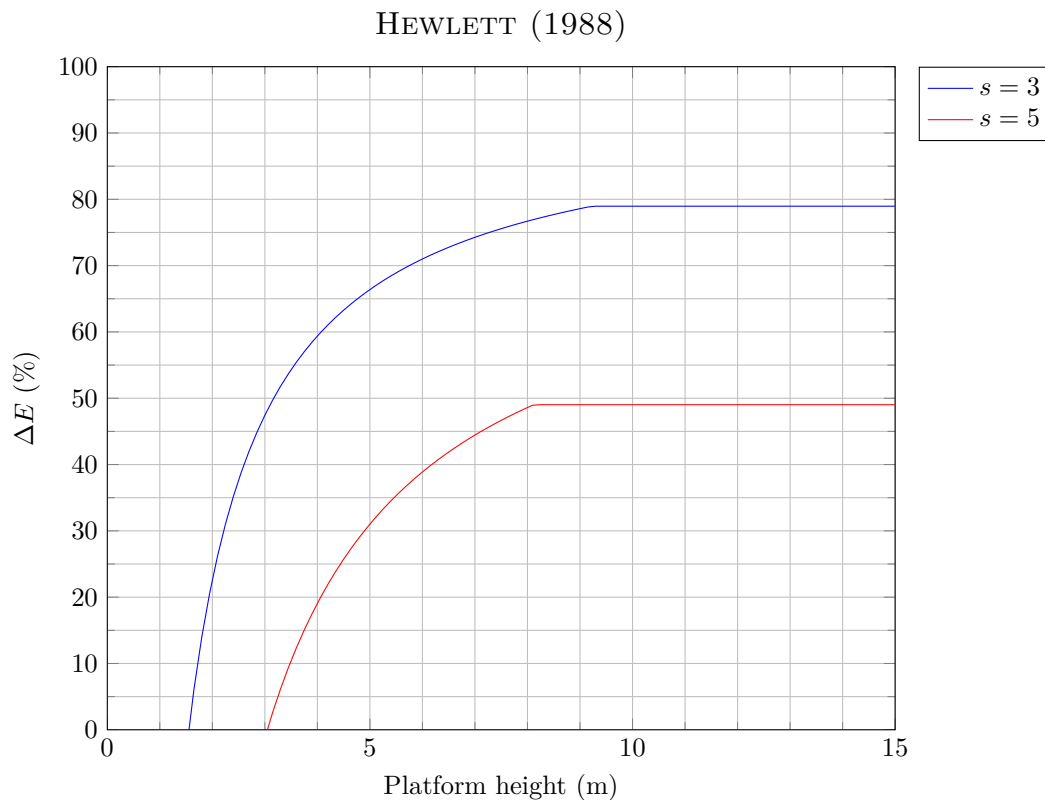
Figure 10.1: Hewlett's design plots for $s = 3$ and $s = 5$ m, $H = 0 - 15$ m and $\varphi = 38°$

It can be observed in figure 10.1 that the efficiency is determined by the equilibrium in the crown rather than at the column cap. The plots imply that soil improvement (arching) develops at platform heights greater than 1.25 m for a column spacing of 3 m. The maximum efficiency for a platform of 10 m is approximately 88%, which is quite high.

Figure 10.1 also shows that at greater column spacings, i.e. 5 m in this case, the efficiency is determined by the crown up to a platform height of 8 m. For higher platforms, the efficiency is determined by the column cap equilibrium. The figure implies that the minimum platform thickness should be 3 m in order to develop (partial) arching.

10.3   Design Plots Zaeske (2001)

The efficiency calculation by Zaeske (2001) is described in the literature study. The variables in Zaekse's equation (given in equation:B.6) are d, s, q, H, H_g, φ, γ. It was shown in section B.4.1 that neither the efficiency nor the incremental efficiency change for a varying q. The values that are used for the plots in figure 10.2 are summarized in table 10.3.

TUDelft

Delft
University of
Technology

Table 10.3: Variable values for the Zaeske calculations

Variable	Unit	Value
d	m	1
s	m	3.0, 5.0
q	kPa	100
H	m	0 - 15
H_g	m	1.5, 2.5
φ	°	38
γ	kN/m³	17.13
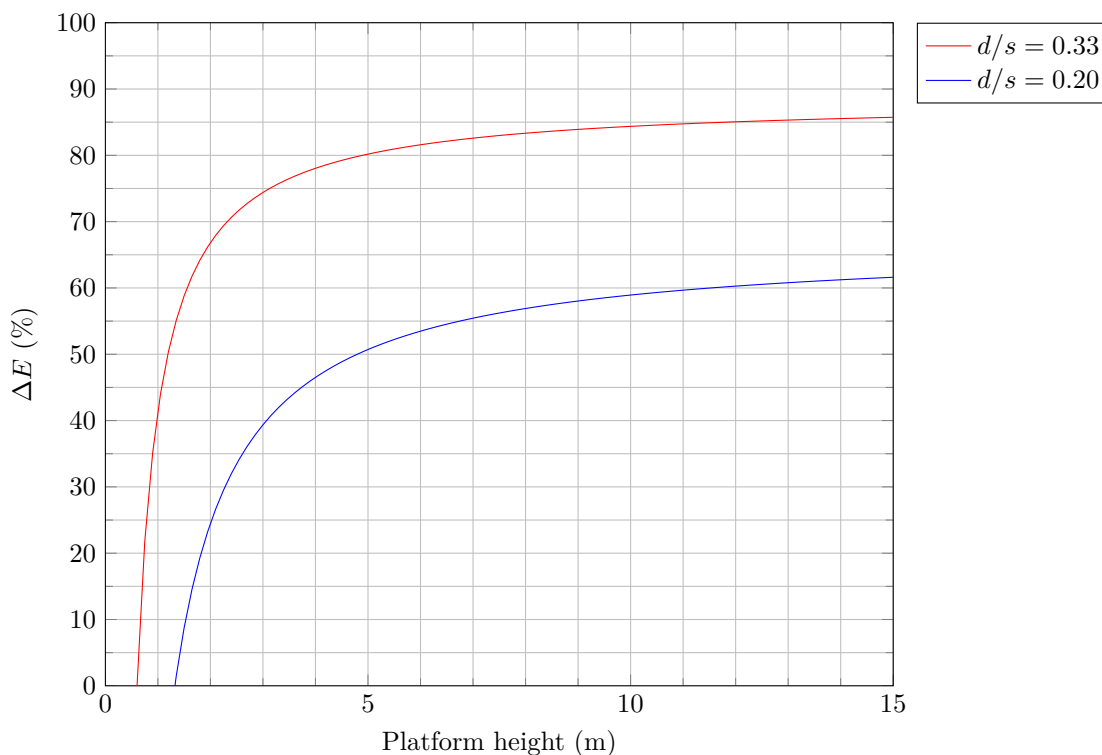
Figure 10.2: Zaeske's design plots for $s = 3$ and 5 m, $H = 0 - 15$ m and $\varphi = 38°$

10.4   Stiffness Ratio Method

The method that is used to estimate stress distribution and settlement for the ZOR project is elaborated in B.5 and H.2. The result of the calculation is the vertical stress in the column σ_c. The only input are the geometry (A and A_c, the total and column area respectively) and stiffness of the column and soft soil. Input of this model is summarized in table 10.4. The efficiency is plotted in figure 10.3 as a function of the platform height for varying stiffness ratios $m = \frac{E_c}{E_s}$, for $s = 3$ m and in figure 10.4 for $s = 5$ m.

Table 10.4: Variable values for the Stiffness Method calculations

Variable	Unit	Value
d	m	1
s	m	3.0, 5.0
E_s	kPa	4000
E_c	kPa	100,000
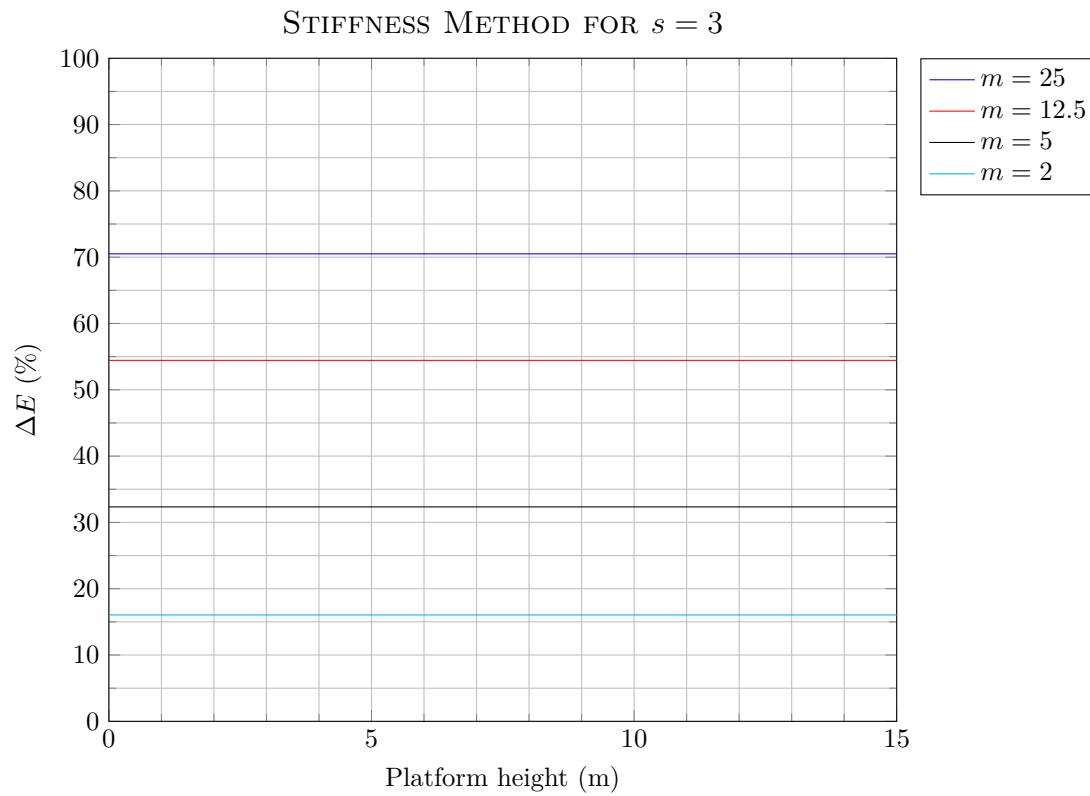
Figure 10.3: Stiffness method varying stiffness for $s = 3$ m
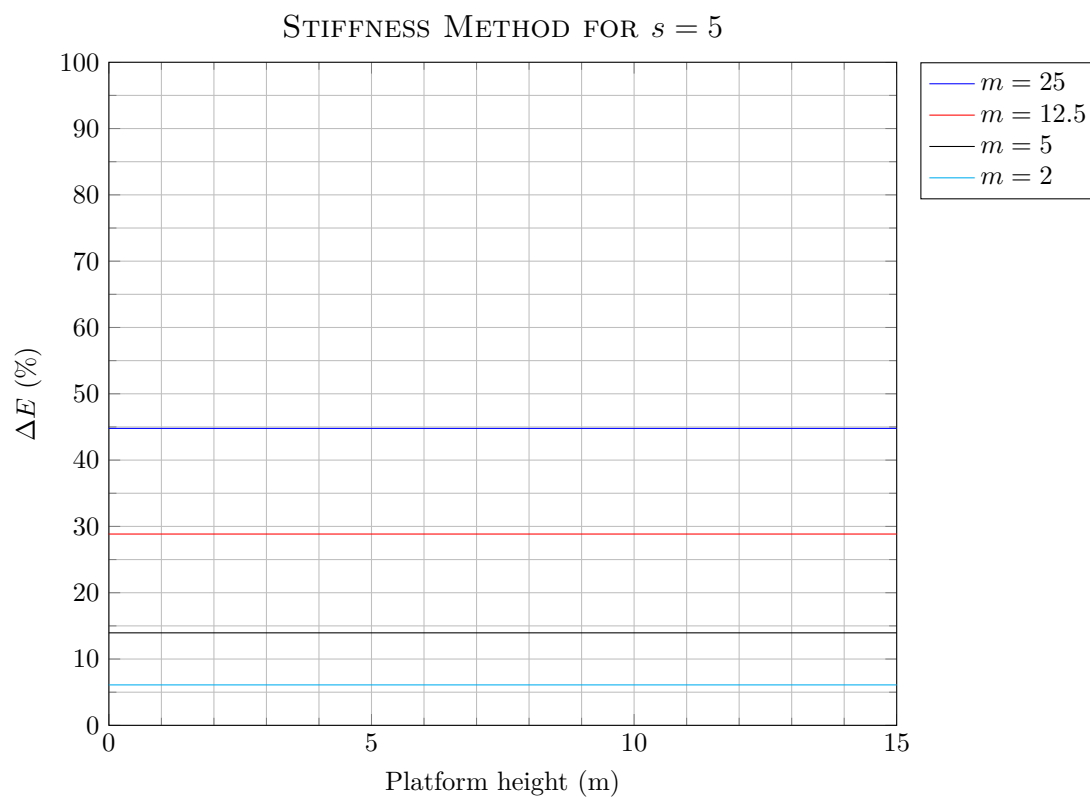
Figure 10.4: Stiffness method varying stiffness for $s = 5$ m

As can be observed by the horizontal plot, the efficiency is no function of the platform height. It is noted

that, based on experience and to introduce some conservatism, the maximal stiffness ratio $m = 25$ in the ZOR project. The same approach will be taken in this report, as higher values for m seem very unlikely, especially when taking the method of column installation into account.

10.5 Comparison and Analysis

The theories presented above are combined with the results from the PLAXIS calculations for a spacing of $s = 3$ in figure 10.5 and for $s = 5$ in figure 10.6.
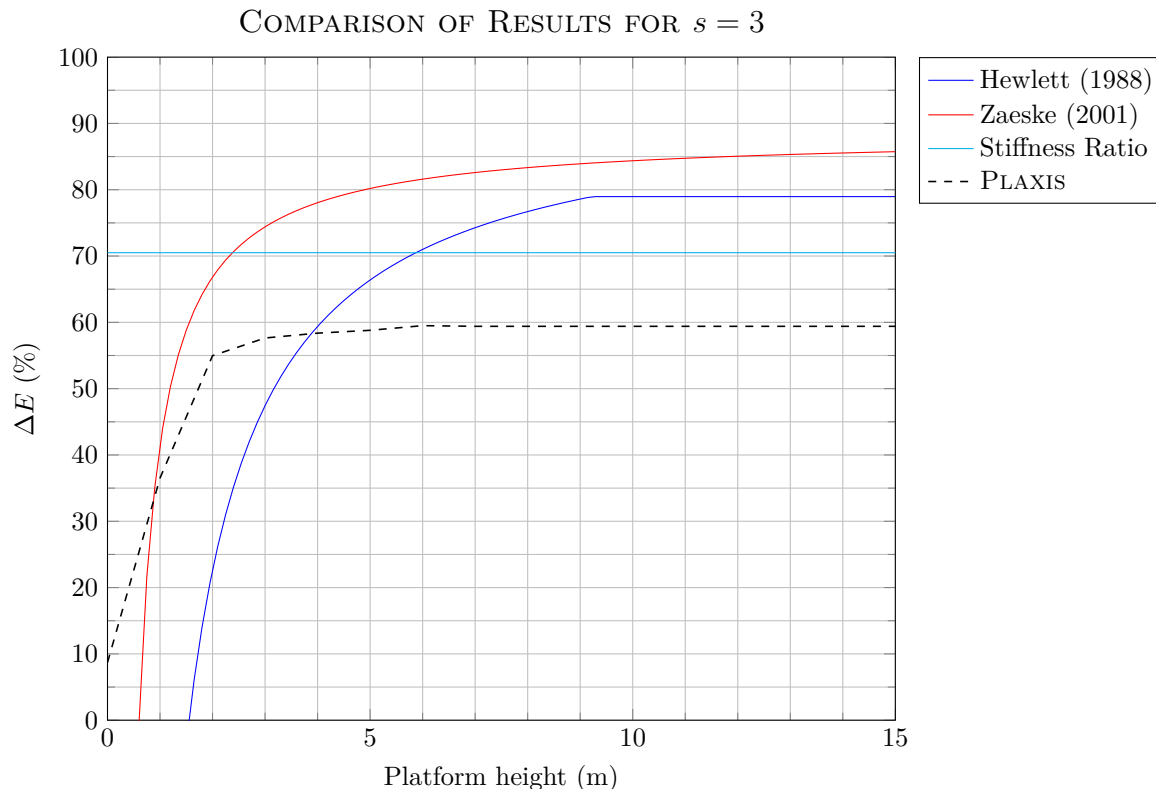
Figure 10.5: Comparison of the different efficiency theories and PLAXIS calculations for $s = 3$ m

COMPARISON OF RESULTS FOR $s = 5$
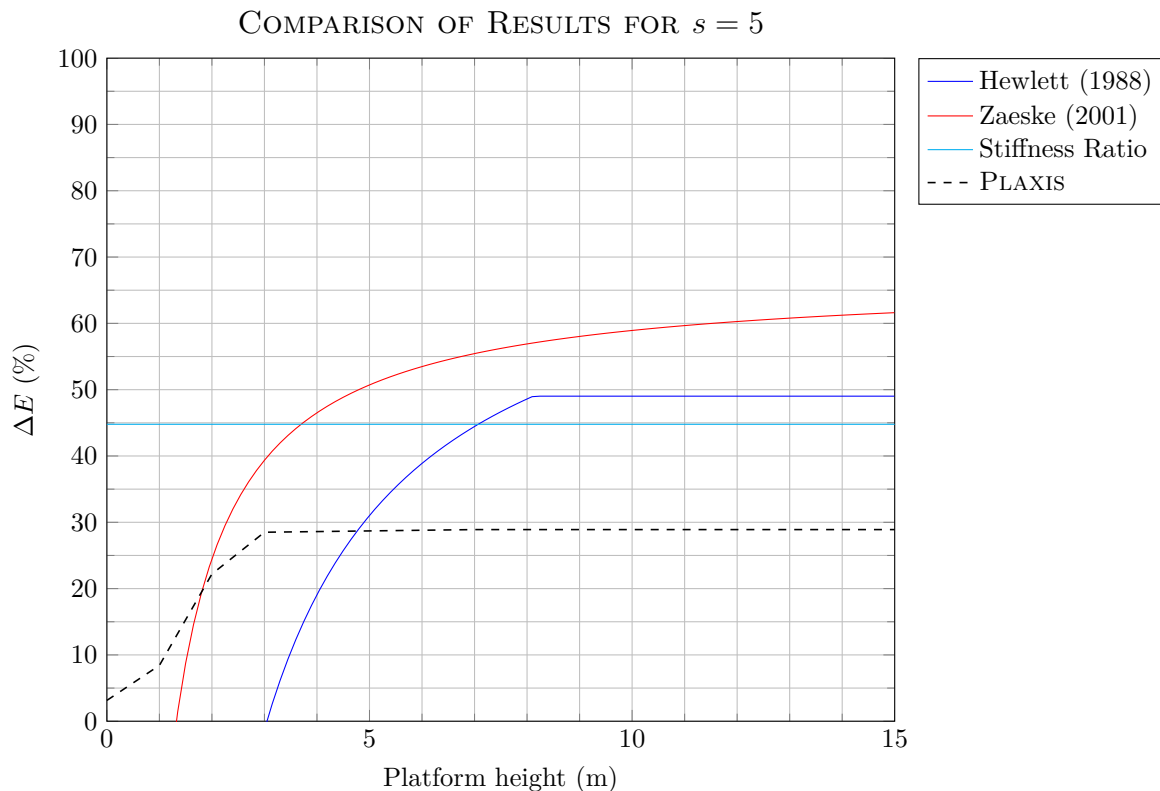
Figure 10.6: Comparison of the different efficiency theories and PLAXIS calculations for $s = 5$ m

Figure 10.5 shows that the methods by Hewlett and Randolph (1988) and Zaeske (2001) generally overestimate ΔE. While the method based on the stiffness ratio predicts lower ΔE compared to the other theories, the efficiency is still approximately 10% higher than the results from the PLAXIS calculations. The pink and blue line show that improvement effects start can be observed from 0.5 m for Zaeske (2001) and 1.25 m for Hewlett and Randolph (1988), PLAXIS shows however that the efficiency starts from H = 0 m.

The stiffness method seems to predict the efficiency for $H > 3$ m the best, relative to the PLAXIS calculations. The overall shape of the PLAXIS plot shows more comparison with the plot based on Hewlett and Randolph (1988).

Figure 10.6 shows once more that the existing theories overestimate the efficiency compared to the calculations. The method based on the stiffness ratio predicts a lower ΔE compared to the other theories.

The stiffness method predicts an efficiency which is 15% higher compared to the PLAXIS results. The method by Hewlett and Randolph (1988) over predicts the efficiency by 20%. The overall shape of the PLAXIS plots shows comparison with the theory by Hewlett and Randolph (1988).

Part IV

Discussion, Conclusions and Recommendations

11

Discussion of the Results

During the project a series of assumptions and decisions may have lead to errors in the results presented in the chapters before. One should take account of these errors in order to be able to estimate the value of the conclusions. The source of errors and their respective impact are discusses in this chapter.

In the ZOR project a sand platform of approximately 2 m is placed on top of the existing surface level. After the sand is placed DR works are carried out. When the DR works are finished another 3-4 m sand layer is placed on top of the existing sand platform. The soil samples that were used for the parameter determination were taken after the DR works. At this point the soft soil is consolidated due to the weight of the sand platform. When the PLAXIS calculations varying platform height were run, the sand platform was modeled as a sand layer of the entire final thickness (i.e. no staged construction where first a 2 m platform was present, followed by another sand platform). This results in a significant error, because the K_0 procedure in PLAXIS assumes at-rest stress distribution, while actually the subsoil is loaded by the sand platform that is placed in the second phase. The result of this chronological error is an underestimation of the settlement. It may however also imply a different efficiency compared to the efficiency values found in the previous chapter. To quantify the error another calculation has been performed where a staged construction of the sand platform was used.

The calculation was performed with an initial sand platform of 2 m and a column spacing of $s = 5$ m. After the K_0 procedure a volume of 3 m($\cdot s^2$) sand was placed on top of the existing 2 m. After placing the second sand layer a consolidation phase was calculated until 99%. In the subsequent phase the 100 kPa uniformly distributed load (UDL) was activated, followed by another consolidation phase. The results are given in table 11.1. Note that the first sand layer with a height of 2 m is referred to as sand 1, the second sand layer of 3 m is referred to as sand 2.

Table 11.1: Calculation results from regular and staged platform construction calculations

Phase	Load	U (%)	σ'_s (kPa)	U_z (mm)	ΔE (%)	ΔS_r (%)	σ'_s (kPa)	U_z (mm)	ΔE (%)	ΔS_r (%)
			Phased				*Regular*			
1	Sand 1	99	0	0	-	-	0	0	-	-
2	Sand 2	0	28.3	9.45	-	-	-	-	-	-
3	Sand 2	99	74.3	28.14	-	-	79.0	-	-	-
4	Sand 2 + UDL	0	75.2	40.43	-	-	79.0	9.45	-	-
5	Sand 2 + UDL	99	142.2	60.12	34	18	152.6	33.41	29	14

The results from the table above suggest that the settlement due to the placement of the sand platform equals 28.14 mm. The settlement due to the activation of the 100 kPa load equals $60.12 - 28.14 = 31.98$ mm. It can be concluded that the absolute value of the settlement after activating the load is smaller for the staged construction of the platform. It can also be seen that the effective stress in the soft soil is lower for the staged construction calculation.

It is shown in table 11.1 that the efficiency is higher for the staged construction compared to the regular calculations. This is also shown in figure 11.1, as it can be seen that arching develops from the moment the second platform is activated. The arching continues to increase as the top load is activated and the soft soil consolidates. This is also seen in the regular calculations.

Based on the observations above it may be concluded that the calculations executed in this thesis (presented in the previous part) are a upper bound of both stress in the soil as well as settlement. Figure 11.1 shows a cross-section through the sand column at different loading and consolidation intervals.
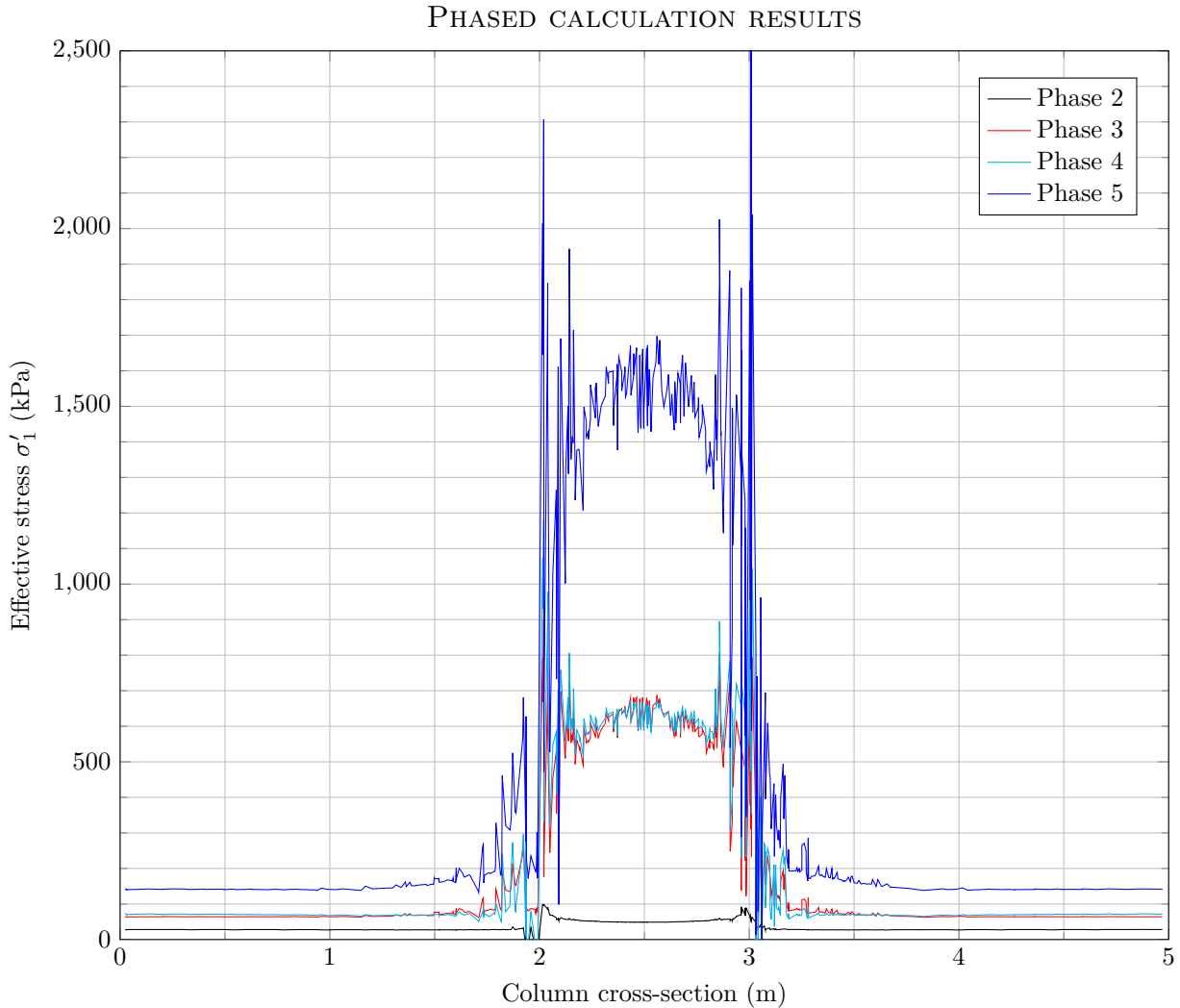
Figure 11.1: Phased platform construction

11.1 Sources of Error

11.1.1 PLAXIS Calculations

As most of the results presented in this thesis are calculations from PLAXIS calculations, it is sensible to determine the accuracy of the model. The most significant source of error are the simplifications that were assumed when the PLAXIS model was built. A selection of the most important simplifications is enumerated below.

1. The columns are assumed to be perfectly cylindrical;

2. The sand platform is assumed to be uniform over the entire area;

3. The sand columns are assumed to be uniform;

4. The soil layers are assumed to be horizontal.

Impact on the results

The impact of the error sources described in the enumeration above will be discussed below.

1. It was concluded during the excavation of the sand columns that the column diameter is at least 1 m. Assuming a cylindrical column of 1 m diameter thus results in an underestimation of the bearing capacity.

2. The sand platform is in fact not uniform because of the local DR works. The sand parameters have been correlated to multiple CPTs and are thus averaged.

3. Because of the method of installation, the level of compaction varies with column depth. The columns are however assumed to be uniformly compacted over the depth. Again the soil parameters are correlated to CPT results and thus averaged.

4. While it may be suitable to model horizontal soil layers for the platform and soft soil, the interface between the lower silt layer and silty sand layer is not horizontal. The result of this simplification may be an over- or underestimation of the settlement in the soft soil layer.

11.1.2   Zone Load Test

The ZLT were performed in three different locations. The temperature during the tests has been measured, although it was not used.

The ZLT was performed in areas where a large amount of CPT have been performed in order to model the soil layering as accurately as possible. Also the sand parameters were correlated with the CPT.

The method of performing of a ZLT is described in section D.2. It can be concluded that the execution is different from the manner it was modeled in PLAXIS, particularly because there are no columns supporting the weight of the ZLT in the model. While the exact disturbance is not known nor quantified, it is sensible that the difference in actual test and model conveys a difference in the results.

Impact on the results

An error in the ZLT results influences all the calculations, as the soil parameters have been fit to the ZLT load/settlement results.

The error in the following calculations will be quantitative, as the settlement or stress distribution may be (slightly) different. The qualitative consideration of the function of a CSE is however valid for a range of soil parameters.

11.1.3   Soil Sampling

The area that was available for the ZLT was a different area from the soil sampling location. While the CPT suggests that the results are comparable, there is no certainty that the sabkha characteristics are the same for both locations.

Impact on the results

Because of the relatively small amount of soil samples, the amount of tests was limited. Though it is believed that the tests that have been performed are reliable, more results should be acquired to deliver accurate information about the soil.

The samples that were taken were sent to The Netherlands by airmail. Even though the samples were packaged correctly, the long transportation distance has had an influence on the samples. The samples most likely have been dehydrated and compacted due to vibration. These influences generally result in a stiffer soil sample, any subsequent test results in an overestimation of the stiffness.

Van Oord
Marine ingenuity

12

Conclusions

In this thesis project the soil improvement for a running Van Oord project at Al-Zour, Kuwait has been investigated. The improvement consists of dynamically replaced sand columns in a soft silty clay layer locally known as sabkha. Above these sand columns a layer of sand with varying thickness is placed.

The combination of columns and platform increases bearing capacity and reduces settlements, and is referred to as a *Column Supported Embankment* (CSE). The columns used in the ZOR project have a center-to-center distance of 5.0 m and a column diameter of 2.2 or 1.0 m, depending on exact installation technique.

When the columns are loaded they should bear more stress compared to the surrounding soil. The weight that is borne by the columns is defined as the column force $A = \sigma_c A_c$. The total force acting in the soft soil is defined as $C = \sigma_s(s^2 - A_c)$. The efficiency of a CSE is then defined as the ratio of force in the column over the total force in a unit cell, which equals $E = \frac{A}{A+C}$. The geometry is sketched in figure 12.1.

(a) Vertical (side-view) embankment cross-section

(b) Horizontal (top-view) embankment cross-section
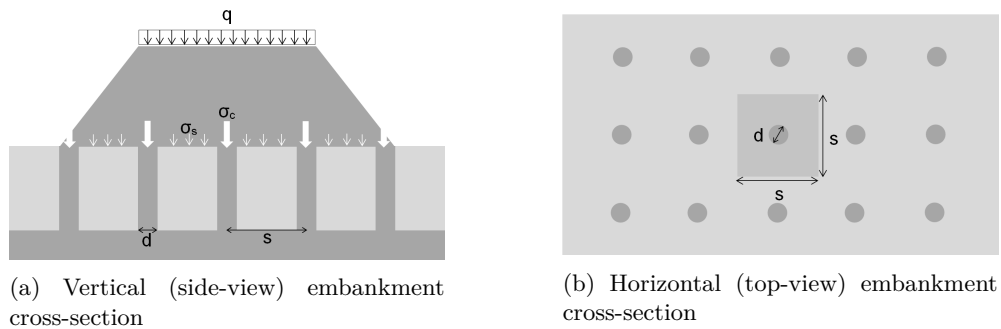
Figure 12.1: Embankment cross-sections, $d = 1$, $s = 5$

To determine the increase of the force in the column under a surcharge, an incremental efficiency was introduced. The incremental efficiency is defined as the column force increase over the surcharge increase, $\Delta E = \frac{\Delta A}{\Delta q s^2}$.

To determine the improvement in terms of settlement, a settlement reduction ratio is used, defined as the settlement of improved soil over the settlement of unimproved soil, $S_r = \frac{U_z}{U_z^*}$. An incremental settlement reduction ratio was defined as the increase in settlement of improved soil (due to a surcharge) over the settlement of unimproved soil, $\Delta S_r = \frac{\Delta U_z}{\Delta U_z^*}$.

The long term behavior of a CSE was analyzed using PLAXIS calculations, in which a uniformly distributed load of 100 kPa was modeled. To simulate consolidation the consolidation tool was used in PLAXIS. An exploded view of the PLAXIS model is given in figure 12.2.

Van Oord
Marine ingenuity
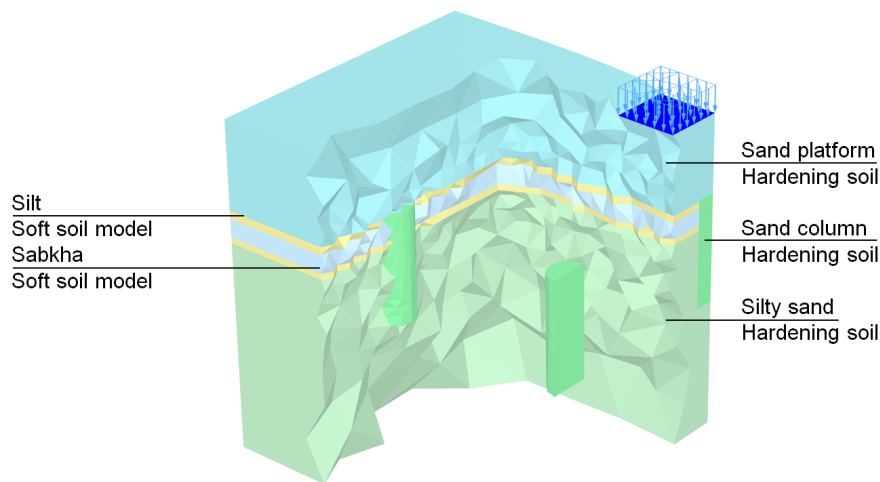
Figure 12.2: Exploded view of the PLAXIS model

After all the calculations had been performed, it was concluded that there was a significant deficiency in the model. Instead of using a K_0 procedure on a 2 m sand platform and adding the second layer after this procedure, the full sand platform was modeled as initial situation. While the soil was consolidated to the weight of the platform, no account was taken of the fact that the 2 m soil platform may have arched already, changing the stress distribution and any distribution of any second sand layer. To investigate the consequences of the deficiency, an extra calculation was run, of which the results are given in the discussion. It was found that ΔE is 5% higher for the phased construction and S_r is 4% lower for the phased construction, compared to the regular calculations. While account should be taken of this deficiency, it is assumed that a qualitative consideration based on the in chapter 9 given results is still valid.

12.1   Research Questions

The subquestions that were defined in the introduction are discussed below.

12.1.1   Subquestions

i *Are there existing methods to determine stress transfer and settlement?*
During the literature study it was found that many theories exist determining stress transfer. Two of these theories (Hewlett and Randolph (1988) and Zaeske (2001)) that seemed most promising were elaborated. Most theories found assume presence of a geosynthetic reinforcement, this is however not used in the ZOR project.

ii *How is the load, imposed by a surcharge, transferred in a CSE?*
The stress imposed by a surcharge on surface level is drawn to the stiffer elements (the columns) in a CSE. The drawing of stress towards the columns is called arching. Rather than full arches as can be seen in for instance masonry, partial arches develop above the columns. The stress is transferred through the sand column. Under the soft soil layer the stress is transferred to the silty sand layer using end bearing and shear resistance at the column interface. The efficiency is dependent on the friction angle φ of the platform. A higher friction angle leads to a more favorable stress transfer and thus to more arching.

In PLAXIS a cross-section of the column including platform was inspected to determine the soil volume that is influenced by the sand column. The soil volume that is influenced by the presence of a sand column is determined for both a column spacing of three and five meters. The efficiency based on this volume agrees well with the efficiency based on column force.

iii *How does platform height and column spacing influence stress distribution?*
It was shown that the efficiency rapidly increases with increasing platform height for a spacing of $s = 3$ m. The efficiency increased to approximately $\Delta E = 60\%$. The top figure in figure 12.3 shows the increase in efficiency for $s = 3$ m.

For $s = 5$ m the increase was less steep and ΔE increased to approximately 28%, where it reached a threshold value and thus remained constant. The bottom figure in figure 12.3 shows the increase in efficiency for $s = 5$ m.

Efficiency Calculations
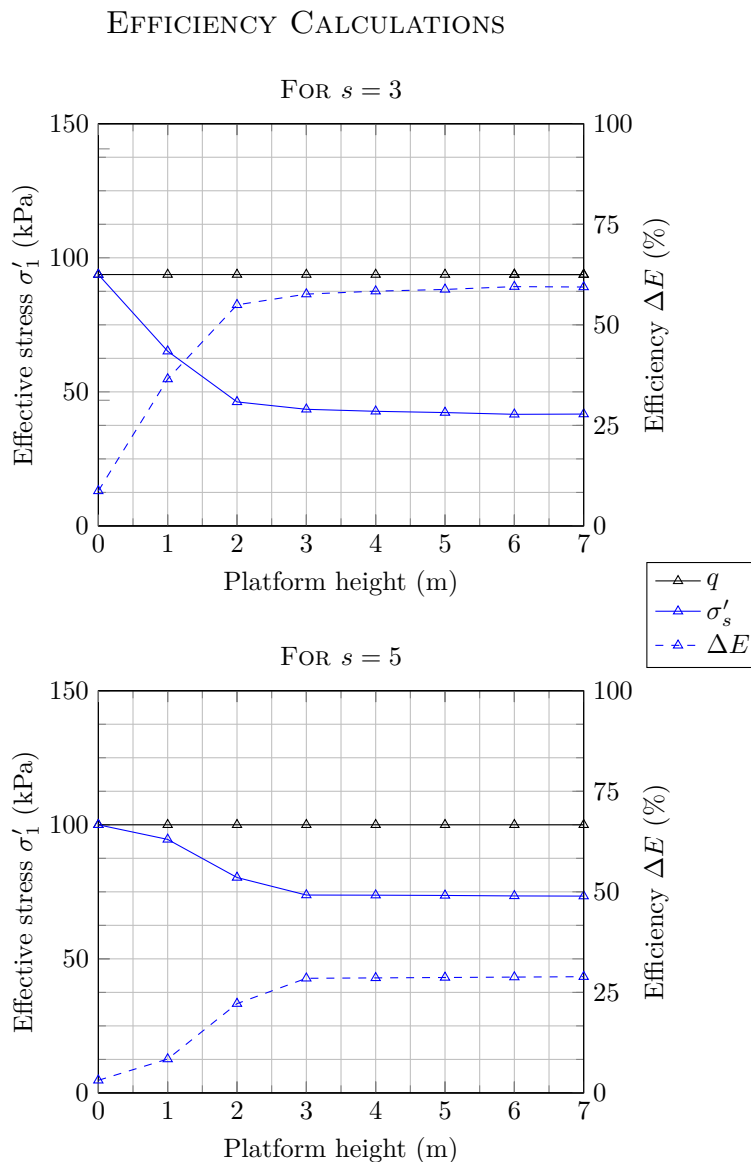
Figure 12.3: Efficiency for increasing platform height for $s = 3$ and $s = 5$

iv *How does platform height and column spacing influence settlement?*
It can be seen in figure 12.4 that the incremental settlement reduction ratio ΔS_r increases with platform height, up to a platform height of two meters for $s=3$ m and three meters for $s=5$ m. It can be concluded that the maximum settlement reduction equals 36% for $s=3$ m and 15% for $s=5$ m when the surface is loaded with a 100 kPa surcharge. The settlement reduction increases for greater platform height. The settlement reduction also increases for a narrow column spacing.
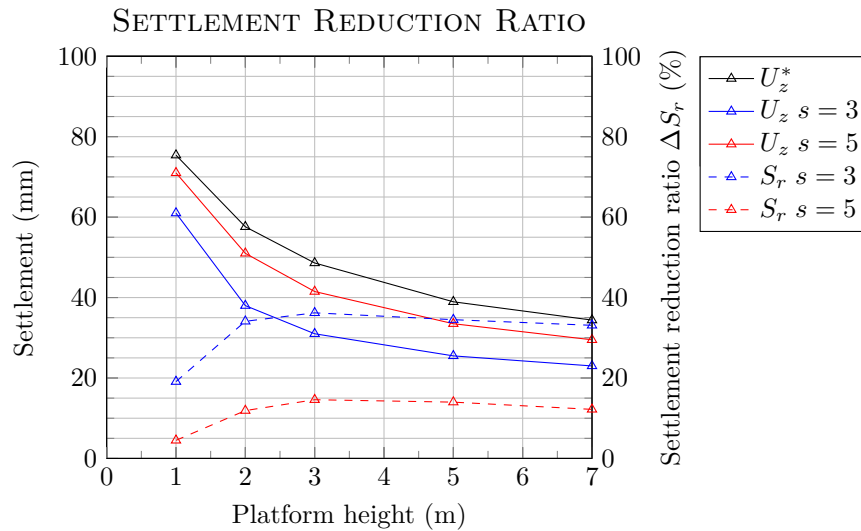
Figure 12.4: Settlement reduction ratio with platform height for $s = 3$ and $s = 5$ m

v *Does the local soil composition influence the efficiency and settlement of a CSE?*
Although no (long-term) parametric analyses have been performed on the soft soil, multiple calculations have been performed varying column and platform stiffness for short-term analysis. It was found that the column friction angle and stiffness do not influence the settlement significantly for short-term analysis. It was found that the platform stiffness and friction angle do influence the settlement of a discrete load. A higher friction angle results in a lower settlement, a relatively stiff platform results in lower settlements.

It was also found that soils with low permeability, such as sabkha, take some time to consolidate. The efficiency and settlement reduction increase with consolidation progress, this will be described in the following research subquestion.

vi *How does consolidation influence the efficiency of a CSE?*
The excess pore pressure in the soft soil increases under activation of the load to approximately 100 kPa. The distributed load, like the ZLT, is thus carried by the water in the soft soil layers. The excess pore pressures in the soft soil start to dissipate via the sand columns and sand layer below. As the pore pressures decrease the horizontal stress on the sand columns starts to decrease, while the vertical force in the column increases under redistribution of stress in the sand platform. Consequently the sand column starts to bulge in the soft soil layer. As consolidation continues the horizontal strain in the outer ring of the sand column increases, lowering the stress. Subsequently the stress distribution in the top part of the column is funnel-shaped. It can be concluded that arching increases during consolidation.
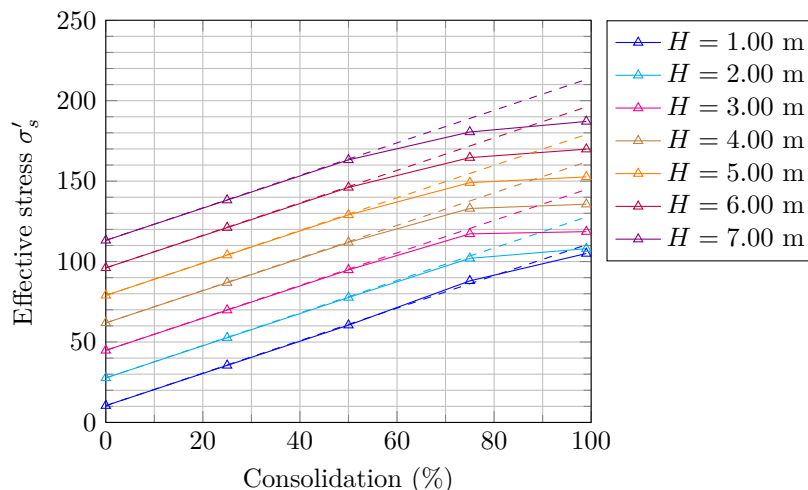
Figure 12.5: Effective stress increase with consolidation progress, dashed lines represent the normal consolidation line

It can be seen in figure 12.5 that the effective stress increase follows the normal consolidation progress. From a certain point, while consolidation continues, the effective stress does not increase anymore: arching develops. Based on the fact that consolidation implies displacement, it can be concluded that a displacement of the sand platform is necessary to develop arching. The latter statement agrees with the theory by Terzaghi (1943).

vii *What are the requirements for an efficient Column Supported Embankment?*
It can be concluded that the following parameters and design requirements are most important for an efficient CSE:

- **Sufficiently compacted platform:** the platform of a CSE should be well compacted in order to have a high friction angle. A high friction angle leads to a more favorable stress distribution and thus higher efficiency. Also a well compacted platform has a high stiffness leading to lower settlements.

- **Sufficient platform height:** in order to develop partial arching in the soil on top of the columns, there should be sufficient platform height to facilitate the arches. From the PLAXIS calculations follows that a height of $H = 0.75(s - a)$ is generally enough to reach maximum efficiency.

- **Narrow column spacing:** it was shown in the calculations that efficiency drastically increases with a narrower column spacing. For the spacings that were calculated, s=3 and 5 m, the efficiency decreased from 60% to 28%.

- **Consolidation of soft soil layers:** it was shown in the long-term PLAXIS calculations that the efficiency increases with consolidation.

viii *Can existing theories be used to design unreinforced CSE?*
In chapter 10 the theories by Hewlett and Randolph (1988) and Zaeske (2001) and a method based on the stiffness ratio $m = \frac{\sigma_c}{\sigma_s}$ are compared with the PLAXIS results. It should be noted that the theory by Zaeske (2001) assumes that geosynthetic reinforcement is used, which is not the case for the ZOR project. The theories all predict higher ΔE compared to the PLAXIS calculations. It seems that the shape of the plots are comparable by shape, however the maximum ΔE based on the theories may be up to >30% higher than the efficiency based on PLAXIS calculations. Since the overall shape is comparable, the theory on which the methods were based may be suitable if a correction, which is to be determined, is applied.

ix *Can a composite stiffness be applied to calculate settlements?*
It was found that the efficiency and thus settlement reduction of a CSE is dependent on platform height, column spacing, consolidation and soil parameters. A composite soil stiffness calculation would thus be a function like $E = f(H, \alpha, U, \varphi, E)$. Taking into account the numerous variables, it may not be suitable

Comparison of Efficiency Calculations
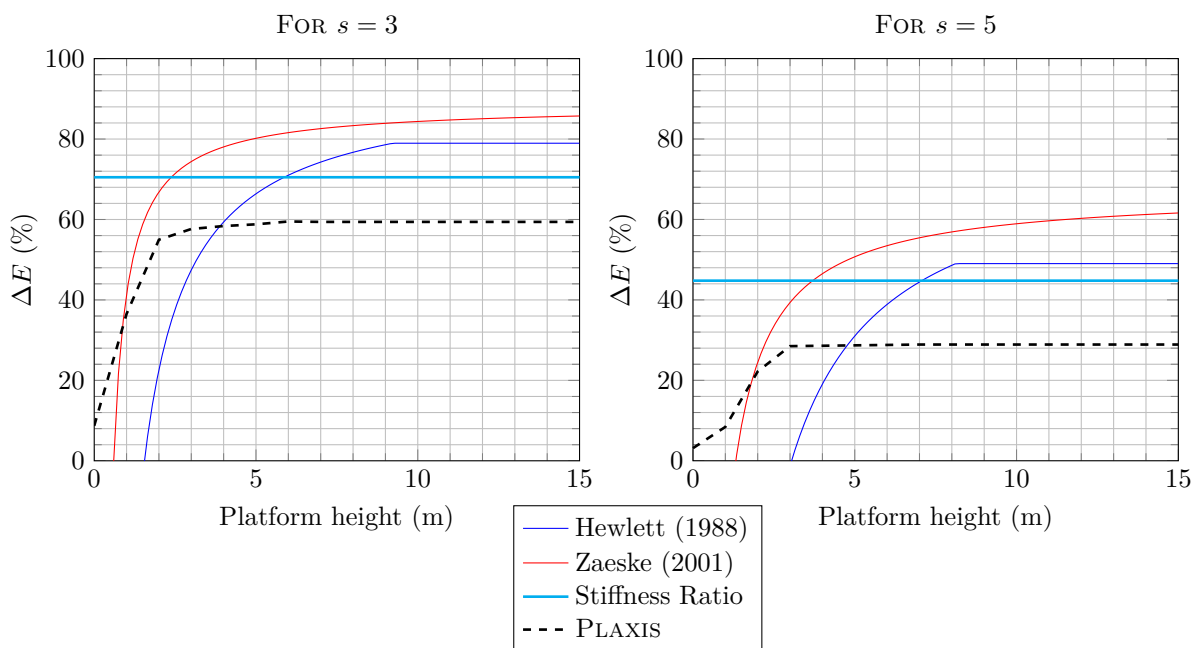
Figure 12.6: Comparison of efficiency calculations for $s = 3$ and 5 m

to take a composite soil approach. Due to limited time and viability of the method this approach was not further investigated.

x *When should a CSE be used as a soil improvement technique?*
A CSE is a feasible and efficient soil improvement technique for relatively large areas. With settlement reductions of up to 36% the method may facilitate a shallow foundation where normally deep foundations would be necessary. In areas where the soft soil has a low permeability (which is usually the case) there is the additional advantage that the sand columns serve as a drain, reducing consolidation periods. As a CSE requires a transfer platform with considerable requirements (compaction, height) the feasibility of the method may be less definite when the platform is not necessary for the end use of the improved area. In that case one can turn to a platform with an even higher friction angle, e.g. rock or pebbles.

12.1.2   Main Question

The subquestions discussed above lead to a conclusion of the main research question. The main question reads: *What is the efficiency of a Column Supported Embankment in sabkha soil?*

In the literature study of this thesis the efficiency of a CSE was defined in terms of stress distribution and settlement reduction. As these parameters are dependent on column spacing, platform height and soil characteristics, the efficiency cannot be unambiguously defined.

During consolidation, the effective stress increase in the soil is approximately equal to the decrease of pore pressure. However, starting at some point near $U = 50\%$, of which the exact location is dependent on platform height, the effective stress does not increase anymore: arching develops. As consolidation results in displacement, it may be concluded that displacement of the sand platform is necessary to develop arching. The latter conclusion is confirmed by the findings of Terzaghi (1943), described in the first chapter.

The efficiency was determined based on the calculations that have been performed. These suggest that a CSE with a column spacing of three meters results in an incremental efficiency of up to 60%. A CSE with a spacing of five meters results in an incremental efficiency of up to 28%. The efficiency thus increases with a denser column spacing. As the efficiency increases, the load part that is transferred to the columns

increases. The load that is borne by the soft soil decreases. This results in lower settlements. The settlement reduction for a column spacing of three meters equals approximately 36%, and approximately 15% for a column spacing of five meters.

As a last concluding summary, the advantages of a CSE are threefold:

1. **Increased bearing capacity:** the load from a surcharge is transferred to sand columns with a high friction angle rather than soft soil with a low friction angle and cohesion.

2. **Reduced settlement:** the load from a surcharge is transferred to sand columns with a relatively high stiffness modulus, resulting in lower settlements.

3. **Shorter consolidation period:** the sand columns also serve as a drain for the excess pore pressures that are generated as a result of a surcharge on the CSE surface.

Van Oord
Marine ingenuity

13

Recommendations

The last chapter of this thesis report is concerned with recommendations. The recommendations are divided into two sections, the first section elaborates the recommendations for the contractor. The second section discusses recommendations for further research in the field of (unreinforced) column supported embankments.

13.1 Recommendations for the Contractor

This section summarizes the attention points for a contractor in the preliminary design phase of an unreinforced CSE.

General Recommendations

- The platform height is an important design requirement for an efficient CSE. The existing theories overestimate the required platform height. It was found in the PLAXIS calculations that a $\frac{H}{s-a}$ ratio of 0.75 leads to maximum efficiency.

- In general a narrower column spacing will lead to a more efficient CSE with a more favorable settlement reduction. The settlement reduction can be determined for multiple columns spacings.

- A narrower column spacing not only leads to a more efficient CSE, it also leads to a shorter consolidation period. The maximum efficiency is reached at 100% consolidation. In projects where time is of the essence, which is usually the case, one may prefer a narrower column spacing in order to reach maximum (or required) efficiency (and thus settlement reduction) at an earlier stage.

- When the settlement of a CSE is tested, for instance with a ZLT, time should be allowed for consolidation. It follows from the PLAXIS calculations that the stress imposed by a surcharge is first borne by the water in the soft soil.

Suggested Design Methodology

In this paragraph a suggested design methodology is presented for the design of a CSE over relatively large areas. It is assumed that the governing requirement is defined in terms of maximum settlement when a distributed load is placed on the surface. It is furthermore assumed that a platform of considerable strength is used (i.e. $\varphi \approx 38°$). A column diameter of one meter is considered, however the design methodology described below is valid for greater diameters (which can be determined based on the replacement ratio α).

1. Identify soil layering, composition and characteristics based on a boring campaign. Correlate soil boring results with CPT to build a 3D soil model of the project site.

2. Determine governing design criteria:

   - **Platform:** when a platform height of $H < 2.5$ m is used the platform height is usually governing.

Van Oord
Marine ingenuity

- **Column spacing:** if the platform height is $H > 2.5$ m, the column installation is relatively expensive, or the project should be finished over a very short time period the column spacing is usually governing.

If platform height is governing and H = 1 - 1.5 m:

  3a Identify areas of equal soft soil layer thickness.

  3b Perform PLAXIS calculations for a column spacing of s =3 for every area identified in the previous step.

  3c Determine whether the column spacing leads to an acceptable settlement. If not, use a different transfer platform material, e.g. rock or pebbles.

If platform height is governing and H = 1.5 - 2.5 m:

  3a Identify areas of equal platform height.

  3b Perform PLAXIS calculations for two or three column spacings (e.g. s =5, 4 and 3 m) based on an unfavorable soil composition (i.e. thickest soft soil layer) in the area identified in the previous step.

  3c Determine the maximum column spacing that leads to an acceptable settlement.

If column spacing is governing:

  3a Identify areas of equal soft soil layer thickness.

  3b Perform PLAXIS calculations for multiple column spacings for every area identified in the previous step.

  3c Determine the maximum column spacing that leads to an acceptable settlement.

4. Combine the areas. In transition zones one should design conservatively, that is to say with the lesser efficiency or settlement reduction.

As with all calculations in this thesis and thus this design methodology, the columns are assumed to be end-bearing.

13.2   Recommendations for Further Research

The scope of this project was to determine the functioning of a CSE using DR for a specific project at Al-Zour, Kuwait. One of the main shortcomings in this thesis is the fact that no settlement or stress redistribution due to the placement of the sand platform is taken into account. This is partly overcome by the introduction of incremental values for the settlement and efficiency. It would be recommended for a follow-up research to determine the settlements from the start of the project all the way up to the final platform.

The main elements of this thesis that can be used for further research are elaborated below.

13.2.1   Dynamic Replacement

To determine the shape of the DR columns, more sand columns should be excavated. The possibility of performing scaled DR experiments should be investigated.

To more accurately determine the stiffness in the sand columns the energy of the DR pounder should be considered. Based on that energy one can determine important stiffness parameters such as $E_u r$. An energy consideration may also be used to determine whether the sand will deform elastic or plastic upon loading, as the yield cap has presumably shifted considerably during DR operation.

The soil around a sand column that has been installed using the DR technique should be monitored using e.g. piezometers, CPT and PMT. This would lead to an additional soil improving feature of the DR technique, that has not yet been taken into account.

13.2.2   Soil Sampling and Testing

To accurately determine soil parameters a more extensive soil sampling and testing campaign should be performed. For this thesis a limited number of soil samples and tests were available.

A more elaborate study investigating the reliability of CPT correlations should be executed. The correlations used in this thesis produced values for φ in the order of 45°- 50°in some locations, which is very high.

13.2.3   Shear Resistance

The sand columns in a CSE increase the (total) shear resistance of soil against shear failure. This favorable feature should be further investigated so that it can be quantified. Perhaps the use of a CSE may prevail other soil improvement methods when shear resistance is included, while it may have been rejected based only on bearing capacity increase or settlement reduction.

13.2.4   Stress Distribution

To validate the results acquired by PLAXIS calculations, field tests should be performed to accurately determine stress distribution and settlement. To this extent, the following recommendations are given.

Designate a testing area in which settlement etc. are recorded starting day 1:

1. Survey the area;

2. Perform an extensive soil boring campaign. Take samples of the soil and install piezometers;

3. Record settlement and GWL when the sand is brought in.

4. Record heave, displacements and pore pressures when DR works are executed.

5. Compare the results from the previous step with the boring campaign. Is there more or less penetration in some areas? Is more heave observed for some locations? These observations can be compared with a 3D soil profile.

6. Install Total Pressure Cells (TPC) on top of the columns and in between the columns, preferably on the interface of the former surface level and the sand platform, to determine the stress distribution.

7. Compact the platform.

8. Perform FDT, DSS and CPT to determine the compaction of the sand.

9. Continue to monitor consolidation of the soft soil layers and settlement of the platform.

10. Install a distributed load on top of the platform, continuously monitor settlements, stresses and pore pressures.

11. Hold the load until there is no more excess pore pressure.

With the data from the above enumeration the stress distribution can be determined. When above procedure is repeated for multiple platform heights the height-dependency of the efficiency and settlement ratio can be determined.

13.2.5   Parametric Analyses

While a parametric analyses was performed based on a ZLT, no analyses were executed determining the sensitivity for long-term calculations. A recommendation would be to determine the effect of varying stiffness of the sand columns. It may be interesting to determine the effect of different column stiffness in a column field.

Van Oord
Marine ingenuity

Furthermore an analysis determining the influence of the subsoil should be carried out. In this thesis one specific soil layering was investigated. No effects of varying soft soil layers and compressibility were determined.

13.2.6 Centrifuge Testing

Instead or complimentary to field testing centrifuge tests may be executed. Using centrifuge testing one can determine the stress distribution between the columns. Also, when TPC the size of the columns are used, one can reliably determine the force in the column. It was observed in the Plaxis calculations that FEM require a highly refined mesh to accurately calculate the stresses in a column.

13.2.7 Plaxis Calculations

It is the author's believe that more accuracy of the calculations can be gained by determining sand column shapes and a more elaborate soil sampling and testing investigation. One can also refine the Plaxis calculations, however this would lead to unacceptable calculation times on regular computers (in the order of weeks).

Bibliography

Abduljauwad, S. and Al-Amoudi, O. (1995). Geotechnical behaviour of saline sabkha soils. *Géotechnique*, 45(3):425–445.

Akili, W. and Ahmed, N. (1983). The sabkhas of eastern Saudi Arabia: geotechnical considerations. *Proceeding of the 1st Saudi Engineering Conference.*

Akili, W. and Al-Joulani, N. (1988). Cone penetration tests on artificially cemented sands. *Proc. of 1st ISOPT*, pages 607–614.

Akili, W. and Torrance, J. (1981). The development and geotechnical problems of sabkha, with preliminary experiments on the static penetration resistance of cemented sands. *Quarterly Journal of Engineering Geology and Hydrogeology 14.1*, pages 59–73.

Al-Amoudi, O. and Abduljauwad, S. (1991). Geotechnical considerations on field and laboratory testing of sabkha. *Proc. Symp. Recent Advances in Geotechnical Engineering III, Singapore.*

Al-Amoudi, O., Abduljauwad, S., and El-Naggar, Z. (1992). Response of sabkha to laboratory tests: A case study. *Engineering Geology.*

Al-Shamrani, M. a. (2005). Applying the hyperbolic method and Ca/Cc concept for settlement prediction of complex organic-rich soil formations. *Engineering Geology*, 77(1-2):17–34.

ASIRI (2012). Recommendations for the design, construction and control of rigid inclusion ground improvements. Technical report.

Baguelin, F. (1978). The pressuremeter and foundation engineering. *Trans Tech public.*

Bates, L. and Merifield, R. (2010). Evaluation of the CPT for assessing ground improvement by dynamic replacement. *2nd International Symposium on Cone Penetration Testing. No. 2-52.*

Brinkgreve, R. and Swolfs, W. (2015). PLAXIS 3D 2015. *Plaxis Manual.*

BS8006 (1995). Code of practice for strengthened/reinforced soils and other fills. *British Standard Institution, London, UK.*

Carlsson, B. (1987). Reinforced soil, principles for calculation. *Linköping: Terratem AB.*

Chan, S. and Chin, F. (1972). Engineering characteristics of the soil along the Federal Highway in Kuala Lumpur. *Proceedings of the Third South-east Asian Conference on Soil Engineering*, pages 41–45.

Chua, C. H., Lai, M., Hoffmann, G., and Hawkins, B. (2008). Ground Improvement using Dynamic Replacement for NCIG CET3 Coal Stockyard. *Australian Geomechanics.*

Collin, J. (2007). US State-of-practice for the design of the geosynthetic reinforced load transfer platform in column supported embankments. *Proceedings of GeoDenver.*

Costa, Y. D., Zornberg, J. G., Asce, M., Bueno, B. S., and Costa, C. L. (2009). Failure Mechanisms in Sand over a Deep Active Trapdoor. *Journal of geotechnical and geoenvironmental engineering 135.11*, pages 1741–1753.

CUR226 (2010). Eisen aan paalmatrassystemen.

Demerdash, M. (1996). An experimental study of piled embankments incorporating geosynthetic basal reinforcement. *Master Thesis.*

Dhowian, A., Erol, A., and Sultan, S. (1987). Settlement predictions in complex sabkha soil profiles. *Bulletin of the International Association of Engineering Geology-Bulletin de l'Association Internationale de Géologie de l'Ingénieur*, pages 11–21.

EBGEO (2010). Empfehlung für den Entwurf und die Berechnung von Erdkörpern mit Bewehrung aus Geokunststoffen. *Deutsche Gesellschaft für Geotechnik e. V.*

Eekelen, S. V. and Bezuijen, A. (2012). Model experiments on piled embankments. Part II. *Geotextiles and Geomembranes.*

Van Oord
Marine ingenuity

Eekelen, S. V., Bezuijen, A., and Tol, A. V. (2013). An analytical model for arching in piled embankments. *Geotextiles and Geomembranes.*

Ellis, C. (1973). Arabian salt-bearing soil (sabkha) as an engineering material. *No. Lr 523 R&d Rpt.*

Ellis, E. and Aslam, R. (2009a). Arching in piled embankments: comparison of centrifuge tests and predictive methods-part 1 of 2. *Ground Engineering.*

Ellis, E. and Aslam, R. (2009b). Arching in piled embankments: comparison of centrifuge tests and predictive methods-part 1 of 2. *Ground Engineering 42.6.*

Fadl, M. (1981). The behaviour of plate anchors in sand. *Journal of Geotechnical Engineering 113.3*, pages 202–215.

Filz, G., Sloan, J., and McGuire, M. (2012). Column-supported embankments: settlement and load transfer. *Geotechnical Engineering State of the Art and Practice - Keynote Lectures from GeoCongress.*

Fookes, P. (1978). Middle East - Inherent ground problems. *Quarterly Journal of Engineering Geology and Hydrogeology 11.1*, pages 33–49.

Fugro (2013). Hydrogeologic Study New Refinery Project - Revision B. Technical report, Fugro.

Hamidi, B., Nikraz, H., and Varaksin, S. (2011). Application of Dynamic Replacement in a Steel Pipe Factory. *International Conference on Advances in Geotechnical Engineering*, pages 867–871.

Han, J. and Gabr, M. (2002). Numerical analysis of geosynthetic-reinforced and pile-supported earth platforms over soft soil. *Journal of geotechnical and geoenvironmental engineering 128.1*, pages 44–53.

Hewlett, W. (1984). the analysis and design of bridge approach support piling. *Pile foundation analysis and design. No. Monograph.*

Hewlett, W. and Randolph, M. (1988). Analysis of piled embankments. *International Journal of Rock Mechanics and Mining Sciences and Geomechanics Abstracts*, 25(6):297–298.

Horgan, G. and Sarsby, R. (2002). The arching effect of soils over voids and piles incorporating geosynthetic reinforcement. *Proceedings of the 7th International Conference on Geosynthetics, Nice*, 1:373–378.

Hossain, D. and Ali, K. (1990). Mackintosh-vs-vane estimation of undrained shear strength correlation for a Sabkha Clay of Saudi Arabia. *Quarterly Journal of Engineering Geology and Hydrogeology 23.3*, pages 269–272.

Hossain, D. and Sabtan, A. (1994). Pressuremeter and Static Cone Penetration Tests in abhor Sabkha, Saudi Arabia. *Earth Sciences.*

Hso, K. and Schneider, J. (1973). Progress report on dolomitization - hydrology of Abu Dhabi sabkhas, Arabian Gulf. *The Persian Gulf*, pages 409–422.

Huat, B., Craig, W., and Ali, P. (1994). The mechanics of piled embankment. *Proc., Int. Conf. on Design and Construction of Deep Foundations.*

Ilamparuthi, K. and Muthukrishnaiah, K. (1999). Anchors in sand bed: delineation of rupture surface. *Ocean Engineering.*

Ismael, N. F. (1993). Laboratory and Field Leaching Tests on Coastal Salt-Bearing Soils. *Journal of Geotechnical Engineering*, 119(3):453–470.

Jamiolkowski, M. and Lancellotta, R. (1984). Embankment on vertical drains-pore pressure during construction. *International Conference on Case Histories in Geotechnical Engineering.*

Janbu, N. (1963). Soil compressibility as determined by oedometer and triaxial tests. *Proc. ECSMFE Wiesbaden.*

Jenck, O. (2004). Renforcement des massifs de fondations par inclusions rigides verticales. Modélisation physique et numérique. *Revue Française de Génie Civil*, 8(1):120–120.

Jenck, O., Dias, D., and Kastner, R. (2007). Two-dimensional physical and numerical modeling of a pile-supported earth platform over soft soil. *Journal of Geotechnical and Geoenvironmental Engineering 133.3*, pages 295–305.

Jenck, O., Dias, D., and Kastner, R. (2009). Discrete element modelling of a granular platform supported by piles in soft soil - Validation on a small scale model test and comparison to a numerical analysis in a. *Computers and Geotechnics*.

Johnson, D. and Kamal, M. (1978). Sabkhas of eastern Saudi Arabia. *Quaternary Period in Saudi Arabia 1*, 1:84–93.

Juillie, Y. and Sherwood, D. (1983). Improvement of sabkha soil of the Arabian Gulf coast. *Proc. of the Eighth European Conference on Soil Mechanics and Foundation Engineering, Helsinki,(Pub.), AA Balkema*, pages 781–785.

Kempfert, H. and Gobel, C. (2004). German recommendations for reinforced embankments on pile-similar elements. *EuroGeo3-third European geosynthetics conference, geotechnical engineering with geosynthetics. Munich, Germany: Deutsche Gesell schaft fur Geotechnik*, pages 279–284.

Khan, I. and Hasnain, S. (1981). Engineering properties of sabkha soils in the Benghazi plain and construction problems. *Engineering Geology*.

Khan, I. and Layas, F. (1984). Settlement of a building founded on difficult soil. *International Conference on Case Histories in Geotechnical Engineering*.

Kinsman, D. (1969). Modes of formation, sedimentary associations, and diagnostic features of shallow-water and supratidal evaporites. *AAPG Bulletin*.

Kulhawy, F. and Mayne, P. (1990). Manual on estimating soil properties for foundation design. *Electric Power Research Inst., Palo Alto, CA (USA); Cornell Univ., Ithaca, NY (USA). Geotechnical Engineering Group*, No. EPRI-E.

Kumar, J. and Kouzer, K. (2008). Vertical uplift capacity of horizontal anchors using upper bound limit analysis and finite elements. *Canadian geotechnical journal*.

Lee, M., Choi, Y., Kim, M., and Lee, W. (2010). Evaluation of cementation effect of sand using cone resistance. *2nd International Symposium on Cone Penetration Testing, Huntington Beach, CA, USA*.

Long, M., Hadj, N., and Hagberg, K. (2009). Quality of Conventional Fixed Piston Samples of Norwegian Soft Clay. *Journal of Geotechnical and Geoenvironmental Engineering*, 135(2):185–198.

Lunne, T., Berre, T., Andersen, K. H., Strandvik, S., and Sjursen, M. (2007). Effects of sample disturbance and consolidation procedures on measured shear strength of soft marine Norwegian clays. *Canadian Geotechnical Journal*, 44(1):111.

Lutenegger, A. (2006). Cavity expansion model to estimate undrained shear strength in soft clay from dilatometer. *Proceedings from the Second International Flat Dilatometer Conference*.

Maurenbrecher, P. and der Harst, M. V. (1989). The geotechnics of the Coastal Lowlands of the United Arab Emirates. *Coastal Lowlands*.

Mayne, P. (2014). Interpretation of geotechnical parameters from seismic piezocone tests. *Proceedings 3rd international symposium on cone pentrometer testing, CPT*, 14:47–73.

Mcguire, M. P. (2011). Critical heigt and surface deformation of column-supported embankments. *Diss. Virginia Polytechnic Institute and State University*.

McNulty, J. (1965). An experimental study of arching in sand.

Menard (2015). Dynamic Replacement - Overview of Technique. *http://www.vibromenard.co.uk/techniques/dynamic-replacement/*.

Meyerhof, G. and Adams, J. (1968). The ultimate uplift capacity of foundations. *Canadian geotechnical journal*.

Moseley, M. and Kirsch, K. (2004). *Ground Improvement, Second Edition*. CRC Press.

Murray, E. and Geddes, J. (1989). Resistance of passive inclined anchors in cohesionless medium. *Géotechnique*.

Naughton, P. (2007). The significance of critical height in the design of piled embankments. *Soil improvement (GSP 172)*.

NEN (2012). Geotechnical design of Structures - Part 1: General Rules. Technical report, NEN, The Netherlands.

NGG (2002). Nordic Handbook: Reinforced Soils and Fills. Technical report, Nordic Geotechnical Society, Stockholm, Sweden.

Peet, T. (2014). *Arching in basal reinforced piled embankments.* PhD thesis.

Puppala, A., Acar, Y., and Senneset, K. (1993). Cone penetration in cemented sands: bearing capacity interpretation. *Journal of geotechnical engineering, 119(12).*

Puppala, A., Acar, Y., and Tumay, M. (1995). Cone penetration in very weakly cemented sand. *ournal of geotechnical engineering, 119(12).*

Rad, N. and Tumay, M. (1986). Effect of cementation on the cone penetration resistance of sand: A model study. *ASTM geotechnical testing journal.*

Rathmayer, H. (1975). Piled embankment supported by single pile caps.

Robertson, P. and Cabal, K. (2015). Guide to cone penetration testing for geotechnical engineering. *Gregg drilling*, 6th Editio.

Robertson, P. and Campanella, R. (1983). Interpretation of cone penetration tests. Part I: Sand. *Canadian geotechnical journal 20.4*, pages 718–733.

Rogbeck, Y. and Gustavsson, S. (1998). Reinforced piled embankments in Sweden-design aspects. *Proc. 1998 Sixth International Conference on Geosynthetics.*

Ruiter, J. D. (1982). The static cone penetration test. State-of-the-art report. *Proceedings of the 2nd European Symposium on Penetration Testing, ESOPT-II, Amsterdam*, 2:389–405.

Russell, D. and Pierpoint, N. (1997). An assessment of design methods for piled embankments. *Ground Engineering.*

Sabtan, A. and Shehata, W. (1994). Mackintosh probe as an exploration tool. *Bulletin of the International Association of Engineering Geology-Bulletin de l'Association Internationale de Géologie de l'Ingénieur*, pages 89–94.

Schanz, T. and Vermeer, P. (1998). On the stiffness of sands. *Géotechnique.*

Schmertmann, J. (1975). Measurement of in situ shear strength. *In Situ Measurement of Soil Properties.*

Schmertmann, J. (1978). Guidelines for cone penetration test. *No. FHWA-TS-78-209 Final Rpt.*

Shibata, T. and Sekiguchi, H. (1984). Performance of trial embankment on soft clay. *International Conference on Case Histories in Geotechnical Engineering.*

Sloan, J. (2011). Column-supported embankments: full-scale tests and design recommendations. *Diss. Virginia Polytechnic Institute and State University.*

Spangler, M. and Handy, R. (1982). Soil engineering. *New York.*

Taylor, J. and Illing, L. (1969). Holocene intertidal calcium carbonate cementation, Qatar, Persian Gulf. *Sedimentology.*

Terzaghi, K. (1943). Theoretical soil mechanics.

Uzielli, M., Mayne, P., and Cassidy, M. (2013). Probabilistic assessment of design strengths for sands from in-situ testing data. *Modern Geotechnical Design Codes of Practice*, pages 214–227.

Verruijt, A. and Baars, S. V. (2007). Soil mechanics.

Walker, M. (2012). Hot Deserts: Engineering, Geology and Geomorphology: Engineering Group Working Party Report. *Geological Society of London.*

Wikipedia (2016). Shell Integration.

Yun-min, C., Wei-ping, C., and Ren-peng, C. (2008). An experimental investigation of soil arching within basal reinforced and unreinforced piled embankments. *Geotextiles and Geomembranes*, 26(2):164–174.

TUDelft
Delft
University of
Technology

Zaeske, D. (2001). Zur Wirkungsweise von unbewehrten und bewehrten mineralischen Tragschichten über pfahlartigen Gründungselementen. *Master Thesis*.

Co-operating Companies

Gratitude is expressed to the following companies.

Stichting Deltares
Boussinesqweg 1
2629 HV Delft, The Netherlands
Phone No: +31 (0)88 335 8273

Gulf Inspection International Co.
Area-6, Plot-57, Street 61
Sabhan Industrial Area, Kuwait
Phone. No. +965 (0)24733048

Keller Grundbau GmbH
Mausegatt 45
44866 Bochum, Germany
Phone No. +49 (0)2327 8040

MENARD VIBRO
Al Saraya Avenue Building, Blk. A, Rm. 202
PO Box 36750, Al Garhoud, Dubai, United Arab Emirates
Phone No. +971 4 2925 700

Van Oord Dredging and Marine Contractors N.V.
Schaardijk 211
3063 NH Rotterdam, The Netherlands
Phone No: +31 (0)88 826 0000

Plaxis B.V.
Computerlaan 14
2628 XK Delft, The Netherlands
Phone No. +31 (0)15 251 7720

Appendices

Appendix A

Maps

A map of Kuwait is given in figure A.1.

Figure A.1: Map of Kuwait, retrieved from https://fanack.com/kuwait/ on 22-05-2015

The project location in Kuwait is shown by the circle in the bottom-right side of figure A.2

Figure A.2: Project Location, retrieved from http://www.asia-atlas.com/kuwait.htm on 01-07-2015

Appendix B

Column Supported Embankment

B.1 Design Steps

B.1.1 CUR 2010

The design steps CSE, based on CUR226 (2010), slightly adapted to this project:

Table B.1: Design phases for a CSE

Step	Phase	Objectives
1	Global dimensions	1. Geometry of the platform (taking account of critical height etc. 2. Choose platform material and set environmental and structural requirements
2	Bearing capacity of the columns	1. Determine column diameter, depth and center-to-center distance, based on both geotechnical and structural considerations
3	Structural design mattress	1. Calculate the vertical stress, based on the theory of arching effect.
4	Check settlements and stability	1. Calculate the predicted settlement of the column 2. Check the overall stability

Where CUR226 (2010) notes that the long term settlement of the platform is usually negligible.

B.1.2 Recommendations by Filz et al. (2012)

In order to determine global dimensions, reasonable assumptions have to be made. The assumptions are dependent on local soil conditions and future use of the CSE. Filz et al. (2012) summarized[1] materials and variables which determine the performance of a CSE:

- Strength and compressibility of the soft soil;

- Strength and compressibility of the bearing layer on which the columns are founded

- Strength, compressibility, cross-sectional area, length, spacing, and arrangement of the columns or piles and pile caps

- Strength and gradation of select fill material in the load transfer platform, if used

- Strength and gradation of general embankment fill material

---

[1]Geosynthetic reinforcement related variables have been left out.

- Height of the embankment above the tops of the columns

- Surcharge or traffic loading

B.2 Critical Height

Table B.2: Critical Heights

Source	Recommended relationship between column size, spacing, and minimum embankment height	Remarks
BS8006 (1995)	Full arching is developed when embankment height is at least 1.4(sa). BS8006 (1995) states that H>0.7(sa) to ensure localized differential deformations cannot occur at the surface of embankments	According to Horgan and Sarsby (2002), BS8006 defines critical height as the fill thickness whereby full arching is developed and any additional fill or surcharge is distributed completely to the pile caps.
Carlsson (1987) as reported in Rogbeck and Gustavsson (1998)	To limit surface displacements, the height of embankment should be at least equal to the greater of 1 meter and the distance between pile caps. The area replacement ratio should be at least 10 percent.	The height of the soil arches considered in Carlsson's approach are equal to 1.87(s-a).
Yun-min et al. (2008)	To ensure that no differential settlement occurs at the embankment surface, a minimum embankment height equal to 1.6(s-a) is necessary.	Plane strain experimental testing indicated that the plane of equal settlement occurs at height above the pile caps equal to 1.4 to 1.6 times the clear spacing, (s-a). Yun-min et al. (2008) use the term 'plane of equal settlement' to indicate the embankment height above which no differential settlement occurs and the term 'critical height' to define the height above which all embankment weight and surcharge is carried by the pile caps.
Collin (2007)	The thickness of the load transfer platform reinforced with at least four layers of reinforcement must be equal to or greater than 0.5(s-d).	Soil unsupported by arching forms a pyramid with sides inclined at 45 degrees.
Demerdash (1996)	To prevent differential surface settlement, H>1.7(s-a)	Demerdash (1996) reports the 'Plane of equal settlement', which is the elevation within the embankment where settlement becomes uniform, was experimentally found to equal 1.7 to 2.0 times (s-a).
Ellis and Aslam (2009a);(Ellis and Aslam, 2009b)	No recommendations given.	Based on the results from centrifuge modeling, Ellis and Aslam report that little to no differential surface settlement occurs for unreinforced embankments when the height is equal to or greater than twice the clear span between pile caps, (s-a).
Hewlett and Randolph (1988)	For square grid of square pile caps, the minimum height of high-grade (Kp>3) fill should not be less than the pile spacing and the total embankment height should not be less than twice the pile spacing. The pile cap width should be selected such that a/s ≥ 1/3.	Soil arching forms hemispherical domes between adjacent pile caps with a height equal to $\frac{s}{\sqrt{2}}$. Failure of the arches can occur either at the base or crown of the arch. The recommendations select geometries where the limiting condition for the arch is at the base where bearing capacity can be improved by use of high quality fill and geosynthetics.

TUDelft
Delft
University of
Technology

Horgan and Sarsby (2002)	No recommendations given.	Based on the results of model tests, Horgan and Sarsby (2002) report a significant increase in load transfer by arching when embankment height increases from 1.545 to 1.92 times the clear spacing, (s-a).
Huat et al. (1994)	The thickness of high quality fill need not extend higher than the pile spacing. Higher area replacement ratio increases arching.	Huat et al. (1994) report no significant increase in load transfer to the columns for fill thicknesses greater than 1 to 2 times the pile spacing, depending on area replacement ratio.
Kempfert and Gobel (2004)	Kempfert and Gobel (2004) defines s as the greatest column spacing. For a square array, s equals √2 times the center-to-center spacing. The clear spacing, (s-d), should be less than or equal to 3.0 m for static loads, 2.5 m for heavy live loads. The clear spacing should also be less than or equal to 1.4 times the embankment height above the reinforcement. The ratio of cap diameter to column spacing, d/s, should be equal to or greater than 0.15.	Using Kempfert's definition for s, the height of the soil arches is considered to equal s/2. When the embankment height is less than s/2, the height of the arches is considered to equal the embankment height.
Naughton (2007)	Assuming the shear planes follow a log spiral path, the critical height is equal to $C(s-a)$, where $C = 0.5\, e^{0.5\pi tan\varphi}$, typically $C = 1.24 - 2.40$.	The term 'critical height' is defined as the distance from the top of the pile caps to the height of the plane of equal settlement in the embankment.
NGG (2002)	To limit surface deformation, the embankment height should at least be as large as 1.2 times the distance between pile caps. The area replacement ratio should be at least 10 percent. Lower embankment heights are permitted if the design includes finite element calculations	No remarks.

B.3 Hewlett (1988)

In the model a plane-strain case is assumed. The band of soil containing the arch is considered weightless. The soil in the infilling between the arches and beneath the arches is assumed to be in isotropic stress state. Within the arch critical state is reached., so the ratio between tangential and radial stress is equal to the passive earth pressure coefficient, K_p. The equilibrium of an element in the arch is elaborated, resulting in equation B.1 (Please note that in equation B.1 an error made in Hewlett and Randolph (1988) is corrected).

$$E \;=\; 1 - \frac{b\,\sigma_i}{H\,\gamma\,s} \;=\; 1 - \delta(1 - \frac{s}{2H})(1-\delta)^{(K_p-1)} \tag{B.1}$$

Where δ=b/s.

The interpretation of a CSE by Hewlett and Randolph (1988) is illustrated in figure B.1.
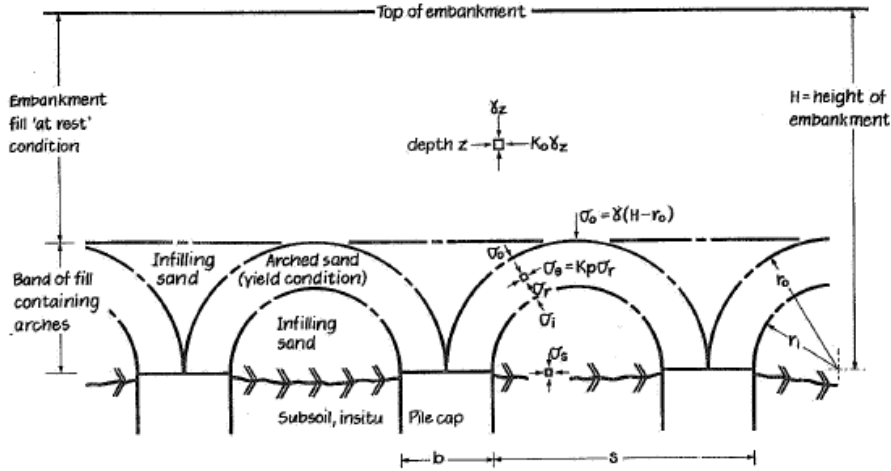
Figure B.1: Interpretation of a CSE by Hewlett and Randolph (1988)

Hewlett and Randolph (1988) refers to Hewlett (1984) for the case where self-weight of the arch is considered. It is shown there that in that case the critical zone is at the crown the arch. This may however not be the case in a 3D model; in this case limit state may develop at the contact with the pile caps. For this case an additional equilibrium is considered. Hewlett and Randolph (1988) proposes to take the lowest efficiency E value of both calculations.

In the 3D model the self-weight of the arch is considered. By including the weight of the soil wedge under the arch, a pressure can be calculated on the soft soil. This pressure is assumed to be constant over the area within the arches. The arching E (referred to as efficacy by Hewlett and Randolph (1988)) is then determined by equation B.2.

$$E = 1 - \frac{s^2 - b^2}{s^2 \ \gamma \ H} = 1 - (1 - \delta^2)(A - AB + C)$$

$$A = (1 - \delta)^{2(K_p - 1)}$$

$$B = \frac{S}{\sqrt{2}H} \left(\frac{2K_p - 2}{2K_p - 3} \right)$$

$$C = \frac{s - b}{\sqrt{2}H} \left(\frac{2K_p - 2}{2K_p - 3} \right)$$

(B.2)

For the total load on a pile, four 2D arches are integrated across the cap, resulting in equation B.3.

$$E \ = \frac{\beta}{1 + \beta}$$

$$\beta \ = \frac{2K_p}{K_p + 1} \frac{1}{1 + \delta} \left[(1 - \delta)^{-K_p} - (1 + \delta K_p) \right]$$

(B.3)

An illustrative design graph is given in figure B.2.

B.3.1   Incremental Efficiency

The method by is modified fairly straightforward to represent ΔE. The formula calculating the efficiency for the case where the cap is governing, given in equation B.3, is only dependent on K_p and δ. For the case at hand only H is varied so the efficiency remains constant.

TUDelft
Delft
University of
Technology
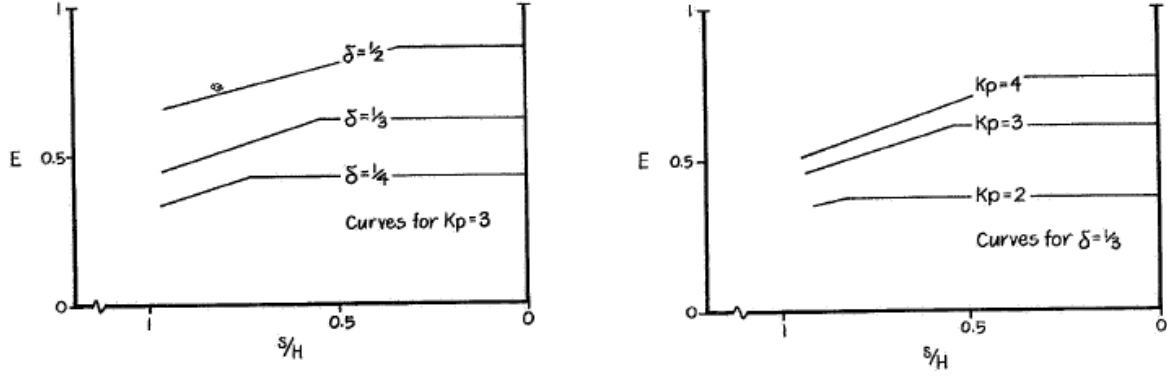
Figure B.2: Design graphs by Hewlett and Randolph (1988)

The formula calculating the efficiency for the case where the crown is governing is presented below.

$$E_{Hewlett} \; = \; 1 - \frac{s^2 - b^2}{s^2 \, \gamma \, H} \; = \; 1 - (1 - \frac{b^2}{s^2 \, \gamma \, H}) \; = \; 1 - (1 - \delta^2) \, \frac{\sigma_s}{\gamma \, H} \; = \; 1 - (1 - \delta^2)(A - AB + C)$$

$$= \; 1 - (1 - \delta^2) \, SRR \; \rightarrow \; SRR \; = \; (A - AB + C) \tag{B.4}$$

Where A, B and C are independent of γ and q. Based on equation B.4 it may be concluded that the efficiency based on Hewlett and Randolph (1988) is independent of q for a given H so that:

$$E_{Hewlett} \; = \; \Delta E \tag{B.5}$$

B.4   Zaeske (2001)

Zaeske (2001) assumes arches to form between the columns, with an increasing radius towards the outer arch. The method to calculate the stress in the subsoil is calculated using equation B.6.

$$\sigma_{z0} \; = \; \lambda_1^\chi \, (\gamma + \frac{q}{H}) \Big[H(\lambda_1 + H_g^2 \lambda_2)^{-\chi} \; + \; H_g \, ((\lambda_1 + \frac{H_g^2 \, \lambda_2}{4})^{-\chi} \; - \; (\lambda_1 + H_g^2 \lambda_2)^{-\chi}) \Big]$$

$$\lambda_1 \; = \; \frac{1}{8}(s_d - d)^2$$

$$\lambda_2 \; = \; \frac{s_d^2 + 2ds_d - d^2}{2s_d^2} \tag{B.6}$$

$$\chi \; = \; \frac{d(K_{krit} - 1)}{\lambda_2 s_d}$$

$$K_{krit} \; = \; \tan^2(45 + \frac{\varphi}{2}) \; = \; \frac{1 - \sin \, \varphi}{1 + \sin \, \varphi}$$

Zaeske (2001) elaborates and plots equation B.6 for a set of friction angles and platform heights to serve as design graphs. An example of such a graph is given in figure B.4.

Note that Zaeske (2001) uses the SRR rather than efficiency in his plots (y-axis).

Van Oord
Marine ingenuity
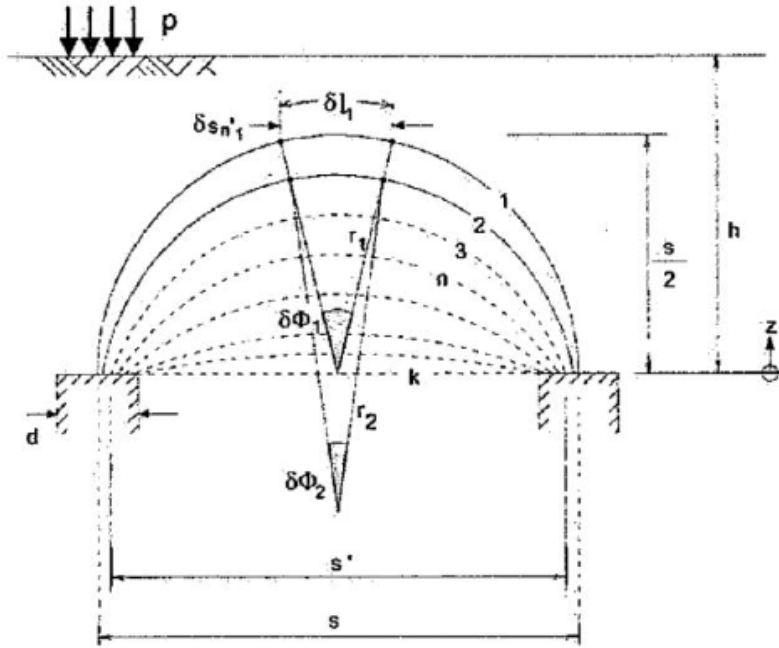
Figure B.3: Soil arches by (Zaeske, 2001)
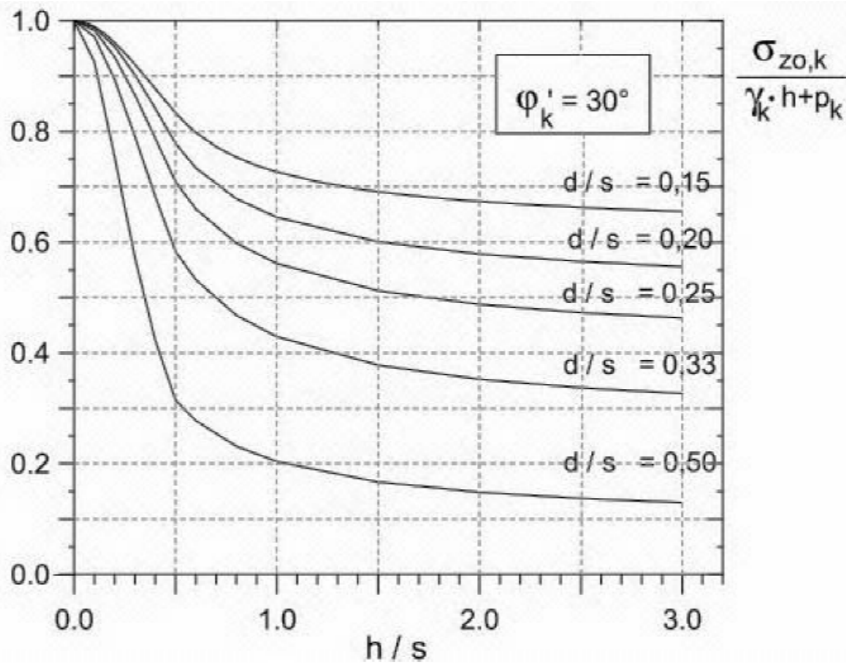
Figure B.4: Example design graph by Zaeske (2001) for $\varphi = 30°$

B.4.1   Incremental Efficiency

The elaboration to determine ΔE based on Zaeske (2001) is given below.

$$\sigma_{z0} = \lambda_1^\chi \left(\gamma + \frac{q}{H}\right)\left[H(\lambda_1 + H_g^2\lambda_2)^{-\chi} + H_g\left((\lambda_1 + \frac{H_g^2\,\lambda_2}{4})^{-\chi} - (\lambda_1 + H_g^2\lambda_2)^{-\chi}\right)\right]$$

(B.7)

$$= Z\left(\gamma + \frac{q}{H}\right)$$

Where Z is **independent** of q and defined as:

$$Z = \lambda_1^\chi \left[H(\lambda_1 + H_g^2 \lambda_2)^{-\chi} + H_g \left((\lambda_1 + \frac{H_g^2 \lambda_2}{4})^{-\chi} - (\lambda_1 + H_g^2 \lambda_2)^{-\chi} \right) \right] \tag{B.8}$$

The efficiency can be defined as follows (using Zaeske's σ_{z0} rather than σ_s:

$$E_{Zaeske} = 1 - \frac{\sigma_{z0}}{\gamma H q} (1 - \alpha) = 1 - Z \frac{\gamma + \frac{q}{H}}{\gamma H + q} (1 - \alpha) \tag{B.9}$$

Using common denominator H results in:

$$E_{Zaeske} = 1 - Z \left(\frac{\gamma + \frac{q}{H}}{H(\gamma + \frac{q}{H})} \right) (1 - \alpha) = 1 - Z \frac{\frac{\gamma + \frac{q}{H}}{\gamma + \frac{q}{H}}}{H}(1 - \alpha) = 1 - \frac{Z}{H} (1 - \alpha) \tag{B.10}$$

It can be concluded that the efficiency is independent of q for a given H. The incremental efficiency thus equals the efficiency calculated for a particular platform height, i.e. E remains constant for a varying q for a given H resulting in:

$$E_{Zaeske} = \Delta E \tag{B.11}$$

B.5   Stiffness Ratio Method

The stress distribution is based on a stiffness difference between the columns and soft soil. The following equations are given:

Balance of areas:

$$A = A_c + A_s, \text{ and } \alpha = \frac{A_c}{A}$$

$$\tag{B.12}$$

this becomes:

$$A_c = \alpha A \text{ and } A_s = (1 - \alpha)A$$

Balance of settlement:

$$\frac{\Delta H}{H} = \frac{\sigma_c}{E_c} = \frac{\sigma_s}{E_s} \rightarrow \frac{\sigma_c}{\sigma_s} = \frac{E_p}{E_s} = m \tag{B.13}$$

Balance of load:

$$A \sigma = A_c \sigma_c + A_s \sigma_s \rightarrow \sigma = \alpha \sigma_c + (1 - \alpha)\sigma_s \tag{B.14}$$

It follows that $\sigma_c = m \sigma_s$. Using equation B.12, $A_c = \pi r^2$ and $A_s = s^2 - A_c$ leads to:

$$\sigma_c = \frac{\sigma A}{\pi d^2 + \frac{s^2 - \pi r^2}{m}} \tag{B.15}$$

The efficiency and subsequently the incremental efficiency can be calculated using equation B.16.

$$E = \frac{\sigma_c A_c}{\sigma A} \rightarrow \Delta E = \frac{(\Delta\sigma_{c,1} - \Delta\sigma_{c,0}) A_c}{\Delta q s^2} \tag{B.16}$$

Van Oord
Marine ingenuity

B.6 Parametric Study

Some studies (Rathmayer, 1975), (Hewlett and Randolph, 1988), (Zaeske, 2001), (Han and Gabr, 2002),(Jenck et al., 2007), (Eekelen et al., 2013) and (Peet, 2014) report on a parametric study. A summary of these studies is given in this section, elaborated per parameter.

B.6.1 Parametric study of the columns and platform

Friction angle

From the tests performed by Rathmayer (1975), it was concluded that the friction angle of the material in the fill has an influence on the embankment height. The tests were performed without GR and it was found that the embankment height was lower for the same coverage by pile for higher friction angles (crushed stone compared to gravel fill). Jenck et al. (2007)[2] carried out experiments and compared those with numerical modelling. He uses a reference friction angle of 24°and calculates the efficiency E for different values between 10 and 40°. He found that an increasing friction angle increases the arching. However, a friction angle beyond 30°does not significantly increase arching. Jenck et al. (2007) highlights that friction angle is of importance on the arching, this is due to the fact that arching is controlled by shear mechanisms.

Eekelen and Bezuijen (2012) performed tests with sand and another granular material with a friction angle of 39-40°and 45-49°, respectively. The tests included a GR. At the end of her tests for both materials, it was found that load part B (the load on the GR) was 39% higher for the sand compared to the granular fill.

Peet (2014) showed with Plaxis calculations that the arching increases with an increasing friction angle. Graphs were plotted for different models ((Eekelen et al., 2013), (Zaeske, 2001), (Hewlett and Randolph, 1988) and the Plaxis calculation) and an approximately linear relation was found between friction angle and arching. The starting points of the lines were different for the models.

Cohesion

The reference material that Jenck et al. (2007) used in the physical is cohesionless. Calculations using the numerical modelling were performed though, with a cohesion of 10 kPa. He found that, compared to the reference case, the efficiency E increased by 21% and the settlements reduced by 53%.

Dilatancy Angle

As the arching effect in the platform is driven by shearing mechanisms it is important to focus on the platform material dilatancy angle ψ influence. In the modified Mohr Coulomb model the dilatancy angle actually plays a role when shear failure occurs (Jenck et al., 2007). In the tests performed by Jenck et al. (2007), the reference value for ν is 4°. Calculations were also carried out for a ν of 0°and 10°, both with- and without GR. For the GR case it was found that settlements increased with 20% for a ν of 0°. For a ν of 10°a settlement reduction of 13% was found. Compared to the reinforced case the settlement reduction is always in the range of 70-80% for every dilatancy angle tested.

Young's Modulus

In the calculations in Han and Gabr (2002) different elastic moduli of the pile were used. The results show a decrease in maximum settlement with an increase in elastic modulus. The difference in settlement was found to be about 5%. Furthermore the stiffness of the GR was varied in the calculations. In figure 7 in Han and Gabr (2002) it can be seen that there is a sharp reduction in maximum settlement for a strength between 0 and 1000 kN/m. A stiffer GR will result in less settlements up to approximately 4000 kN/m.

---

[2]For the numerical calculations by Jenck et al. (2007), one should keep in mind that the contribution of the parametric study results is limited due to the material used (Schneebeli's rods) which is different from the material used in a real earth platform, additionally to the two-dimensional aspect of the modelling (Jenck et al., 2007).

TUDelft
Delft
University of
Technology

Jenck et al. (2007) investigated the influence of a Young's modulus ten times larger and ten times smaller than the reference value (for the piles, ref. value 12 MPa). It was found that an Young's modulus ten times larger has no impact on either the efficiency E or surface settlements, whereas a smaller value leads to a weaker arching (reduction of 20%) and larger surface settlement (increase of 180%)

B.6.2 Parametric study of the soft soil

Jenck et al. (2007) used foam in his experiment to investigate the influence of the Young's modulus on settlements and aching, he used foams with a Young's modulus three times smaller and three times larger than the reference value of 35-82 kPa. The smaller Young's modulus, thus a more compressible soil, has no impact on the arching compared to the reference case. The higher Young's modulus however leads to a reduction of arching of about 13%. Jenck et al. (2007) notes that this may be the result from insufficient arch formation in the platform due to a lack of settlement (as described in Terzaghi (1943)).

Yun-min et al. (2008) performed experimental investigations both on reinforced and unreinforced piled embankments. The test set-up consists of water bags in between which beams were placed. On top of the beams and water bags soil stress transducers (SST) were placed. After the embankment was filled, the water was drained from the bags, inducing settlements (to simulate consolidation). It was found in figure 3b citepTunmin2008 that a configuration of h/s = 0.7 led to a continuous increase in soil pressure. At higher ratios of h/s, starting at 0.9, an arching effect was noticed. In the latter case the soil pressure decreased with pile-subsoil relative displacement (induced by the draining water bags), down to a threshold value. In figure 4 in (Yun-min et al., 2008) a diagram is given showing the relative displacement plotted against the SCR. For all values of h/s the SCR increases with relative displacement. A peak is found at 10-15mm displacement, after which the SCR decreases and then remains constant.

The findings from Yun-min et al. (2008) can be compared with the results from Jenck et al. (2007). Where the former used water bags to induce settlement, the latter used a more compressible foam to induce settlement. Jenck et al. (2007) notes that the arching remains the same for a lower Young's modulus, and that is reflected in the results from Yun-min et al. (2008), who found a treshold value for the SCR. Also, the latter found a peak in the settlement/SCR diagram. The 'rigid' Young's modulus Jenck et al. (2007) chose may have led to a settlement just after the peak in the settlement/SCR diagram. This would lead to a lower SCR, or, in Jenck's terminology, efficacy.

Eekelen and Bezuijen (2012) showed with experiments that during consolidation both the A% and the B% increase. In the experiments multiple loading/consolidation phases were induced. The fact that an increase in A% was noticed during consolidation agrees with the data found by Yun-min et al. (2008). Since geotextile was used in the tests by Eekelen and Bezuijen (2012), the results will not be elaborated further.

An extensive elaboration on the soft soil found at ZOR is given in chapter 3 and chapter C.

TUDelft

Appendix C

Soil investigations

This section describes a selection of relevant soil investigations that have been performed in the area of Kuwait.

C.1 Site investigation Al-Amoudi et al. (1992)

This section is based on site investigations described by Al-Amoudi et al. (1992) and Abduljauwad and Al-Amoudi (1995). The location of the investigation is the Eastern Province of Saudi Arabia, the Ras Al-Ghar, approximately 450 km south of the Al-Zour site.

C.1.1 Brine analysis

By virtue of its chemical nature, analysis of the sabkha's brine is regarded as the prerequisite test to elucidate the spontaneously perpetual interaction between the sediments and the groundwaters of the sabkha and, ultimately, the system (Abduljauwad and Al-Amoudi, 1995). As described in paragraph 3.3.2, the brine may be up to six times as high in concentrations compared to seawater. The tests on brine from the Ras Al-Gahr site agree with the latter statement, having salt concentrations of approximately five times the concentration found in seawater.

C.1.2 Borelog

The borelog revealed loose, brown, fine to medium sand with salt crystals. The layer is underlain by a rock salt layer. The bottom layer is characterized by the presense of light grey calcareous sand increasing in density with depth. Groundwater was encountered at a depth of 0.8 m. X-ray diffraction analysis on the top (sabkha) layers indicated that the sediments are mainly quartz (49%), cemented with halite (23%), calcite (21%), gypsum (6%) and traces of clay and iron oxides.

C.1.3 Permeability

Tests were performed both with brine and distilled water. The results are shown in figure 15 a & b in Abduljauwad and Al-Amoudi (1995). It can be seen that the permeability coefficient does not (significantly) change in the test with brine. This is due to the high salt concentration in the brine, which renders it incapable of dissolving salts. The permeability increased when distilled water was used, with approximately 120%. The increase in permeability can be attributed to the washing away of the natural cementation and the development of voids and flow channels between the quartz particles (Abduljauwad and Al-Amoudi, 1995). When leaching occurs under loading, the permeability coefficient initially increases and then decreases, finally tending to a constant value. Leaching of salts under loads will be accompanied by consolidation of soil and by the formation of large, partially closes caverns. This leads to an increase in the overall porosity, but permeability reduces due to consolidation of the main soil mass. Abduljauwad and Al-Amoudi (1995).

C.1.4 California Bearing Ratio

CBR[1] tests were performed on-site and in the laboratory, both with brine and distilled water. The results can be found in figure 16 in Abduljauwad and Al-Amoudi (1995). It can be concluded that the tests which have been soaked with distilled water show higher penetration compared to the tests soaked with brine. The latter statement is valid for both the field and the laboratory tests. This indicates a significant reduction is strength and the susceptibility of sabkha to collapse when it is soaked or leached with water. Soaking under load results in softening and weakening of structural colloidal bonds and dissolution of crystalline bonds produced by salts. (Abduljauwad and Al-Amoudi, 1995)

C.1.5 Plate Load Test

PLTs were performed with a plate diameter of 460 mm at a depth of 40 cm. The test pit was excavated with a diameter of approximately four times the diameter of the plate. The tests were conducted under natural conditions, with brine and with distilled water. The test results show in figure 16 in Abduljauwad and Al-Amoudi (1995) the leaching the site with brine has no major effect. Leaching the site with water reduced the bearing capacity and increased settlement at all applied pressures. Abduljauwad and Al-Amoudi (1995) used the intersecting tangents method from Spangler and Handy (1982). The bearing capacities were found to be 100 kPa, 95 kPa and 70 kPa for the natural conditions, the test with brine and the test with water, respectively.

C.2 Dhowian et al. (1987)

The tests performed by Dhowian et al. (1987) were located in the town of Jazan, situated on the South-West coast of Saudi Arabia. This location may not be very relevant for the NRP, the results will be shortly discussed however because of the long term test that are available and lacking from other investigations.

The sabkha layer in this investigation is 9.5 m thick, and underlies a 1.0 m sabkha crust. The sabkha base is at 10.5 m minus surface. The top part of the sabkha profile consists of highly plastic organic clays.

The load on top of the sabkha is an embankment. In the first stage a volume of 40x40 m with a height of 1 m was placed. In the second stage the height was increased with 2 m on an area of 15x15 m. at the centre. Settlement plates were installed at the corners and center of the second stage embankment, as well as piezometers.

It can be seen in figure 9 in Dhowian et al. (1987) that there is a very long secondary consolidation period, still settling after ten weeks. This is typical for soils which are high in organic content.

The graph in figure 12 in Dhowian et al. (1987) shows the excess pore pressure with time. The initial increase in pore pressure is comparable with the increase in the total vertical stress due to the loading. During the second stage however, the piezometer shows a sudden drop in pore pressure. This behaviour is expected due to the fact that the stratum under consideration possesses a well developed macro fabric which consists of thin seams, lenses and pockets of fine sand. These permeable sublayers allow spontaneous dissipation of the pore pressures during the construction period. (Shibata and Sekiguchi, 1984), (Jamiolkowski and Lancellotta, 1984)

The results show the relevance of organic content for (long-term) settlements. The presence of organic content will lead to greater settlements, and longer settlement periods. Furthermore, because of the presence of lenses consisting of fine sand, the consolidation characteristics may show high spatial variability.

The results from the investigation presented are in line with the results from Al-Shamrani (2005) and the latter investigation will thus not be discussed.

---

[1]The test is performed by measuring the pressure required to penetrate a soil sample with a plunger of standard area. The measured pressure is then divided by the pressure required to achieve an equal penetration on a standard crushed rock material. The CBR test is described in ASTM Standards D1883-14.

C.3 Ismael (1993)

Ismael (1993) performed tests on sabkha for the design of a multi-story building in downtown Kuwait city, requiring deep excavations and dewatering. The field leaching tests included penetration and plate-bearing tests before and after leaching with fresh water over a period of six months. Two borings were done, one hollow auger system to retrieve samples and perform SPTs and one boring taking Shelby tube samples. Furthermore CPTs were performed.

The samples were subjected to a permeability test. During the test the electrical conductivity (EC) and total dissolved salts (TDS) were measured. Soil permeability was also measured after every litre of (fresh) water. Comparable with the tests reported by Al-Amoudi et al. (1992), the permeability increased with 100% from $1.75 \cdot 10^{-5}$ to $3.5 \cdot 10^{-5}$ m/s. The TDS and EC decreased sharply during the initial stage of the test, followed by a gradual decrease to residual values. After the test small cavaties, irregular channels and holes were seen in the sample. The sample was described as honeycombed (Ismael, 1993). Chemical analysis on the sample revealed that nearly al chlorides had dissolved, sulphates partially dissolved. Is was found that gypsym and anhydrite were less soluble. It was also found that the strength had decreased 33.5 to 2.3 kPa (in terms of unconfined compressive strength). Consolidation test showed that the initial void ratio e was higher for the leached sample compared to the natural sample. This was expected based on the text above. During loading it can be seen in figure 9 in (Ismael, 1993) that high pressures (approximately 1300 kPa) the e decreased past the e of the natural sample. During unloading, the e of the leached sample remained lower than the natural sample. The consolidated undrained (CU) triaxial tests resulted in a lower axial stress σ_1 for equal confining pressures σ_3 for the leached samples compared to the natural samples. From an undrained $q' - p'$ diagram the friction angle ϕ was determined: 36.5 °for the natural sample and 34°for the leached sample.

Part of the investigation were field tests. A test area of 5 x 10 m was selected for leaching tests. Drill holes (diameter 0.3 m) of 1.5 m depth were made along the edges of the area, every 1.5 m. The holes were filled with gravel to enhance water drainage. The site was leached with water (3785 l) every two weeks. After two weeks, the same amount was poured every day for another two weeks. After a total of four weeks samples were taken out of a depth of 0.3 m and tested for TDS and EC. It was found that the leached soil had not yet reached the residual value (as mentioned before), for either TDS or EC. The inital value for both TDS and EC were however lower for the leached sample compared to the natural sample. It can thus be conlcuded that only partial leaching had occured. Ismael (1993) attributes this limited leaching to evaporation and the fact that the leaching in field conditions occur under different confining stresses compared to the laboratory. After samples were taken, CPT tests were performed. It can be seen in figure 2 in Ismael (1993) that there is an approximately 50% reduction in cone resistance at a depth between 1 - 1.5 m. Below this depth no significant effect is noticed. A plate load test was performed in the area after the CPT. It turned out that there is a 42% reduction in bearing capacity due to field leaching. As the soil clearly failed in punching shear, it is assumed that the failure occurred in the topsoil until a depth of 1 -1.5 m.

From the test results by Ismael (1993), for instance shown in figure 10 in the paper, one can conclude that the reduction in strength of the sabkha is most severe for low to medium confining pressures (50-200 kPa). For higher pressures (300 kPa), the reduction is less severe (in CU tests). This conclusion can also be drawn for the void ratio and indirectly for the permeability; the oedometer shows a lower void ratio for a leached sample at high pressures (>1300 kPa).

Appendix D

Field testing

D.1 Soil Tests

D.1.1 Boring and Sampling

For borings in sabkha soil, the conventional soft soil boring techniques are used. Because of the strength loss under saturation, water-less techniques are preferred. The Auger boring system can very well be used. SPT tests can be done in intervals (usually when adding an auger). When tubes samples are needed, the rotary hollow-stem auger system can be used. This system allows lowering down a pushed or driven tube to the borehole bottom. Penetration of weakly cemented layers is possible, but the auger is likely to meet refusal in strongly indurated layers (e.g. in floating duricrusts) (Walker, 2012)

D.1.2 Cone Penetration Test

The cone penetration test (CPT) is used to check the requirements concerning level of compaction, bearing capacity and (future) settlements. To this extent, it seems useful to determine the applicability of CPT in the soils that are found at ZOR. One of the soils found here is sabkha, as described in chapter 3. The platform and columns consist of a hydraulic fill, which is sand.

Based on the CPT results, settlements and dry densities can be predicted. In the ZOR project, this is done by the method described in section H.2.

Cementation

It is already described that the sabkha soil has cementation between the grains, this is illustrated in figure 3.1. It is known from previous studies (Puppala et al., 1995), (Lee et al., 2010), that cementation of soil has an influence on the cone resistance and sleeve friction. Rad and Tumay (1986), Akili and Al-Joulani (1988) and Puppala et al. (1993) test results showed that cementation increases the cone resistance and sleeve friction and decreases friction ratio. These findings have once more been confirmed by tests by Puppala et al. (1995). In the latter tests sand was used which was cemented with 0%, 1% and 2% Portland cement. It was found that at a vertical stress of less than 100 kPa, the cone resistance may increase up to two to three times the uncemented values (for the 1% and 2% test, respectively). The confinement effect overshadows the weak cementation at higher vertical stresses, e.g. 15-25% and 40-45% increase in cone resistance (for the 1% and 2% test, respectively) at a confinement of 300 kPa (Puppala et al., 1995). It is furthermore noted in the latter reference that predictions of relative density and peak friction angle from charts developed for clean, uncemented sands may be significantly biased in very weakly cemented sand deposits. The higher tip resistances recorded in cemented sands result in significantly higher relative density estimates.

CPT Literature

Hossain and Sabtan (1994)

Hossain and Sabtan (1994) performed a site investigation in what is referred to as 'Obhor sabkha'. With Obhor Hossain and Sabtan (1994) refers to a sea bay (Red Sea) approximately 30 km North of Jeddah City, Saudi Arabia. The site investigation described here is the second investigation at the same site. The first one was described by Hossain and Ali (1990) and involved Mackintosh probing[1] and field Vane

---

[1]The Mackintosh probe is one of most widespread penetrometers in use in Saudi Arabia. Mackintosh probe with its 30°apex angle, 1.1 in diameter cone, 4.5 kg hammer and 30 cm drop height is a light dynamic cone penetrometer that can be operated manually. (Sabtan and Shehata, 1994)

shear tests. The 1994 investigation compares the results from the 1990 investigation with pressuremeter test (PMT) and CPT results. The subsoi layering was known from the 1990 investigation.

The results of the CPT show the crust layer on top and the end of the soft layer. The fluctuations in $(q_c - p_{v,0})$ and s_u observed in figure 13 in Hossain and Sabtan (1994) are considered to be interference of gypsum crystals and shells and partly due to the random variations in strength of clay. It also shows in figure 14 of the 1994 investigation that the CPT correlations for undrained strength, s_u, tend to over predict compared to the undrained strength from the FVT. The strength is calculated based on the correlation in equation D.1

$$s_u = \frac{q_c}{14} \tag{D.1}$$

Moreover, in figure 15 and 16 in Hossain and Sabtan (1994) it can be seen that there is no clear relation between the undrained strength and the cone resistance for neither the soft clay nor the stiff clay. The trend is however that the undrained strength seems to increase with cone resistance, which is a well established finding (e.g. (Schmertmann, 1975), (Ruiter, 1982)).

Bates and Merifield (2010)

An evaluation of using the CPT for assessing ground improvement by DR for a project on Koorang Island, Newcastle, Australia. For the project, a new coal loading facility, a hydraulic fill was placed on top of 1 - 4 m of silty clay q_c 0.2 - 0.5 MPa. Under the clay layer a fine to medium sand of medium density was present.

The tests by Bates included CPT, DMT and PLT. It is believed that the Oedometer modulus, E_{oed} and the undrained shear strength are the most reliable parameters that can be derived from a DMT. The $E_{oed,DMT}$ is compared with the $E_{oed,CPT}$. The author notes that stiffness parameters are not as reliable as strength parameters from CPT. Young's modulus is derived from the CPT using Schmertmann (1978). The agreement between DMT and CPT was very dependent on the α_E used (see section H.2). With α_E = 8, the CPT tends to over-predict the modulus.

Estimates of the E_{oed} are provided by a ZLT, based on elastic theory of a rigid loaded circular area. Compared to post CPT testing at the same column location, the PLT estimates compared well to the CPT interpreted modulus at shallow depths (i.e. <2m), tending to conservative for depths greater than 2 m (Bates and Merifield, 2010).

It is mentioned in the paper that the ageing is a very real phenomenon and is observed in the results. The author however notes that the CPT are performed immediately after column construction, and sixteen days later. It is the author's opinion that the strength increase over that period is due to consolidation rather than soil ageing.

D.1.3 Standard Penetration Test and Mackintosh Probing

A relatively economical (in terms of investment costs) alternative to the CPT is the Standard Penetration Test (SPT).

Hossain and Ali (1990) discussed the use of FVT and Mackintosh probe (MP) (as described in Chan and Chin (1972)) in a sabkha area North of Jedda, Saudi-Arabia. It was found that the MP suffered less disturbance from the gypsum and shell content of the soil, compared to the FVT. They suggested a tentative relation between the blow count and FVT results.

Maurenbrecher and der Harst (1989) described site investigations for foundation pile design. To this extent borehole sampling, CPT and SPT were performed. In total five sites in Abu Dhabi, United Arab Emirates, were compared. Although the correlation can be considered good by virtue of standard borehole sampling/testing sequence, the SPT fail to measure the strength of the surface crust and often miss relatively lower density layers such as the two SPT profiles from site AD2. In this instance a pile founded at 8 m moved excessively during its loading test (Maurenbrecher and der Harst, 1989). It can

---

During a Mackintosh test the number of blows of the weight is recorded. Contrary to the SPT, no split spoon sample is taken

be seen in figure 13 in Maurenbrecher and der Harst (1989) that the CPT penetrates through a layer of lower density while the SPT value increases.

The benefits, in terms of mobility and speed, of the CPT are not valid for the SPT. The SPT is used in intervals during a boring. This makes the technique more expensive and time consuming. It is however noted that when a SPT is performed complimentary to a regular boring (which is usually the case), the costs are very limited (compared to the boring).

D.1.4 Pressuremeter Test

The standard (Menard) pressuremeter test (PMT) consists of two elements, the probe that is lowered into a pre-drilled hole and the pressure and volume control unit (CPV) that remains on the ground and is connected to the probe by connecting tubes (Walker, 2012). The probe consists of a inflatable membrane. During the test the membrane is inflated until the walls of the borehole begin to deform. The pressure is then held constant for some time. After a pre described period the volume that is required to maintain pressure is recorded.

A special pressuremeter test probe is the flat dilatometer test (DMT). In this test a flat probe is pushed in the ground. Three different pressures[2] are measured on the basis of which undrained shear strength and other parameters can be derived (Lutenegger, 2006).

The results from PMT by Hossain and Sabtan (1994) show that the correspondence between the limit pressure P_l from the PMT, the $s_{u,Vane}$ and the M value from the Mackintosh test is not very good for every borehole. This is also seen in a previous investigation by Hossain and Ali (1990), and is considered to be partly due to the raise of some of the s_u values locally by the interference on the vane rotation by the large gypsum crystals or shells present in these sabkha clays (Hossain and Sabtan, 1994).

The $s_{u,PMT}$ are generally higher compared to the $s_{u,Vane}$. This difference is due to disturbance during boring prior to testing (Baguelin, 1978); (Hossain and Sabtan, 1994).

It is concluded that the PMT is technically feasible in sabkha soil. The correspondence between the undrained shear strength from a PMT and FVT is however not very good.

D.2 Load Test

An estimation of settlement is made using the CPT method. This method is described in section H.2.

The following section describes the Zone Load Test, a test to determine settlement at a given foundation pressure.

The Zone Load Test (ZLT) consists of the following elements:

Element	Description
Precast concrete footing	The footing measures 3 x 3 m and 0.6 m thick. A steel bearing plate with diameter 0.8 m and thickness 0.02 m will be laid directly on the concrete footing.
Load Cell	A hydraulic jack including a load cell will be placed on the steel bearing plate. Between the top of the jack and the steel beams supporting the reaction weight, a bearing plate of sufficient thickness is used.
Settlement recording gauges	Measurement is performed by means of four dial gauges attached to the midpoints between the corners of the steel bearing plate.
Loading blocks	Concrete blocks of 1.50 x 2.40 x 0.60 m will be used and placed on top of the supporting beams. The supporting beams are supported by a bearing plate on top of the hydraulic jack.

---

[2]See http://www.insitusoil.com/dilatometer.html for a more elaborate description of this technique

Van Oord
Marine ingenuity

D.2.1 Set-up

The area of the test base shall be carefully leveled and checked for leve using an engineering level. This prepared area shall be sufficiently large to accommodate kentledge supports and reference beams. The clearance between the steel grillage and the top of the test base must be such hat there is sufficient space to insert jacks and spacers, taking into account that there will be some settlement of kentledge supports prior to commencement of the test which will reduce the clearance beneath the grillage. If there is any evidence of undue total or differential settlement, further application of load shall cease and guidance sought from the technical manager.

The hydraulic jack and calibrated load cell shall be placed between the steel plate and the reaction beam. Four settlement gauges will be fixed on an independent frame to measure displacement.

D.2.2 Procedure

- Records shall be kept promptly throughout the testing period.

- Load shall be increased in 25% increments, each increment shall be applied for a minimum of two hours. The incremental loading shall not be applied until the rate of settlement under the preceding load is less than 0.008 mm/min as determined by the average of readings of the deflection gauges at five minute intervals. The load increments are as follows:

$$
\begin{array}{rlll}
25\% & *\,200\,kPa\, *\, 9\,m^2 & = & 450\,kN \\
50\% & *\,200\,kPa\, *\, 9\,m^2 & = & 900\,kN \\
75\% & *\,200\,kPa\, *\, 9\,m^2 & = & 1350\,kN \\
100\% & *\,200\,kPa\, *\, 9\,m^2 & = & 1800\,kN \\
125\% & *\,200\,kPa\, *\, 9\,m^2 & = & 2250\,kN
\end{array}
$$

- The maximum load shall be held for a minimum of 48 hours.

- After applying the maximum load (125%), the settlement shall be read at the following intervals: 5 min, 10 min, 30 min, 1 hour, 2 hours, 5 hours, 12 hours, 24 hours, 36 hours and 48 hours.

- The load shall be removed in equal increments corresponding to the increments at loading. Immediately after each load is removed the settlement will be recorded. Unloading shall be applied at 0.5 hour intervals.

D.2.3 Settlement Calculation

The total settlement consists of direct settlement and long term settlement, both are discussed in the following sections. Note that direct settlement occurs at t_1, long term settlement occurs over a period of 25 years t_{25}.

Direct settlement

The direct settlement is taken from ZLT readings at design load (250 kPa).

$$
S_{t_1} = S_{ZLT,t_1} \tag{D.2}
$$

Long term settlement

The long term settlement is predicted using the results of the ZLT and CPT. The direct settlement of each layer is determined by multiplying the CPT predicted settlement of that layer (see chapter H.2) by the ratio between the direct measured and total predicted settlement from the CPTs adjacent to the ZLT.

$$
S_{t_1,i} = \frac{S_{ZLT,t_1}}{S_{CPT,t_1}}\, S_{CPT,t_1,i} \tag{D.3}
$$

Where n is defined in H.2.

$\tilde{T}$UDelft

The long term settlement is then calculated:

$$S_{t_{25},i} = ((\frac{t_{25}}{t_1})^n - 1) \, S_{t_1,i} \tag{D.4}$$

Total settlement

The requirement for the ZOR project is met if:

$$S_{total} = S_{t_1} + \sum S_{t_{25},i} \, dz \; \leq \; 25 \, mm. \tag{D.5}$$

Van Oord
Marine ingenuity

Appendix E

Method Statement Soil Sampling

Van Oord
Marine ingenuity

Faculty of Civil Engineering

Department of Geo-engineering

Master Thesis

Dynamic Replacement in Sabkha Soil

Method Statement: Soil Sampling

Student:
R. Lamoré, 4052048

Supervisors:
Ir. W.J. Karreman (Van Oord)
Ing. H.J. Everts (TU Delft)

VERSION: 12 October 2015

Summary

Introduction	This document describes the execution of the soil sampling at Al-Zour in Kuwait, with the purpose of gathering information for the Master Thesis project.
Period	September
Van Oord supervisors on site	J.M. van Duinen, *Operations Manager* J. Beela, *Engineer* W.J. van Hemert, *Engineer*
Van Oord supervisor at HQ	W.J. Karreman, *Thesis project supervisor*

Van Oord
Marine ingenuity

E.1   Site Description

The location of the project is Kuwait. Kuwait is bordered by Iraq in the North and Saudi Arabia in the West. East of Kuwait lies the Arabian Gulf. At the location of the project a new refinery is to be built.

The soil at the New Refinery Project (NRP) is characterized as (very) soft silty sandy clay with salt and carbonate content. This type of soil is prominent in the Arabian Peninsula and locally often referred to as sabkha (sabkha is the Arabic word for salt flat). Sabkhas are salt bearing arid climate sediments of recent age which develop in areas of low relief, and are restricted to coastal inlets where the wave energy is low enough to allow settlement of silt and clay (Akili and Torrance, 1981); (Fookes, 1978).

The project includes distributing a hydraulic fill over a large area, with a thickness of six meters in the East. In the West there is no hydraulic fill. The sand is supplied by pipeline over several kilometres. After placing, the fill is distributed by bulldozers.

The method for improving the soil in this project is dynamic replacement. Dynamic replacement is a method based on dynamic compaction. For dynamic replacement, first a hydraulic fill is placed, then sand is driven to depth by a heavy block dropped by a crane. The column that is formed is then refilled with sand, and in turn compacted. The columns are relatively stiff compared to the surrounding soil, increasing bearing capacity and reducing post-construction settlements. The method is developed and carried out for this project by (Menard, 2015).

The distance between the centers of the sand columns is 6 meters. The diameter of one sand column is 2.2 meters.

After the sand columns are finished, there should be a stress transfer from the surface of the platform to the columns by an arching effect. To achieve this effect, the platform should have sufficient height. Also, the columns should not be spaced too far apart.

The sand platform is compacted by Van Oord. The first one to two meters are compacted by proofrolling. For greater depth compaction the sand is improved by rapid impact compaction method.

E.2   Description of the works

Boreholes down to a maximum of five meters will be made. For the drilling the Auger technique is employed. The Auger system is a well-known system to be used in, among others, (slightly) cohesive, silty soils.

At the bottom of the borehole soil samples will be taken by a thin walled sampler.

Equipment

The main drill rig consists of a rotary machine, driven by hydraulics. The rotary drives the drill rods to depth. The rods for the Auger system consist of pipes with a (very) course thread. At the bottom of the rods a cutter is mounted. While rotating and simultaneously lowering the rods, the cuttings are brought to surface level using the helical flights. The cuttings are considered disturbed soil and thereby not suitable for all lab tests. A casing is used, giving support to the borehole.

When the cutter is near the desired level, the driller stops the advancement. Sometimes a special Auger is used to clean the bottom part of the borehole. This is not standard practice, it is however desirable.

When the required depth is achieved, all the drill rods are pulled from the borehole. A different system, the tube sampler, is mounted on the machine. This system consists of a massive pipe on which a hollow thin walled tube can be mounted. The thin walled tube is lowered to the bottom of the borehole. A sample is taken following ASTM D1587 (see Appendix E.4).

Procedure

The procedure for both Auger borings and tube sampling is described in Appendix E.4.

Location

The location of the borings will be in portion 32. The depth of the layer of interest, the sabkha, is approximately 1.0 - 1.5 m below surface. During the borings printed CPT results from the area will be available.

E.3 Executional Aspects

The quality of the samples is highly dependent on the driller's competence. Table E.2 summarises the executional aspects based on (Lunne et al., 2007) and (Long et al., 2009) and chapter E.4.

Table E.2: Executional aspects

Action	Item	Influence	Probability	Prevention or Mitigation
The tube	Loose tube	+	+	Make sure that the tube is fixed, otherwise notify drilling foreman.
Sampling	Sharpness tube	++	+	Make sure that the cutting edges of the sample tube are sharp.
	Tube surface	+/-	+	Make sure the tube is clean and free of surface damage.
	Cutting too fast	++	+	Slow cutting down by notifying the drill foreman.
	Over-coring	++	++	Notify drilling foreman. Explain that a partially filled tube is better than a tube filled with compacted soil.
	Excessive twisting	+	++	Notify the drill foreman that it is better to very slowly retrieve sample than to twist and lift.
	Resting time	+	++	The tube should be left at final depth for some time.
	Retrieval speed	+	++	The retrieval of the sample tube should be done slowly.
	Hanging sample	++	+/-	If the sample is left hanging longer than necessary, tensile strains will develop. Notify drilling foreman to tak down the sample tube.
Storage	Heat	++	+	The samples should be stored in a cool, dry area. They should not be stored in direct sunlight or in a package subject to direct sunlight.
	Vibrations	+	+	While the samples will undergo disturbance during transport, care should be taken that the samples will not be stored on the (running) drilling rig. Any vibrations that can be prevented should be prevented.

TUDelft
Delft
University of
Technology

E.4   ASTM document

AUGER BORINGS AND TAKING & HANDLING SOIL SAMPLES

ASTM
D1452 – Soil Exploration and Sampling by Auger Borings;
D1587 – Thin-Walled Tube Sampling of Soils for Geotechnical Purposes;
D4220 – Preserving and Transporting Soil Samples.

AUGER BORING

Casing is required in unstable soils; especially below groundwater level. The casing shall not advance the auger. Samples taken directly from the auger are disturbed. During the boring the water level should be measured. Documentation of water levels include datum, date and time.

The log shall include the following:
1. The location,
2. Date of start and completion of boring.
3. Identifying number of boring,
4. The name of the drilling foreman, inspectors and company,
5. Reference datum,
6. Type and size of auger used,
7. Depth of changes in strata,
8. Description of soil in every stratum,
9. Groundwater level and depth of seepage zones (if found),
10. Datum, date and time of water levels,
11. A note whether the hole remains open during auger removal (if this can be seen).

TUBE SAMPLING

Any boring method that minimizes disturbance and does not hinder penetration can be used for tube sampling. The inner diameter of the casing or open borehole diameter shall not exceed 3.5 times the outside diameter of the sample tube. Though it may be necessary to drive the tube in hard formations, this is not recommended. The tube head shall contain a venting area. Attachment of the tube to the head shall be concentric to ensure uniform application of force.

SAMPLE RETRIEVING PROCEDURE
1. Maintain water level equal or higher than groundwater level during sampling.
2. (Bottom discharge bits are not allowed)
3. Lower the tube and record the length to the bottom of the hole.
4. Advance the tube without rotating, recording the length of advancement.
5. In clays: advance no more than 10-15 times the diameter,
   in sands: advance no more than 5-10 times the diameter,
   the advance shall in no case be greater than the tube's length including a allowance of at least 76mm.
6. If the formation is too hard for push-type sampling the tube may be driven, recording weight of the hammer and achieved penetration. The sample shall be labeled 'driven sample'.

TUDelft

Delft
University of
Technology

7. The sampler may be rotated slightly to improve recovery. In soft materials it may be advisable to delay recovery 5-30 minutes.

SEALING PROCEDURE
1. Remove drill cuttings from the sample. Measure the length of the sample and seal of the upper end of the tube. Remove at least 25mm from the lower end of the tube and use this material for soil description. Measure the sample length again. Seal of the lower end of the tube (e.g. paraffin wax).
2. Tubes sealed over the end should be provided with spacers or packing materials prior to sealing to ensure confinement of the sample. The spacers or packing materials shall be non-absorbent.
3. Prepare and affix markings labels or markings necessary to identify the sample. The top end of the tube shall be labeled 'top'.

Where samples are taken, the boring log shall be extended with:
1. The tube size,
2. The sampling depth,
3. The method used (pushed or driven),
4. Length of the sampler advance,
5. Preferably cone recovery in sample tube.

LABELING, PRESERVING AND TRANSPORTING SOIL SAMPLES

Labeling
The samples shall be labeled with:
1. Job name or number,
2. Sampling date,
3. Sampling/boring number and location,
4. Depth/elevation,
5. (Deviating) Transporting/handling instructions,
6. Potential hazardous.

Preserving
1. Use spacers between the sample and end cap (non-absorbent),
2. Use tape to seal the rubber or plastic end caps,
3. The samples shall be protected against (extreme) heat and vibrations,
4. The samples shall be wrapped in plastic foil or cloth,
5. The samples are collected in a container, protecting against heat and vibrations.
6. The samples will either be in a fixed position by slots in a box, or by filling up the space between samples in a container.
Examples of containers are given in the following pages.

Transporting
Care shall be taken so that the samples are exposed to as little disturbance as possible. Transporting between site and laboratory should be without any preventable delay.

Custody of samples must be maintained and documented at all times. It is advised to prepare a chain of custody (COC) document containing all the necessary forms and seals.

In addition to chain of custody records associated with sample handling and packaging, certain standard forms will be completed for sample description and documentation. These shall include sample log sheets, daily record forms, and logbooks. A bound/weatherproof field notebook shall be maintained by the crew. All field activities shall be recorded in the field notebook on a daily basis.

SHIPPING BOX EXAMPLES
From ASTM D4220

25 mm [1 in.] foam or rubber; or 65 mm [2.5 in.] insulation

20 mm [3/4 in.] binding steel

Galvanized steel 25 mm × 40 mm × 1.3 mm [1 in. × 1.5 in., 18 gauge]

76 mm [3 in.] foam or rubber; or 25 mm [1 in.] foam or rubber and 65 mm [2.5 in.] insulation over base
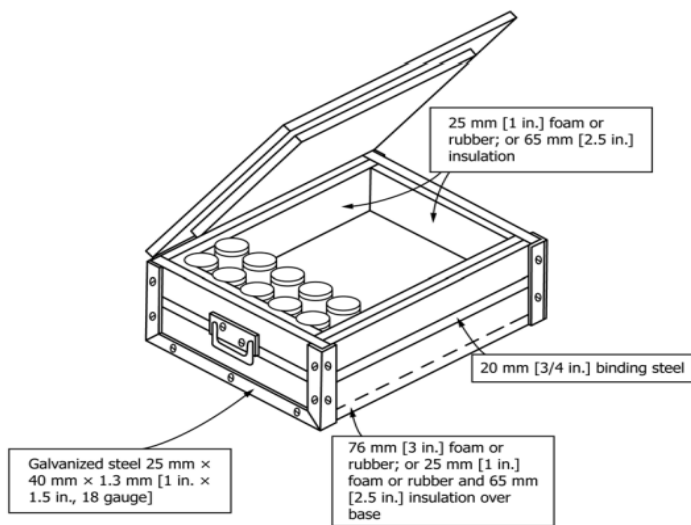
Figure 1 Shipping box for short tube

Figure 2 Shipping box for 127mm tubes

TOP MUST BE SCREWED INTO
PLACE OR HINGED AND LATCHED

340 mm [13 1/2"] SQ.
TOP AND BOTTOM

255 mm [10"]

460 mm [18"]

255 mm [10"]

MINIMUM OF 7 NAILS IN
EACH LONG EDGE
(PREFERABLY ALSO GLUED
WITH WATERPROOF GLUE)

90 mm [3 1/2"]
CENTER OF HOLE
TO EDGE OF DIVIDER (TYP.)

BOTTOM MUST BE
SCREWED INTO PLACE

100 mm [4"] DIA. HOLE
(4 HOLES EACH,
TOP AND BOTTOM DIVIDERS)
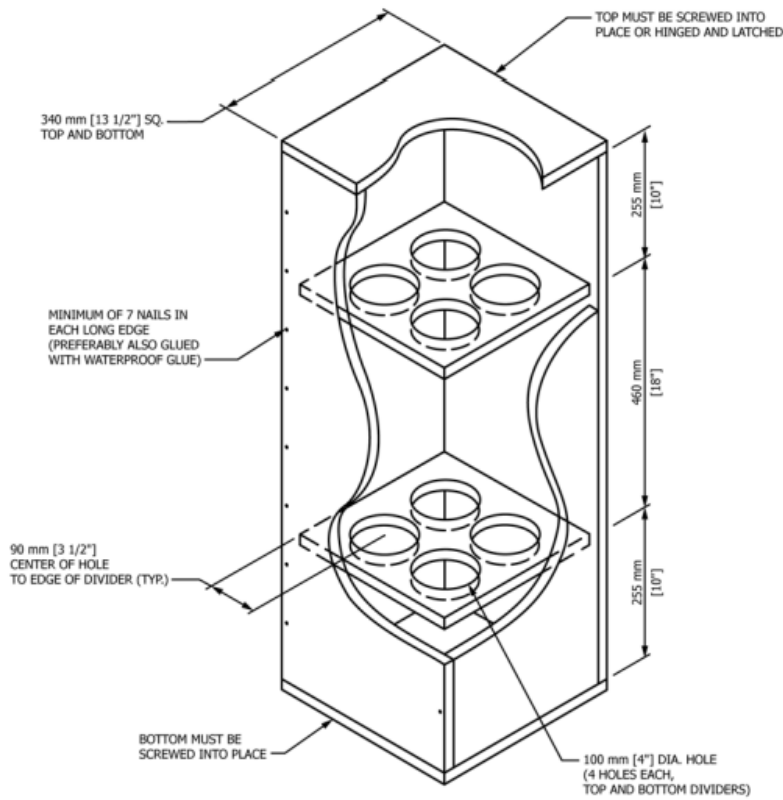
Figure 3 Shipping box for 76mm tubes

Appendix F

Field Test Results

This chapter describes the results from both the field tests performed in Kuwait, as well as the laboratory tests performed at the TU Delft.

F.1   Soil Sampling

In order to determine soil parameters for future PLAXIS calculations, soil samples have been taken. Laboratory soil tests will be performed on these samples. Another advantage of laboratory determined stiffness parameters is that the CPT correlations that are used in this project can be compared qualitatively.

For the borings a local site investigation company was hired. There was constant supervision by Van Oord. In chapter E a brief method statement is included. This method statement also includes a summary of auger borings and tube sampling, based on respective ASTM standards.

During the borings on the first day (Tuesday October 13) no sabkha was found. Before any tubes samples were taken, so-called exploratory boreholes were made. For these type of 'quick and dirty' boreholes, no borehole stabilizer (e.g. slurry or casing) is used. Instead, the auger advances to final depth (6 m - surface) without intermediate retracting. The auger is retracted and put down on the surface. The cuttings can then be examined. Only silty sand was found, that could however be part of the hydraulic fill (clay and silt lenses were previously found in other areas). In some locations the borings may have been made inside a sand column. This could be judged by the fact that the tube could not penetrate the soil at depths in the order of 2-3 m. It was assumed not probable that all the borings were made in a DCDR column, since the multiple locations were staked by the survey department.

The second day started out with the same results as the first day. It was thus decided to move to a different area, also showing very soft soil in the CPT results. No more exploratory holes were performed because it was assumed that the soft sabkha, if present, would not stick to the thread but rather fall of the auger upon retracting. The first two borings were advanced further than the depth at which the sabkha was to be expected. However, neither boring showed any sabkha. Two more borings were done, the tube of the last one was partly filled with soft clay. It was decided to continue with more boreholes close to the latter borehole. Four more samples were taken. The tubes were sealed right away and kept in a air-conditioned car. After two hours the samples were taken to the laboratory.

It was found during the exploratory borings that the groundwater level (GWL) was 1.5 m below surface level.

F.1.1 Photo Report

Soil Borings

Figure F.1: The drilling rig mounted on a truck.

Figure F.2: The drilling rig mounted on a truck.

Figure F.3: A boring being executed.

Figure F.4: The 4-inch Shelby tube that was used.

Figure F.5: An 'exploratory' boring, a quick and dirty method.

Sample Extrusion

The photos presented in this section were taken at the Gulf Inspection International Co. (GIICO) laboratory in Sabhan industrial area in Kuwait.

Figure F.6: Extruding the sample from the Shelby tube.

Figure F.7: Measuring the length of the layers of interest (the sabkha).

Figure F.8: Sawing the tubes in parts. The tubes should contain the samples for transport.

Figure F.9: Sawing the tubes lengthwise to allow for a nearly disturbance-free wrapping of the sample.

Figure F.10: Logging the samples before transport

Figure F.11: Logging the samples before transport

Figure F.12: Logging the samples before transport
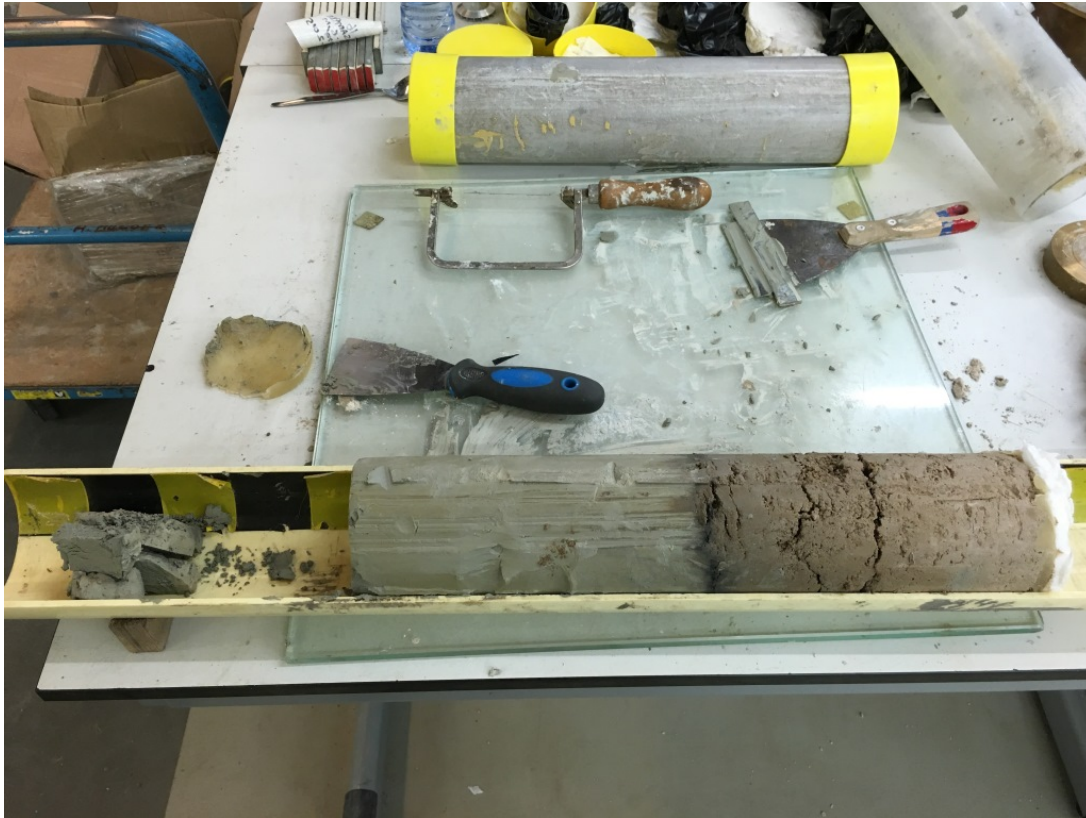
Figure F.13: Extruding samples from the packaged tubes. Note the layering inside the sample.

Figure F.14: Extruding samples from the packaged tubes. Note the layering inside the sample.

F.2 Cone Penetration Tests

The equipment that was used for the Cone Penetration Test (CPT) was already on site.

F.2.1 Sand Column

In the night of September 3rd CPTs were performed in portion 15. The location was in box CV166.

The CPTs were planned to be done in one straight line, from the center of the column to the outside. With this configuration, the hypothesis is that an interface between the sand (column) and soft soil (sabkha) can be recognized. Knowing where the interface is would greatly improve the accuracy of a model of the configuration.

CV166

A drawing of the CPT[1] locations relative to the sand column is given in figure F.15.
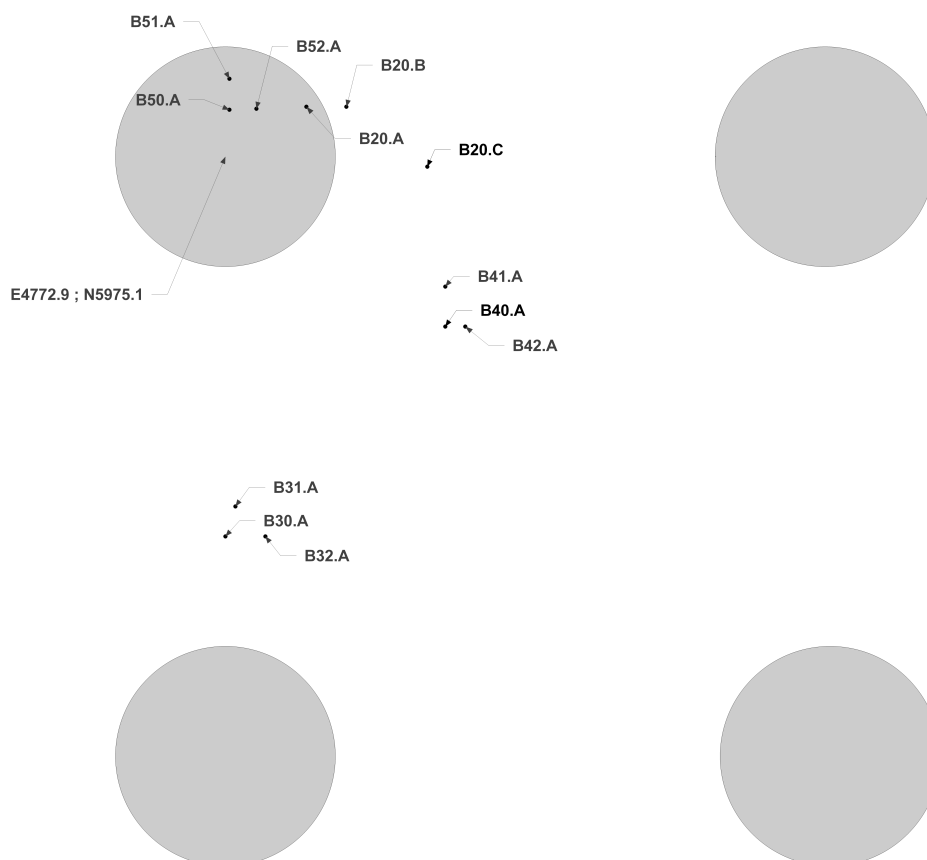
Figure F.15: Locations from the 03-09-15 CPT set at box CV166

After the tests were completed and the results sent for review, it turned out that the CPT locations in OpenEarth did not completely match the map of the columns. CPTB20.B should however be located outside of the column, as well as CPTB20.C. The results from the CPTs are summarised in table F.1.

The sharp, shortlength increase in friction ratio that is seen in B20.B can also be seen in B50.A, although the small layer is present at -2.8 m. while the surface level only differs by 6 cm., furthermore the friction

---

[1]Note that all the CPTs that are analysed in this section are performed within this box. To enhance readability, the first part of the CPT reference has been left out. I.e. CPT-CV166-B50.A will be shortened to B50.A.

Table F.1: CPT in CV166

CPT	Refus. Depth [m]	Remarks
B20.A	4.4	Friction ratio slightly higher than 1% at -3 m. may indicate silt intrusion. There is a clear end of the column reached at -3.7 m. Friction ratio increases at this depth 2.5%, indicating silt soil type. The friction ratio decreases to 1.2% 0.4 m. below this point, this may indicate a mix of silt/sand.
B20.B	5	Slight bump in friction ratio at -2.5 m.. At -3.5 m. there is an sharp increase in friction ratio up to 3%, indicating the bottom of the column is reached and a silt layer is present.
B20.C	5	Significant jump in friction ratio at -2.3 m., up to 3% for 0.3 m.. At -3.5 m. there is an sharp increase in friction ratio up to 1.5%, later 3%, indicating the bottom of the column is reached and a silt layer is present.

ratio reaches only 2%. A small increase at the same depth is seen in B52.A, this increase only extents to 1%. B20.A also shows an increase of 1%, at 2.9 m. The characterising peak at the former CPTs is also present in B51.A, however at a depth of 3.2 m., about 0.5 m. lower than the other tests.

Compared to B20.A and B20.B which have a cone resistance increasing to about 15 MPa at -2.5 m., B20.C has a high cone resistance of 20 MPa between -1 and -1.5 m.. There is however a drop in cone resistance at -2.3 m., decreasing to 2 MPa. This drop is not seen in B20.A or B20.B. It is somewhat unexpected to find the high cone resistance in this CPT, since B20.C is the farthest away from the center of a column. All the CPTs show a silt/sand layer at -3.5 m., except for B50.A which has a silt/sand layer at -3.8 m. It is noted that this CPT is, assuming the co-ordinates are approximately correct, near the center of the column.

Box CW165

A drawing of the CPT locations relative to the sand column is given in figure F.16.
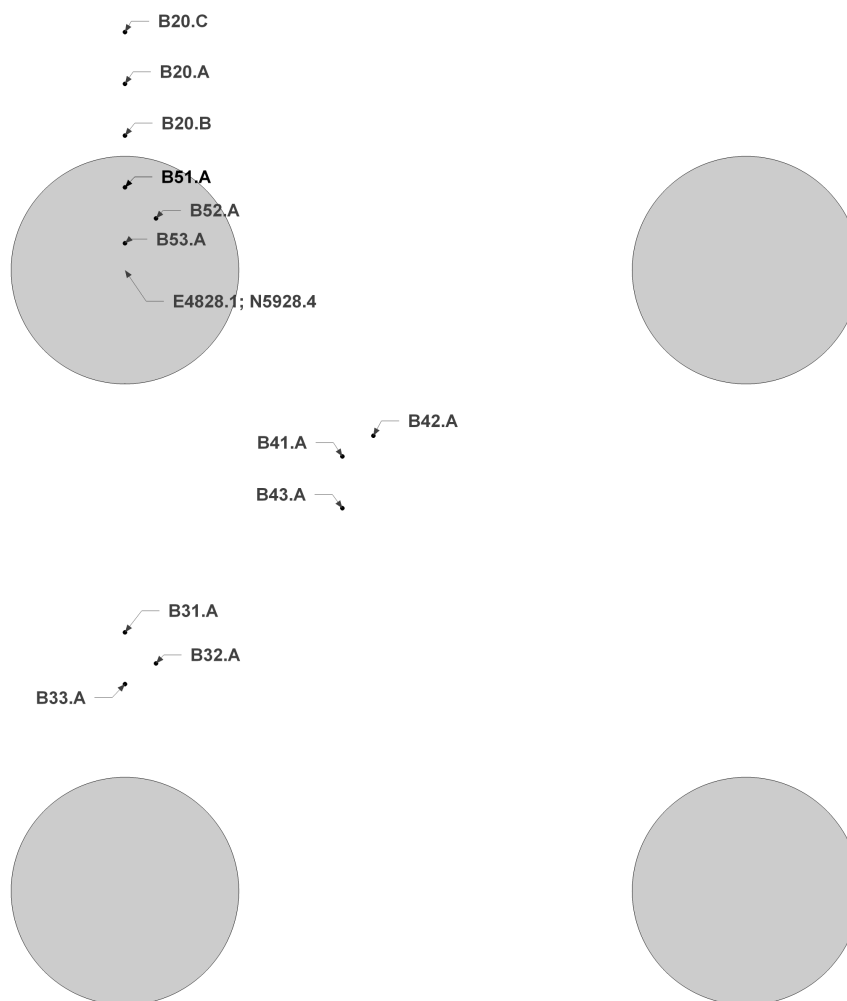
Figure F.16: Locations from the 03-09-15 CPT set at box CW165

CPT	Refus. Depth [m]	Remarks
B20.A	4.7	Friction ratio of well below 1% indicates a clean sand layer. The cone resistance increases with depth to 25 MPa at -3.2 m.. After -3.2 m. there is a decrease in cone resistance, increasing the friction ratio to almost 3% at -3.5 m. The friction ratio fluctuates from 0.5% to 3% hereafter. This may indicate mixing of the silt and sand. The fact that a clean sand column is found is striking since the test location is almost two meters out of the center of the column.
B20.B	4.8	Mostly the same as the previous test. The friction ratio is generally slightly higher due to a higher sleeve friction. The cone resistance shows remarkable similarity with the previous test from -3.5 m. on.
B20.C	5.1	Compared to the previous two tests, test B20.C shows a very capricious friction ratio line. The cone resistance is increasing with depth in the first 0.7 m., however decreasing afterwards. From -1.5 m. to -2.8 m. cone resistance is increasing on average. The sleeve friction shows two peaks at -0.6 m. and -2 m. Higher friction ratios start at -3.4 m.

The CPTs performed in the column (B51.A, B52.A and B53.A) show the same friction ratio compared to the B20 series CPTs. At B51.A and B52.A the higher friction ratio (indicating silt) starts at -3.5 m. At B53.A (the CPT nearest to the center of the column) it shows a friction ratio of more than 3% at -3

m. This probably indicates higher penetration of the sand column in the middle.

The cone resistance is on average the highest in B53.A. It increases with depth to 20 MPa a -2.8 m. After this depth it decreases, to increase again at -3.7 m. B51.A shows a poor cone resistance, increasing to 12 MPa maximum, at -3.4 m. The cone resistance of B52.A is slightly higher on average. It shows four distinct phases. First a phase of increase, between 0 and -0.5 m. to about 5 MPa. Then a phase of no increase; the cone resistance equals 5 MPa down to -1.5 m. This is followed by another phase of increase from 5 to 15 MPa, in a increment of half a meter. After this increase the cone resistance remains at a value of 16-17 MPa (with one short peak of 20 MPa) to a depth of -3.3 m.

The CPT diagrams are given in figure (to be added later).

F.2.2 Parameter Determination Sand

For the calculation of the parameters, reference is made to H.3.

This section is divided into two subsections, referring to the two of the three ZLT locations.

ZLT FC113-1

The CPT diagram of the platform under location FC113-1 is given in figure F.17. The friction angle correlation for the platform is given in figure F.18, for the column the CPT diagram is given in figure F.19 and the correlation of the column is given in figure F.20.
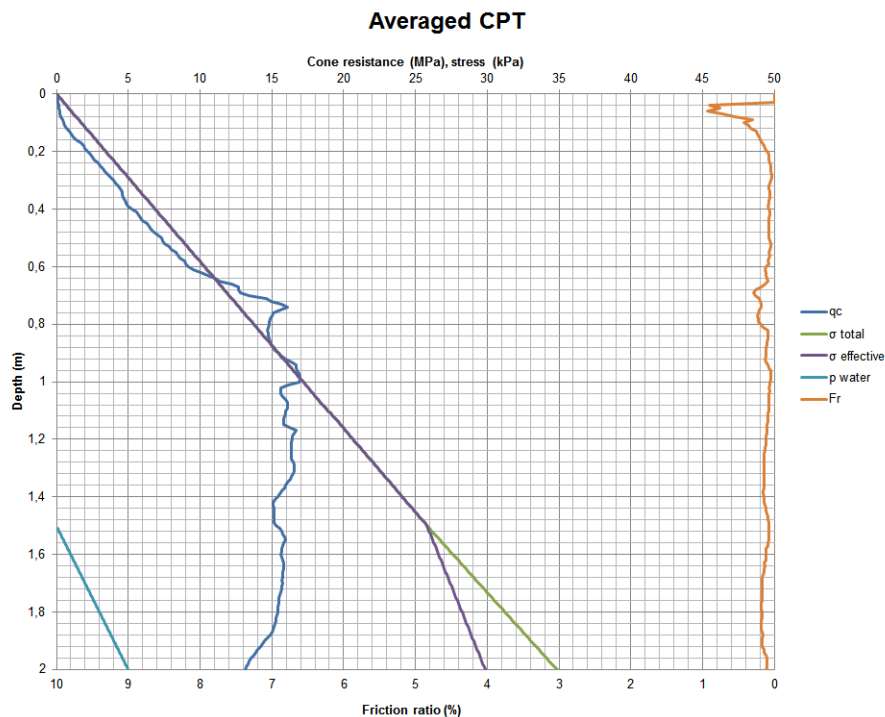
Figure F.17: Averaged CPT diagram for ZLT FC113-1 platform
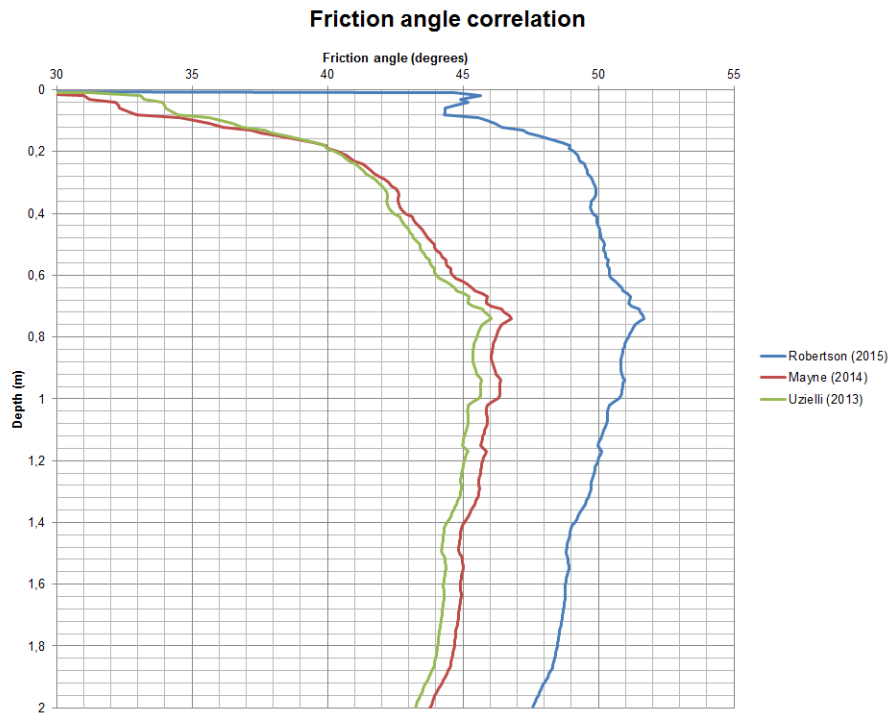
Figure F.18: Friction angle correlations for ZLT FC113-1 platform
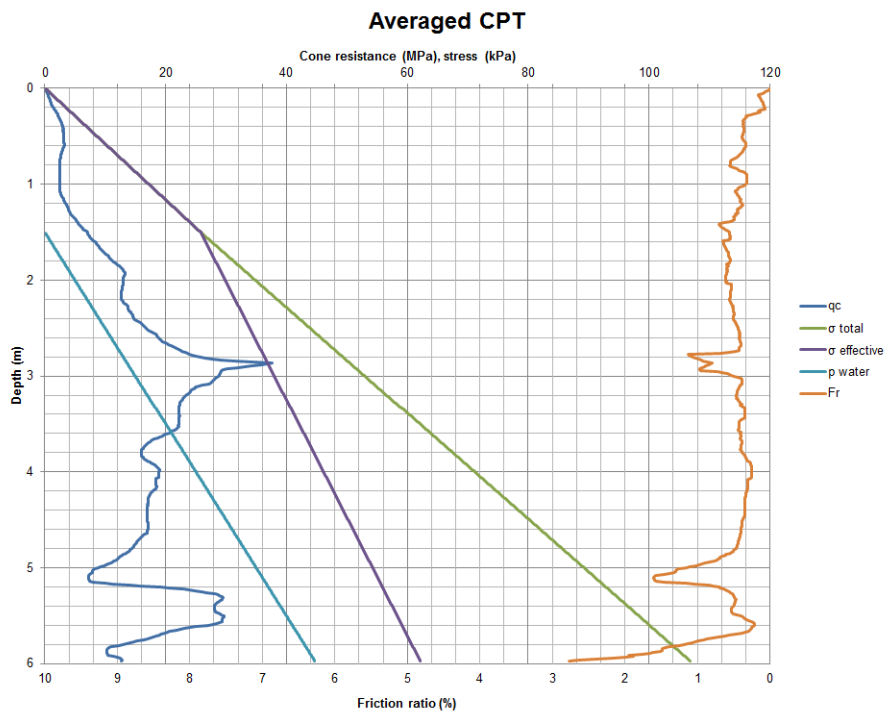
Figure F.19: Averaged CPT diagram for ZLT FC113-1 column
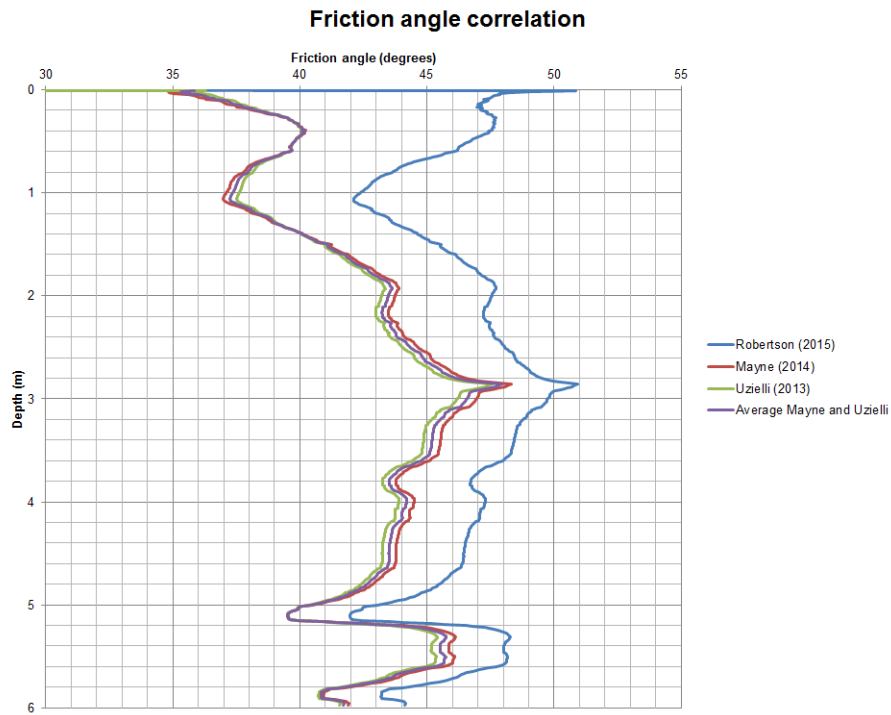
Figure F.20: Friction angle correlations for ZLT FC113-1 column

ZLT FC113-2

The CPT diagram of the column under location FC113-2 is given in figure F.21. The friction angle correlation for the platform is given in figure F.22.
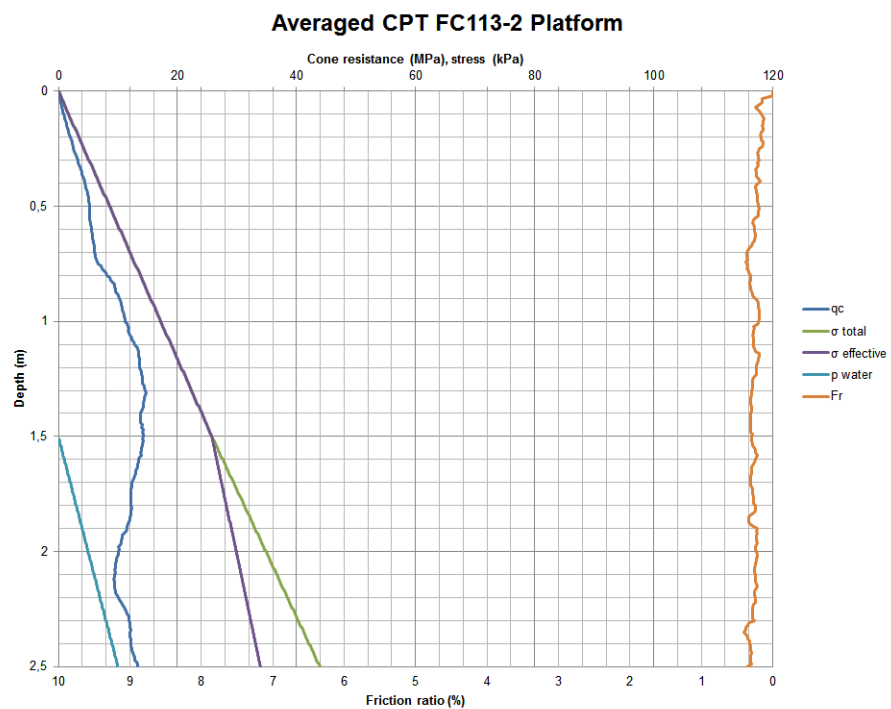
Figure F.21: Averaged CPT diagram for ZLT FC113-2 platform
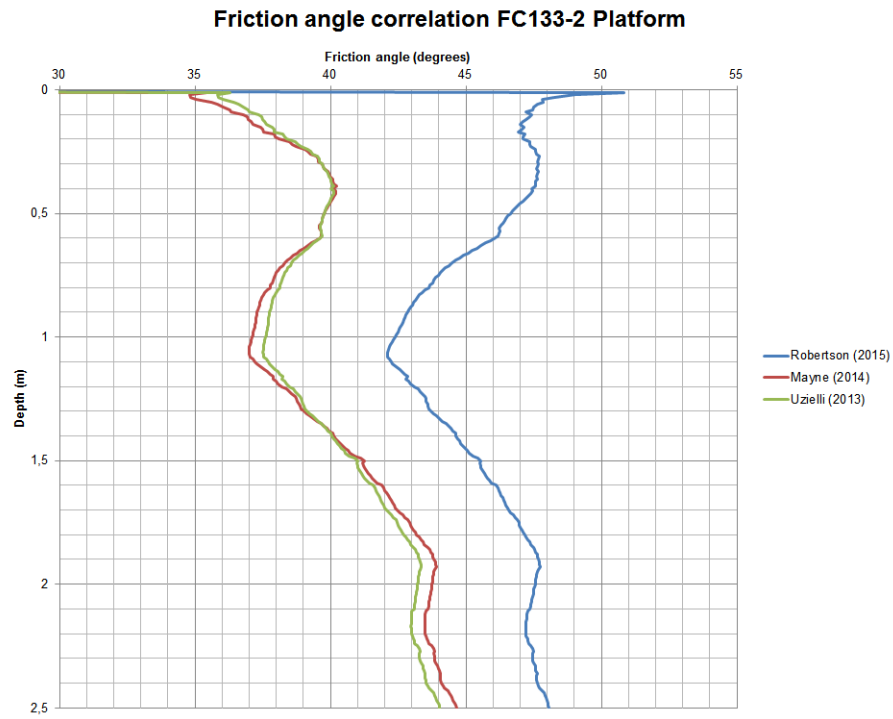
Figure F.22: Friction angle correlations for ZLT FC113-2 platform

F.2.3   Parameter Determination Silty Sand

Under the lower intermediate silt layer, a layer of silty sand is present. The engineering parameters of this layer are derived from CPT tests as described in H.2.

F.3   Zone Load Test

F.3.1   Box 139
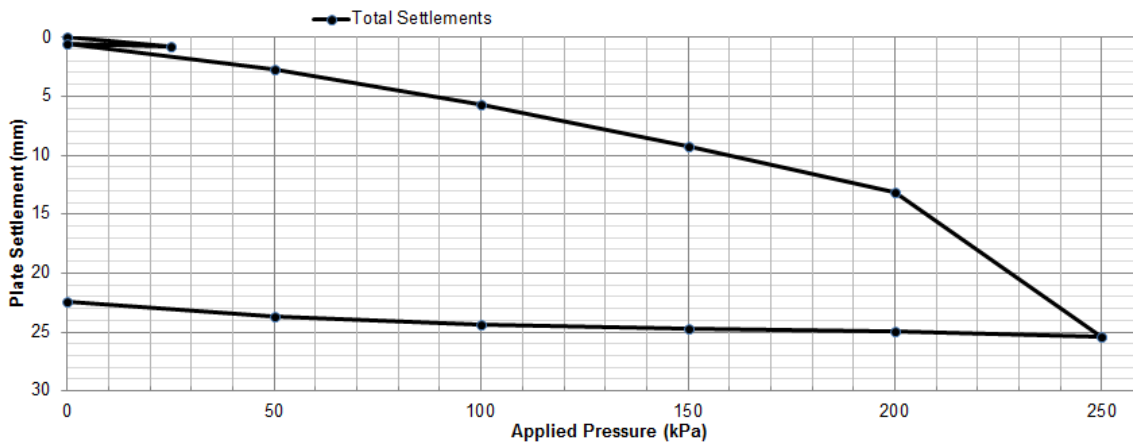
Figure F.23: ZLT settlement at box DR139
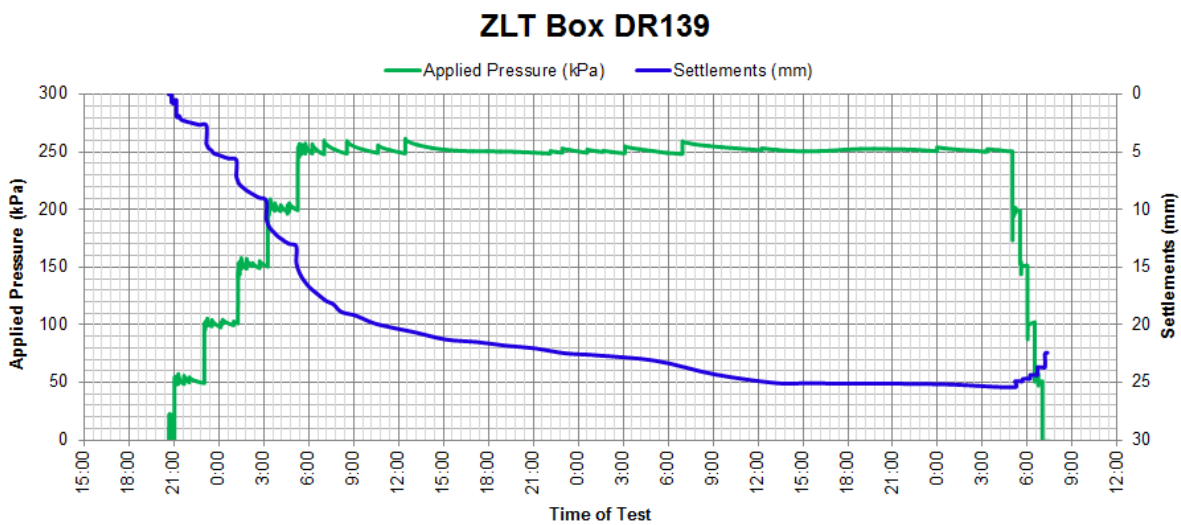
Figure F.24: ZLT settlement and pressure at box DR139

F.3.2   Box FE113-1
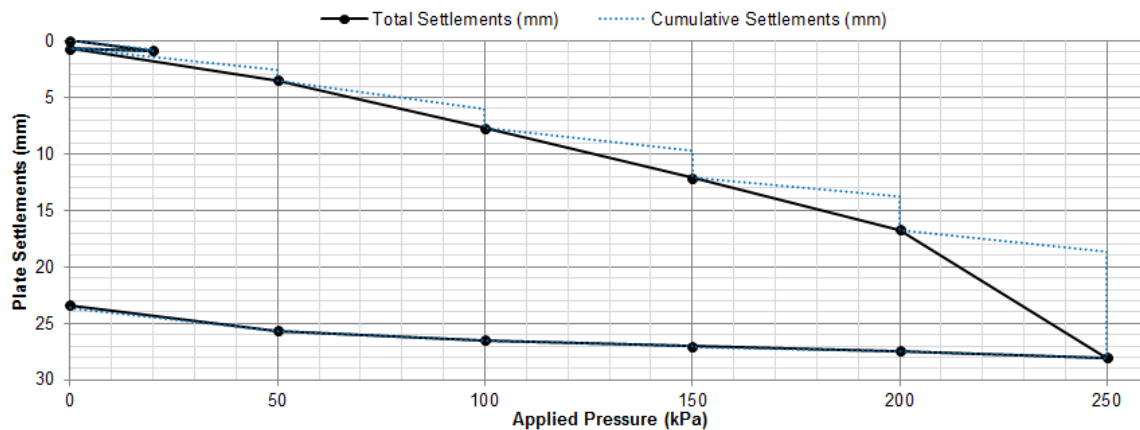
Figure F.25: ZLT settlement at box FC113, location 1
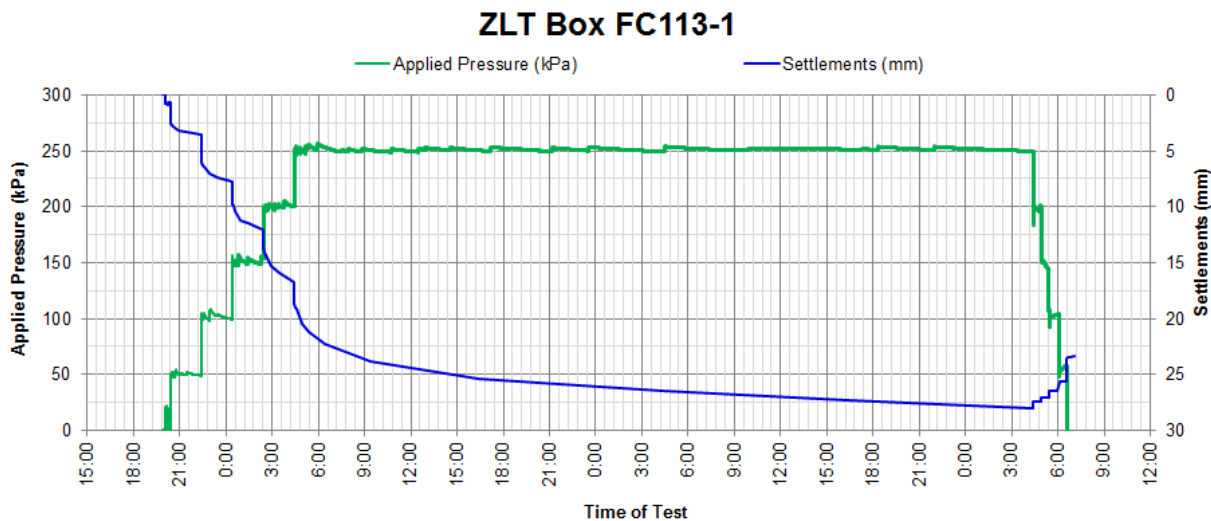
Figure F.26: ZLT settlement and pressure at box FC113, location 1

F.3.3   Box FE113-2
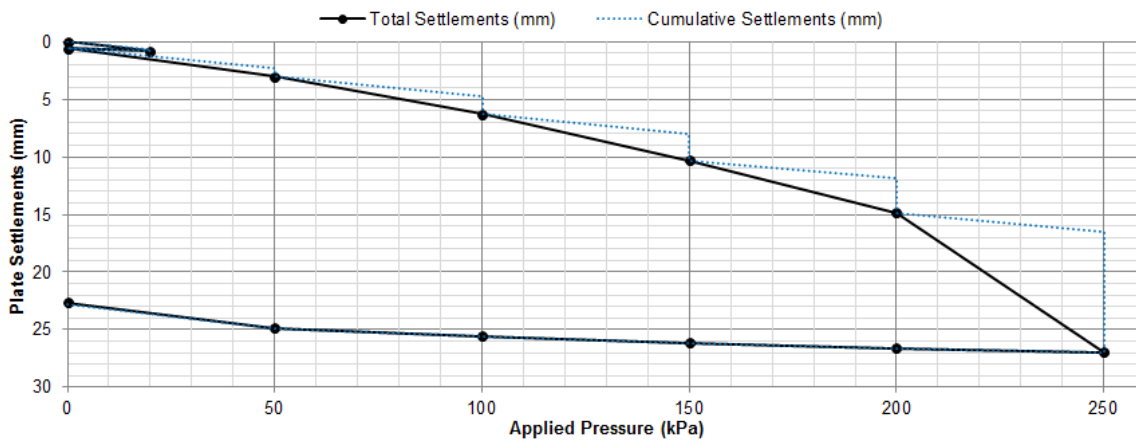
Figure F.27: ZLT settlement at box FC113, location 2
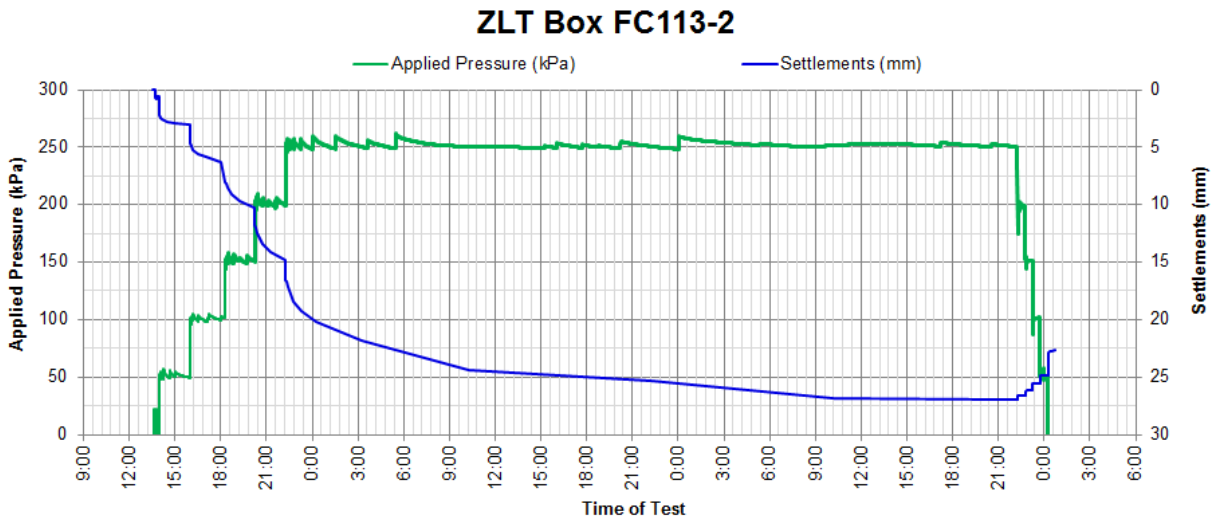
Figure F.28: ZLT settlement and pressure at box FC113, location 2

F.4   Field Density Tests

The FDT is used to determine wet and dry density of soil. If the maximum dry density is determined in a lab, with for instance a Proctor test, the relative compaction can be determined.

The FDT is used to determine both the density and compaction in this report. Table F.2 summarizes FDTs that have been performed near the ZLT area.

Parameter	Unit	FDT1	FDT2	FDT3	FDT4	FDT5	Average
Wet dens.	g/cm^3	1.815	1.786	1.836	1.801	1.826	1.813
Dry dens.	g/cm^3	1.715	1.714	1.719	1.732	1.720	1.720
Max. dry dens.	g/cm^3	1.803	1.803	1.797	1.803	1.803	1.802
Relative compaction	%	95.1	95.1	95.7	96.1	95.4	95.5

Table F.2: Density and relative compaction

Appendix G

Laboratory Test Results

This chapter describes the results from the laboratory tests. In the laboratory two types of soil have been tested, i.e. soft clay and silt. The silt was recovered from the samples very close to the soft clay. That silt layer is referred to as intermediate silt layer and should not be confused with the deeper silty sand layer. Layering is clearly visible in figures F.13 and F.14. The engineering parameters of the silt layer are determined using CPT correlations and reference tables.

G.1 Classification Tests

In this subsection the results of the classification tests are given.

Sieve Test and Hydrometer

The grain size distribution of the samples can be found below.
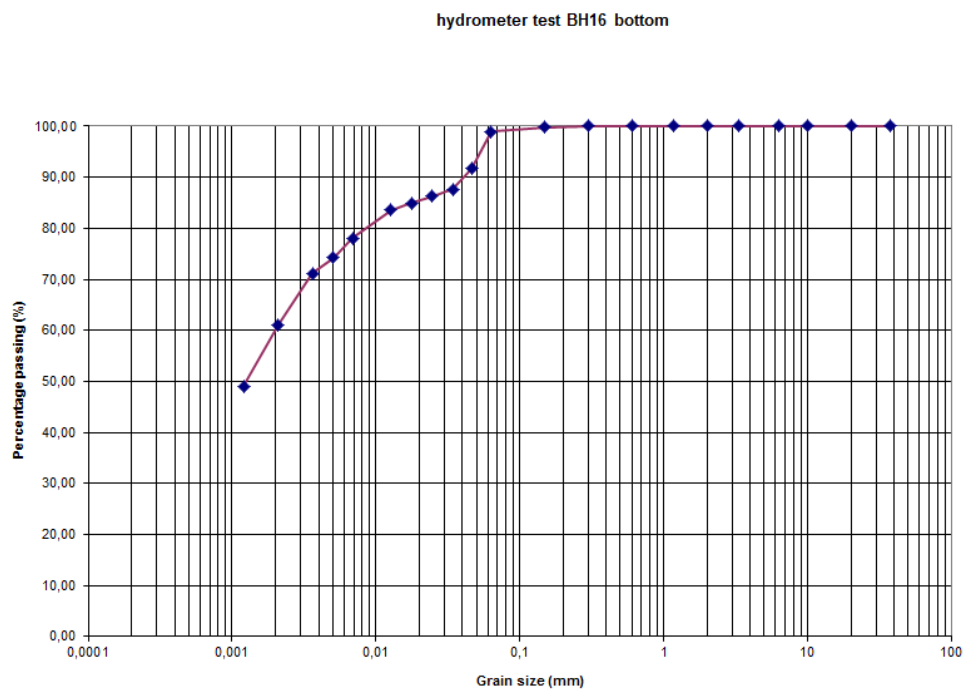
Figure G.1: Grain size distribution for the BH16 bottom sample
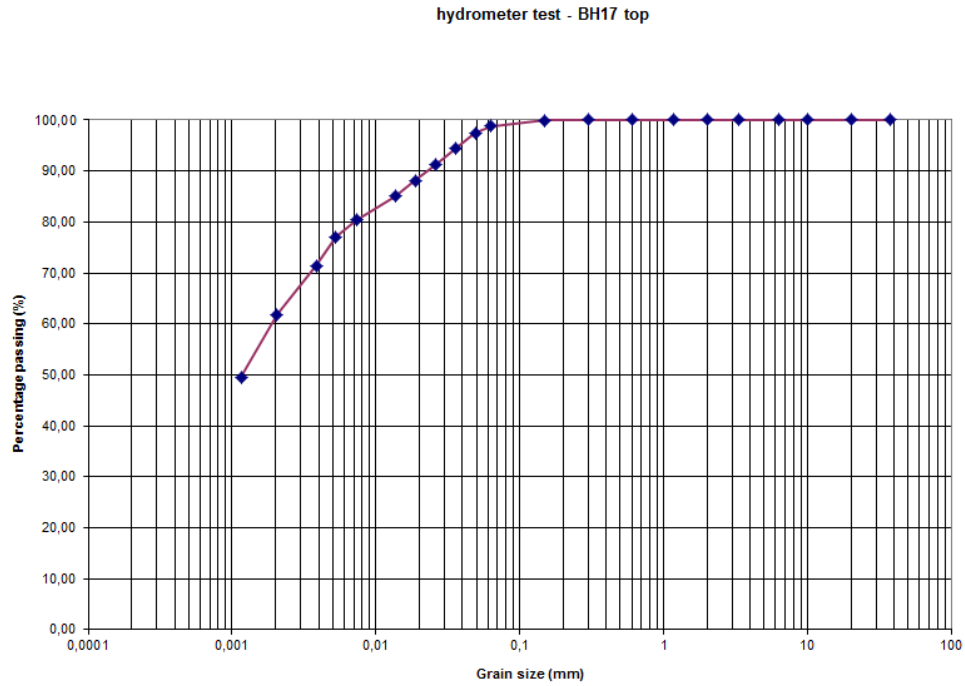
Figure G.2: Grain size distribution for the BH17 top sample
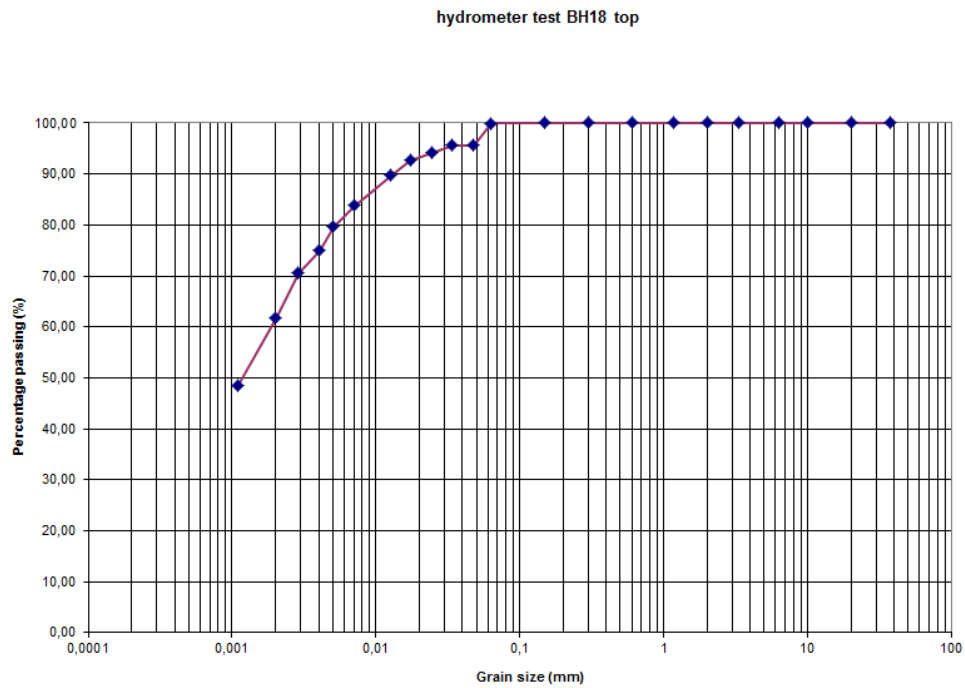
Figure G.3: Grain size distribution for the BH18 top sample

Water Content

The water content of the samples was determined using ISO 17892-1:2004.

Location	Water Content (%)
BHSILT	40.5
BH17 top	84.6
BH16 bottom	83.3
BH18 top	73.6

Table G.1: Water content of the soil samples

Density

The density of the samples was determined using ISO 17892-2:2004. The results are given in table G.2.

Location	Density (kg/m^3)
BH 17 Silt	1607.25
BH17 top	1535.5
BH16 bottom	1536.9
BH18 top	1527.9

Table G.2: Density of the soil samples

The average density of the sabkha samples is 1533.4 kg/m^3. The density of the intermediate silt layer is 1607.25 kg/m^3.

Particle Density

The particle density was determined using a Pyknometer, following ISO 17892-3:2004. The results are given in table G.3.

Location	Particle Density (g/cc)
BHSILT	2.7238
BH17 top	2.5909
BH16 bottom	2.6099
BH18 top	2.6211

Table G.3: Particle of the soil samples

Atterberg's Limits

To determine both the plastic and the liquid limit of the samples, hand rolling was used for the former limit and a cone penetrometer was used for the latter limit. Both tests have been performed following ISO17892-12.

The diagrams showing the water content against the penetration are given in figures G.4 through G.6.
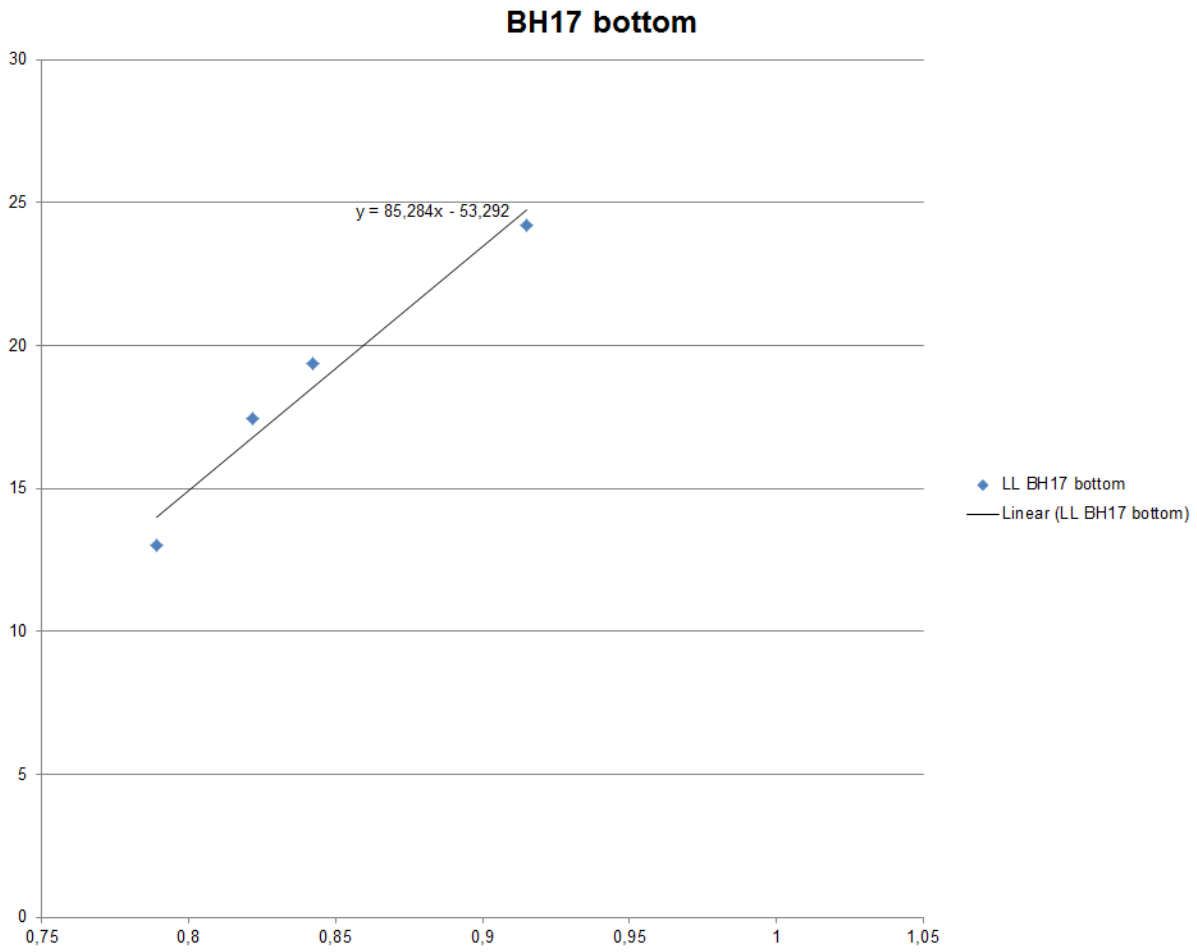
Figure G.4: Borehole 16 bottom

Borehole 17 top

Liquid Limit:	86%
Plastic Limit:	37%
Plasticity Index:	49 %
Classification:	Silt, very high plasticity
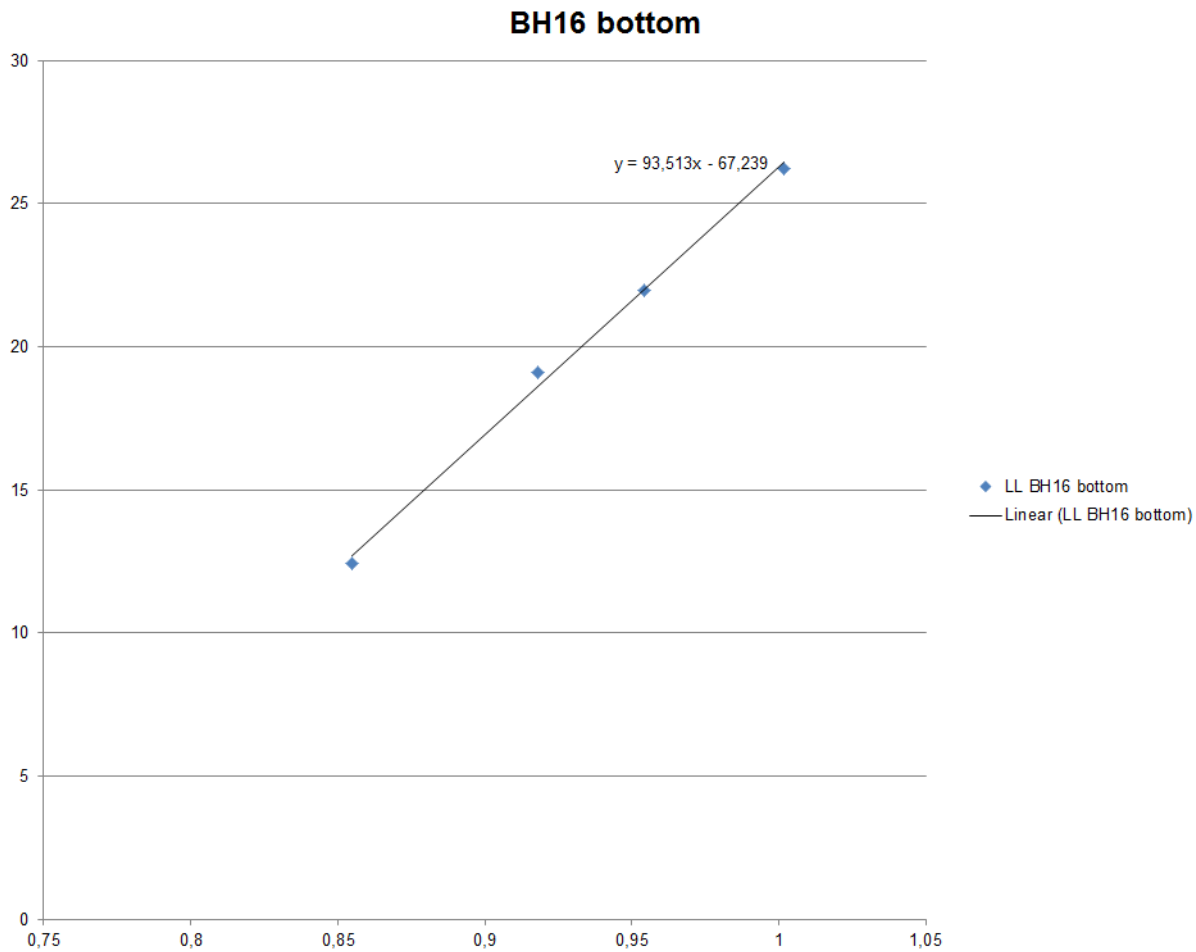
Figure G.5: Borehole 17 top

Borehole 16 bottom

Liquid Limit:	93%
Plastic Limit:	55%
Plasticity Index:	38%
Classification:	Clay, extremely high plasticity
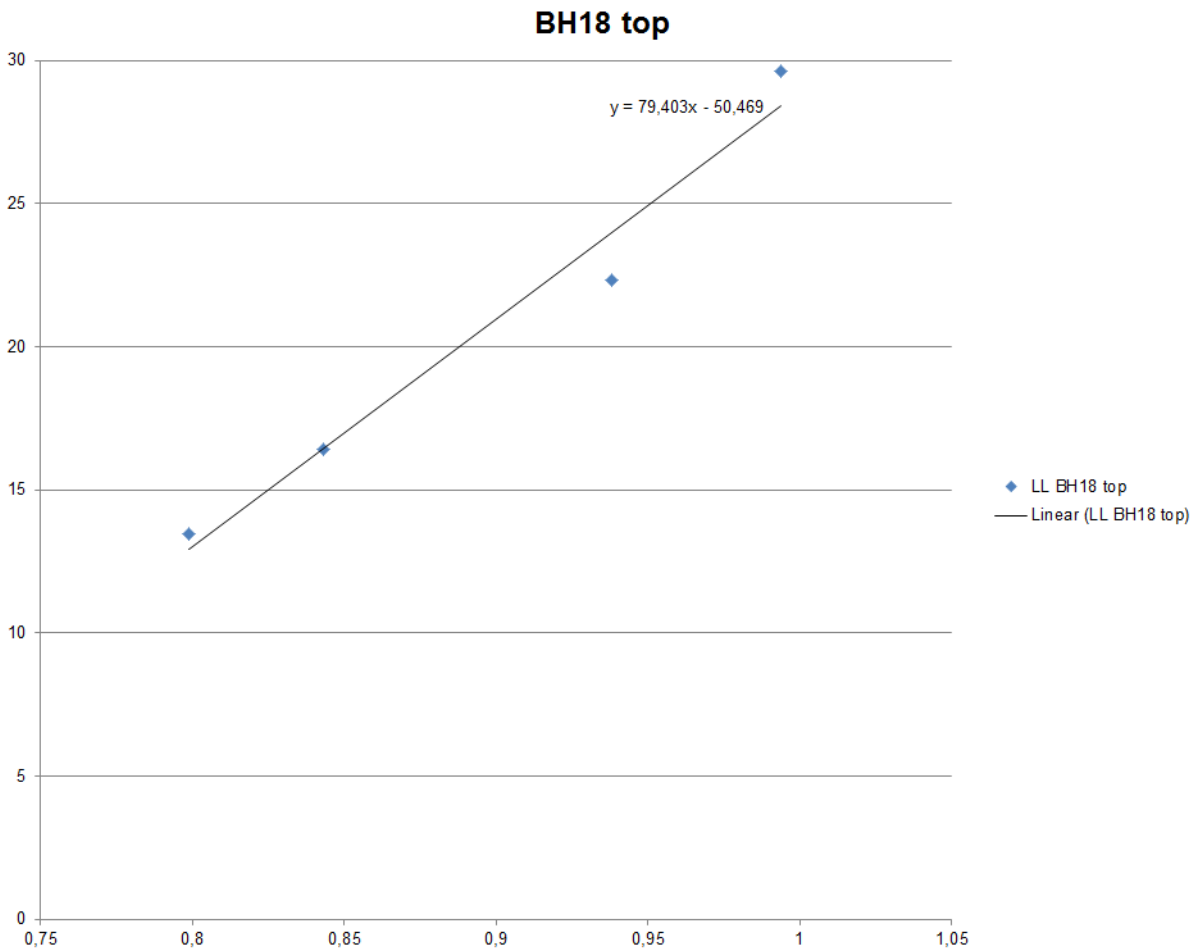
Figure G.6: Borehole 18 top

Borehole 18 top	
Liquid Limit:	89%
Plastic Limit:	38%
Plasticity Index:	51%
Classification:	Silt, very high plasticity

G.1.1   Consolidation Tests

Sample	C_c	C_s
BH16 bottom (E)	0.21 (12.9) 0.46 (35.4) 0.60 (79.9) 0.49 (157.7)	0.13 (157.7) 0.10 (51.9) 0.13 (6.9)
BH16 silt (B)	0.11 (14.8) 0.23 (27.7) 0.19 (55.5) 0.13 (111.0)	
BH17 top 1(A)	0.14 (14.8) 0.42 (27.7) 0.50 (55.5) 0.48 (111.0)	
BH17 top 2(F)	0.13 (11.1) 0.41 (33.7) 0.57 (78.4) 0.59 (156.1)	0.11 (156.1) 0.08 (49.9) 0.12 (6.6)
BH17 silt (C)	0.04 (12.6) 0.09 (40.5) 0.09 (85.0) 0.34 (162.6)	0.02 (35.1)
BH18 top (D)	0.20 (12.9) 0.47 (35.4) 0.63 (79.9) 0.60 (157.7)	0.08 (157.7) 0.11 (51.9) 0.13 (6.9)

Table G.4: Consolidation test results

The consolidation data and diagrams are given on pages 190 through 197. Note that the unloading part of the consolidation diagram (time vs. displacement) could not be drawn for the silt sample due to a defect displacement gauge.

TU**Delft**
Delft
University of
Technology

Oedometer data interpretation
Delft University of Technology, Department of GeoScience & Engineering

Test data		
Name	BH17 top	
Sample height, H	21,1	(mm)
Sample diameter, D	63	(mm)
Sample wet weight, m_b	110	(g)
Sample dry weight, m_d	65,23	(g)
Particle density, rho_p	2,61	(g/cm3)

Loads and deformations											
Load Step	Load (kg)	Stress (kPa)	δ_{inc} (mm)	δ_{total} (mm)	Final Thickness (mm)	Incremental Strain (-)	Total strain (-)	V (cm3)	e (-)	v (-)	w (%)
0	0	0,0	0,00	0,00	21,10	0	0	65,8	1,63	2,63	63
1	3,315	10,4	0,2400	0,24	20,86	0,01	0,01	65,0	1,60	2,60	61
2	6,665	21,0	0,3400	0,58	20,52	0,02	0,03	64,0	1,56	2,56	60
3	11,665	36,7	0,8100	1,39	19,71	0,04	0,07	61,4	1,46	2,46	56
4	26,665	83,9	1,4300	2,82	18,28	0,07	0,13	57,0	1,28	2,28	49
5	46,665	146,9	0,9300	3,75	17,35	0,05	0,18	54,1	1,16	2,16	45

δ_{inc} *Deformation occuring in a load increment*

δ_{total} *Cumulative deformation for all of the load increments. This is calculated automatically from the δ_{inc} data.*

V *Volume*

e *void ratio: V void/V solid*

v *specific volume: 1 +e*

mc *moisture content: mass water/mass solid*

Consolidation parameters						
Step interval	Average Stress	mv [1/Pa]	cv [m2/s]	kv [m/s]	Cc [-]	Cs [-]
1-2	14,8	1,55E-06			0,14	
2-3	27,7	2,51E-06			0,42	
3-4	55,5	1,54E-06			0,50	
4-5	111,0	8,08E-07			0,48	

Figure G.7: Borehole 16 bottom

Oedometer data interpretation
Delft University of Technology, Department of GeoScience & Engineering

Test data		
Name	BH16 silt	
Sample height, H	21,1	(mm)
Sample diameter, D	63	(mm)
Sample wet weight, m_b	104	(g)
Sample dry weight, m_d	74,12	(g)
Particle density, rho_p	2,72	(g/cm3)

Loads and deformations										
Load Step	Load (kg)	Stress (kPa)	δ_{inc} (mm)	δ_{total} (mm)	Final Thickness (mm)	Incremental Strain (-)	Total strain (-)	V (cm3)	e (-)	v (-)	w (%)
0	0	0,0	0,00	0,00	21,10	0	0	65,8	1,41	2,41	52
1	3,315	10,4	0,2800	0,28	20,82	0,01	0,01	64,9	1,38	2,38	51
2	6,665	21,0	0,3000	0,58	20,52	0,01	0,03	64,0	1,35	2,35	50
3	11,665	36,7	0,4900	1,07	20,03	0,02	0,05	62,4	1,29	2,29	47
4	26,665	83,9	0,6100	1,68	19,42	0,03	0,08	60,5	1,22	2,22	45
5	46,665	146,9	0,2700	1,95	19,15	0,01	0,09	59,7	1,19	2,19	44

δ_{inc} Deformation occuring in a load increment

δ_{total} Cumulative deformation for all of the load increments. This is calculated automatically from the δ_{inc} data.

V   Volume

e   void ratio: V void/V solid

v   specific volume: 1 +e

mc   moisture content: mass water/mass solid

Consolidation parameters						
Step interval	Average Stress	mv [1/Pa]	cv [m2/s]	kv [m/s]	Cc [-]	Cs [-]
1-2	14,8	1,37E-06			0,11	
2-3	27,7	1,52E-06			0,23	
3-4	55,5	6,45E-07			0,19	
4-5	111,0	2,21E-07			0,13	

Oedometer data interpretation
Delft University of Technology, Department of GeoScience & Engineering

Test data		
Name	BH17 Silt (C)	
Sample height, H	21,3	(mm)
Sample diameter, D	63	(mm)
Sample wet weight, m_b	109	(g)
Sample dry weight, m_d	79,12	(g)
Particle density, rho_p	2,72	(g/cm3)

Loads and deformations												
Load	Load	Stress	δ_{inc}	δ_{total}	Final Thickness	Incremental Strain	Total strain	V	e	v	w	
Step	(kg)	(kPa)	(mm)	(mm)	(mm)	(-)	(-)	(cm3)	(-)	(-)	(%)	
0	0	0,0	0,00	0,00	21,30	0	0	66,4	1,28	2,28	47	
1	1,81	5,7	0,1740	0,17	21,13	0,01	0,01	65,9	1,26	2,26	46	
2	8,81	27,7	0,2410	0,42	20,89	0,01	0,02	65,1	1,24	2,24	46	
3	18,81	59,2	0,2660	0,68	20,62	0,01	0,03	64,3	1,21	2,21	44	
4	38,81	122,1	0,2570	0,94	20,36	0,01	0,04	63,5	1,18	2,18	43	
5	68,81	216,5	0,7980	1,74	19,56	0,04	0,08	61,0	1,10	2,10	40	
6	1,81	5,7	-0,3000	1,44	19,86	-0,02	0,07	61,9	1,13	2,13	41	

δ_{inc}	*Deformation occuring*		V	*Volume*	
	in a load increment		e	*void ratio:*	
				V void/V solid	
δ_{total}	*Cumulative deformation for all of the*		v	*specific volume:*	
	load increments. This is calculated			*1 +e*	
	automatically from the δ_{inc} data.		mc	*moisture content:*	
				mass water/mass solid	

Consolidation parameters						
Step	Average	mv	cv	kv	Cc	Cs
interval	Stress	[1/Pa]	[m2/s]	[m/s]	[-]	[-]
1-2	12,6	5,18E-07			0,04	
2-3	40,5	4,05E-07			0,09	
3-4	85,0	1,98E-07			0,09	
4-5	162,6	4,15E-07			0,34	
5-6	35,1	7,27E-08				0,02

Figure G.8: Borehole 16 bottom

Oedometer data interpretation
Delft University of Technology, Department of GeoScience & Engineering

Test data		
Name	BH16 (E)	
Sample height, H	21,3	(mm)
Sample diameter, D	63	(mm)
Sample wet weight, m_b	98,29	(g)
Sample dry weight, m_d	53,6	(g)
Particle density, rho_p	2,61	(g/cm3)

Loads and deformations											
Load Step	Load (kg)	Stress (kPa)	δ_{inc} (mm)	δ_{total} (mm)	Final Thickness (mm)	Incremental Strain (-)	Total strain (-)	V (cm3)	e (-)	v (-)	w (%)
0	0	0,0	0,00	0,00	21,30	0	0	66,4	2,23	3,23	86
1	2,301	7,2	0,6300	0,63	20,67	0,03	0,03	64,4	2,14	3,14	82
2	7,301	23,0	0,6970	1,33	19,97	0,03	0,06	62,3	2,03	3,03	78
3	17,301	54,4	1,1260	2,45	18,85	0,06	0,12	58,8	1,86	2,86	71
4	37,301	117,4	1,3180	3,77	17,53	0,07	0,18	54,6	1,66	2,66	64
5	67,301	211,8	0,8350	4,61	16,69	0,05	0,22	52,0	1,53	2,53	59
6	37,301	117,4	-0,2270	4,38	16,92	-0,01	0,21	52,7	1,57	2,57	60
7	7,301	23,0	-0,4580	3,92	17,38	-0,03	0,18	54,2	1,64	2,64	63
8	0,65	2,0	-0,8660	3,06	18,25	-0,05	0,14	56,9	1,77	2,77	68

δ_{inc} *Deformation occuring*
in a load increment

δ_{total} *Cumulative deformation for all of the*
load increments. This is calculated
automatically from the δ_{inc} data.

V   *Volume*
e   *void ratio:*
     V void/V solid
v   *specific volume:*
     1 +e
mc   *moisture content:*
     mass water/mass solid

Consolidation parameters						
Step interval	Average Stress	mv [1/Pa]	cv [m2/s]	kv [m/s]	Cc [-]	Cs [-]
1-2	12,9	2,14E-06			0,21	
2-3	35,4	1,79E-06			0,46	
3-4	79,9	1,11E-06			0,60	
4-5	157,7	5,05E-07			0,49	
5-6	157,7	1,44E-07				0,13
6-7	51,9	2,87E-07				0,10
7-8	6,9	2,38E-06				0,13

Figure G.9: Borehole 17 top

Oedometer data interpretation
Delft University of Technology, Department of GeoScience & Engineering

Test data		
Name	BH17 top (F)	
Sample height, H	21,3	(mm)
Sample diameter, D	63	(mm)
Sample wet weight, m_b	106,79	(g)
Sample dry weight, m_d	61,52	(g)
Particle density, rho_p	2,59	(g/cm3)

						Loads and deformations					
Load Step	Load (kg)	Stress (kPa)	δ_{inc} (mm)	δ_{total} (mm)	Final Thickness (mm)	Incremental Strain (-)	Total strain (-)	V (cm3)	e (-)	v (-)	w (%)
0	0	0,0	0,00	0,00	21,30	0	0	66,4	1,80	2,80	69
1	1,8323	5,8	0,4530	0,45	20,85	0,02	0,02	65,0	1,74	2,74	67
2	6,8323	21,5	0,5600	1,01	20,29	0,03	0,05	63,2	1,66	2,66	64
3	16,8323	53,0	1,2120	2,23	19,08	0,06	0,10	59,5	1,50	2,50	58
4	36,8323	115,9	1,4850	3,71	17,59	0,08	0,17	54,8	1,31	2,31	51
5	66,8323	210,3	1,1690	4,88	16,42	0,07	0,23	51,2	1,16	2,16	45
6	36,8323	115,9	-0,2220	4,66	16,64	-0,01	0,22	51,9	1,18	2,18	46
7	6,8323	21,5	-0,4720	4,19	17,12	-0,03	0,20	53,4	1,25	2,25	48
8	0,65	2,0	-0,9530	3,23	18,07	-0,06	0,15	56,3	1,37	2,37	53

δ_{inc} *Deformation occuring*
in a load increment

δ_{total} *Cumulative deformation for all of the*
load increments. This is calculated
automatically from the δ_{inc} data.

V   *Volume*

e   *void ratio:*
    V void/V solid

v   *specific volume:*
    1 +e

mc *moisture content:*
    mass water/mass solid

Consolidation parameters					
Step interval	Average Stress	mv [1/Pa]	cv [m2/s]	kv [m/s]	Cc [-]	Cs [-]
1-2	11,1	1,71E-06			0,13	
2-3	33,7	1,90E-06			0,41	
3-4	78,4	1,24E-06			0,57	
4-5	156,1	7,04E-07			0,59	
5-6	156,1	1,43E-07				0,11
6-7	49,9	3,00E-07				0,08
7-8	6,6	2,86E-06				0,12

Figure G.10: Borehole 18 top

Oedometer data interpretation
Delft University of Technology, Department of GeoScience & Engineering

Test data	
Name	BH18 top (D)
Sample height, H	21,3 (mm)
Sample diameter, D	63 (mm)
Sample wet weight, m_b	99,57 (g)
Sample dry weight, m_d	53,95 (g)
Particle density, rho_p	2,62 (g/cm3)

Loads and deformations											
Load Step	Load (kg)	Stress (kPa)	δ_{inc} (mm)	δ_{total} (mm)	Final Thickness (mm)	Incremental Strain (-)	Total strain (-)	V (cm3)	e (-)	v (-)	w (%)
0	0	0,0	0,00	0,00	21,30	0	0	66,4	2,22	3,22	85
1	2,301	7,2	0,4400	0,44	20,86	0,02	0,02	65,0	2,16	3,16	82
2	7,301	23,0	0,6500	1,09	20,21	0,03	0,05	63,0	2,06	3,06	79
3	17,301	54,4	1,1600	2,25	19,05	0,06	0,11	59,4	1,88	2,88	72
4	37,301	117,4	1,3800	3,63	17,67	0,07	0,17	55,1	1,67	2,67	64
5	67,301	211,8	1,0200	4,65	16,65	0,06	0,22	51,9	1,52	2,52	58
6	37,301	117,4	-0,1400	4,51	16,79	-0,01	0,21	52,3	1,54	2,54	59
7	7,301	23,0	-0,5100	4,00	17,30	-0,03	0,19	53,9	1,62	2,62	62
8	0,65	2,0	-0,9000	3,10	18,20	-0,05	0,15	56,7	1,76	2,76	67

δ_{inc} *Deformation occuring in a load increment*

δ_{total} *Cumulative deformation for all of the load increments. This is calculated automatically from the δ_{inc} data.*

V *Volume*

e *void ratio: V void/V solid*

v *specific volume: 1 +e*

mc *moisture content: mass water/mass solid*

Consolidation parameters						
Step interval	Average Stress	mv [1/Pa]	cv [m2/s]	kv [m/s]	Cc [-]	Cs [-]
1-2	12,9	1,98E-06			0,20	
2-3	35,4	1,82E-06			0,47	
3-4	79,9	1,15E-06			0,63	
4-5	157,7	6,11E-07			0,60	
5-6	157,7	8,91E-08				0,08
6-7	51,9	3,22E-07				0,11
7-8	6,9	2,49E-06				0,13

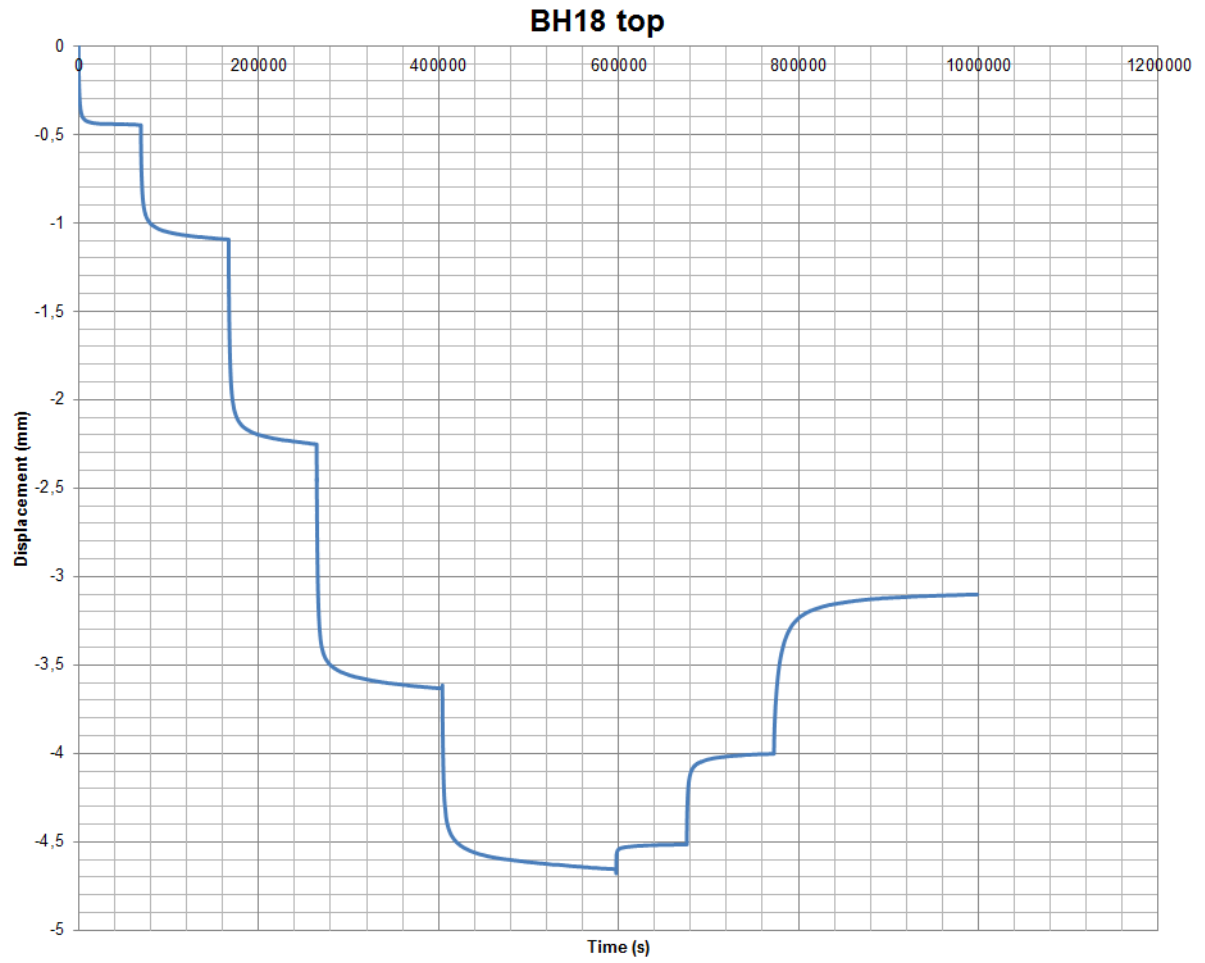**Photos**

Figure G.11: Consolidation test

Figure G.12: Consolidation test, note the salt deposition

Figure G.13: Consolidation test, note the salt deposition

G.1.2   Shear Strength Tests

The shear strength tests were performed in a Direct Shear Strength (DSS) device. All the tests have been executed using ISO17892-10:2004.

BH17

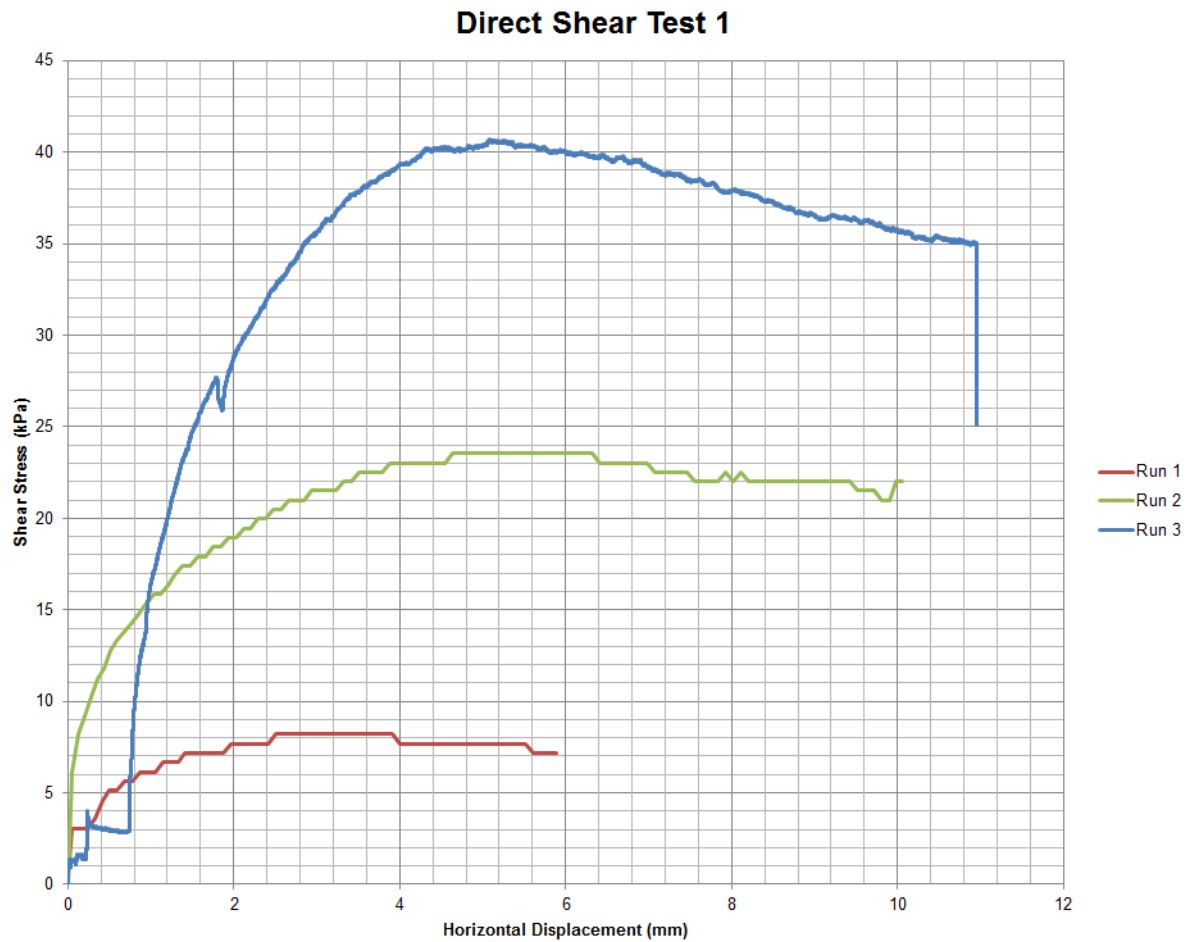The results from DSS test 1 from BH17 are given in figures G.14 and G.15.

Figure G.14: Shear strength test 1 - horizontal displacement vs. shear stress

Van Oord
Marine ingenuity

Table G.5: Consolidation pressure and shear strength from test 1

Test	σ_c (kPa)	τ (kPa)
1	15.65	8.19
2	32.95	23.54
3	71.03	40.69

Table G.6: Cohesion and friction angle from test 1

Run	c (kPa)	ϕ (°)
1-2	0	46.8
2-3	10	24.2
Trendline	1.5	29.9
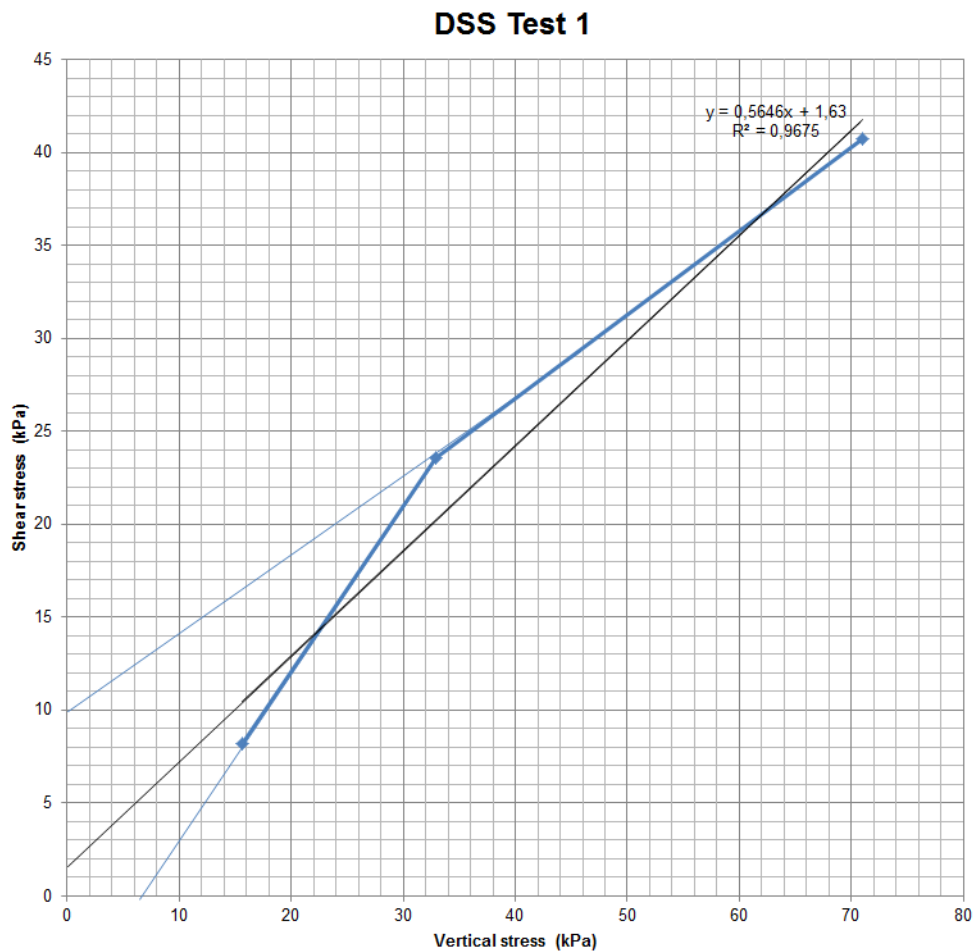
Figure G.15: Shear strength test 1 - consolidation stress vs. shear stress

The parameters that can be derived from test 1 are given in tables G.5 and G.6.

BH16

The results of DSS test 2 from BH16 are given in figure G.17. Note that during the start of run 2 the horizontal displacement gauge failed. The shear box had run for one millimeter, this however remains an estimation. The graph in figure G.16 is corrected for the non-recorded displacement.

TUDelft
Delft
University of
Technology
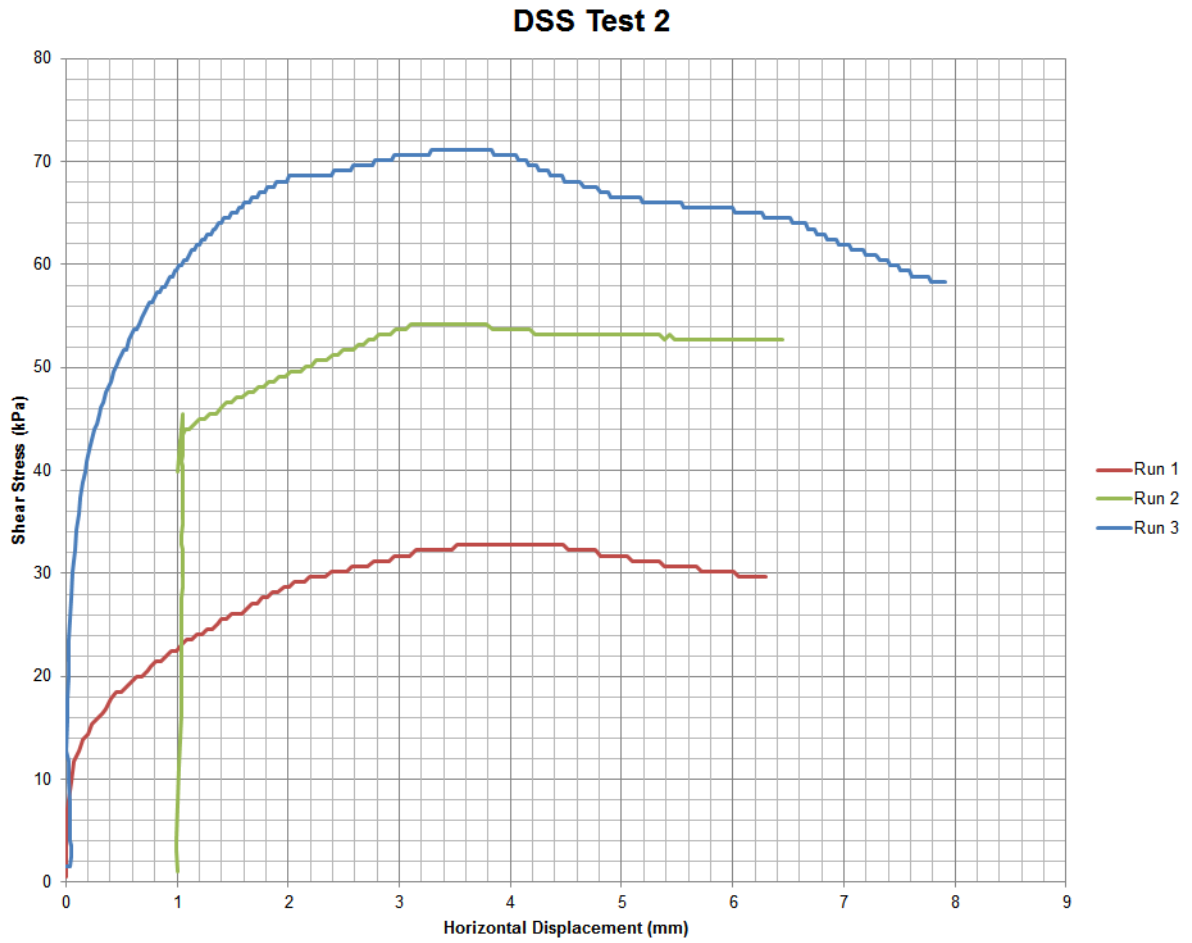
Figure G.16: Shear strength test 2 - horizontal displacement vs. shear stress

Table G.7: Cohesion and friction angle from test 2

Run	c (kPa)	ϕ (°)
1-3	14	22.6

DSS Test 2
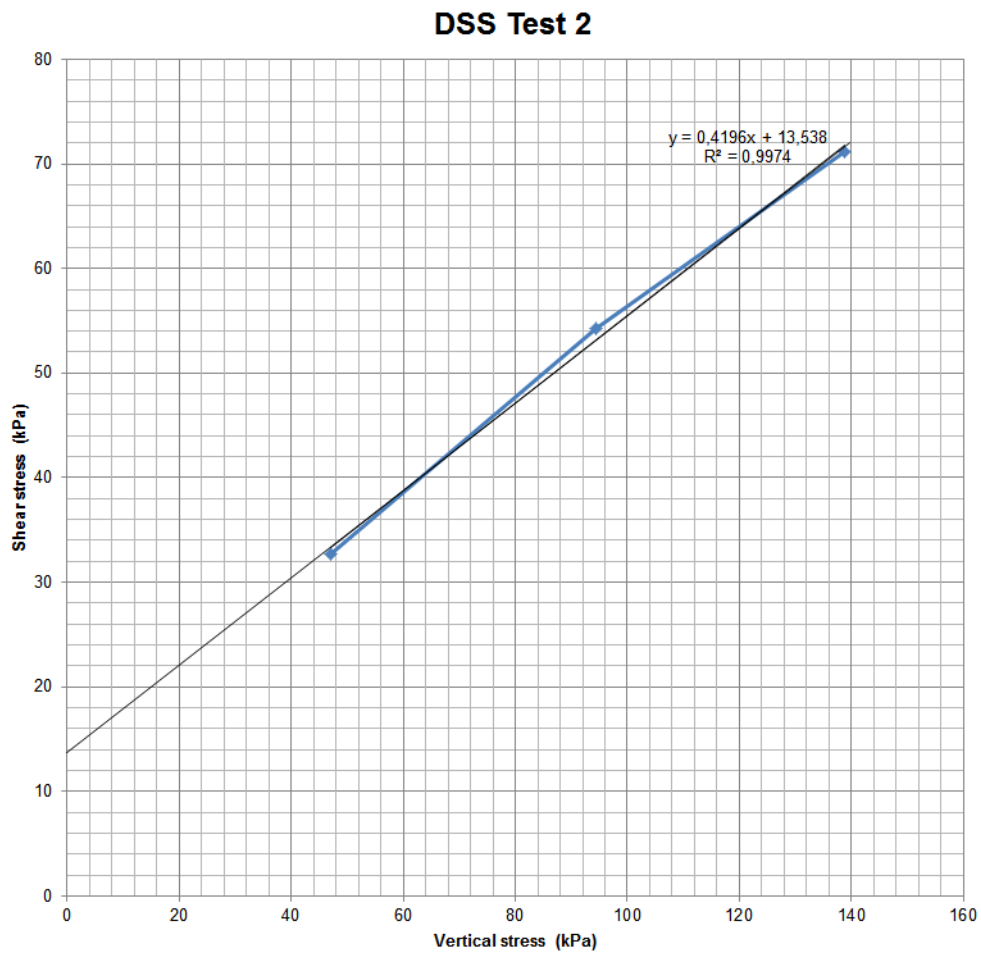
Figure G.17: Shear strength test 2 - consolidation stress vs. shear stress

The parameters that can be derived from test 2 are given in table G.7.

Photos

Figure G.18: Shear strength test sample after shearing

Figure G.19: Shear strength test sample after shearing

Appendix H

Parameter Correlations

Both stiffness and strength parameters were determined by field and laboratory testing in F. This chapter is concerned with refining the estimations and correlations that were elaborated in the aforementioned chapter.

H.1   Hardening Soil - Stiffness
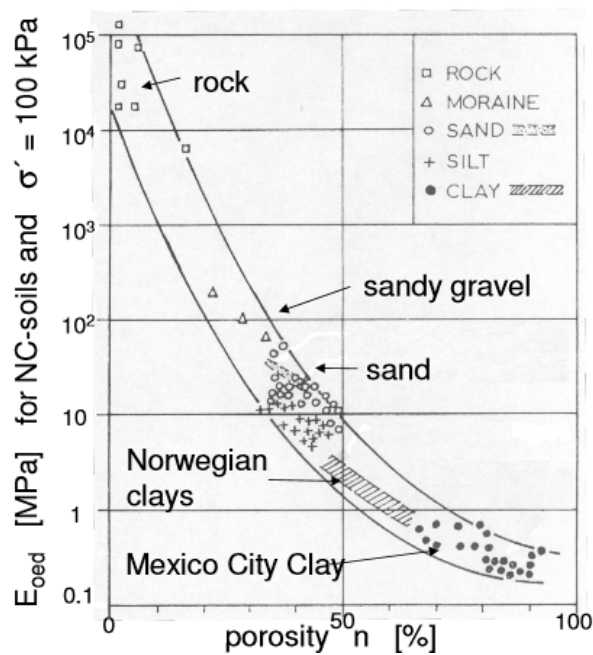
Figure H.1: Oedometer modulus by Janbu (1963)

The Oedometer modulus relative to a reference vertical stress, $p_{ref,v} = \sigma_1$, can be calculated with equation H.1 (Janbu, 1963).

$$E_{oed} = E_{oed}^{ref} \left(\frac{\sigma_1}{p_{ref,v}}\right)^m \tag{H.1}$$

Experimental data was presented by Schanz and Vermeer (1998) on three types of sand.
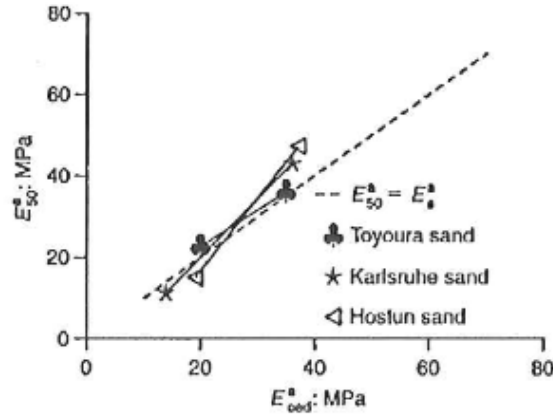
Figure H.2: Comparison of normalized moduli, by Schanz and Vermeer (1998)

It was found that $E_{50}^{ref} \approx E_{oed}^{ref}$.

According to equation H.1,

$$E_{50} = E_{50}^{ref} \left(\frac{\sigma_3}{p_{ref,h}}\right)^m \tag{H.2}$$

$$E_{oed} = E_{oed}^{ref} \left(\frac{\sigma_1}{p_{ref,v}}\right)^m \tag{H.3}$$

and from this

$$\frac{E_{oed}}{E_{50}} = \frac{E_{oed}^{ref}}{E_{50}^{ref}} \left(\frac{\sigma_1}{\sigma_3}\right)^m \approx \frac{\sigma_1}{\sigma_3}\right)^m = \frac{1}{(K_0)^m} \tag{H.4}$$

For sands $m \approx 0.5$, and assuming $K_0 \approx 0.4$ results in equation H.5.

$$E_{oed} = 1.5 \, E_{50} \tag{H.5}$$

H.2   CPT Correlations

Bearing capacity, the level of compaction and settlement predictions (in terms of cone resistance) are checked with CPT testing. Also a selection of soil parameters can be derived from CPT. Please note that for the settlement predictions, results are retrieved from both CPT and zone load testing (ZLT). The latter is not included in this chapter. Multiple CPTs are performed before and after ground improvement works.

CPT results are corrected for surcharge, carbonate and shell content, fines content and transition layers.

H.2.1   Bearing capacity

As described in the Introduction, the bearing capacity is checked by averaging cone resistance in the column $q_{c,p}$ and in the (sabkha) soil $q_{c,s}$ to find the composite (column and soil, respectively) cone resistance. With the composite cone resistance, or equivalent cone resistance $q_{c,eq}$, the performance of dynamic replacement can be verified. The calculation for the equivalent cone resistance is calculated as follows:

$$q_{c,av} = D_{Load,column} \, q_{c,p} + D_{Load,soil} \, q_{c,s} \tag{H.6}$$

Where:

$D_{Load,column}$	= Weighting factor for the load on the column;
$q_{c,p}$	= Cone tip resistance in the column;
$D_{Load,soil}$	= Weighting factor for the load on the soil;
$q_{c,s}$	= Cone tip resistance in the soil.

The weighting factors are calculated as follows:

$$D_{Load,column} = \frac{A_p \sigma_p}{A\sigma}$$

and   (H.7)

$$D_{Load,soil} = \frac{A_s \sigma_s}{A\sigma}$$

With A (A_p and A_s) and σ (σ_p and σ_s) the area and the stress for the compaction grid, respectively.

Using the following equations:

Balance of areas:

$$A = A_p + A_s, \text{ and suppose } \alpha = \frac{A_p}{A}$$

this becomes: (H.8)

$$A_p = \alpha A \text{ and } A_s = (1-\alpha)A$$

Balance of settlement:

$$\frac{\Delta H}{H} = \frac{\sigma_p}{E_p} = \frac{\sigma_s}{E_s} \rightarrow \frac{\sigma_p}{\sigma_s} = \frac{E_p}{E_s} = m \qquad (H.9)$$

Balance of load:

$$A\,\sigma = A_p\sigma_p + A_s\sigma_s \rightarrow \sigma = \alpha\,\sigma_p + (1-\alpha)\sigma_s \qquad (H.10)$$

With equation H.7 and the implementation of the balance equations, equation H.6 can be rewritten to:

$$q_{c,av} = \alpha\frac{\sigma_p}{\sigma}q_{c,p} + (1-\alpha)\frac{\sigma_s}{\sigma}q_{c,s} \qquad (H.11)$$

To arrive at:

$$q_{c,av} = \alpha\frac{m}{1+\alpha(m-1)}q_{c,p} + (1-\alpha)\frac{1}{1+\alpha(m-1)}q_{c,s} \qquad (H.12)$$

Where α is the replacement ratio and m is the stiffness ratio, as defined above.

H.2.2 Dry density

Because of the depth of the columns, it is not practical nor safe to use field density testing method (FDT) over the complete depth. Therefore, two steps are considered:

- For the top 0.5 meter the density will be determined from a FDT.

- Below 0.5 meter depth the density will be determined using the corrected average of the cone resistance.

Van Oord
Marine ingenuity

H.2.3   Settlement

The settlement prediction from the CPT is used to base the locations of the zone load test on. The method is based on correlations with the cone tip resistance. Because the method is relatively straightforward, it is only used for the mentioned zone locations. It is not used for actual settlement predictions (which are used to verify whether the requirements are met).

Young's modulus

The method first calculates the Young's Modulus of the soil. With Young's modulus both the direct and long term settlement is calculated. The method is elaborated below.

$$E \ = \ \alpha_E \ (q_c - \sigma_{v0}) \tag{H.13}$$

Where:
α_E = Coefficient depending on soil behaviour;
q_c = Corrected cone tip resistance;
σ_{v0} = Total overburden stress.

The α_E coefficient is dependent on the Soil Behaviour Index, I_c, which is defined as follows:

$$I_c \ = \ \sqrt{((3.47 - log\,Q_t)^2 \ + \ (logF_r + 1.22)^2} \tag{H.14}$$

Where:
Q_t = Normalized cone penetration resistance, calculated below;
p_a = Reference stress of 100 kPa;
F_r = Normalized friction ratio, calculated below.

The normalized cone penetration resistance, Q_t is calculated as follows:

$$\begin{aligned} Q_t \ &= \ \frac{q_c - \sigma_v 0}{p_a} \ C_N \\ C_N \ &= \ (\frac{p_a}{\sigma'_{v0}})^n \\ n \ &= \ 0.381 \ I_c \ + \ 0.05 \frac{\sigma'_{v0}}{p_\alpha} \ - \ 0.15 \ \leq \ 1.0 \end{aligned} \tag{H.15}$$

Where n is iterated until the change is less than 0.01.

The normalized friction ratio, F_r is calculated as follows:

$$F_r \ = \ \frac{f_s}{(q_c - \sigma_{v0})} \ \times 100\% \tag{H.16}$$

With I_c known, α_E can be calculated:

if $I_c \leq 2.2$ $\alpha_E \ = \ 0.015 \ 10^{0.55 I_c \ + \ 1.68}$

if $I_c > 2.2$ $\alpha_E \ = \ \frac{\alpha_M}{1.35}$

Where α_M is calculated as follows:

For $Q_t < 7$ $\alpha_M \ = \ Q_t$

For $Q_t > 7$ $\alpha_M \ = \ 7$

TUDelft
Delft
University of
Technology

H.2.4   Total Settlement

The total settlement consists of direct settlement and long term settlement, both are discussed in the following sections. Please note that direct settlement occurs at t_1, long term settlement occurs over a period of 25 years t_{25}.

Direct settlement
The direct settlement for a layer i is:

$$S_{t0,i} = C_1(q - \sigma'_{v0})\frac{I_z}{E\ C_3}\ dz \tag{H.17}$$

Where:

C_1	=	Correction factor, calculated below;
C_3	=	Shape correction factor, 1.2 for square footings;
q	=	Foundation load pressure;
σ'_{v0}	=	Effective vertical in-situ stress at foundation depth;
E	=	Young's modulus correlated from CPT, see previous section;
dz	=	Thickness of layer i;
I_z	=	Vertical strain influence factor, calculated below.

The depth correction factor,C_1, is calculated as follows:

$$C_1 = 1 - 0.5(\frac{\sigma'_{v0}}{q - \sigma'_{v0}}) \tag{H.18}$$

The maximal strain influence factor,$I_{z,max}$, is calculated as follows:

$$I_{z,max} = 0.5 + 0.1\sqrt{\frac{q - \sigma'_{v0}}{E\ C_3}} \tag{H.19}$$

For other values reference is made to figure H.3.
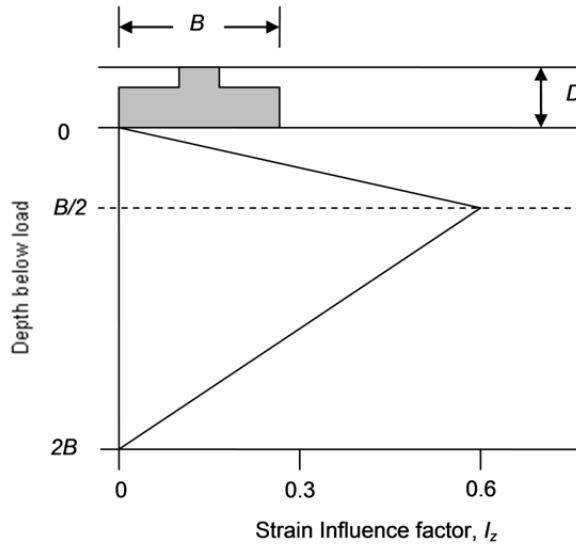
Figure H.3: Strain influence factor from Schmertmann, 1970 for axisymmetric footing

Long term settlement
Long term settlement is calculated using:

$$\frac{S_{t_{25}}}{S_{t_1}} = (\frac{t_{25}}{t_1})^n \tag{H.20}$$

Van Oord
Marine ingenuity

Where:
S_{t_1} = Settlement after 2 hours;
$S_{t_{25}}$ = Settlement after a period of 25 years;
n = Briaud's coefficient (dependent on Soil Behaviour Type, I_c) given in table H.1.

Table H.1: Briaud's coefficient

Soil	**I_c**	**n**
Organic soils - clay	≥ 3.6	0.08
Clayey silt to clay	2.6-3.6	0.025-0.08
Clean sand to sandy silt	1.31-2.6	0.005-0.025
Gravelly sand to dense sand	≤ 1.31	0.005

The long term settlement is then calculated as follows:

$$S_{t_{25},i} = ((\frac{t_{25}}{t_1})^n - 1)\, S_{t_1,i} \tag{H.21}$$

Total settlement
The total predicted settlement is then calculated as follows:

$$S_{total} = \sum(S_{t1,i} + S_{t_{25},i})\, dz \tag{H.22}$$

H.3 Friction Angle

A prediction of the friction angle, φ, can be made based on CPT. The following sections describe three theories to determine φ. The results of these theories was already shown in figures F.18 and F.22 in section F.2.2.

H.3.1   Mayne et al. (1990)

The friction angle can be approximated using equation H.23 from Kulhawy and Mayne (1990).

$$\varphi' = 17.6 + 11\log(Q_{tn}) \tag{H.23}$$

H.3.2   Uzielli et al. (2013)

The friction angle can be approximated using equation H.23 from Uzielli et al. (2013).

$$\varphi' = 25 + q_t^0.10 \tag{H.24}$$

H.3.3   Robertson et al. (1983)

The friction angle can be approximated using equation H.25 from Robertson and Campanella (1983).

$$\tan\varphi' = \frac{1}{2.68}\left[\log(\frac{q_c}{\sigma'_{v0}} + 0.29\right] \tag{H.25}$$

Appendix I

PLAXIS Benchmarking and Meshing

As described in the main document in chapter 7, the PLAXIS model should be benchmarked using ZLT results from the site investigation (described in chapter 6).

The PLAXIS benchmarking together with the mesh used will be elaborated in section I.1. Section I.3 describes the mesh used for the consolidation calculations.

I.1 Benchmarking

The parameters used were derived from soil tests (see chapter F). It is worth mentioning that for the stiffness simulations equations I.1 and I.2 are used:

$$E_{50}^{ref} = E_{oed}^{ref} \tag{I.1}$$

$$E_{ur}^{ref} = 3E_{50}^{ref} \tag{I.2}$$

Furthermore, the dilation angle, ψ, was implicitly changed during the $\varphi_{platform}$ and φ_{column} simulations, using equation I.3.

$$\psi = \varphi - 30° \tag{I.3}$$

I.1.1 ZLT on top of Column

The simulations that were performed for the initial benchmarking of the ZLT on top of the column are given in table I.1. Note that

Table I.1: Simulations on top of Column

Calculation	$\varphi_{platform}$ [°]	φ_{column} [°]	E [MPa]	H [m]
1,1	34	40	110	2,2
1,2	36	40	110	2,2
1,3	38	40	110	2,2
1,4	40	40	110	2,2
1,5	42	40	110	2,2
2,1	38	34	110	2,2
2,2	38	36	110	2,2
2,3	38	38	110	2,2
2,4	38	40	110	2,2
2,5	38	42	110	2,2
2,6	38	44	110	2,2
3,1	38	40	70	2,2
3,2	38	40	80	2,2
3,3	38	40	90	2,2
3,4	38	40	100	2,2
3,5	38	40	110	2,2
3,6	38	40	120	2,2
3,7	38	40	130	2,2
4,1	38	40	110	2,2
4,2	38	40	110	2,5
4,3	38	40	110	2,8
4,4	38	40	110	3,1
4,5	38	40	110	3,4
4,6	38	40	110	3,7
4,7	38	40	110	4
4,8	38	40	110	5
4,9	38	40	110	6
5	38	40	110	7

Figures I.1 through I.4 show the results from the calculations summarized in table I.1.

TUDelft
Delft
University of
Technology
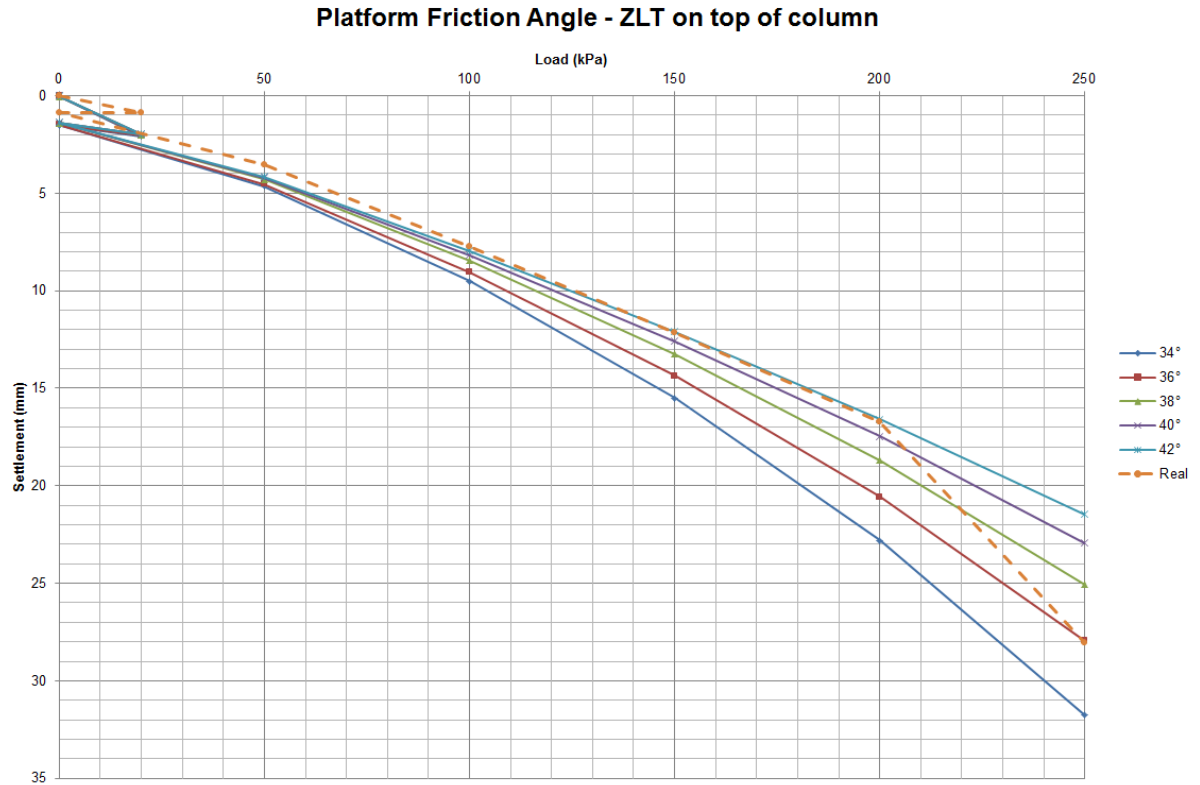
Figure I.1: ZLT between columns, varying platform friction angle
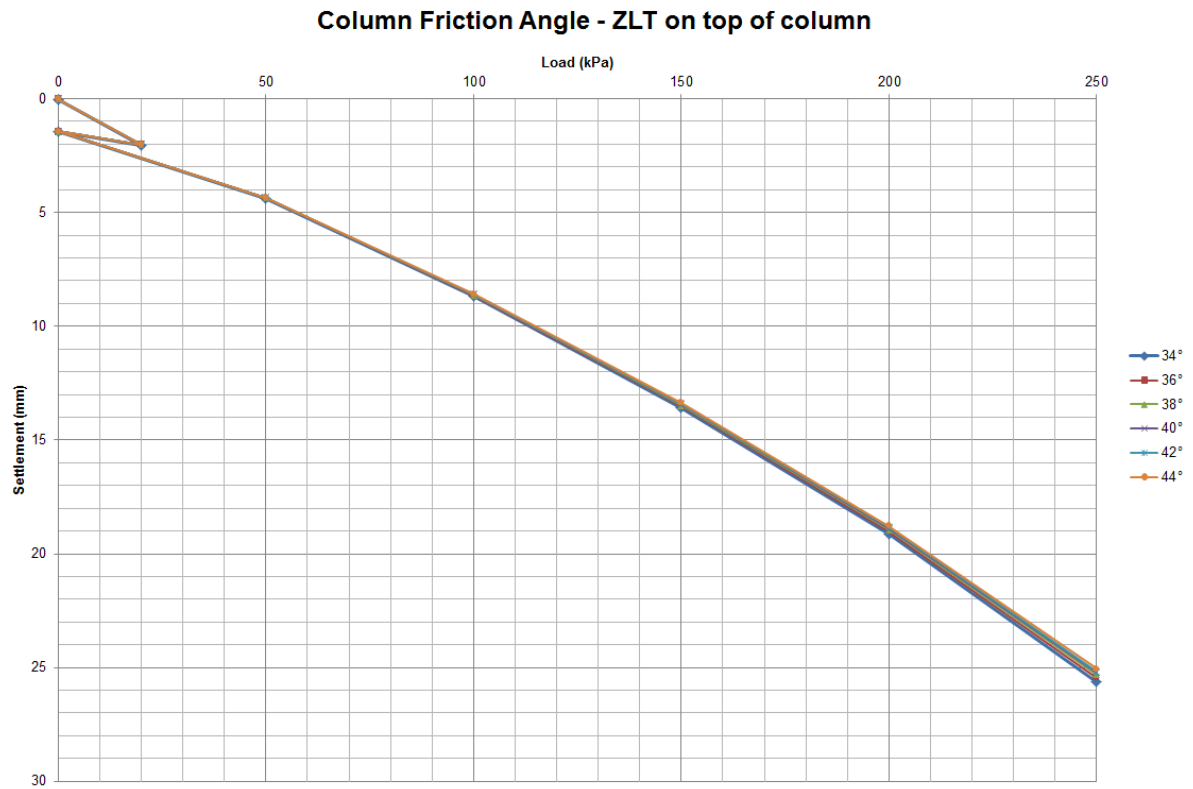
Figure I.2: ZLT between columns, varying column friction angle

213

Stiffness - ZLT on top of column

Figure I.3: ZLT between columns, varying platform stiffness

Platform Height - ZLT on top of column
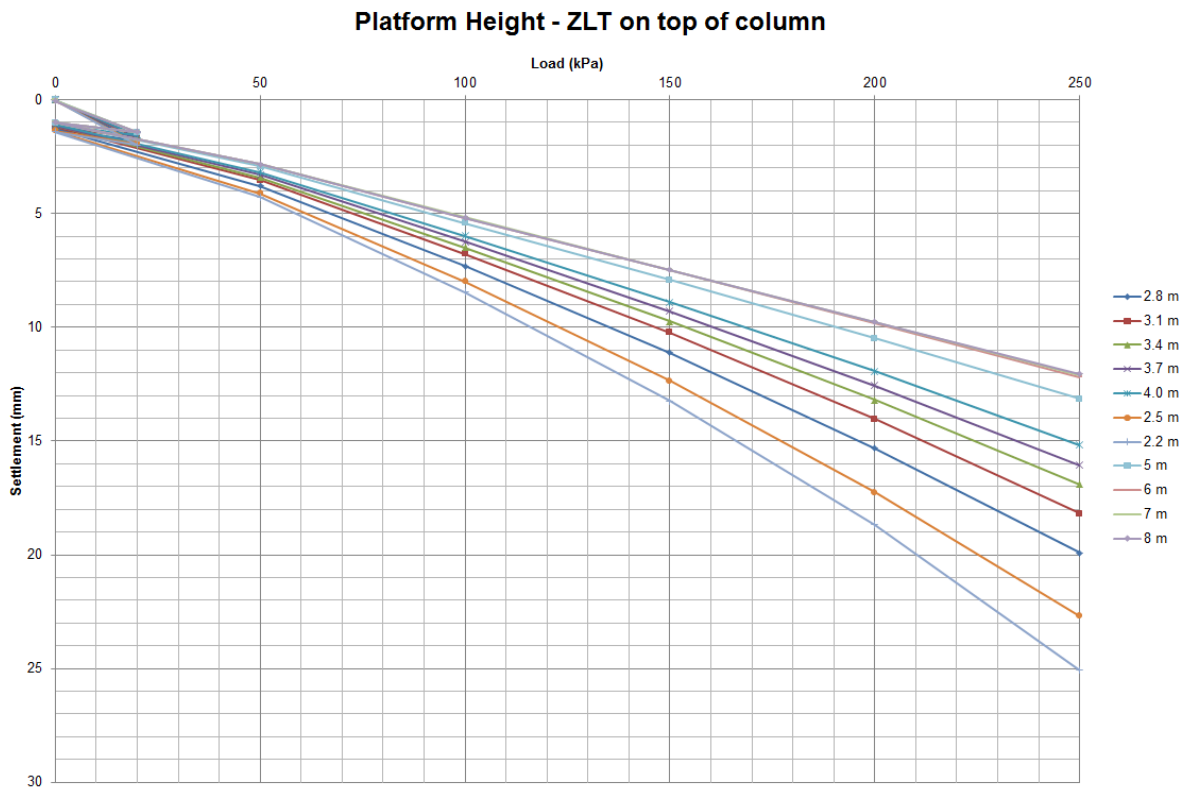
Figure I.4: ZLT between columns, varying platform height

214

I.1.2 ZLT between Columns

The simulations that were performed for the initial benchmarking of the ZLT on top of the column are given in table I.2.

Table I.2: Simulations between Columns

Calculation	$\varphi_{Platform}$ [°]	$\$\varphi_{Column}$ [°]	E [MPa]	H [m]
1,1	34	40	110	2,2
1,2	36	40	110	2,2
1,3	38	40	110	2,2
1,4	40	40	110	2,2
1,5	42	40	110	2,2
2,1	38	34	110	2,2
2,2	38	36	110	2,2
2,3	38	38	110	2,2
2,4	38	40	110	2,2
2,5	38	42	110	2,2
2,6	38	44	110	2,2
3,1	38	40	70	2,2
3,2	38	40	80	2,2
3,3	38	40	90	2,2
3,4	38	40	100	2,2
3,5	38	40	110	2,2
3,6	38	40	120	2,2
3,7	38	40	130	2,2
4,1	38	40	110	2,2
4,2	38	40	110	2,5
4,3	38	40	110	2,8
4,4	38	40	110	3,1
4,5	38	40	110	3,4
4,6	38	40	110	3,7
4,7	38	40	110	4
4,8	38	40	110	5
4,9	38	40	110	6
5	38	40	110	7

Figures I.5 through I.8 show the results from the calculations summarized in table I.2.

Van Oord
Marine ingenuity

Platform Friction Angle - ZLT in between columns
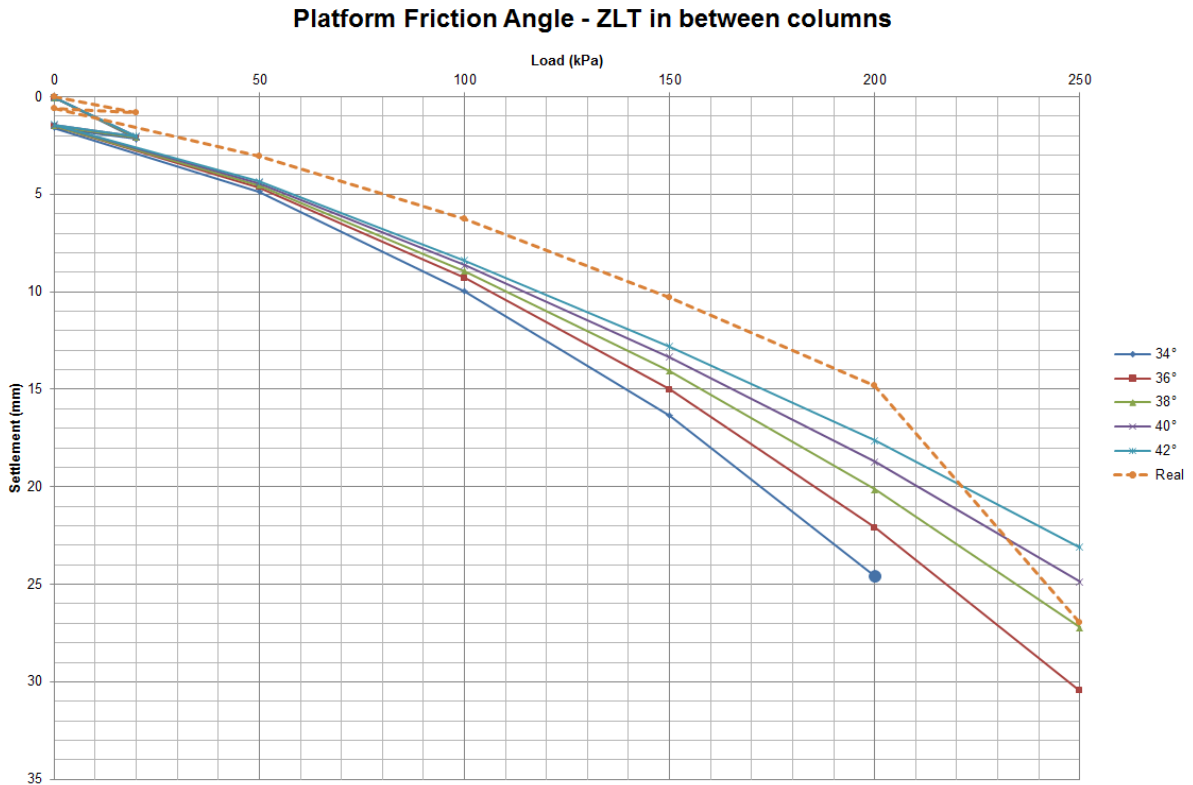
Figure I.5: ZLT on top, varying platform friction angle

Column Friction Angle - ZLT between columns
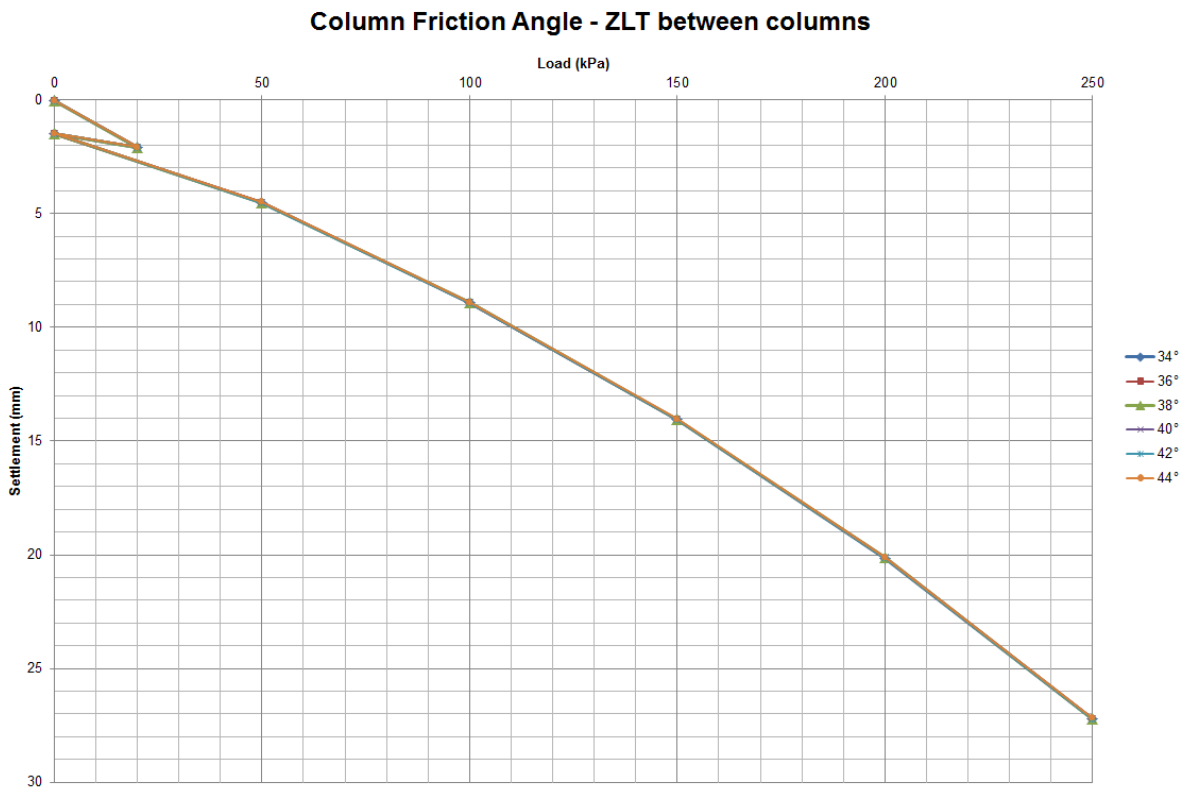
Figure I.6: ZLT on top, varying column friction angle

Figure I.7: ZLT on top, varying platform stiffness
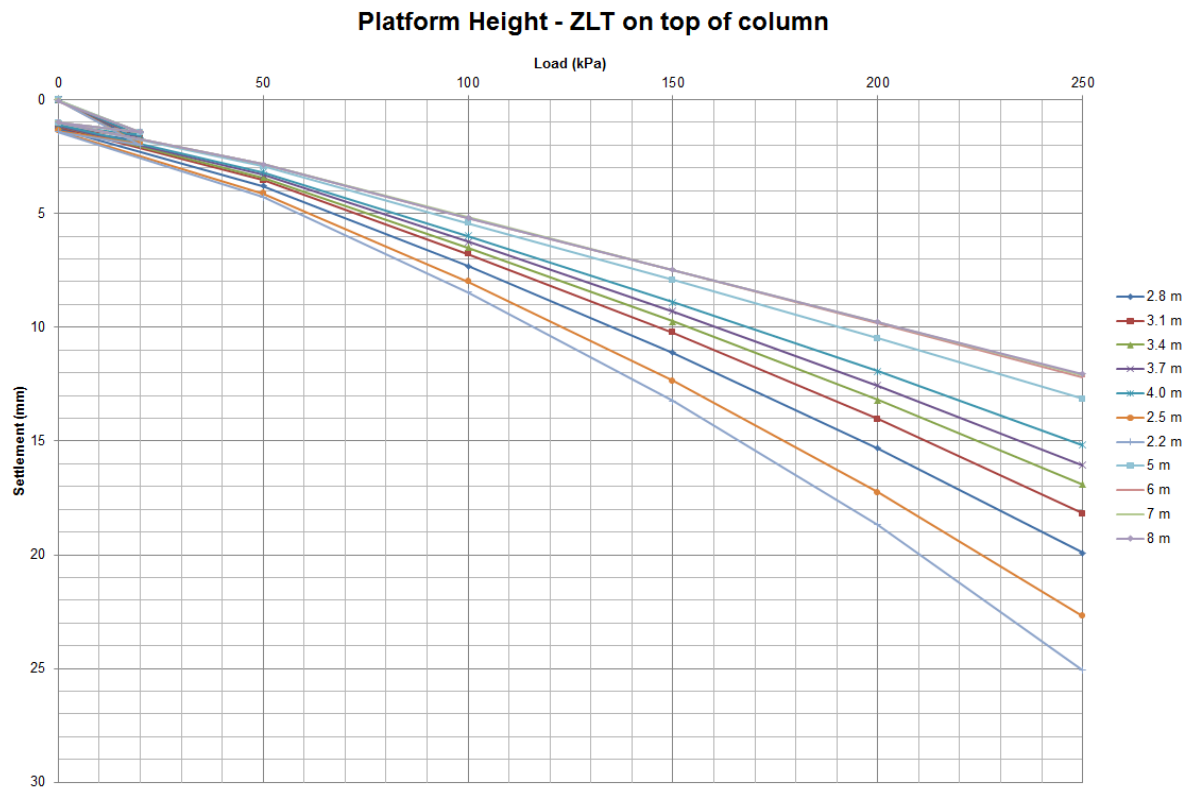
Figure I.8: ZLT on top, varying platform height

Table I.3: Element PLAXIS coarseness factor

Element	Coarseness
Area under ZLT	0.282
Area <3 m XY from ZLT	0.400
Volume <5 Z from ZLT	0.400
Sand platform	0.707
Sand columns	0.707
Silt	1.000
Sabkha	1.000
Deep silt	1.000

I.2 Parametric Analysis Mesh

To determine the model's sensitivity to meshing, different mesh coarsenesses have been used. For all meshes holds that the platform and the columns have a refined mesh compared to the surrounding (soft) soil. All the calculations were performed with $\varphi_{platform} = 38°$ and $\varphi_{column} = 40°$.

The model with a printed mesh is given in figure I.9.
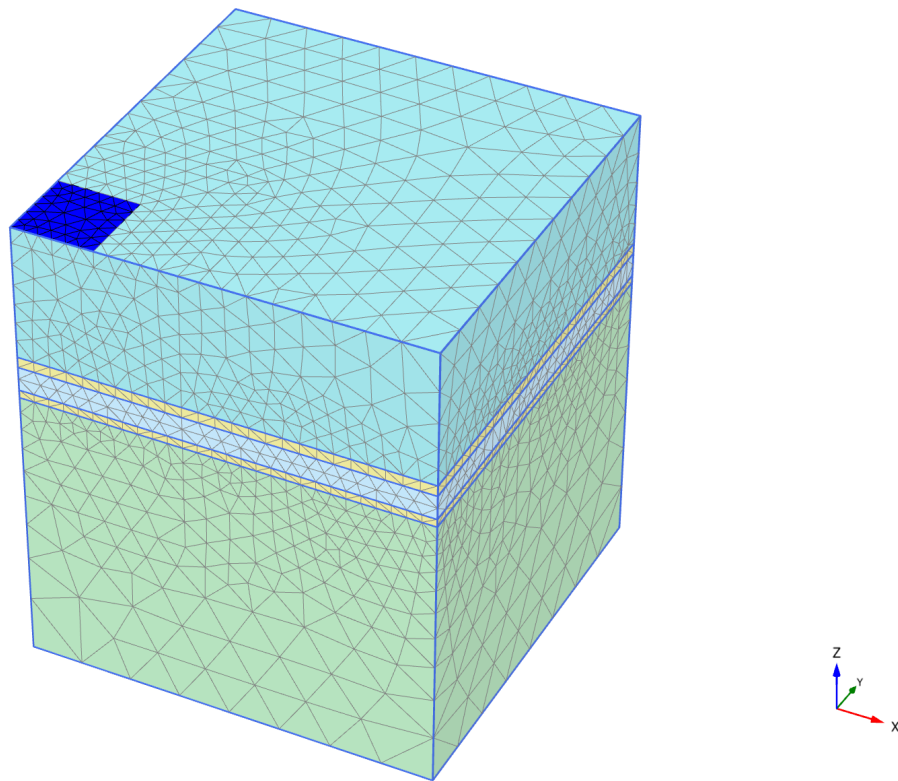
Figure I.9: The mesh for the simulations with the ZLT in between the columns

The coarseness of the mesh is varied between very coarse and medium (in PLAXIS terms). This results in a set of coarseness factors, given in table I.3. For the simulations where the ZLT is located on top a column the same factors hold.

The mesh sensitivity analysis for the ZLT on top of a column is given in table I.4, the sensitivity analysis for the ZLT between the columns is given in table I.5.

Based on the maximum accuracy difference of 5% (between the coarse and medium coarse mesh for the ZLT between columns simulation), it is decided to continue using the very coarse general mesh with local refinements, as summarized in table I.3.

Table I.4: Mesh sensitivity, on top of column

Pressure	Very Coarse	Coarse	Medium	Difference V-C [%]]	Difference C-M [%]]
0	0,01623	0,0295	0,01456	81,76	-50,64
20	1,823	1,848	1,871	1,37	1,24
0	1,295	1,317	1,339	1,70	1,67
50	3,909	3,972	4,062	1,61	2,26
100	7,793	7,973	8,126	2,31	1,91
150	12,49	12,89	13,15	3,20	2,02
200	18,13	18,96	19,3	4,58	1,79
250	24,9	26,28	26,73	5,54	1,71

Table I.5: Mesh sensitivity, between columns

Pressure	Very Coarse	Coarse	Medium	Difference V-C [%]]	Difference C-M [%]]
0	0,01741	0,1676	0,0452	862,67	-73,03
20	1,877	1,895	1,872	0,96	-1,21
0	1,338	1,353	1,34	1,12	-0,96
50	4,044	4,134	4,07	2,23	-1,55
100	8,189	8,341	8,149	1,86	-2,30
150	13,26	13,64	13,24	2,87	-2,93
200	19,53	20,32	19,51	4,05	-3,99
250	27,17	28,52	27,09	4,97	-5,01

The default maximum number of 250 steps was used. The maximum number of iterations was kept at 60. The default tolerated error was 0.010.

I.3   Consolidation Calculations Mesh

The connectivity plot of the mesh that is used for the main calculations is given in figure I.10. The coarseness factors are summarized in table I.6.

Van Oord
Marine ingenuity
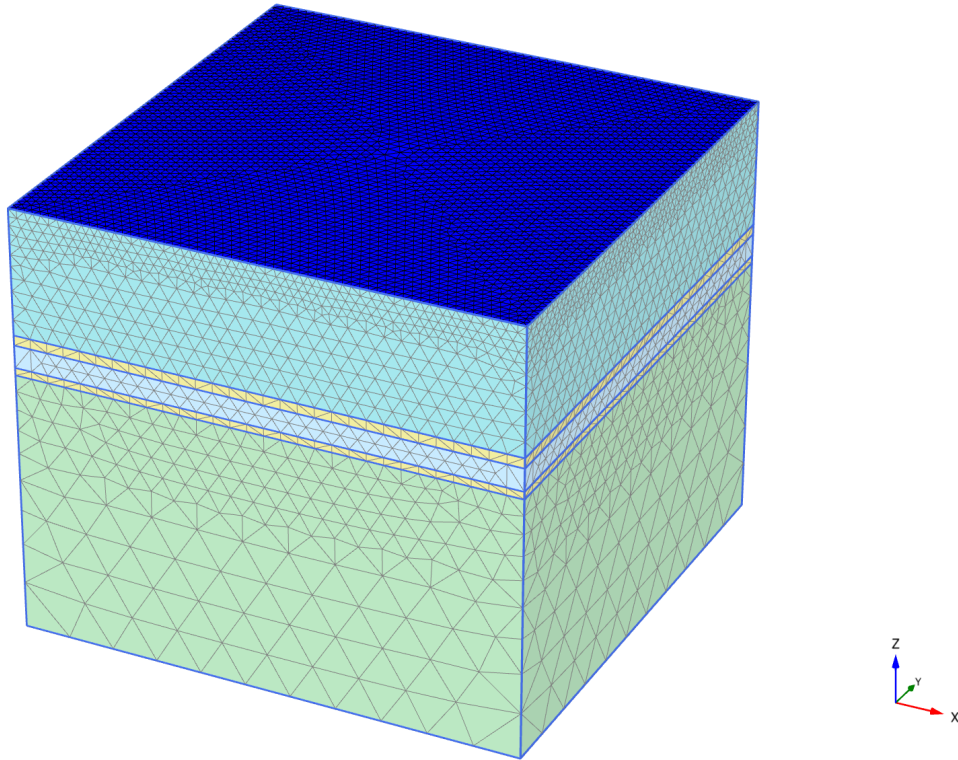
Figure I.10: The mesh for the main calculations

Table I.6: Element coarseness

Element	Coarseness factor
Area under ZLT	0.200
Sand platform	0.400
Sand columns	0.1000
Silt	0.707
Sabkha	0.707
Deep silt	0.5657

The above mentioned model leads to effective stresses in the order of 3000 kPa, which is not realistic. A plot of the stresses in a cross-section of the column is given in figure I.11.
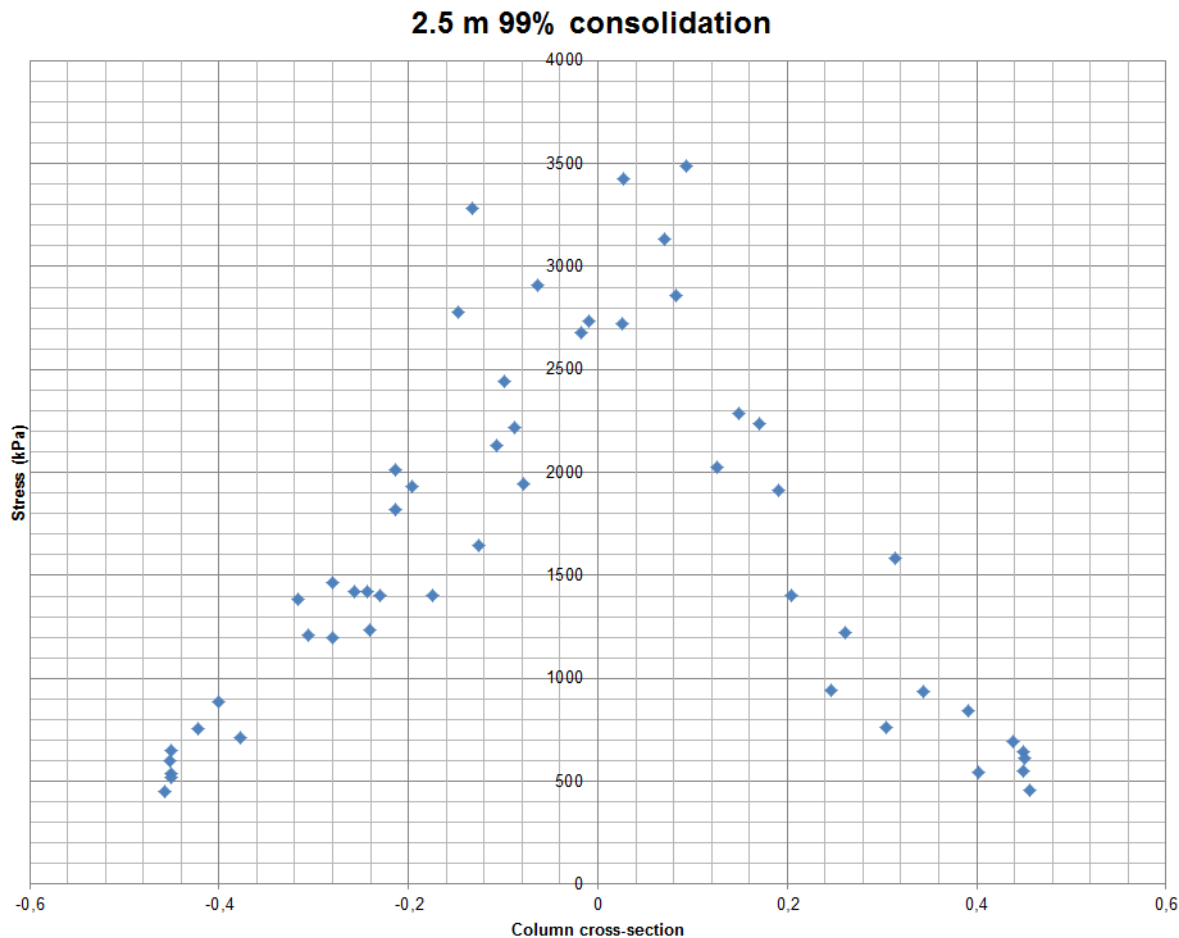
TU Delft

Delft
University of
Technology

Figure I.11: Unrealistically high stresses in the column

The high effective stresses values are located and concentrated ("peaks") between the Sand column and Sand Platform. These stresses appear to be caused by an interpolation error. Stresses in nodes are interpolated from Gauss points (or stress points) and the interpolation error will increase the farther away the nodes and Gauss points are from each other (i.e more coarse mesh). The error is more severe in circular elements. These elements consist of many straight lines, at the edges of which high stresses occur. The interpolation error can be seen in figure I.12. The stress is extremely high near the edge of the sand column.

Figure I.12: Interpolation error near the edges of the sand column

To reduce the interpolation error it was decided to refine the mesh. The model as illustrated in figure I.10 leads to a calculation time of approximately 30 hours for one consolidation ($U = 50\%$) which is not feasible. Instead of the unit cell that was chosen before, a column-centered (see chapter 2) is used. The connectivity plot of the mesh that is used for the consolidation analysis is given in figures I.13 and I.14
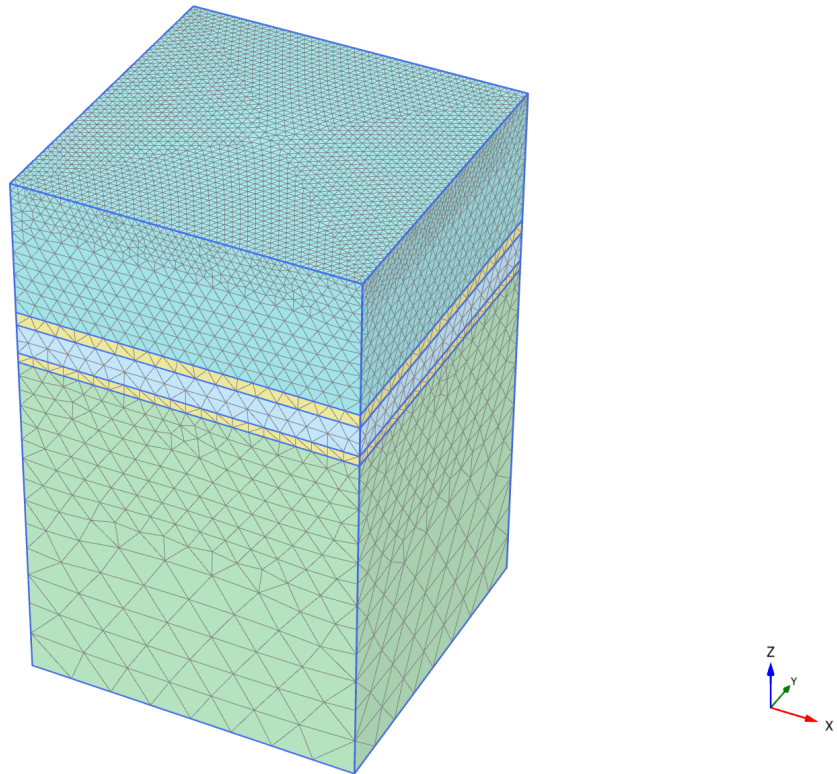
Figure I.13: The mesh for the consolidation calculations
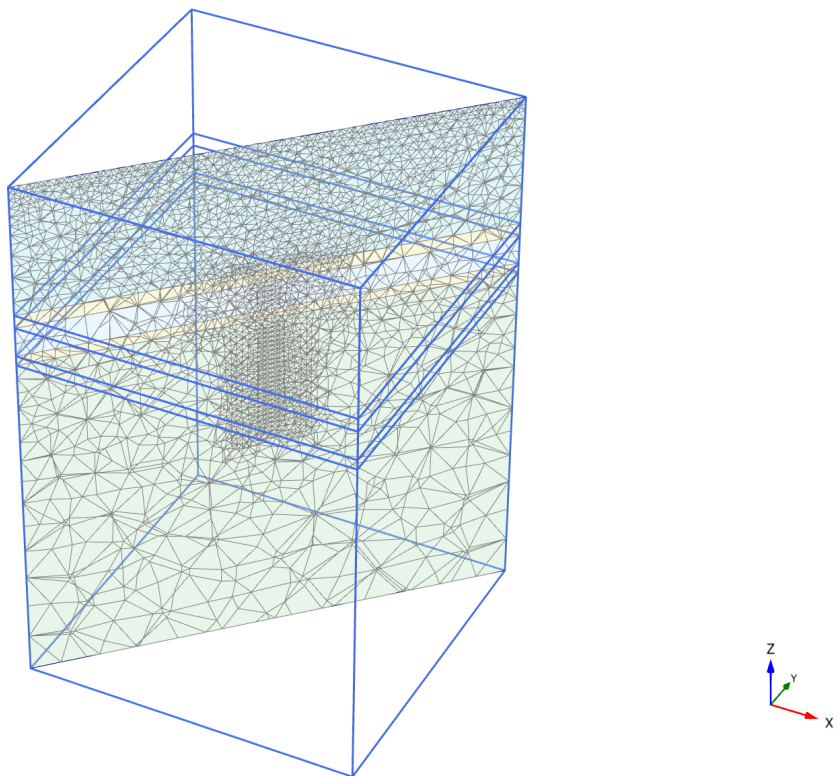
Figure I.14: The mesh for the consolidation calculations, a cross-section

The coarseness factors are summarized in table I.7.

Table I.7: Element coarseness

Element	Coarseness factor
Area under ZLT	0.100
Sand platform	0.200
Sand columns	0.07071
Silt	0.707
Sabkha	0.707
Deep silt	0.5657

The maximum number of steps was adjusted to 800 steps. Especially for the lower embankment heights, this proved not sufficient. Consequently the number was increased once more to 1500 steps. The maximum number of iterations was kept at 60. The default tolerated error was 0.010.

Appendix J

Column Force and Arching Calculation

The current PLAXIS version does not include a tool to integrate stress over a non-structural area or in a non-structural volume.

To determine the force in a column, the following methods were used.

J.1 Shell Integration

To integrate the stress over the cross-section of the column, shell integration is employed. The shell method "is a means of calculating the volume of a solid of revolution, when integrating along an axis perpendicular to the axis of revolution" (Wikipedia, 2016). A sketch of the method is given in figure J.1.
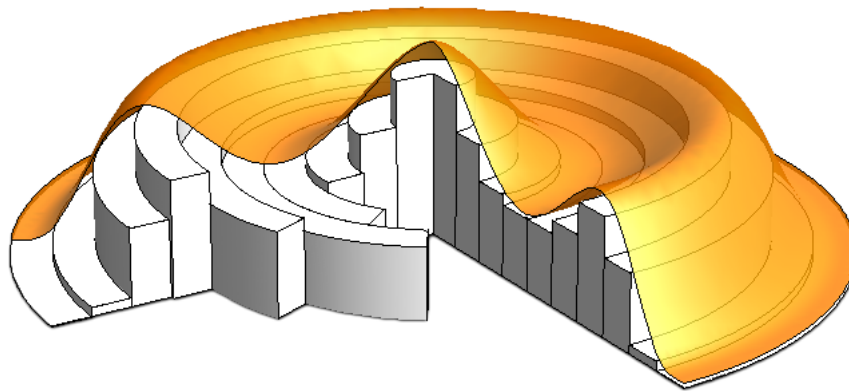
Figure J.1: Shell integration, taken from Wikipedia (2016)

$$2\pi \int_a^b x\,\sigma(x)\,\mathrm{d}x. \tag{J.1}$$

Where a is the lower bound, 0, and b is the upper bound, $0.5 \cdot a$.

Two plots of the stress in a column cross-section are given in figures J.2 and J.3.
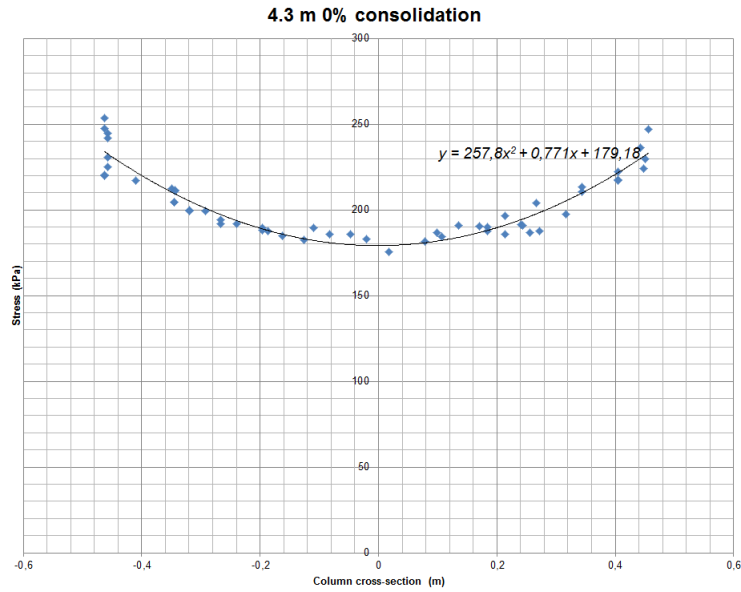
Figure J.2: Example column cross-section for consolidation = 0%

Integrating by the Shell Method leads to a force in the column from figure J.2 of 166 kN.
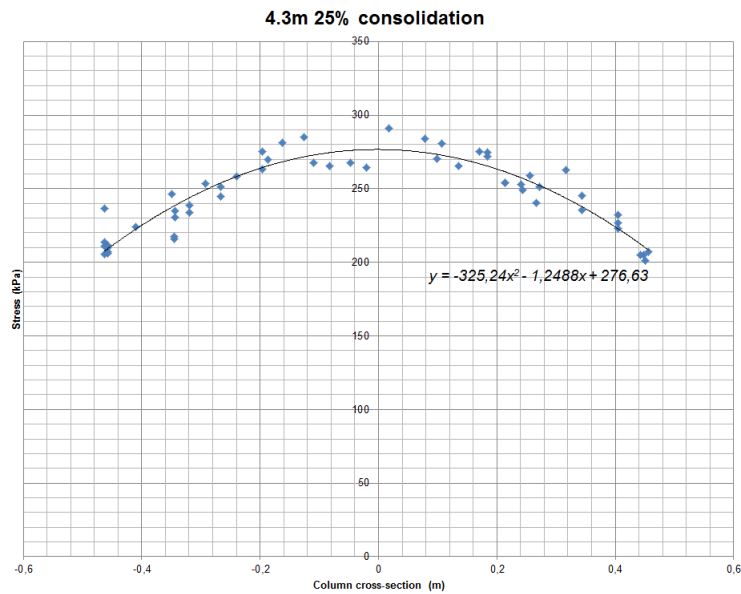

Figure J.3: Example column cross-section for consolidation = 25%

Integrating by the Shell Method leads to a force in the column from figure J.3 of 185 kN.

The result of the above calculation is the Arching A in kN/pile. The Efficiency can be now calculated using equation J.2.

$$E = 1 - \frac{B+C}{A+B+C} = \frac{A}{A+B+C} = \frac{A}{(H\gamma + q)s_x s_y} \tag{J.2}$$

In equation J.2 A equals the force in the column, B can be calculated based on equilibrium and C equals zero. The equilibrium can be considered using equation J.3.

$$A + B = \gamma H + q \tag{J.3}$$

If one would however only be interested in the increase in arching due to the distributed load, an incremental arching parameter can be defined using equation J.4.

$$\Delta E \;=\; \frac{\Delta A}{\Delta q S^2} \tag{J.4}$$

J.2   Balance of Load Method

Instead of calculating the force in the column, the stress on the subsoil can be integrated over a unit cell and then subtracted from the total load. The efficiency calculation is then rewritten to equation J.5

$$E = \frac{W - \sigma_s(s^2 - A_c)}{W} = 1 - \frac{\sigma_s(s^2 - A_c)}{W} \tag{J.5}$$

Where W is defined in equation J.6. For the other parameters reference is made to the nomenclature on page ix.

$$W = (\gamma H + q)s^2 \tag{J.6}$$

Assuming a unit cell of s width, s length, column diameter d and no arching, leads to equation J.7.

$$E \;=\; \frac{\sigma_s(s^2 - \frac{1}{4}\pi d^2)}{W} = \frac{(\gamma H + q)(s^2 - \frac{1}{4}\pi d^2)}{(\gamma H + q)s^2} = \frac{\pi d^2}{4s^2} = 3.14\% \tag{J.7}$$

The efficiency is thus equal to $\frac{\pi}{100}$, which is the same result one obtains when considering the balance of area, $\frac{A_c}{s^2} \;=\; \frac{\frac{1}{4}\pi d^2}{s^2}$. It should be realized that the lowest efficiency E, in case no arching occurs, equals the ratio of column area over total area.

J.3   Cross-sections

This section shows the cross-sectional stress distributions corresponding to the consolidation calculations elaborated in section 9.2.
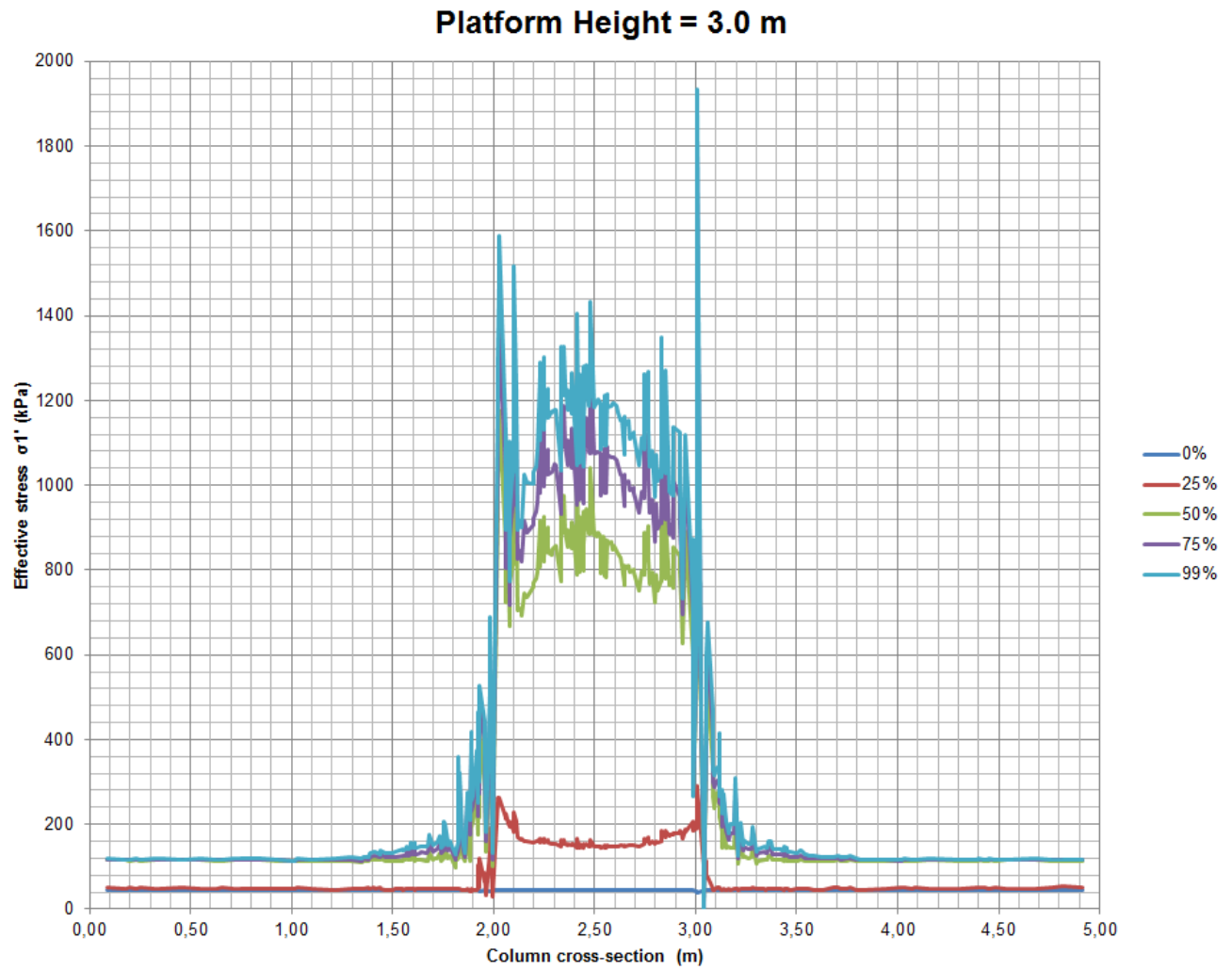
Van Oord
Marine ingenuity

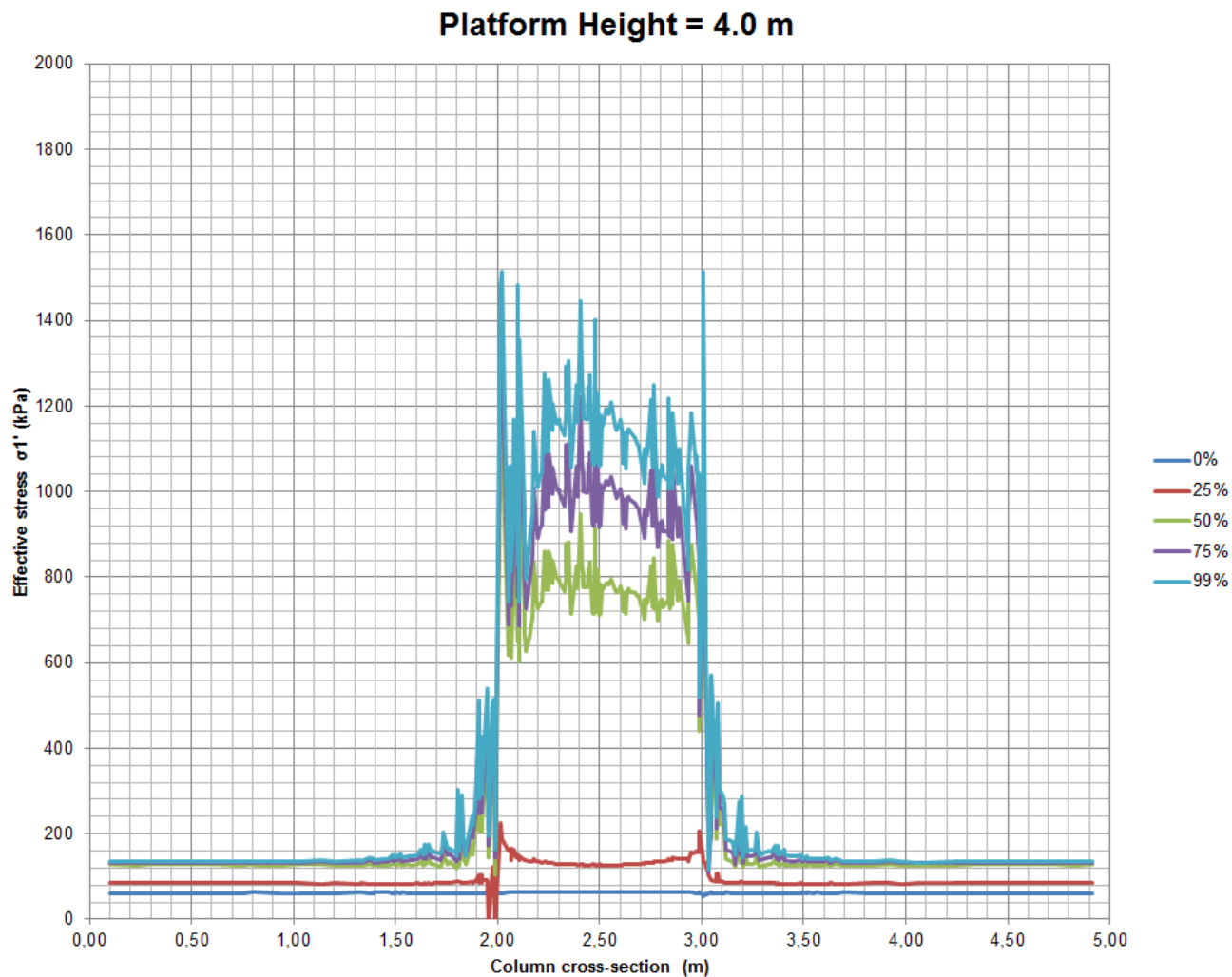Figure J.4: Cross-section of the stress distribution for platform height = 3.0 m

Figure J.5: Cross-section of the stress distribution for platform height = 4.0 m
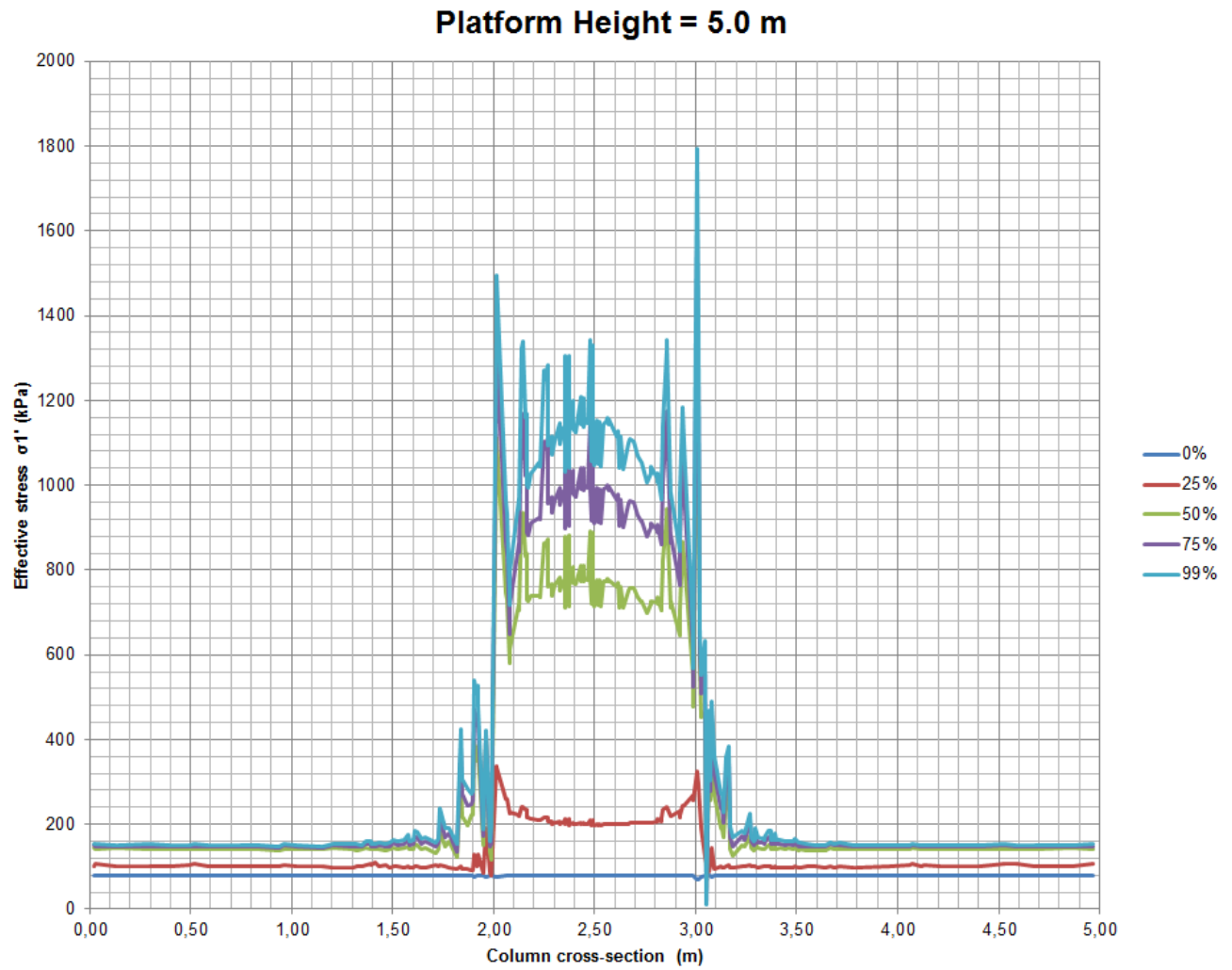
Figure J.6: Cross-section of the stress distribution for platform height = 5.0 m
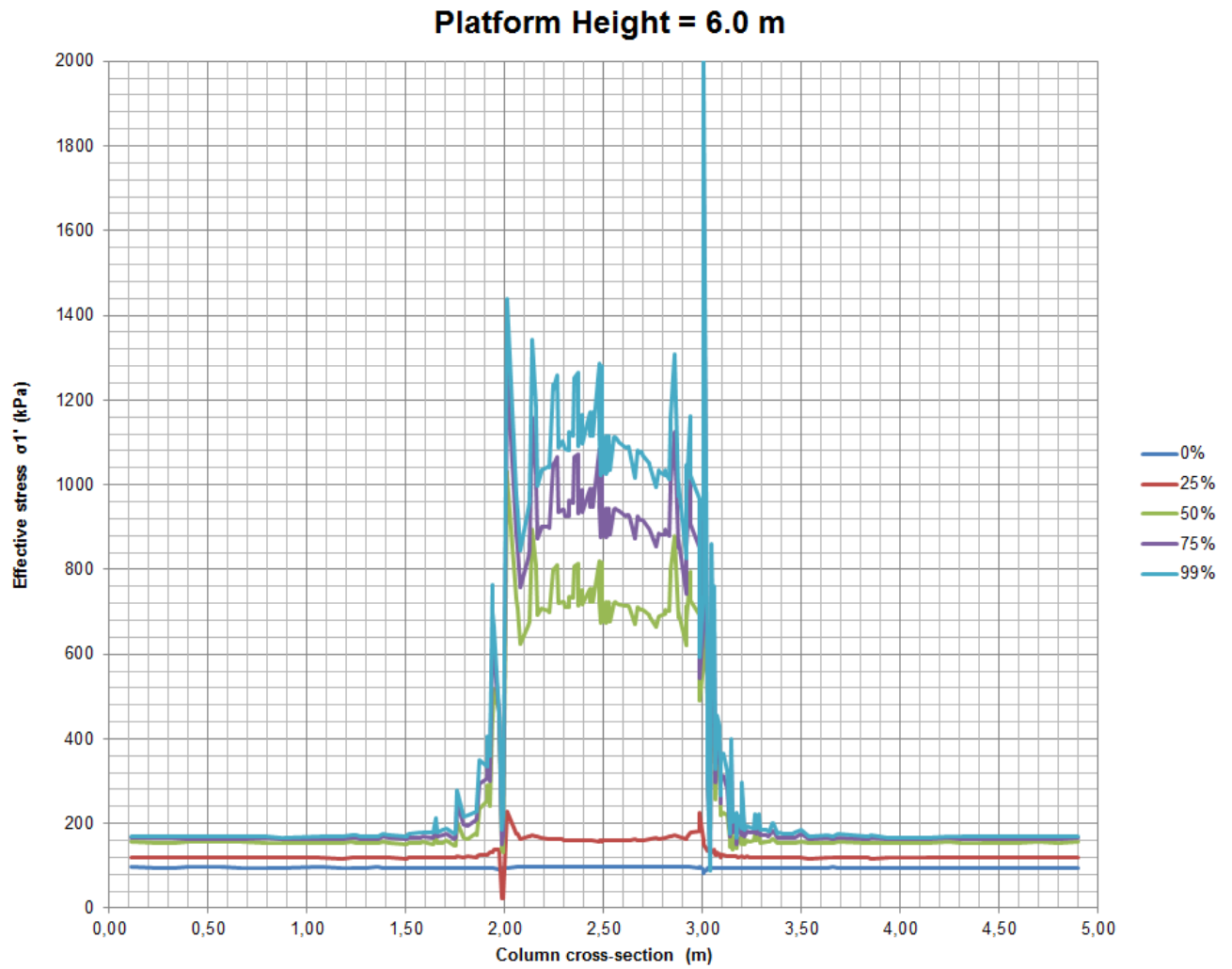
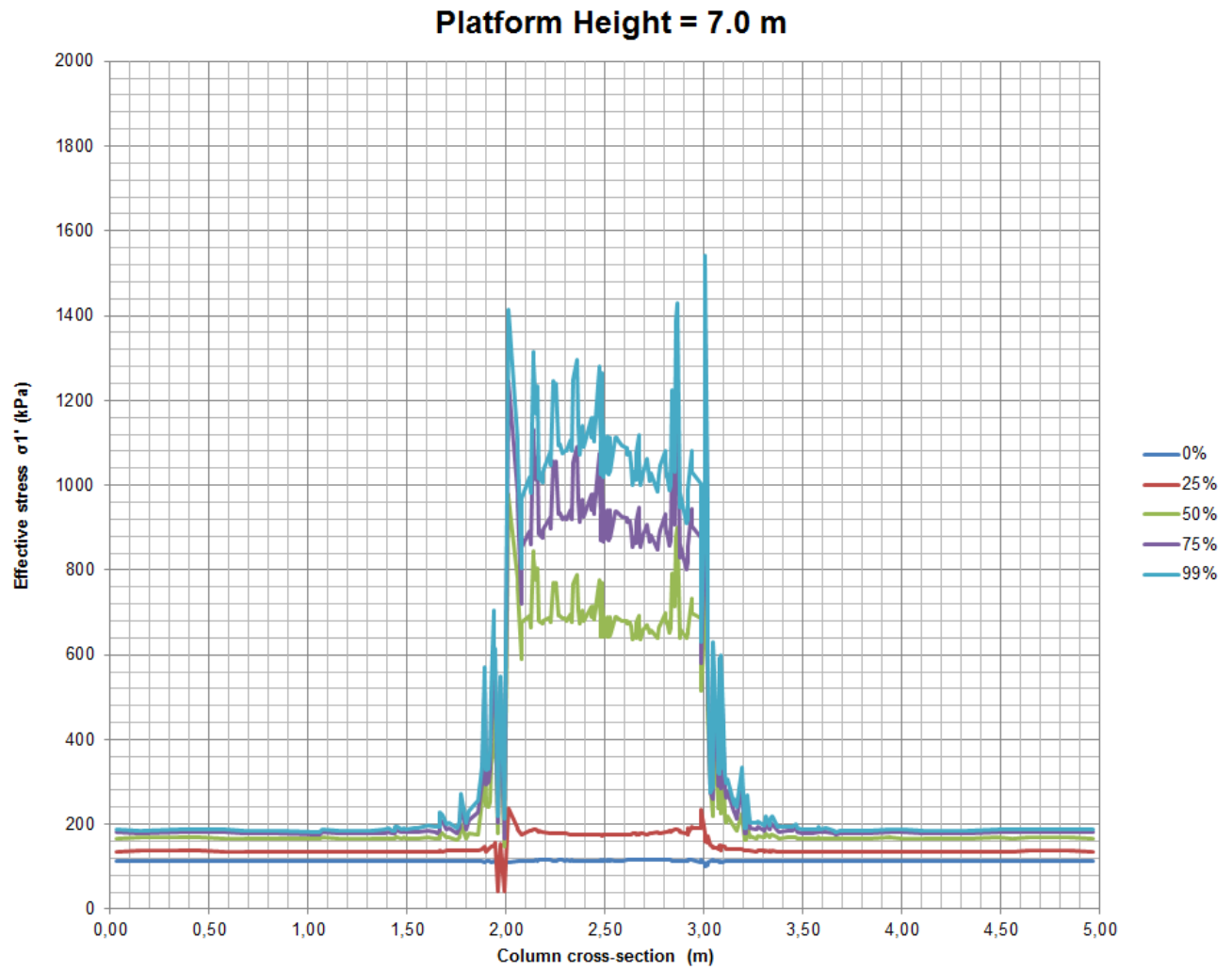Figure J.7: Cross-section of the stress distribution for platform height = 6.0 m

Figure J.8: Cross-section of the stress distribution for platform height = 7.0 m

Appendix K

PLAXIS Calculations

In this chapter the calculation results complimentary to chapters 8 and 9 are given.

K.1 Short-Term calculations

K.1.1 Parametric Analysis of the Columns

The columns are modeled using sand with stiffness moduli $E_{50}^{ref} = E_{oed}^{ref} = 70$ - 130 MPa. The friction angle φ is varied between 34°- 42°.

Column Friction Angle

The results from the column friction angle calculations are given in figures K.1 and K.1.
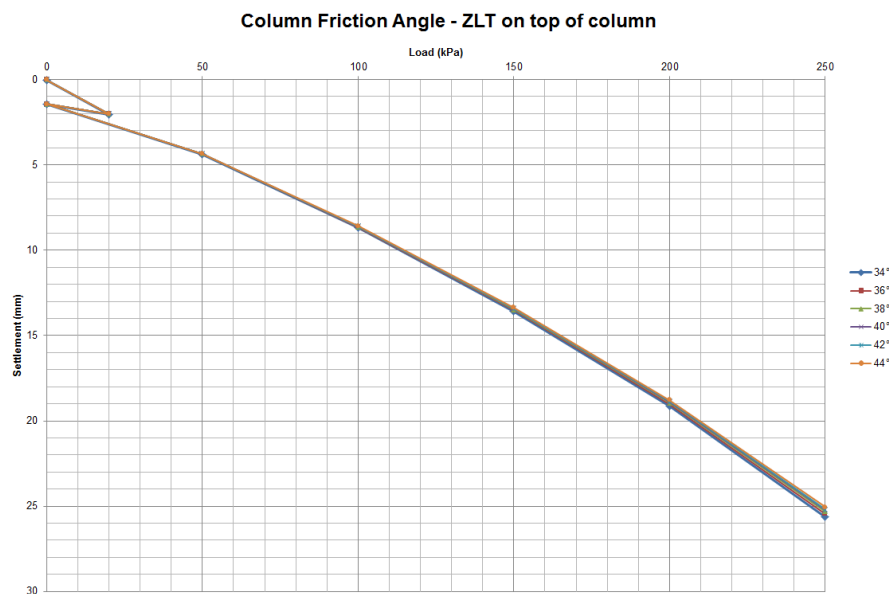

Figure K.1: Friction angle calculations, ZLT on top of column

It can be seen in the figures above that the friction angle of the sand columns does not have a significant influence on the settlement. This strengthens the hypothesis that nearly all pressure (imposed by the ZLT) is carried by water in the sabkha and silt.

It can be seen in figures K.3 and K.4 that the horizontal displacement is higher for a low friction angle, resulting in more surface settlement.

K.2 Column Stiffness

The results from the column stiffness calculations are given in figures K.5 and K.6.

It can be seen in the figures above that the stiffness of the columns only has minor influence on the surface settlement.
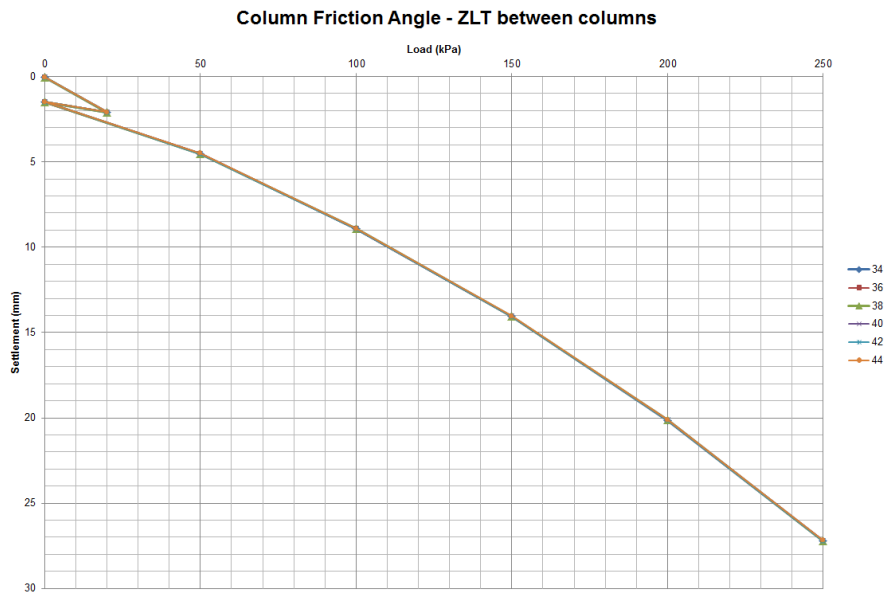
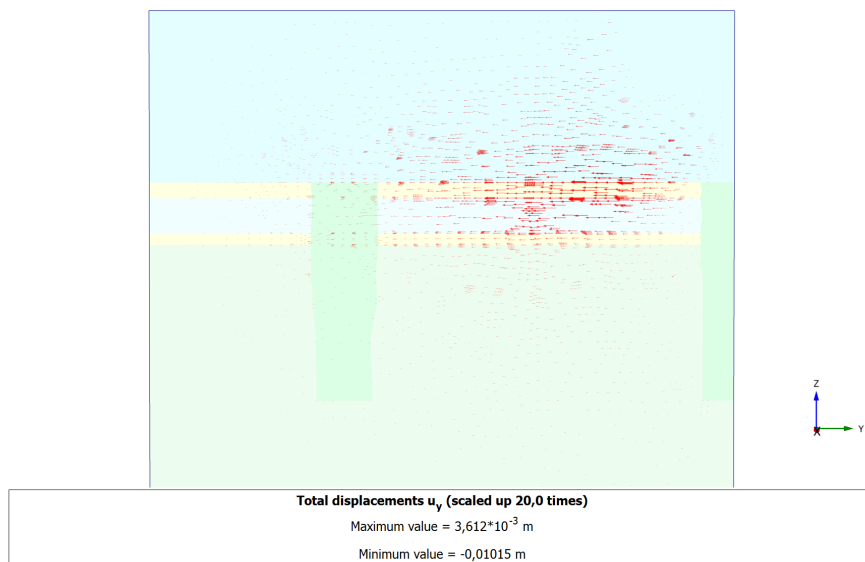Figure K.2: Friction angle calculations, ZLT between columns

Figure K.3: Displacement in direction of the y-axis for $\varphi = 36°$

It was already concluded in section 8.3 that the settlement of the ZLT is governed by horizontal displacement of soft soil. Figures K.7 and K.8 show the horizontal displacement for $E = 70$ and 130 MPa.

It can be seen that the horizontal displacement is almost similar and thus only marginally dependent on column stiffness.

K.3 Long-Term calculations

It was observed in the calculations described in section 9.2 of the main report, that the stress on the soft soil linearly increases with platform height. When the efficiency is calculated based on the calculation results, the parameters A and B are calculated as follows:
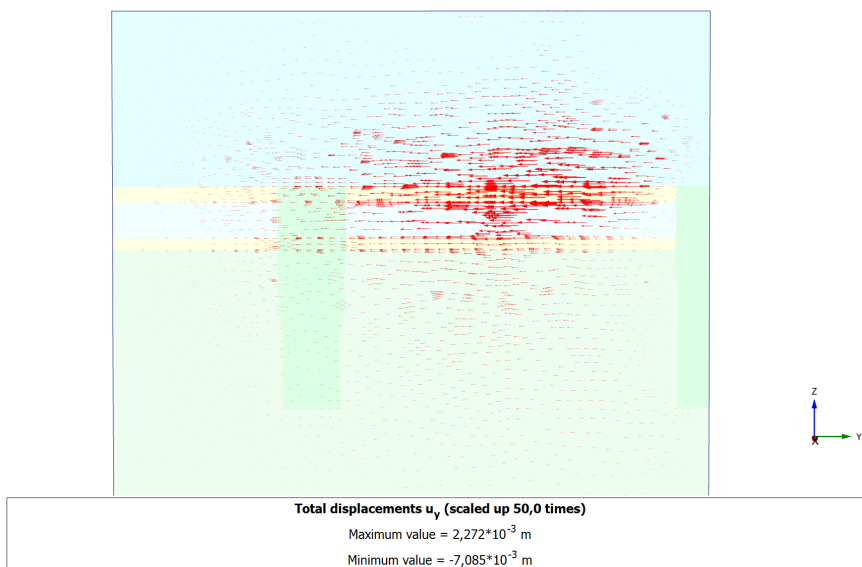
Figure K.4: Displacement in direction of the y-axis for $\varphi = 44°$

Figure K.5: Friction angle calculations, ZLT on top of column

$$A = (\gamma H + p) - \sigma_s \left(s^2 - \tfrac{1}{4}\pi d^2\right)$$

$$B = 0$$

$$C = \sigma_s \left(s^2 - \tfrac{1}{4}\pi d^2\right)$$

$$A + C = \sigma s^2 = (\gamma H + p)s^2$$

Where σ_s can be approximated (after consolidation) by $\sigma_s \approx \gamma H + p - \sigma_{arch}$, where σ_{arch} represents
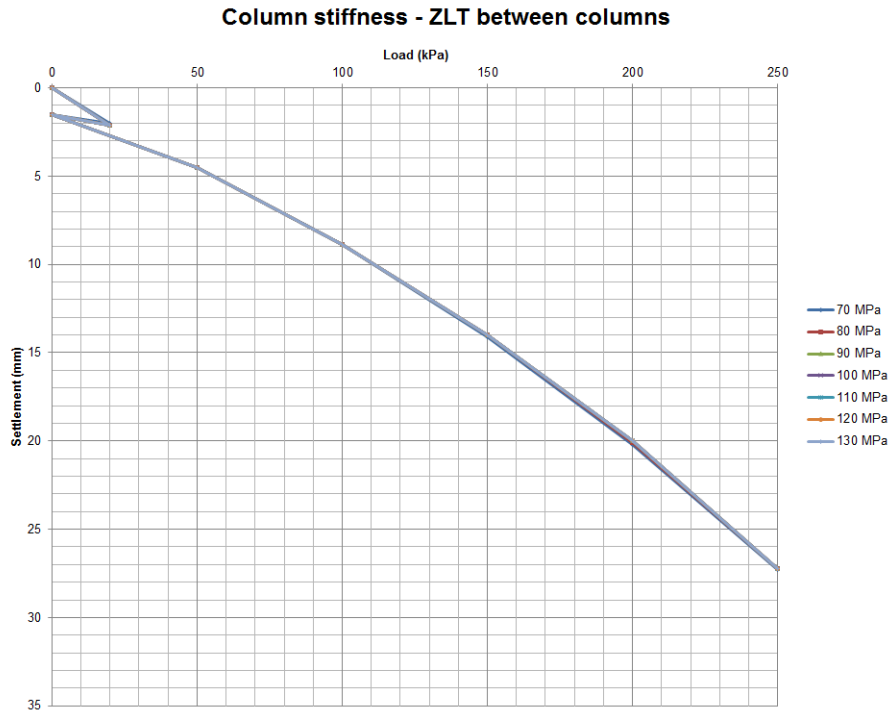
Figure K.6: Friction angle calculations, ZLT between columns
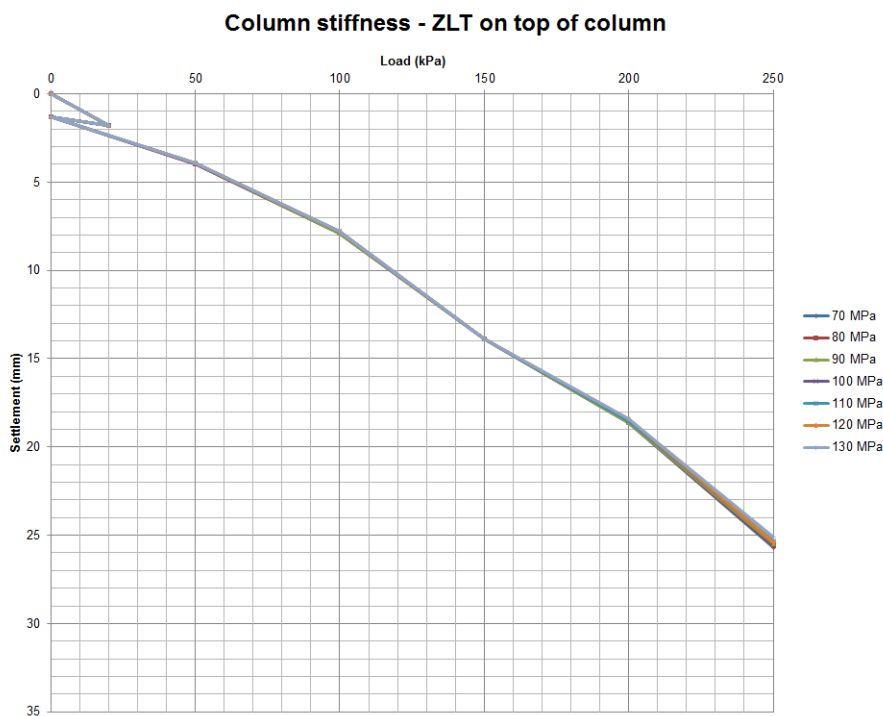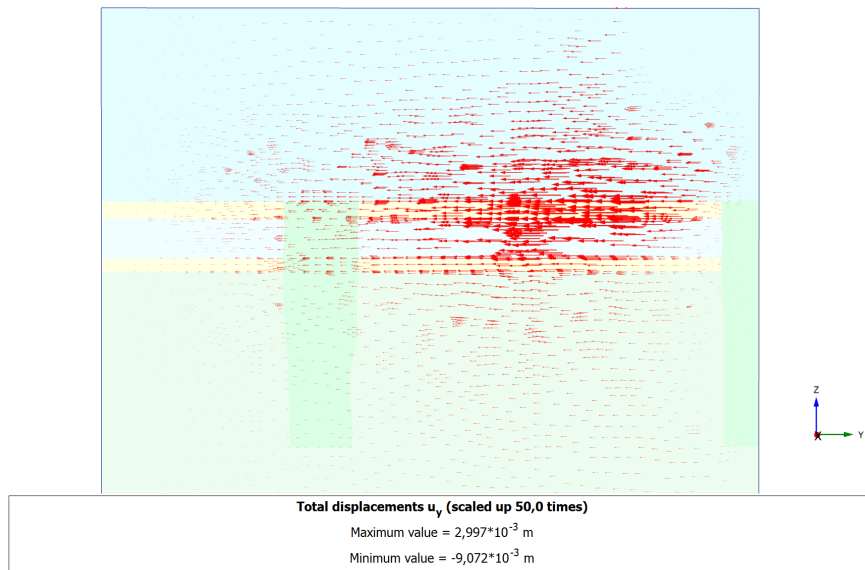

Figure K.7: Displacement in direction of the y-axis for $E = 130$ MPa

the relieved stress due to arching effect. Then equation K.3 can be rewritten to, using $s=5$ and $d=1$:

$$E = 1 - \frac{C}{A + C} = 1 - \frac{\sigma_s(s^2 - \frac{1}{4}\pi\, d^2)}{\gamma H + p}$$

$$\approx 1 - \frac{(\gamma H + p - \sigma_{arch})(s^2 - \frac{1}{4}\pi d^2)}{(\gamma H + p)\, s^2} \tag{K.1}$$

$$\lim_{H \to \infty} E(H) = \frac{\pi}{100} = \alpha$$
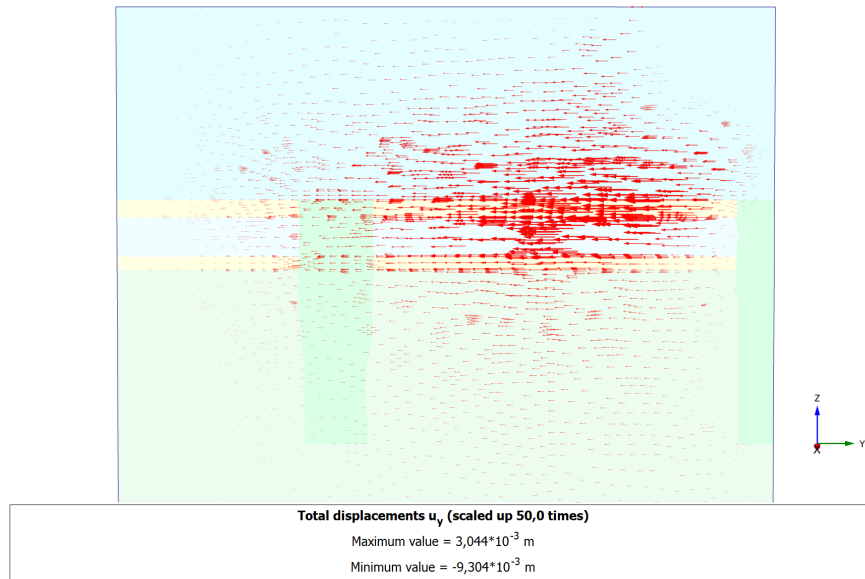
Figure K.8: Displacement in direction of the y-axis for $E = 70$ MPa

The efficiency of the CSE would in this case converge to the replacement ratio, α.

TU Delft

Delft
University of
Technology

Appendix L

CPT Diagrams

The CPT diagrams that are referred to in the main text can be found in this chapter.

L.1   ZLT CPTs

Van Oord
Marine ingenuity

L.1.1 :

ZLT FC113-1

Test according ASTM 5778-12	Predrill: **0.00 m Predrilled**
G.L.: **105.04 m** W.L.: **0.00 m**	Date: **17-12-2015**
Project: **Al Zour Refinery Project**	Cone no.: **S10CFIIP.S13331**
Location: **P 39**	Project no.: **313688**
Position: **7728, 3335.94 E-N**	CPT no.: **CPT-FC113-B60.A** **1/1**

Van Oord — Marine ingenuity

Elevation: 4.34 m

TUDelft
Delft
University of
Technology

| Cone resistance (qc) in MPa | Sleeve friction (fs) in MPa | u2 in MPa | Friction ratio (Rf) in % |
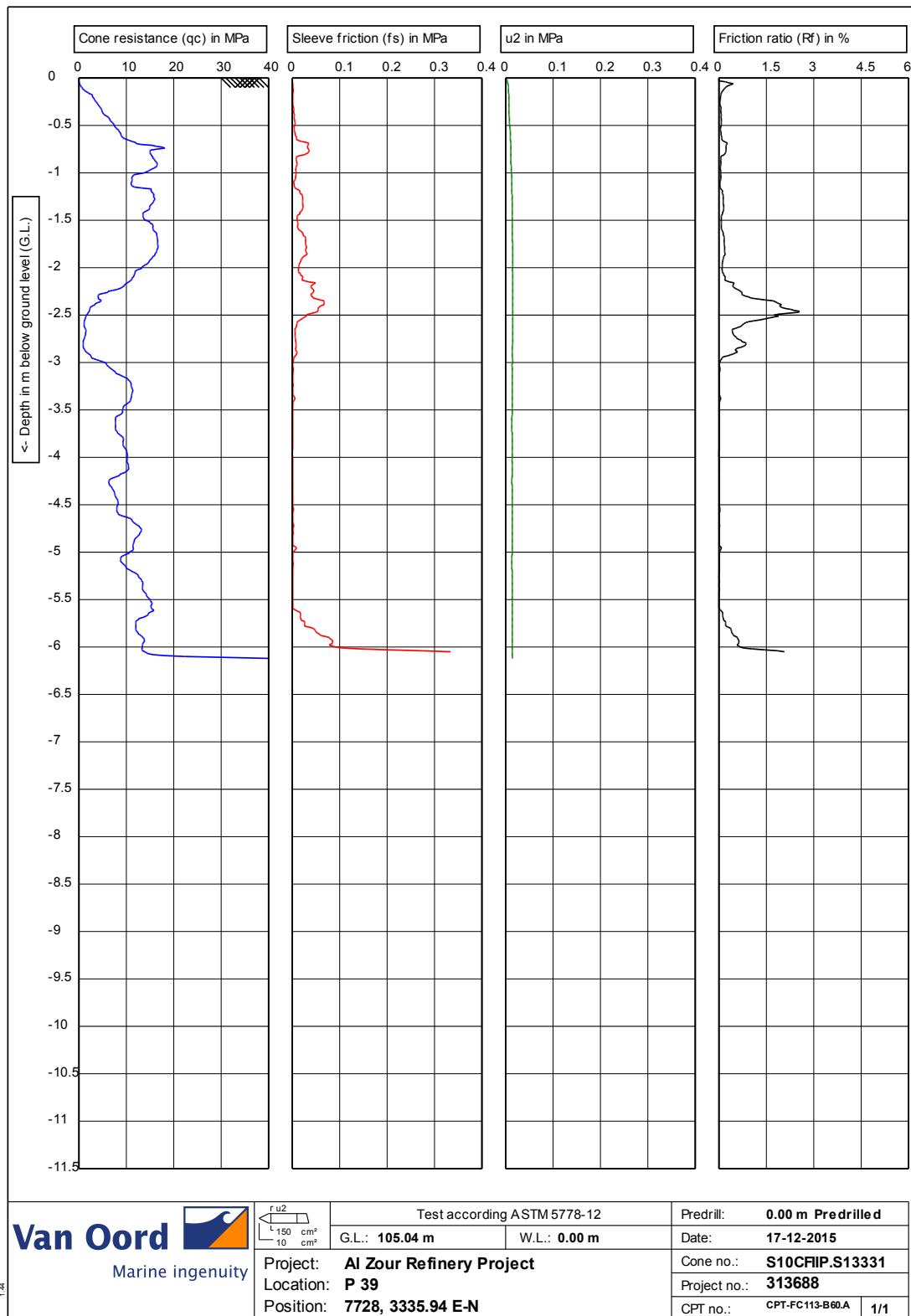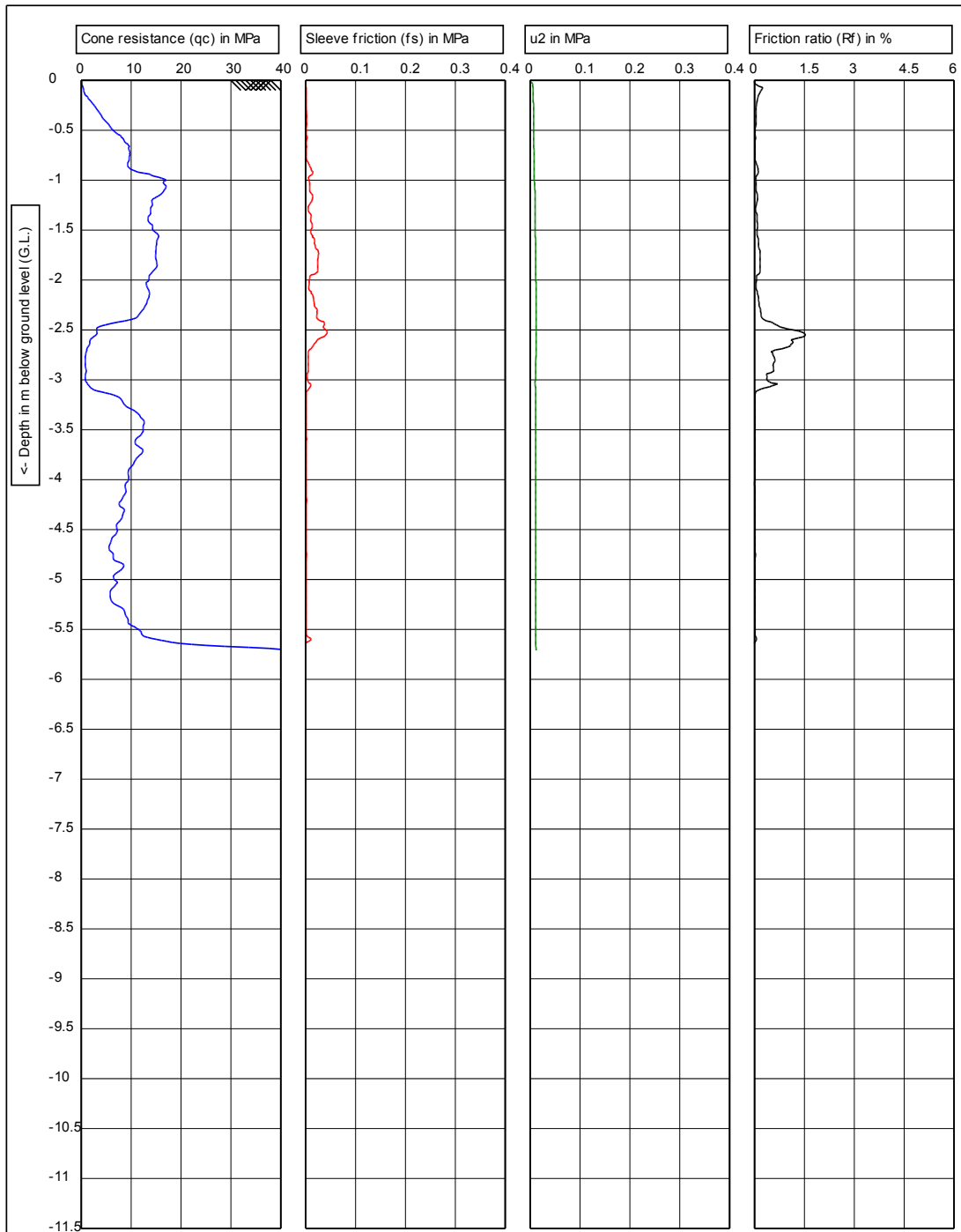
Test according ASTM 5778-12

Predrill:	**0.00 m Predrilled**	
G.L.: **105.14 m**	W.L.: **0.00 m**	Date: **17-12-2015**
Project: **Al Zour Refinery Project**		Cone no.: **S10CFIIP.S13331**
Location: **P 39**		Project no.: **313688**
Position: **7728, 3332.95 E-N**		CPT no.: **CPT-FC113-B70.A** **1/1**

Van Oord
Marine ingenuity

r u2
150 cm²
10 cm²

Elevation: 4.42 m

Van Oord
Marine ingenuity

Cone resistance (qc) in MPa | Sleeve friction (fs) in MPa | u2 in MPa | Friction ratio (Rf) in %

L.1.2   ZLT FC113-2

| Cone resistance (qc) in MPa | Sleeve friction (fs) in MPa | u2 in MPa | Friction ratio (Rf) in % |

	r u2	Test according ASTM 5778-12	Predrill:	**0.00 m Predrilled**
	150 cm²	G.L.: **105.27 m**	W.L.: **0.00 m**	Date: **17-12-2015**
	10 cm²			Cone no.: **S10CFIIP.S13331**
Van Oord	Project:	**Al Zour Refinery Project**		Project no.: **313688**
Marine ingenuity	Location:	**P 39**		CPT no.: **CPT-FC113-B60.B** 1/1
	Position:	**7730.51, 3324.46 E-N**		

Elevation: 4.55 m

Van Oord
Marine ingenuity

Cone resistance (qc) in MPa	Sleeve friction (fs) in MPa	u2 in MPa	Friction ratio (Rf) in %

Test according ASTM 5778-12

			Predrill:	**0.00 m Predrilled**
G.L.: **105.29 m**		W.L.: **0.00 m**	Date:	**17-12-2015**
Project:	**Al Zour Refinery Project**		Cone no.:	**S10CFIIP.S13331**
Location:	**P 39**		Project no.:	**313688**
Position:	**7730.52, 3320.44 E-N**		CPT no.:	**CPT-FC113-B70.B** **1/1**

Van Oord
Marine ingenuity

Elevation: 4.57 m

Cone resistance (qc) in MPa | Sleeve friction (fs) in MPa | u2 in MPa | Friction ratio (Rf) in %

<- Depth in m below ground level (G.L.)

Test according ASTM 5778-12

Van Oord Marine ingenuity	
r u2 / 150 cm² / 10 cm²	
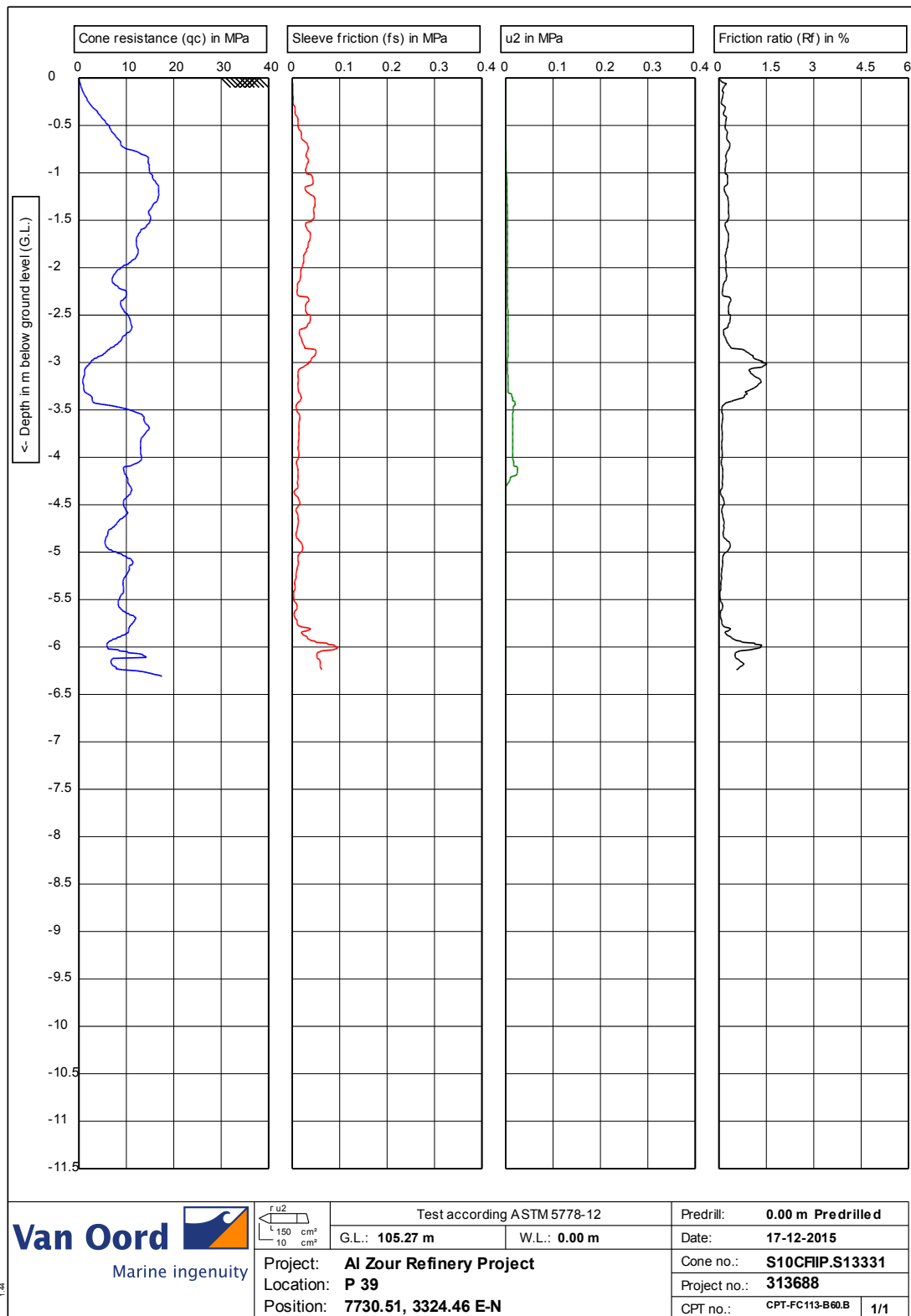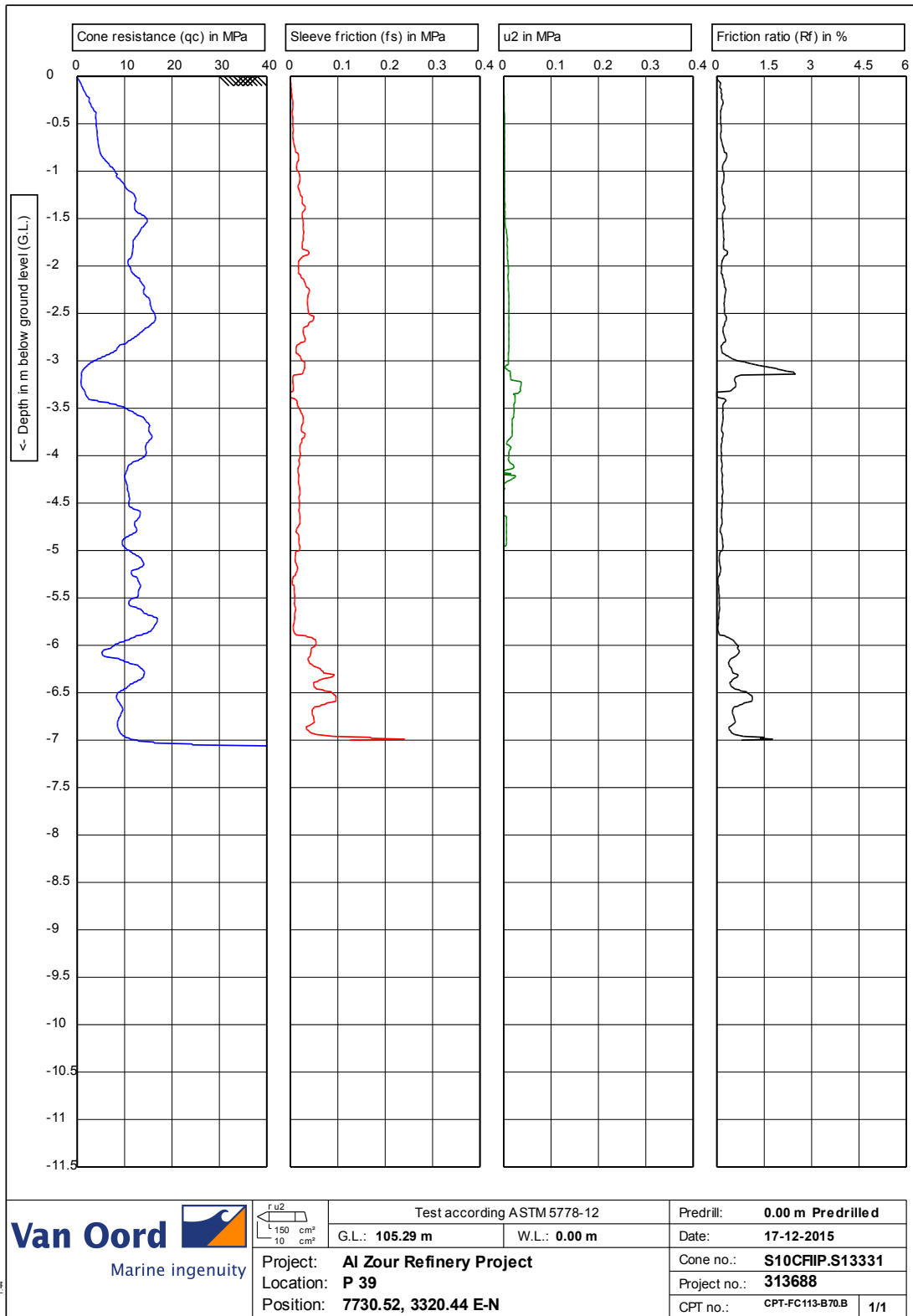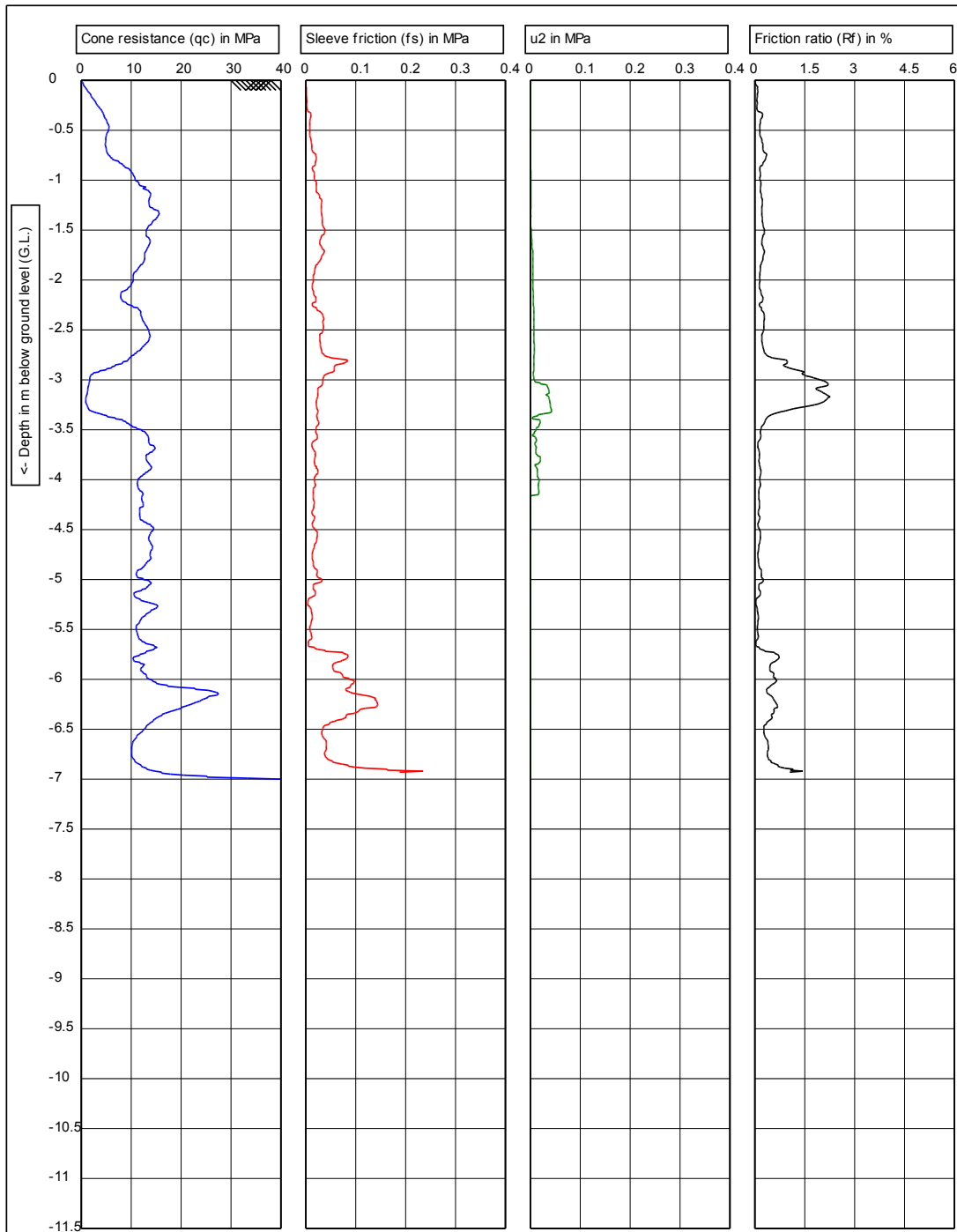
Test according ASTM 5778-12		Predrill:	**0.00 m Predrilled**
G.L.: **105.25 m**	W.L.: **0.00 m**	Date:	**17-12-2015**
Project: **Al Zour Refinery Project**		Cone no.:	**S10CFIIP.S13331**
Location: **P 39**		Project no.:	**313688**
Position: **7727.48, 3320.47 E-N**		CPT no.: **CPT-FC113-B80.B**	**1/1**

Elevation: 4.53 m

Van Oord
Marine ingenuity